



HAL
open science

Multi-scale modelling of structure and mass transfer relationships in nano- and micro-composites for food packaging

Caroline Wolf

► **To cite this version:**

Caroline Wolf. Multi-scale modelling of structure and mass transfer relationships in nano- and micro-composites for food packaging. Polymers. Université Montpellier II - Sciences et Techniques du Languedoc, 2014. English. NNT : 2014MON20217 . tel-02178975

HAL Id: tel-02178975

<https://theses.hal.science/tel-02178975>

Submitted on 10 Jul 2019

HAL is a multi-disciplinary open access archive for the deposit and dissemination of scientific research documents, whether they are published or not. The documents may come from teaching and research institutions in France or abroad, or from public or private research centers.

L'archive ouverte pluridisciplinaire **HAL**, est destinée au dépôt et à la diffusion de documents scientifiques de niveau recherche, publiés ou non, émanant des établissements d'enseignement et de recherche français ou étrangers, des laboratoires publics ou privés.

THÈSE

Pour obtenir le grade de
Docteur

Délivré par
l'Université de Montpellier 2

Préparée au sein de l'école doctorale
Science des procédés – Science des aliments

Et de l'unité de recherche
Ingénierie des Agro-polymères et des Technologies Emergentes

Spécialité : **Génie des procédés**

Présentée par
Caroline WOLF

**Multi-scale Modelling of Structure and Mass
Transfer Relationships in Nano- and Micro-
Composites for Food Packaging**

Soutenue le 16 septembre 2014 devant le jury composé de

Dr. Véronique COMA	Maitre de Conférence Université de Bordeaux	Rapporteur
Pr. Jack LEGRAND	Professeur Université de Nantes	Rapporteur
Dr. Julien BRAS	Maitre de Conférence Grenoble INP-Pagora	Examineur
Pr. Ferruccio DOGHIERI	Professeur Université de Bologne	Examineur
Pr. Nathalie GONTARD	Professeur Université de Montpellier	Examineur
Dr. Valérie GUILLARD	Maitre de Conférence Université de Montpellier	Directeur de thèse



TABLE OF CONTENT



TABLE OF CONTENT	3
INTRODUCTION	9
Scientific and technical context in the field of food packaging	11
Scientific objectives of the PhD project.....	15
Scientific questions of the PhD project	16
Scientific strategies of the PhD project	16
Glossary	18
CHAPTER 1 : Understanding of mass transfer properties in composites filled with impermeable particles and comparison of experimental data with available predictive models	21
Publication 1 : How various particle shapes affect structure & mass transfer relationships of nanocomposite material ?.....	23
1. Introduction	24
2. Overview of particle types and brief recall of the processing and structures of the composites.....	28
3. Effect of the particles shape on the modulation of mass transport properties	38
4. In-depth investigation and understanding of the modulation of the permeability of nanocomposites	43
5. Conclusion	62
Publication 2: State of the art and beyond on multi-scale modelling of structure & mass transfer relationships in nanocomposite materials	77
1. Introduction	78
2. Basics on mass transfer.....	81
3. General overview of available analytical tortuosity-based model for permeability prediction.....	85
4. Toward a multi-scale modelling of the structure / mass transfer properties relationship.....	111
5. Conclusion	116
PERSPECTIVES	117

CHAPTER 2 : In depth understanding of mass transfer and development of a 2D numerical model for the prediction of these properties into composites filled with permeable particles	119
Publication 3: Water vapour sorption and diffusion in wheat straw fibres and impact on mass transfer in PHBV based bio-composites	121
1. Introduction	122
2. Experimental	124
3. Results and discussion	134
4. Conclusion	145
Publication 4 : Prediction of water vapour permeability in biocomposites using theoretical models	147
1. Introduction	148
2. Theory on analytical biphasic models	150
3. Experimental	156
4. Results and discussion	159
5. Conclusion	168
PERSPECTIVES	169
Publication 5 : A numerical model for predicting mass transfer in bio-composites : assesment of the permeable particles impact on the water vapour properties	171
1. Introduction	172
2. Mathematical modelling and simulation	176
3. Materials and experimental modelling parameters determination	180
4. Results and discussion	184
5. Conclusion	196
PERSPECTIVES	198

CONCLUDING REMARKS AND GENERAL DISCUSSION	199
REFERENCES.....	207
PUBLICATIONS AND COMMUNICATIONS	229
Scientific papers.....	231
Oral communication	231
Posters.....	232
ANNEXES.....	233



INTRODUCTION



Scientific and technical context in the field of food packaging

In the last decades, food packaging R&D attempts were mainly devoted to the design of new and improved (active and intelligent packaging) barrier materials (new polymers, complex and multilayer materials) that extend shelf-life while maintaining and monitoring food safety and quality. Simultaneously, with the global growing conscience related to the intensive use of petro-sourced plastics in food packaging applications, a significant interest has been dedicated to the study of biobased materials [Petersen et al. (1999)]. Despite the increasing number of studies related to the development of new materials, the main limitation is the absence of approaches that combine food requirements and materials development for implementation of “food/packaging systems” into integrated food chain concepts, from processing to consumption.

One main role of packaging material in food quality and safety preservation is to control mass transfer of gases and vapours between the food, the packaging material and the environmental atmosphere; three types of mass transfer can occur (figure 1):

- ➔ from the environment through the packaging and toward the headspace and the food product, the permeation of environmental gases and vapour need to be controlled for the preservation of food quality by avoiding food degradation reactions;
- ➔ from the packaging toward the food, the migration of undesirable molecules such as chemical additives should not exceed the maximum limit in order to be not toxic for human in long term exposure conditions;

- ➔ from the food product toward the packaging, the sorption and diffusion of food components such as aroma compound need to be controlled for the conservation of organoleptic properties of the food product.

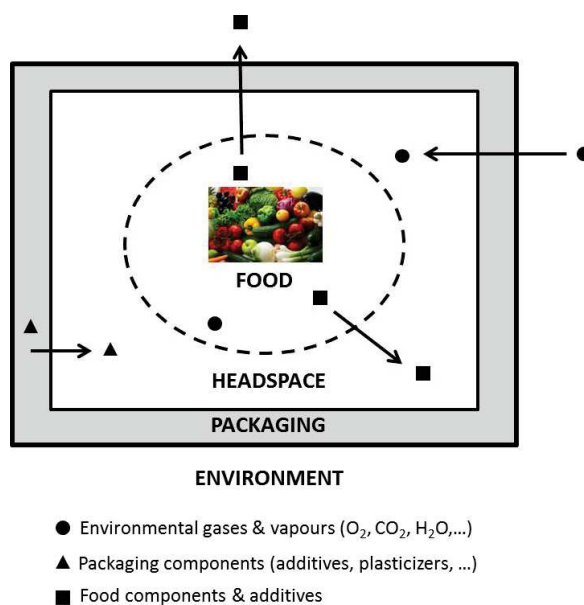


Figure 1: Mass transfer representation in food packaging

An essential step to promote the application of new complex materials, such as composites for example, by the food packaging industry is to develop decision-aid numerical tools based on mathematical modelling of mass transfer to favour the tailoring of composite structures well adapted to the targeted food requirements. In a perspective of multi-scale modelling an in-depth understanding of the knowledge of the relationships between structure and mass transfer properties is required based on the characterization of the composite structures (in-situ size, shape, dispersion, orientation of the particles), of the particles impact on both polymer matrix structure and properties, and on the resulting modulation of the mass transfer in the composites. Each type of particles is unique in terms of size, shape, nature (impermeable or permeable for example) and so their effects on the mass transfer of

the composites are not the same. If the effect of impermeable particles addition on the modulation of mass transfer properties has already proven many times by experimental approach [Azeredo et al. (2009)], the formalisation (e.g. modelling) of structure and mass transfer relationships remains limited because it is still difficult to reach an optimal structure and barrier properties characterization due to two major hindrances:

- ➔ the difficulty to reach a good structural characterization of composite materials, especially an accurate description of the size, dispersion and orientation of the particles in-situ in the polymer;
- ➔ the lack of experimental methodologies and tools to characterize mass transfer properties in permeable particles.

Actually, there is a wealth of experimental data in the available scientific literature on the mass transfer properties of composite structures, especially nanocomposites with impermeable particles. Indeed composite materials represent a promising source of development for active and intelligent packaging but also for the development eco-friendly materials based on the use of biopolymers. While the latter present high sensibility to environmental conditions, such as temperature or moisture, which limited their use in food packaging to a narrow range of applications, water and mechanical resistance could be improved by incorporating fillers [Rhim et al. (2013)] in order to obtain materials with reinforced functional properties. Such property enhancements are generally attained at low nanoclays content, less than 5% compared to that of conventional fillers which are in the range of 10–50%. Nowadays, vegetable fibres are raising interests in food packaging applications for their affordable convenience; indeed, nanocrystalline cellulose may

be only one-tenth as strong as carbon nanotubes but its production cost is 50-1000 times lesser to produce [Faruk et al. (2012)]. Incorporation of vegetal fibres in a polymer contributes to decrease the overall cost of the material (especially when high content up to 40wt% of fibres are added) and permits to modulate the mass transfer properties such as water vapour permeability.

Modelling approach have either been based on the application of analytical tortuosity-based models or on the development of numerical approach (computational fluid dynamic modelling (CFD), such as finite element method (FEM)) for the prediction of mass transfer properties in composites. Currently, the use of analytical models relies on the prediction of the permeability of composites from experimental structural characterization of few geometrical inputs (aspect ratio, volume fraction, dispersion and orientation of the particles) supposed constant and homogeneous for all the material and from the permeability of the neat polymer matrix. These models were developed for homogeneous distribution of particles and exhibited restrictions of use for heterogeneous composite structures. Using numerical approach, more complex structures could be investigated, by applying FEM to 2D or 3D geometries representing the composite structure. For instance, Bhunia et al. (2012) have developed a model based on finite element method which overcame the limitations from most of the tortuosity-based by taking into consideration structural phenomena such as particle orientation or agglomeration.

Scientific objectives of the PhD project

In this context, my PhD work aimed to contribute to increasing the scientific knowledge on mass transfer properties in composite materials by reaching a better understanding of the modulation of the barrier properties with the incorporation of nano- and micro- permeable and impermeable particles in polymer matrix; and to developing an innovative multi-scale approach based on finite element method for the prediction of mass transfer in bi-phasic composites considering both the particle and the polymer matrix properties with realistic 2D geometry of the composite structures. This PhD was realized within the framework of the research activities of the Joint Research Unit "Agropolymer Engineering and Emerging Technologies" and funded through state resources coming from the French government (Ministry grant). The innovative aspect of this project was to consider composite with either impermeable particles or permeable ones (such as vegetal fibres) which hugely contribute to the overall water vapour mass transport. A composite material based on a biopolyester matrix and wheat straw fibres was used as a basis to develop the numerical model and validated it. This composite has been developed within the EcoBioCAP European Project (<http://www.ecobiocap.eu/>); using advanced composite structures based on constituents derived from food industry by-products.

Scientific questions of the PhD project

To achieve my PhD objectives, several questions should be first answered:

- ➔ What is the impact of the particles nature, shape and size on the composite permeability?
- ➔ What are the most commonly used models for predicting structure & mass transfer relationships?
- ➔ What is the contribution of the particle to the overall mass transfer in the case of permeable particles such as vegetal fibres?
- ➔ How can structural characteristics and mass transfer characteristics of composites, getting from structural and mass transfer analysis, be gathered and linked to the mass transfer of composite in a multi-scale modelling approach?

Scientific strategy of the PhD project

To answer to the aforementioned questions, the scientific strategy presented in figure 2 was adopted; the PhD work plan is divided in two chapters according to the nature of the particle either permeable or impermeable.

The first chapter is dedicated to an exhaustive analysis of mass transfer in composites and a gathering of all mathematical models proposed for the prediction of mass transport through composites from data available in the literature. The analysis of barrier properties lead to the determination of parameters impacting mass transfer in composites and the analysis of the models highlight the bottlenecks encounter to

the development of models able to provide good prediction of composite barrier properties.

The second chapter is first aimed at providing a better understanding of the impact of permeable fibres on the modulation of water vapour transfer through wheat straw fibres/biopolyester composites with the help of experimental and modelling support. It is then intended to present a new multi-scale approach using COMSOL Multiphysics Software to predict mass transfer properties in a bi-phasic composite, considering both mass transfer properties of the permeable particles and polymer matrix with realistic 2D geometry of the composite structures.

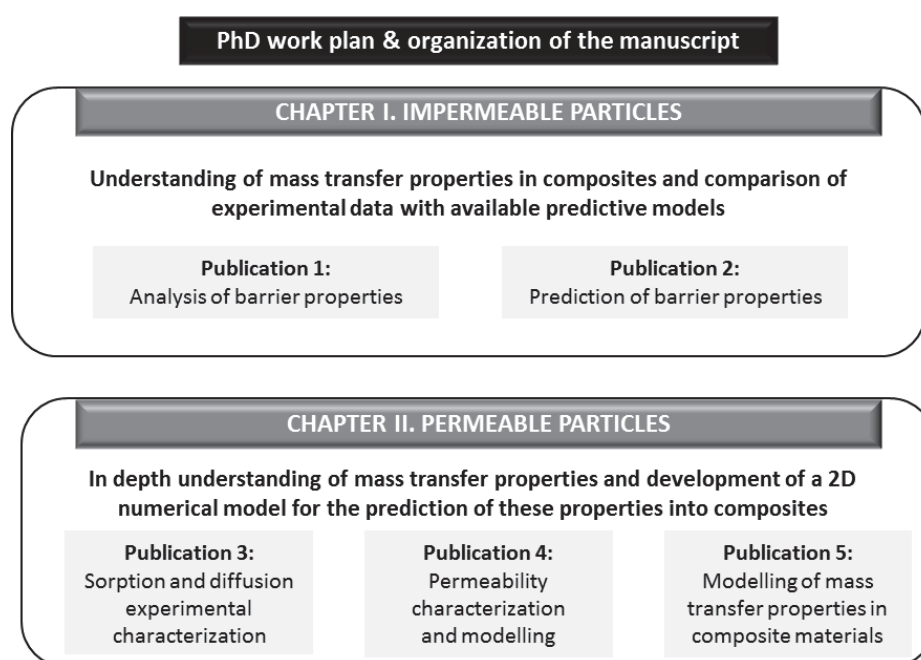


Figure 2: PhD work organization

In order to facilitate the understanding of the different discussions provided in the next chapters, a glossary with the definitions of the main terms used in the following is proposed to the reader in the next pages.

Glossary

- ➔ **Analytical tortuosity based-model:** predict the permeability of a composite material exhibiting permeable polymer matrix and impermeable particle, dependant from the permeability of the polymer matrix and geometrical input such as particle volume fraction, aspect ratio, dispersion, orientation, etc...
- ➔ **Analytical biphasic model:** predict the permeability of a composite material exhibiting permeable particles and permeable polymer matrix, dependant from the particles and the matrix permeability, the particle volume fraction and geometrical input such as the shape and the maximum volume packing of the particles.
- ➔ **Aspect ratio:** ratio of the length to the thickness of one particles
- ➔ **Composites:** materials consisting of at least two non-miscible constituents with different properties, whose synergism creates properties unavailable from individual single constituents
- ➔ **Effective diffusivity:** isotropic diffusion of molecular species through the entire materials
- ➔ **Diffusing molecular species:** any molecule other than a polymer chain that diffuses through the material
- ➔ **Diffusion:** conductive transport of a chemical species through a single phase from a macroscopic point of view always occur from a region of high concentration to a region of low concentration. Diffusion obeys to the (phenomenological) Fick's law.
- ➔ **Diffusivity (diffusion coefficient / D):** constant between the molar flux due to molecular diffusion and the gradient in the concentration of the species at a specific section according to Fick's law
- ➔ **Numerical modelling:** simulation to predict and reproduce the behaviour of a system, to explore and gain new insights into new technology and to estimate the performance of systems too complex for analytical solutions

- ➔ **Permeability (permeation coefficient / P):** measure of the ability of a material to allow a molecular specie to pass through it and in the case of permeability to gases and vapours, the combination of Fick's first law and Henry's law
- ➔ **Permeation:** penetration of a molecular species through a solid and directly related to the concentration gradient of the permeate and the material diffusion coefficient
- ➔ **Phenomenological model:** relate several different empirical observations of phenomena to each other, in a way which is consistent with fundamental theory, but is not directly derived from this theory
- ➔ **Solubility (solubility coefficient / S):** amount of diffusing molecular species that dissolve in a given amount of material and directly proportional to the partial pressure of the molecular specie above the solvent according to Henry's law
- ➔ **Tortuosity:** represents the ratio of the pathway that a molecular specie must follow through the composite thickness with particles to the pathway through the neat polymer thickness without particles
- ➔ **Tortuosity factor:** parameter that represents the tortuosity and depends on the aspect ratio, the shape and the orientation of the particles
- ➔ **Transfer:** conductive or convective transport of a chemical species between two phases; in the case of a packaging material, transfer between a material toward atmosphere
- ➔ **Transport:** conductive or convective motion of chemical species through a single phase



CHAPTER 1: Understanding of mass transfer properties in composites filled with impermeable particles and comparison of experimental data with available predictive models



Publication 1

How various particle shapes affect structure & mass transfer relationships of nanocomposite materials?

Caroline Wolf, Nathalie Gontard, Valérie Guillard

ABSTRACT: *More than 1000 published experimental data of oxygen (O₂), carbon dioxide (CO₂) and water vapour (H₂O) permeabilities in nanocomposites containing either spherical, cylindrical or platelet particles were collected, assorted and compared in order to decipher the role of particle shapes on the reduction of the relative permeability of the nanocomposite. This paper extensively discussed the impact of the shape of the particles on the structure and, thus on, permeability values in order to draw meaningful conclusions on the structure/mass transfer relationships and to give directions for the development of next generation of packaging materials with tailored mass transfer properties. The results generated had revealed that the expected decrease of permeability due to a tortuosity effect was not systematically achieved, even for platelets that displayed higher aspect ratio than spheres and cylinders. Attempts of explanation will be made throughout the text to explain this unexpected behaviour.*

KEYWORDS : Particle shape, Nanocomposites, Structure & mass transfer relationships, Permeability

1. Introduction

1.1. Context

Nanostructuring by different processing techniques is one of the promising directions in the development of packaging materials with advanced mass transfer properties. A lot of reviews present the last advancement in elaboration strategies of nanocomposites and the resulting functional properties, mainly mechanical properties [Le Baron et al. (1999), Alexandre et al. (2000), Ray et al. (2003), Ray et al. (2005), Chung et al. (2007), Cong et al. (2007), Pavlidou et al. (2008), Chivrac et al. (2009), Faruk et al. (2012)]. Some authors have made a slight focus on the mass transfer properties [Ray et al. (2003), Ray et al. (2005), Chung et al. (2007), Cong et al. (2007), Pavlidou et al. (2008), Mittal et al. (2009)] in nanocomposites elaborated with a given type of particle, i.e. spheres or platelets for instance. In the scope of optimal food packaging conditions, one of the main purposes is to design and provide food packaging's able to protect the food from the external environment and to maintain the quality of the food throughout the shelf life of the foods [Pertersen et al. (1999)]. To optimally achieve this purpose, the properties of composite materials and especially mass transfer properties should be understood according to the structure of the composites, i.e. particles nature, shape, size, dispersion and orientation in order to respond to the needs of the food. In the field of food packaging, some reviews [Azeredo et al. (2009), Arora et al (2010), Silvestre et al. (2011), Rhim et al (2013)] have already dealt with the study of nanocomposites for food packaging applications, from the choice of the polymers and nano-reinforcements to the industrial applications and the safety consideration, including the nanocomposites properties such as mass transfer properties. Actually, there is a wealth of information available in scientific literature on barrier properties of nanocomposites containing

platelets, spherical or cylindrical particles, but there is a lack of systematic analysis of all these data in the perspective of deciphering the role of particle shape on the mass transfer properties of the resulting material. As far as we knew, there is no review associated with exhaustive analysis of experimental nanocomposite permeabilities from the open literature.

1.2. General background on mass transport

The transfer of small molecules through a polymer packaging film occurs due to a random molecular motion of individual molecules where the driving force behind sorption, diffusion and permeation is the concentration difference between the two sides of the film. This process can be described by Fick's first law of diffusion, according to which the flux (J) normal to the direction of the flux is proportional to the concentration gradient $\left(\frac{\partial c}{\partial x}\right)$:

$$J = -D \left(\frac{\partial c}{\partial x}\right) \quad [1]$$

where (D) is the diffusion coefficient. This equation is applicable when the concentration does not vary with time. The molecular penetrant sorption, in the case of transfer of gases or vapours can be described according to Henry's law:

$$c = S \times p \quad [2]$$

where p is the pressure and S the solubility coefficient. In the steady state and after integration of equation 1, the flux can be expressed as follow:

$$J = \frac{D(c_1 - c_2)}{h} \quad [3]$$

where h is the thickness of the packaging film and c_1 and c_2 are the concentration on the two sides of the film. The combination of equation 2 and equation 3 give the permeation equation:

$$J = \frac{D S(p_1 - p_2)}{h} \quad [4]$$

where p_1 and p_2 are the pressure on the two sides of the film. The product $P=D \times S$ represent the permeability coefficient and then in term of permeability, the flux equation can be written as:

$$J = \frac{P(p_1 - p_2)}{h} \quad [5]$$

The relation $P=D \times S$ was initially developed for the description of gases permeability in a homogeneous pure polymer has also been considered for the description of gas transport properties through a nanocomposites with impermeable, non-porous particles dispersed in a polymer matrix [Cornelius et al. (2002), Takahashi et al. (2006)]. This relation in nanocomposites was valid only under the assumption that the polymer matrix was not affected by the incorporation of nanoparticles, and that the particles/polymer matrix interactions were strong enough to avoid the creation of an interphase at the interface particles/polymer matrix. In general, when impermeable particles are incorporated in a polymer matrix, particles acted as an obstacle to the permeation of gas molecules which had to follow a more tortuous path and lead to a decrease of the effective permeability of the nanocomposite. This effect is called

tortuosity¹ and depends on the volume fraction of particles and the shape and the size of the impermeable particles, i.e. on the aspect ratio (W/t) of the particles. The tortuosity outcome is forecasted to be particularly efficient in the case of nanoplatelets, as can be seen in figure 1, due to their large aspect ratios when compared to other nanoparticle shapes.

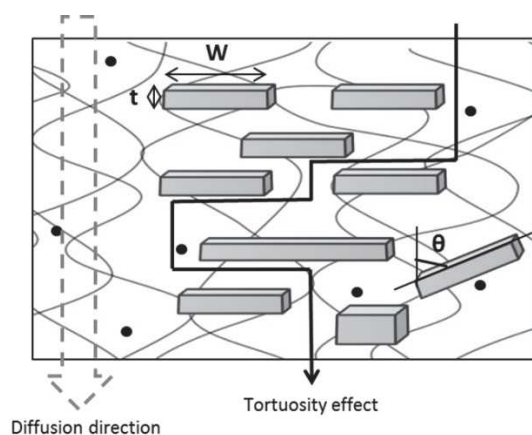


Figure 1: Representation of the tortuosity effect in platelet-based composites

1.3. Aim of the paper

With the recent developments in the nanotechnologies and nanosciences field, the correlation of material mass transfer properties with the nanocomposites structure has generated much interest. From this standpoint, the objective of the present article is to comprehensively discuss the role of the particle shape on the modulation of the mass transfer properties in nanocomposites. In this purpose, more than 700 values (i.e. 100 articles) of the most recently measured values of O_2 , CO_2 and H_2O permeability in agro-, bio and petroleum-based nanocomposites were collected from the available literature. Particles considered were classified in three categories:

¹ Tortuosity (τ) represents the ratio of the distance that a molecular specie must follow through the nanocomposite thickness (d') to the distance through the neat polymer (d): $\tau = d'/d$

spheres, cylinders and platelets, all belonging to the nanosize except in specific case such as that of natural vegetal fibres where some particles were more in the microsize. Aside the meaningful conclusions on the role of particle shape, the main objective of this paper is to give some recommendations for the design of nanocomposite packaging materials with tuneable mass transport properties.

In the present work the modulation of the barrier properties is investigated according to the shape of the particles through (1) a presentation of the particles and the processing techniques of the composites, (2) general and numerical observations of the modulation of the permeability and (3) a qualitative analysis of the structure and mass transfer properties relationships in composites.

2. Overview of the particles type and brief recall of the processing and structures of the composites

The following section will be focused on particle types and shapes divided in three main categories (spheres, cylinders and platelets) and on the main elaboration strategies for (nano)-composites processing.

2.1. Particle type and shape

In the pool of studies collected, most of them dealt with nanoparticles and only exceptionally with microparticles (case of natural vegetal fibres); therefore the following section will present principally the nanoparticles the most frequently

encountered in the present work². The particles considered in this review are impermeable, non-porous ones; zeolites were, for example, excluded of this analysis and were not described in the present section.

Nanoparticles are defined as inclusions that have at least one dimension in the range of 1-100nm. Nanoparticles can be divided in three families, depending on how many dimensions are in the nano-scale. If three dimensions are in the order of the nanometers, the particles can be considered as spherical particles; if two dimensions are in the order of the nanometers, the particles can be considered as elongated cylinder particles and if only one dimension is in the order of the nanometres, the particle can be considered as platelet particles.

2.1.1. Spherical particles

The two most widely studied non-porous spherical nanoparticles are silicon dioxide (SiO₂) particles and titanium dioxide (TiO₂) particles. TiO₂ particles have been used in food packaging materials [Rhim et al. (2013)], since it is inert, non-toxic, inexpensive, and environmentally friendly with antimicrobial activity against a wide variety of microorganisms [Fujishima et al. (200)]. Besides, for membrane applications, TiO₂ particles, as SiO₂ particles have been widely used and incorporated in dense polymer matrix in order to modulate the barrier properties of gases and vapours and to increase the selectivity; one of the most important characteristics a membrane should reach [Koros et al. (1993)]. These particles could be used in their native form or synthesized from inorganic precursors through sol-gel method. The average

² All the information about the composites; type, size and modification of particles, type of polymer matrix and processing techniques of the composites were gathered in table 1-2-3. These data were collected from the material and methods section of the publication analysed in this work.

diameter of these particles is in the range from 5 to 150nm; the characteristics of the spherical particles-based composites studied in this paper were gathered in table 1.

2.1.2. Cylinder particles

Cylinder particles could either be synthetic one such as carbon nanotubes (CNT) which consisted in one-atom thick single wall nanotubes (SWNT) or a number of concentric tubes called multi-walled nanotubes (MWNT) with respectively average length in the range from 0.1 to 1 μ m and from 1 to 100 μ m and with respectively average diameter in the range from 0.8 to 1.4nm and 10-200nm. Due to their exceptional mechanical, thermal and chemical, carbon nanotubes have been used as polymer fibre reinforcement to improve the polymer matrix properties [Liu et al. (2014)]. In the field of food packaging they have recently been used and the resulting nanocomposites have shown migration levels of simulants below the overall migration limits required by current legislative standards for food packaging materials [Yu et al. (2014)]. Cylinder particles included also natural fibres such as cellulose nanofibres and cellulose nanowhiskers with respectively average length in the range from 0.1 to 1 μ m and from 20 to 300nm and with respectively average diameter in the range from 0.8 to 1.4nm and 10-30nm. Natural vegetal fibres are cheaper [Fabruk et al. (2012)] than most of other nanoparticles since they come from readily available natural sources. They are therefore often proposed as filler reinforcement agent to modulate the properties of the composites and particularly to decrease the cost of the final material as regard to the high price of the neat polymer matrix. Besides nanoparticles, micro-particles such as cellulose micro-fibres have also been used as fillers; all the characteristics of the cylinder particles-based composites studied in this paper were gathered in table 2.

2.1.3. Platelets

One of the most widely used nanoplatelets is usually montmorillonite (MMT), i.e. hydrated alumina-silicate layered clay consisting of in an edge-shared octahedral sheet of aluminium hydroxide between two silica tetrahedral layers exhibiting average length, width and thickness in the range from 80 to 300 nm, from 15 to 50 nm and from 1 to 8 nm respectively. Montmorillonites and other nanoplatelets shaped particles such as cellulose and starch nanocrystals, silicon carbide or boron nitride were initially incorporated into a polymer matrix to enhance its mechanical properties. However, researchers very soon realized that they had a great impact on the improvement of barrier properties, even at very low filler content (< 5 wt/wt%), provided that a homogeneous exfoliation of the platelets into the neat matrix was achieved and that the mean aspect ratio of the particle was the highest possible. The concept of tortuosity makes perfect sense in that case. All the characteristics of the platelet particles-based composites studied in this paper were gathered in table 3.

For the three aforementioned categories, the dispersion state of the particles in the neat matrix strongly impacts the homogeneity of the structure and the resulting mass transfer properties. It is all the more important for mass transfer that even a single channel in a homogeneous nanostructure could completely counteract the barrier performance. Bad dispersion of particles could provoke their agglomerations in the polymer matrix, leading to the formation of particle clusters in the micro-size. The tortuosity effect is then lost and barrier properties of the composite are the same than those of the neat matrix or even worse ("permeabilisation" of the neat matrix). Besides loss of barrier properties is enhanced by bad particles/polymer matrix

interactions which lead to apparition of an interphase at the interface particles/polymer matrix [Kim et al. (1998), Chung et al. (2007)], with creation of defected interface particles/polymer matrix or change in polymer matrix properties that could favour the diffusion of the molecule [Chaiko et al. (2005), Sanchez-Garcia et al. (2009)]. By definition, the interphase could be seen as a third compartment at the interface particle/polymer matrix where the local properties change from the filler bulk properties to the matrix bulk properties [Kim et al. (1998)].

2.1.4. Native or chemically modified particles

To enhance the dispersion of the particles into a polymer matrix, a chemical modification of the particle surface, with the aim to match the polymer matrix polarity, is often carried out [Ray et al. (2005), Fabruk et al. (2012)]. For instance, in the case of clay platelets, cationic exchange of the inorganic interlayer cations by organic ones, such as alkylammonium surfactants, is one of the most common used techniques. But other original techniques are also used [Alexandre et al. (2000)]. In the case of spherical particles such as SiO₂, the surface of the particles can be modified with -silyl [Kono et al. (2007), Ahn et al. (2008), Yu et al. (2011)] or with -silane groups [Joly et al. (1999), Romero et al. (2011), Rafiq et al. (2012)].

Besides chemical modification of the particles, dispersion in the polymer matrix strongly depends on the elaboration process used. Generating ideal and defect-free nanocomposites structures is very challenging and draws considerable effort. A necessary condition for acceptable interfacial interaction between the particle and the matrix is determined by the surface free energy of the two components. Usually this means that the surface energy of the particle must be greater than that of the

matrix. For example, in case of solution blending, an ideal system would be one where the particle has a stronger affinity for the polymer than the solvent, while the polymer has a stronger affinity for the particle surface than the solvent. These relations could be quantified with the help of Hildebrand solubility parameters for the polymer-solvent interaction, using the solvent-particle interaction strength parameter for the particle, the higher the parameter, the stronger the interaction. This approach was experimented by (Mahajan & Koros, 2000) on mixed matrix membranes for gas separation and zeolite and sieve as nanoparticles. Another approach would be to use measurements of surface free energy (though contact angle measurements) to predict a work of adhesion, which gives an expression of the thermodynamic work necessary to separate two solid phases [Berthet et al. (2014)]. However, this approach is not yet well expanded in the field of packaging science probably because of the lack of data for the calculation of Hildebrand solubility parameters for the polymer and nanoparticle encountered in this field. As regard measurement of work of adhesion, experimental bias prevents an accurate determination of the free surface energy that prevents the use of this technique to predict compatibility between particle and matrix. The main elaboration strategies used for nanocomposites processing will be thus described in the following section.

2.2. Nanocomposites elaboration

Several strategies have been considered for the preparation of nanocomposites and are gathered in figure 2; the most commonly used preparation techniques can be divided in three main processes for all the particle types and shapes with the addition of one particular method for the spherical particle (e.g. sol gel method) and platelets (e.g. template synthesis).

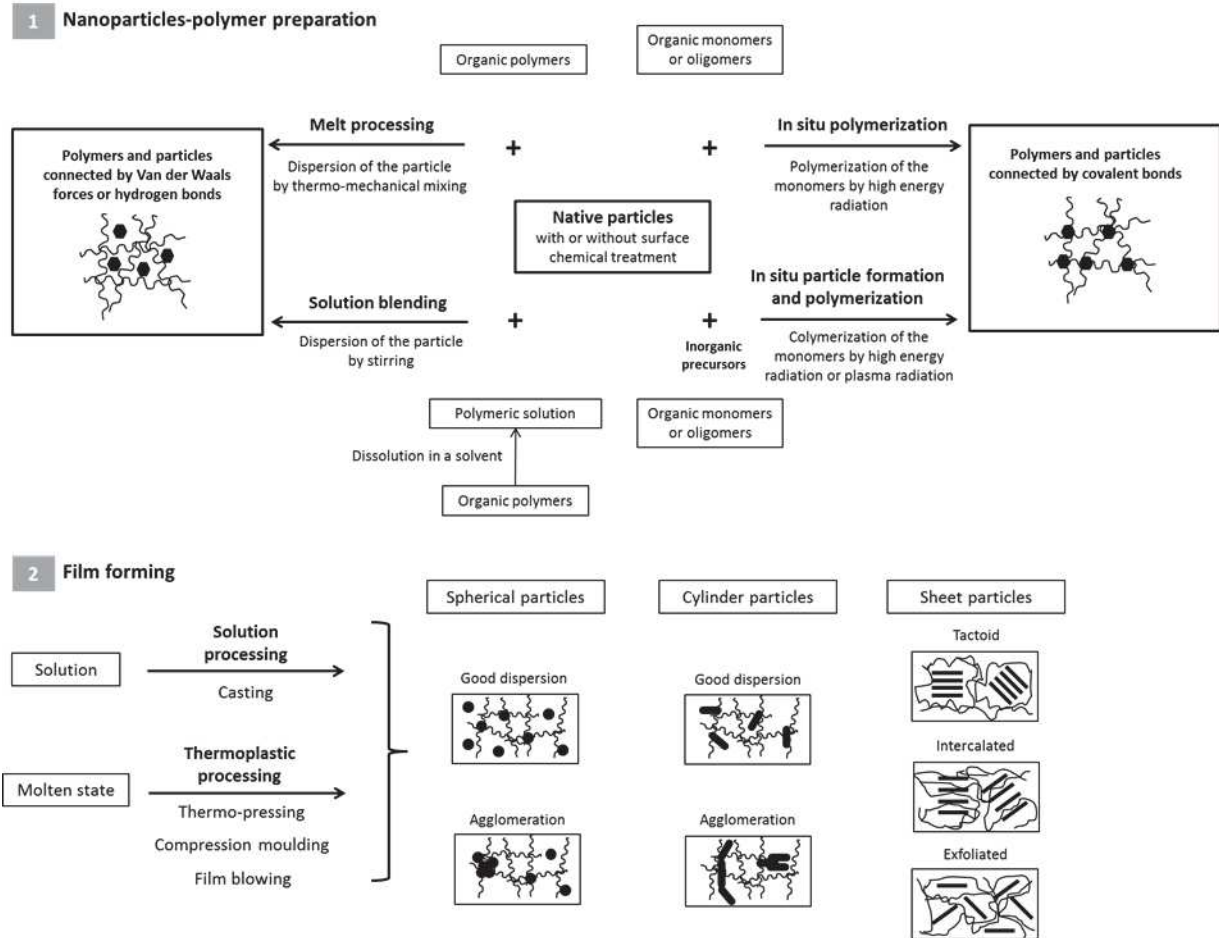


Figure 2: Outline of the processing, with the preparation techniques and film-forming of composite and their structures according to the particle shapes

All the preparation technologies have already been extensively detailed in reviews dedicated to specific nanocomposites such as for example, polymer-layered silicate based-nanocomposites [Alexandre et al. (2000), Ray et al. (2003), Pavlidou et al. (2008), Mittal et al. (2009)], polymer-natural fibre based-composites [Saheb et al. (1999), Siqueira et al. (2010)] and polymer-inorganic spherical based nanocomposites [Cong et al. (2007), Chung et al. (2007)]. Due to the physical and chemical differences of the polymer matrixes and the particles it is very complicated to propose one universal processing technique. Indeed the choice of the nanocomposites processing technique is based on the convenience and ease of

use of the techniques according to the nature of the raw materials, both the particles and the polymer matrix. At laboratory scale, solution blending, in-situ polymerization and melt-processing are very often used. However at industrial scale, it is very difficult to implement solution blending and in-situ polymerization due to the huge volume of solvent needed and the complexity of the processing techniques respectively. Thus at industrial scale, due to the large amount of materials produced, melt-processing is preferred.

Solution blending. In solution blending, a polymer is dissolved in a solvent and the particles are dispersed in the solution by stirring; finally the solvent is removed either by vaporization or by precipitation. In order to reach a good dispersion of the particles, both the polymer matrix and the particles unmodified/modified chemically should dissolve in the solvent and thus the experimental conditions, such as the temperature and the stirring rate should be optimized according to the couple particles/polymer matrix.

Melt-processing. In melt-processing, the particles are dispersed by thermo-mechanical mixing in a polymer matrix in the molten state. In order to reach a good dispersion of the particles the shear conditions should be optimized, requiring in some cases high processing conditions which could come close to matching the temperature of degradation of the polymer matrix.

In-situ polymerization. In in-situ polymerization, the native particles or modified particles with functional groups on their surfaces such as hydroxyl or carbonyl are dispersed in a solution of monomers. The polymerization is generated by initiating

radicals, cations or anions under high energy radiation (plasma, heat,...) on the surface of the particles.

Sol-gel method / Template synthesis. In the sol-gel method for spherical particles and template synthesis for the platelets, monomers and inorganic precursors are mixed together in solution. The inorganic precursors hydrolyse and condense into well dispersed nanoparticles and get trapped into the polymeric matrix chains during polymerization. This processing is often used in the cases of spherical particles, as can be seen in table 1 but less often used for platelets, and never used in the publications quoted in the present paper. This technique leads to well-dispersed particles in-situ in the polymeric matrix and seemed to be used in a large number of works in the membrane science field.

2.2.5. Resulting (nano)-structures

Depending on the process conditions and on the particles/polymer matrix affinity, different morphologies can be obtained which can be divided in distinct categories that depend on the particle shape. For spherical and cylinder, there are usually two possible arrangements: particles are either (i) well-dispersed or (ii) agglomerated. For platelets, three distinct morphologies could be obtained: (i) tactoid (micro-composites), (ii) intercalated or (iii) exfoliated nanocomposites. Tactoid structure appears when the polymer chains have not penetrated into the inter-layer spacing due to, mainly, poor particle/polymer matrix affinity and not inefficient shearing. Intercalated structures are obtained when the polymer chains have diffused between platelets leading to separation of silicate layer and increasing of interlayer space. Exfoliated structures display complete delamination and homogeneous

dispersion of the clay layers. Depending on the process, a random or specific orientation (for example platelets orthogonal to the diffusion flux) could be achieved.

In solution blending and melt intercalation, the particles are connected to the polymer matrix through Van der Waals forces or hydrogen bonds [Cong et al. (2007)]. If particles/polymer matrix interactions are weaker than the particles/particles interactions, particles could form clusters and lead to agglomeration phenomena. Process conditions are generally tentatively optimized to avoid this phenomenon (e.g. shearing in the extrusion process, type of solvent in the solution blending, etc ...) concomitantly with the used of chemically modified particles to fit the polymer polarity. Contrary to solution blending and melt intercalation, in-situ polymerisation and sol-gel method lead to covalent particle/polymer bonds which usually favour the dispersion of the particles within the matrix [Cong et al. (2007)] For example, in sol-gel method, based on self-assembly forces, the polymer aids the nucleation and growth of the inorganic host crystals and gets trapped within the layers as they grow [Alexandre et al. (2000)]. Therefore, these two techniques are usually preferred, when possible, to limit particles agglomeration during nanocomposites elaboration. But in the case of in-situ polymerization, a complete state of particles exfoliation in the polymer matrix was not always reached [Gain et al. (2005), Herrera-Alonso et al. (2010)]. Gain et al. (2005) have compared different processing techniques and showed that the dispersion of the platelets was greatly improved with in-situ processing if compared to melt-processing. However, even with a chemical modification of the platelets, they still remained some stacks of intercalated clays.

3. Effect of the particles shape on the modulation of mass transport properties

3.1. Explanation of the analysis approach

The publications which were considered in the following part were collected from peer-reviewed scientific journals in different field of research such as membrane, materials and packaging sciences. All these papers presented one or more value of permeability of (nano)-composites material according to the composition of the composite. Only gases (O_2 and CO_2) and water vapour permeability data were considered in the following because of their high interest in food packaging field. These data were analysed as regard to particle shape (sphere, cylinder, platelet) and size, (nano and micro), the filler volume fraction used in the composite formulation, the eventual chemical and functionalization treatments applied to the particle and elaboration technique used for (nano)-composite processing. Almost all the cited papers used nano-size particles and the particles were also considered as impermeable.

The objective of the study was to decipher the role of the particle shapes on the obtained variation of composite permeability compare to that of the neat matrix as a function of filler volume fraction and in the light of the composite structure achieved. To do that, the modulation of the permeability was represented through the evaluation of the relative permeability, i.e. the ratio of the composite permeability to the matrix permeability (P/P_0) as function of particle volume fraction (ϕ_{vol}). Generally, in experimental work, the weight fraction (ϕ_{wt}) of particles was given instead of volume fraction. However, ϕ_{vol} is always the main input in tortuosity based model [Nielsen (1957), Cussler et al. (1988), Baradwaj (2001) ...] used to

predict effect of particles addition on the permeability of nanocomposite based-materials, and therefore, volume fraction was preferred in this study. This implied to convert all the ϕ_{wt} given in the original papers. In order to calculate the particle volume fraction, the density of both particles and polymer matrix was needed but in most of the publications these values were not provided and it was therefore necessary to extract the information in other publications, in supplier data sheets or even to approximate the value. ϕ_{vol} could be calculated from the weight fraction and the density of both particle and polymer using the following expression:

$$\Phi = \frac{\frac{w}{\rho_{particles}}}{\frac{w}{\rho_{particles}} + \frac{1-w}{\rho_{matrix}}} \quad [6]$$

where ρ_{matrix} and $\rho_{particles}$ are the density of the matrix and the particles respectively and w the weight fraction of particles. This conversion and hypothesis made to do it leads to unavoidable uncertainty on the ϕ_{vol} . To further analysis evolution of composite permeability, plots of P/P_0 as a function of ϕ_{vol} were done for each particle shape.

3.2. Modulation of mass transport properties in nanocomposites (global evolution of P/P_0) : first screening approach

While a lot of experimental work has been performed in the area of polymer-based nanocomposites, the challenge is yet to reach the understanding on how nanoparticles with various shapes can affect the permeability of the nanocomposites. As can be seen from figure 3, the evolution of the relative permeability as function of particle volume fraction is really complex and do not follow the same trend according to the nanoparticles shapes.

Due to the high number of studies found for each particle shapes, for O₂, CO₂ and H₂O permeability, the figures are not actually readable but they permit to draw the general tendencies of P/P₀ as function of ϕ_{vol} and to give an idea of the amplitude of variation of the P/P₀ ratio depending on the particle shape. Most of the studies of O₂, CO₂ and H₂O permeability in nanocomposites were carried out in platelets-based nanocomposites with about 100 publications on the topic resulting in a total of 710 permeability values. All of them have been represented in Figure 2c leading to a scatter graph in which each individual study could not, of course, be distinguished. For comparison, 45 publications were found for spheres-based nanocomposites and 35 for cylinder-based nanocomposites resulting in about 380 and 190 values of permeability respectively (Figures 2a and 2b).

These figures, aside their overloaded aspect that underlined the intensive works on the topic, permit to draw general trends on P/P₀ variation as a function of ϕ_{vol} :

- As it can be observed in figure 2a and 2b the ϕ_{vol} range investigated remains always higher for spherical and cylinder particles than for platelets with a maximal ϕ_{vol} value reaching 40 vol% and 45 vol% respectively against 15 vol% only for platelets (figure 2c). We noted that for platelet-based nanocomposites, only 3 publications (i.e. 11 permeability values) were in the range of 15 to 40 vol% (not shown in Figure 2c). This feature could be ascribed to the fact that, usually only a small platelets volume fraction (generally between 1 to 5 wt%) is necessary to gain an effect on the material functional properties [Lange et al. (2013)].

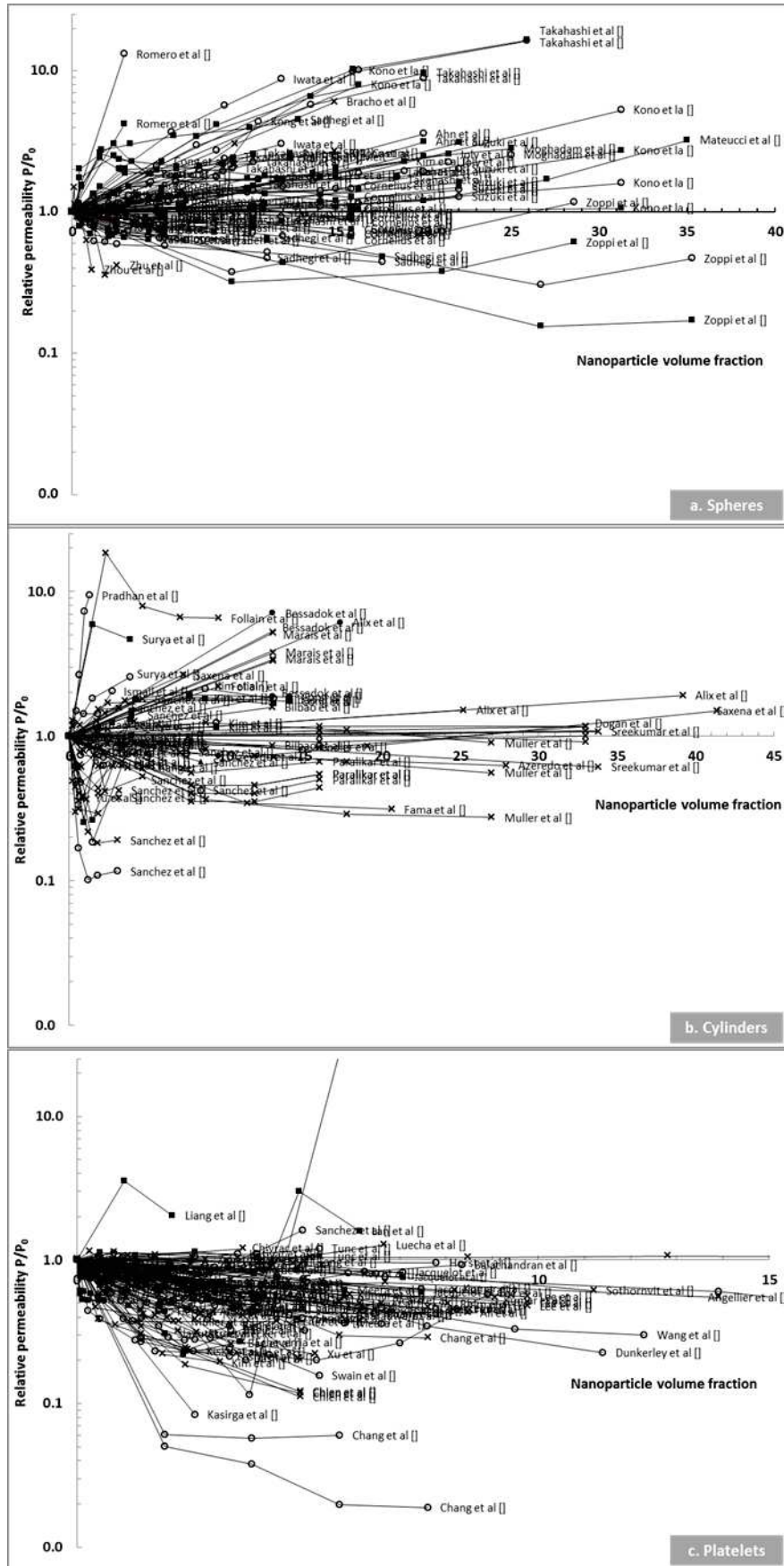


Figure 3: Evolution of the relative permeability P/P_0 in spheres (a), cylinders (b) and platelets (c) - based composites as function of particle volume fraction

- The amplitude of variation of P/P_0 depends on the particle shape. Figures 2a and 2b permit to point out that spheres and cylinders addition in a polymer generally provoke either a monotonic decrease or increase of P/P_0 with amplitude of variation of 0.15 to 16 and 0.1 to 18 respectively. This leads to a scatter graph of P/P_0 with a general aspect in herringbones centred on $P/P_0 = 1$. On the contrary, figure 2c shows that for platelets, except one or two cases, the relative permeability values remains always below P/P_0 equal to 1.
- The maximum drop in P/P_0 is much higher for platelets-based nanocomposites, with a P/P_0 reaching a minimum value of 0.01, i.e. up to 10 folds lower than the minimum value that could be reached with cylinder and particles, and in spite of the lower filler volume fractions used.
- For all kinds of particles, some non-monotonic variations of P/P_0 were noted with simultaneously increase and decrease of the relative permeability for the nanocomposites. It represents approximately 12% of the studies for spherical nanoparticles, 21% of the study for cylinder nanoparticles and only 7% of the studies for platelets.

Among the aforementioned conclusions of this first general analysis of P/P_0 evolution in nanocomposites, some trends were expected as in the fact that platelets generate, more often and with higher amplitude than the cylinders and/or the spheres, a decrease of the permeability. This could be easily ascribed to the particle geometry and the more pronounced tortuosity effect induced by platelets compare to spheres and cylinders. This analysis has also revealed that the behaviour of P/P_0 was more complex than expected with non-monotonic behaviours especially in the

case of cylinders. However, straightaway it could be asserted that the evolution of the relative permeability and thus the modulation of the barrier properties were affected by the shape of the nanoparticles. Some general tendencies have emerged for each kind of particles that will be in depth analysed in the following sections.

4. In-depth investigation and understanding of the modulation of the permeability of nanocomposites

Some material properties such as mechanical properties have already been in-depth studied [Jordan et al. (2005), Al-Saleh et al. (2011)], Suvorova et al. (2013)] and have provided a better understanding of the relationships between nanocomposites properties and structures. But among these functional properties, mass transfer properties were never extensively analysed in the perspective of comparing effect of particle shape on permeability. In the following section the evolution of the relative permeability P/P_0 will be in depth investigated by first, a statistical analysis of available data according to the shape and volume fraction of particles and second, an attempt of qualitative explanation case by case of the modulation of the permeability according to particles morphology by focusing on the (nano)structure obtained and its relationship with mass transfer properties.

4.1. Statistical analysis of the modulation of mass transport properties

In order to perform a quantitative analysis of “performance” of each particle shape to modulate/change the permeability value of the neat matrix, all the permeability

data collected were gathered on a histogram showing the number of studies per class of modulation represented by a range of value for the relative permeability P/P_0 . The maximum number of permeability values for spheres (43%), for cylinders (29%) and for platelets (30%) was obtained for the classes $1 < P/P_0 < 2$, $1 < P/P_0 < 2$, and $0.6 < P/P_0 < 0.8$ respectively, confirming the fact that only platelets leads to largely decrease of permeability (figure 4).

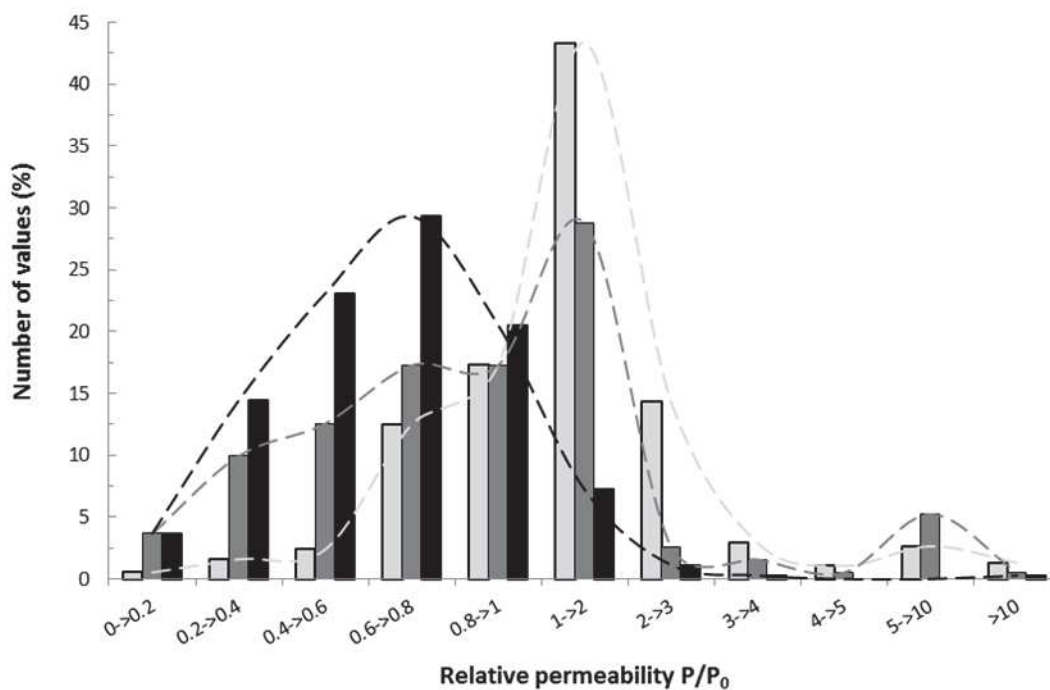


Figure 4: Representation of the number of permeability value in composites (%) according to the particle shapes (spheres: light-grey, cylinders: dark-grey and platelets: black) as function of the classes of the relative permeability P/P_0 evolution

Besides this main impact, secondary peaks were observed in figure 4. In the case of spherical particles, 17% of values were obtained for the class $2 < P/P_0 < 3$ and 14% for $0.8 < P/P_0 < 1$ indicating that permeability in spheres-based nanocomposites could be either multiply by a factor 3 in a significant number of times as well as slightly decrease of 20%. This feature confirms well the herringbone scatter graph observed when all data of P/P_0 are represented as a function of ϕ_{vol} (figure 3a). In the case of

cylinders, 17% permeability values belonged to the class $0.6 < P/P_0 < 0.8$ and once again 17% to the class $0.8 < P/P_0 < 1$, indicated that even if the main effect is a weak increasing permeability up to a factor 2, addition of cylinders could statistically decrease the permeability of cylinders-based nanocomposites. In the case of platelets, their overall trend of decreasing permeability was confirmed with secondary peaks which reveal that 23% of permeability values were obtained for $0.4 < P/P_0 < 0.6$ and 21% of for $0.8 < P/P_0 < 1$ in platelet-based nanocomposites.

To verify if the conclusions of this global analysis were still confirmed for different filler fractions, permeability values were also apportioned into classes of filler fraction in addition to the classes of P/P_0 values. Classes chosen for filler fractions were 0 to 5 vol%, 5 to 10 vol%, 10 to 20 vol% and 20 to 30 vol%. Resulting plots are shown in figure 5. Compared to figure 4, the P/P_0 were limited to a maximal value of 3 considering that higher increase of the permeability ratio is an exceptional behaviour (less than 6 % of the studies whatever the particle shape) and result in great structural changes of the nanocomposites.

According to figure 5a, an increase up to a factor 2 of the permeability of the neat matrix was globally obtained in almost 45% of cases whatever the filler fraction considered: that means that the same evolution of P/P_0 was obtained for each filler fraction in the case of spherical particles. This regularity was not observed anymore for cylinders and platelets which displayed some differential behaviour depending on the filler fraction. For cylinders-based nanocomposites, the same trend of P/P_0 evolution was obtained than in Figure 4b for volume fraction until 20vol% with a main peak (between 25 and 30%) centred for P/P_0 values ranging between 1 to 2. At a volume fraction higher than 20 vol% the curve was offset to higher decrease of the

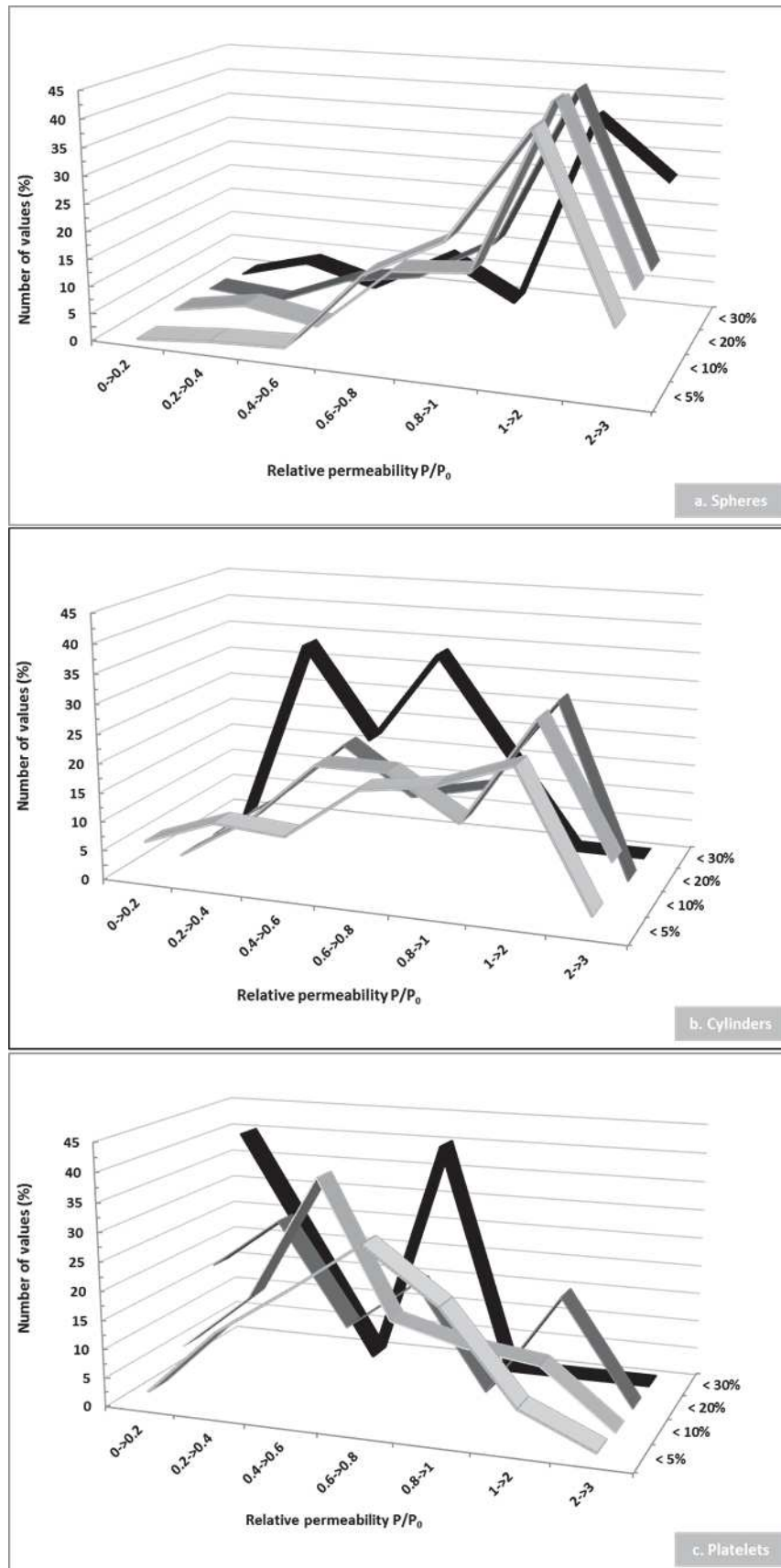


Figure 5: Representation of the number of permeability value of composites (%) in spheres (a), cylinders (b) and platelets (c) -based composites according to the volume fraction various particle as function of the relative permeability P/P_0 evolution

relative permeability but presented a more disordered shape of the curve. For platelets-based nanocomposites the same trend of P/P_0 evolution was obtained than in Figure 4c for particle volume fraction lower than 5 vol% with a main peak (30%) centred for P/P_0 values in the range from 0.6 to 0.8. This main peak was shifted to higher decrease of the relative permeability for particle volume fraction ranging between 5 to 10 vol%, with a main peak (38%) for P/P_0 values in the range from 0.4 to 0.6 while for volume fraction > 10 vol%, the decreasing effect on the permeability was not confirmed anymore. We noted that studies conducted with such high amount of platelets (> 10 vol%) were scarce and it is thus difficult to generalize the effect of high volume fraction of platelets on P/P_0 of the resulting nanocomposites.

To sum up, this statistical analysis has revealed that:

- Whatever the volume fraction, the addition of spherical particles did not statistically impact so much the permeability of the nanocomposites;
- Decrease of permeability could be achieved by either cylinders and platelets addition but for different volume fraction of particles; more than 20 vol% are necessary to achieve a significant decrease of P/P_0 in cylinders based nanocomposites while less than 10 vol% are required when platelets are used instead of cylinders;
- Increasing volume fraction of particles between 5 and 10 vol% in platelet-based nanocomposites decreases the P/P_0 ratio more sharply than filler fraction lower than 5 vol% .

Therefore, the modulation of the permeability is clearly affected by the shape of the particles. In the following, lines of explanation will be tentatively brought in order to

relate this “shape effect” to the morphology of the particle and the (nano)-structure of the composite.

4.2. Qualitative analysis of the relationship between mass transfer properties and structure of the composites

In this section, in order to reach a better understanding of the structure and mass transfer properties relationships, we will try to explain the general tendencies previously observed of the modulation of the permeability relying on a critical discussion of explanation lines provided by the author in their study. In the three following sub-section, three cases will be considered:

- “ideal” case of monotonic decrease of P/P_0 ;
- monotonic increase of P/P_0 ;
- non-monotonic behaviour.

4.2.1. Decrease of the permeability induced by a “tortuosity-based effect”

In theory the incorporation of impermeable particles which present good compatibility with the polymer matrix should favour the decrease of the permeability of gases and water vapour, mainly due to the increase of the tortuous path for the diffusing molecules. Such “ideal” cases were largely observed in data collected from literature as illustrated in figure 3. For instance, for the incorporation of impermeable various shape of nano- and micro-particles, spherical such as TiO_2 [Hu et al. (1997)] and SiO_2 particles [Zoppi et al. (2000), Patel et al. (2003), Patel et al. (2004), Vladimorov et al. (2006), Vassiliou et al. (2007), Zhu et al. (2007), Sadhegi et al. (2013), Sadhegi et al. (2011).], cylinder such as cellulose fibre [Azeredo et al. (2009), Chang et al. (2010)], cellulose nanocrystals [George et al. (2012)], cellulose

nanowhiskers [Saxena et al. (2009), Sanchez-Garcia et al. (2010), Bilbao-Sainz et al. (2011)], cellulose micro-fibres [Fendler et al. (2007)], wheat bran micro-fibres [Fama et al. (2009)] and platelet such as montmorillonites [Straewhecker et al. (2000), Chang et al. (2002), Xu et al. (2002), Choi et al. (2004), Chien et al. (2006), Yeh et al. (2006), Herrera et al. (2010), Katyar et al. (2010), Aloofetileh et al. (2013), Abdollahi et al. (2013)], rectorite silicate [Wang et al. (2005)], and mica silicate [Sanchez et al. (2010), cellulose nanocrystals [Fortunati et al. (2012)], waxy maize [Angellier et al. (2005)], boron nitride [Swain et al. (2013), Kisku et al. (2012)], silicon carbide [Kisku et al. (2014), Dash et al. (2013)] led to a decrease of the gases and vapours permeability. The amplitude of this decrease largely depends on the particle shape and/or particle volume fraction used. In most cases, the authors attributed this effect to the nanostructure created by the incorporation of an impermeable particle (tortuosity effect) and/or in a lesser extend to the impact of particle addition onto the polymer matrix network, or to the modification of the availability of specific sorption sites for the sorption of the diffusing molecule.

Tortuosity effect. Tortuosity effect could be related to the in-situ size aspect ratio of the particle: high size aspect ratio favouring a more tortuous pathway. For example, Gatos et al. [Gatos et al. (20007)] created nanocomposites via melt processing using two different sizes of particles, octadecylamine modified montmorillonites with a size aspect ratio of 100 and synthetic fluorohectorite with size aspect ratio of 200 (measured by transmission electronic microscopy). Both particles were well exfoliated into the hydrogenated acrylonitrile butadiene rubber polymer matrix. The higher decrease of oxygen permeability was achieved using the fluorohectorite composites and it could be related to its highest aspect ratio. It is obvious that, size aspect ratio of a sphere is lower than that of a cylinder which is, in

turn, usually, lower than that of platelets leading to more tortuous pathway in nanoplatelets-based nanocomposites, as can be seen in figure 6.

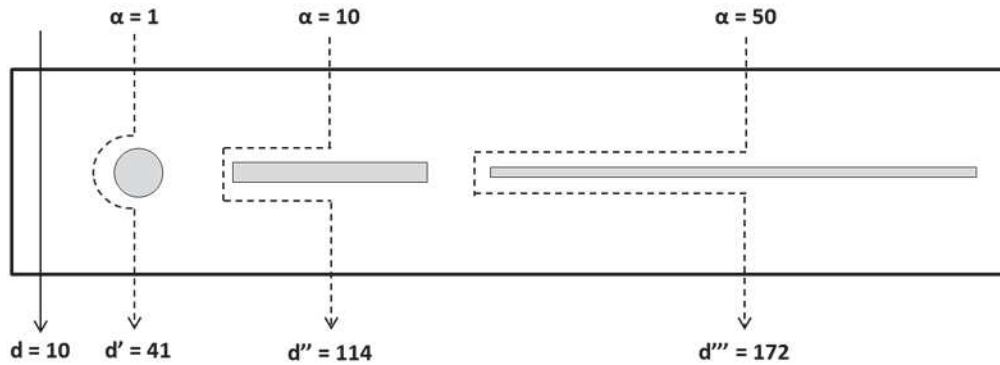


Figure 6: Representation of the tortuous path according to the particle shape and aspect ratio ($\alpha=1$ for spherical particles, $\alpha=10$ for cylindrical particles and $\alpha=100$ for platelets). The calculation of mean aspect ratio was done based on the experimental observations of the size of the in-situ particles made from the authors quoted in table 2 and table 3

The in-situ size aspect ratio, i.e the aspect ratio of the particles ones embedded in the polymer matrix after processing, in turn, strongly depends on the particles **dispersion state**. For instance, in platelets-based systems, different state of dispersion have been identified; exfoliated, intercalated, both intercalated and exfoliated, and tactoid structures. Sanchez et al. [Sanchez et al. (2007)] have demonstrated that the decrease of oxygen permeability was higher in PHBV-PCL nanocomposites displaying exfoliated structure. Koh et al. [Koh et al. (2008)] obtained the same results in their study comparing the effect of three different montmorillonites organo-modifications in PLA. They observed that the highest decrease of the oxygen and carbon dioxide permeability was obtained for the exfoliated structure. Sun et al. [Sun et al. (2008)] also observed that a higher degree of particle exfoliation lead to higher decrease of oxygen permeability in α -zirconium phosphate/epoxy resin nanocomposites compare to samples where only intercalation or mix of intercalation/exfoliation was achieved. In intercalated structures, the platelets

remained in stacks; therefore the apparent size aspect ratio (length to thickness) is much lower than that of the single platelet layer. The structure achieved is thus less tortuous than in case of a full-exfoliated structure.

Complete exfoliation or dispersion of the particles in the polymer matrix was really complicated to achieve and was strongly related to the **processing conditions**. The main elaboration techniques used in the papers collected in this work were solution blending and melt processing. Takahashi et al. (2006) pointed out that the final structure of SiO₂/poly(ether-imide) depend on the processing technique by comparing the structures according to the process, melt-processing and solution casting. They showed that in the case of the melt-processing the particles were better dispersed than in solution casting process due to the higher shearing forces which caused the stretching of the polymer chain and then favoured the dispersion of the nanoparticles between them. Hence in melt processing, the shear forces encountered could highly influenced the dispersion state as proved by many authors such as for example Monsivais-Barron et al. (2013) who pointed out that the barrier properties of montmorillonites/high density polyethylene was impacted by the shear rates during extrusion. In solution blending complete exfoliation and dispersion was dependant to the couple particle/polymer matrix in order to reach the better matching between the particles and the polymer matrix [Cornelius et al. (2002)] and to avoid the formation of "interfacial void" at the interface particles/polymer matrix [Chung et al. (2007)]. In both cases, incomplete dispersion, either by melt-processing [Bharadwaj et al. (2002), Balachadrin et al. (2010), Meera et al. (2012)], or by solution casting [Rhim et al. (2009), Kumar et al. (2010), Kasirga et al. (2012)] is usually achieved such as in the study of Luecha et al. Luecha et al. (2010) who showed that

either solution casting or blown extrusion lead to coexistence of intercalated and exfoliated structures in montmorillonites /corn zein matrix.

Dispersion state is more difficult to achieve, when the filler content increase due to, agglomeration phenomena as evidenced by Rhim et al. (2011) Bharadwaj et al. (2002), Picard et al. (2007) in agar/Montmorillonite, in polyester/montmorillonite and in polyamide/montmorillonite nanocomposites. In the same line, Chang et al. (2001) demonstrated that oxygen permeability was highly dependent on the filler volume fraction in organomodified montmorillonites/polyimide nanocomposites and exhibited non-linear dependency between P/P_0 and particle volume fraction with a less decrease of the ratio P/P_0 at high clay content due to, according to the authors, clay aggregation. From figure 3c, it was highlighted that a lot of curve representing the decrease of the ratio P/P_0 as function of the particle volume fraction exhibited this breaking in the decrease of the curve which lead to constant P/P_0 value at higher particle volume fraction. Even for chemical modified particles, agglomeration still could occur at high loading as evidenced by Zhu et al (2007) with modified SiO_2 particles in poly(vinyl chloride) matrix.

Some techniques would tend to be more effective to gain a good dispersion than solution and melt processing. As exposed previously, spherical and platelet nanoparticles can be synthesized during the processing of the nanocomposites itself (sol-gel or template synthesis) even if for platelets this process was very unusual. It should favour the dispersion of the particle by the establishment of covalent bonding between polymer and particle. Hu et al (1997) in-situ processed TiO_2 particles and Zoppi et al. (2000) SiO_2 particles in a poly(amide) matrix via sol gel method and obtained a well-dispersion of particles. In-situ polymerization would be another

solution to reach complete exfoliation [Messersmith et al. (1995), Ke et al. (2005), Herrera et al. (2010)]. Nevertheless in some cases complete exfoliation was not reached even with this processing technique and there still remained presence of small agglomerates, as shown by Gain et al. (2004) in poly(ϵ -caprolactone) polymer matrix in situ polymerized.

Aside the elaboration technique, another strategy to enhance the dispersion state is the improvement of particles/polymer matrix interaction through the use of **chemical modification or compatibilizer addition**.

Another way to achieve good adhesion between the particles and the polymer matrix is to chemically modify the surface of the spherical [Patel et al. (2003), Patel et al. (2004)], and platelet particles [Fortunati et al. (2012), Choi et al. (2011), Zhang et al. (2012)]. Rhim et al. (2009) showed that the use of montmorillonite without chemical modification lead to an increase of the permeability if compared to the permeability of the neat poly(L-lactide); and when the surface of the particles were organically modified, the permeability of the composite decreased. Aside particle surface modifications, the use of a compatibilizer could improve the dispersion and the adhesion between the particles and the polymer matrix [Osman et al. (2005), Jacquelot et al. (2006), Lee et al. (2005), Horst et al. (2007)].

The **orientation** of the particles also led to the modulation of the permeability; well-oriented particles perpendicular to the permeation flux have more impact on the decrease of the permeability than disoriented particles as regard the tortuosity effect. This feature is of value for cylinder and platelets only and of course, for particles with high size aspect ratio. Importance of the particle orientation was

experimentally and theoretically (with the use of predictive modelling of the permeability) demonstrated by Dunkerley et al (2013) in polystyrene/montmorillonites nanocomposites. The orientation of the particles could be related to the process of the composites, Messersmith et al (2005) showed that the montmorillonites adopted a planar orientation in the poly(ϵ -caprolactone) polymer matrix after in-situ-polymerization and solution casting processing. Besides Sanchez et al (2007) demonstrated that the orientation of montmorillonites in PHBV-PCL polymer matrix adopted different orientation after melt-processing and compression moulding. And Osman et al (2007) highlighted that the incorporation of montmorillonite in polypropylene polymer matrix through melt-processing and compression moulding could lead to partial orientation of the particles. Thus the orientation of the particles seemed to be highly dependent from the composite preparation techniques but nevertheless difficult to master.

Modification of the polymer matrix. Addition of the particle itself could modify the properties of the polymer which thus could contribute to the decrease in P/P0 ratio. This was many related to increase in crystallinity or in free volume in the polymer when used in nanocomposites. Effect on free volume was reported by Sadhegi et al. (2013) polycaprolactone based polyurethane-silica nanocomposites mainly due without doubts to the preparation technique of the nanocomposites via sol-gel method which lead to a reduction of the polymer chain mobility in the amorphous phase.

Impact on cristallinity was reported by Vladimorov et al. (2006) and Vassiliou et al. (2007) for spherical particles, by Fendler et al. (2007) and Fama et al. (2009) for cylinder particles and by Sanchez et al. (2007) and Gashemi et al. (2012) for platelets

particles. Particles can act as nucleating agent and lead to an increase of the crystallinity which decrease the permeability of the polymer in the nanocomposites. Indeed cristallinity acts as an obstacle to migrant diffusion.

Decrease of polymer sorption site. Initially the particles were modified to reach better adhesion and dispersion in the polymer matrix. The secondary effect of this modification is lesser available sites for the sorption especially for highly interactive water molecules due to specific interactions between the particle and the matrix for example montmorillonites and wheat gluten [Tunc et al. (2006)] and montmorillonites and soy protein [Lee et al. (2010)]. Slavutsky et al. [Slavutsky et al. (2014)] went further on the explanation of the modulation of the permeability, making the assumption that the interactions between montmorillonites could hinder the passage of water molecules through the composite film.

4.2.2. Increase of the permeability influenced by imperfect structuring of the composites

No significant modification of permeability or increase of the relative permeability P/P_0 in nanocomposites were related to (1) lack of efficient tortuosity, (2) occurrence of structural defects in the material such as particles agglomeration, (3) significant modification of the polymer matrix and (4) increasing migrant sorption induced by particles (case of water vapour for example).

Lack of tortuosity. In term of modulation of the permeability Tunc et al. (2007) showed that the presence of stacked silicates layers in wheat gluten polymer matrix did not lead to a tortuosity effect sufficient enough to disturb the diffusion pathway of a small molecule as O_2 and the permeability stayed more or less constant. In the

same article, the authors have demonstrated that for bigger molecule such as aroma compounds the same nanostructure display efficient tortuosity to decrease the diffusion of that molecule. This highlighted that the nature, molecular weight and/or steric hindrance of the migrant would be important in addition to that of the particle. Besides Dogan et al. (2007) also noticed no significant change of the water vapour permeability with the addition of microcrystalline cellulose particles, in the range from 0.5 to 3 μm , hydroxyl propyl methyl cellulose polymer matrix. Although they expected a decrease of the diffusion coefficient in the composites, they assumed that this trend could be explained by higher water affinity of the materials due to the presence of the particles which could lead to enhance water sorption which could counteract the decrease of the diffusion; this outcome will be discussed in the following.

Structural defects. Agglomeration phenomena could be considered as structural defects which play a major role in the increase of P/P_0 . In spherical-based composites [Cornelius et al. (2002)] and cylinders-based composites [Bilbao-Sainz et al. (2011)] highlighted the presence of both nanosized and microsized particles representing the particle agglomerates. These agglomeration phenomena could be related to a bad dispersion of the particle which is mainly ascribed to (1) inefficiency of the elaboration technique and/or (2) mismatching of the particle polarity compare to that of the polymer.

For example, insufficient shearing forces during the melt processing could cause agglomeration of particles. During casting, sol-gel method and in-situ polymerisation, coalescence of the particles during drying of the solution could appear through insufficient particle/particle interactions ("bad compatibility"). This last phenomenon

could be triggered by chemical modification of the surface of the particles when the effect of the chemical modification was wrongly anticipated [Zhu et al. (2007)]. Due to agglomeration phenomena, void spaces could be created at the interface particle/polymer matrix and led to the formation of a narrow gap around the agglomerates [Rafiq et al. (2012)].

Interphase at the interface particles/polymer matrix could be created due to weak interfacial interaction between the particles and the polymer matrix. Interphase, defined as a third component in the composite materials was evidenced in spherical-based composites by Matteucci et al. (2008) and Moghadam et al. (2011), and in cylinder-based composites by [Pradhan et al. (2012)]. It could be assimilated as a "third compartment" with its own properties. Interphase could participate to the overall mass transport properties and strongly disturb the permeability of the composite. For instance, Liang et al. (2012) in platelet-based composites noticed that because of poor adhesion between hydrophobic poly(ethersulfone) and hydrophilic particles, huge transfer could happen at the interphase particles/polymer matrix.

Modification of the polymer matrix. Changes of the polymer matrix properties following the incorporation of particles could lead to an increase of the permeability. The incorporation of particles could be linked to the disruption of polymer chain packing which caused an increase of polymer matrix free volume in spherical-based composites [Matteucci et al. (2008), Dougnac et al. (2010), Moghadam et al. (2011), Romero et al. (2011)] and in cylinder-based composites [Murali et al. (2010)]. Increase of free volume was also observed by Mittal et al (2007) following the use of compatibilizer due to bad compatibility between the compatibilizer and the surface

treated particles. This led to a lesser decrease of the permeability than expected. In the same trend, Zhong et al. (2007) observed an increase of the permeability due to the use of a compatibilizer that modulate the space between the polymeric chains and thus an increase of the polymer matrix free volume.

Besides the addition of particles in a polymer matrix could lead to a decrease of the crystallinity because particles could play a role in hindering the crystallisation process [Dougnac et al. (2010)].

Interaction migrant/composite constituents. Another phenomenon responsible for the increase of permeability was the interaction between the molecular penetrant and the composites constituents. In some composites, interaction between the molecular migrant such as water vapour should be considered due to the hygroscopic nature of the particles [Bracho et al. (2012), Dougnac et al. (2010), Dogan et al. (2007)]. Moreover interactions between the organo-modification of the particles and the molecular penetrant such as O₂ should be taken into considerations [Chang et al. (2002), Iwata et al. (2002)] which are also responsible of an increase of the permeability.

4.2.3. Non-monotonic variation of P/P_0

The gases and water vapours permeability did not always monotonically increase or decrease but could follow more complicated tendencies. For example, in the work of Sanchez et al. (2009) on platelets-based composites, the permeability first decrease due to, according to the authors, the tortuosity effect but from 5% volume fraction of particle the permeability began to increase due to the formation

of agglomerates as supposed by the authors. In cylinders-based nanocomposites [Dogan et al. (2007), Saxena et al. (2009), Paralikar et al. (2008)] and microcomposites [Sanchez et al. (2010)], the same trend was observed with the formation of particle agglomerates at high particle volume fraction (generally > 10 vol%). This agglomeration phenomenon led in nanocomposites [Ismail et al. (2011)] to the formation of "interface voids" at the interface particle/polymer matrix and to the formation of a preferential pathway for the migration of molecular penetrant. The formation of void space at the interface particles/polymer matrix could also appear due to bad compatibility and poor adhesion between the particle and polymeric matrix and also lead to an increase of the permeability from a given particle fraction [Zoppi et al. (2000)]. Aside agglomeration that could reverse the trend of variations of P/P_0 , some extensive cracking of the composite film could occur and lead to a complete loss of barrier properties [Chaiko et al. (2005)], which was attributed by the authors to excessive particle agglomeration at high particle fraction.

Another observed but more rarely evolution of the permeability was first an increase of the water vapour permeability caused by enhanced affinity between molecular penetrant such as water vapour and composite components due to the hydrophilic nature of the components of the cellulose nanocrystals/poly(ϵ -caprolactone) composites and, second, a decrease of the permeability induced by the tortuosity effect [Follain et al. (2013)].

4.2.4. Explanation of the evolution of the permeability in line with the evolution of solubility and diffusivity coefficient

Face to the complex evolution of P/P_0 as a function of filler content, the authors tried to find an explanation and to do that, broke down the permeability into diffusivity and solubility through the well-known relation $P=D \times S$. They determined in addition to the permeability, the diffusivity and solubility coefficients in the composite under study.

Permeability is governed by the evolution of both the diffusivity coefficient and the solubility coefficient. In nanocomposites, when P decreases, diffusivity and solubility should do the same because of the formation of a more tortuous path (influence on D) and, the diminution of specific area for the sorption of gases or vapours and of the total amount of free volume which hindered the dissolution of gas molecules and numerous interactions between the particle and the matrix which decrease sorption sites [Cornelius et al. (2002)] (influence on S). For instance [Muller et al. (2009)] observed a decrease of the solubility due to interaction between the fibres and the hydrophilic sites of starch polymer chain which substituted the starch - water vapour interactions that predominates in films without fibres. Decrease of both D and S coefficient is the ideal case. Anyhow this ideal case was not always observed and there was rather a competition between an increase of the solubility and a decrease of the diffusivity.

Indeed, solubility remained sometimes at the same value in the composite compare to that of the neat matrix as observed by [Kim et al. (2001), Cong et al. (2007)] in silica particles/poly(amide-6-b-ethylene oxide) and silica particle/brominated poly(2,6-diphenyl-1,4-phenylene oxide) nanocomposites, or even increase with the

addition of particles. As evidenced by Sadhegi et al. (2009) in silica particles/polybenzimidazole composites for carbon dioxide molecular penetrant, the solubility could increase because of interactions of the molecular penetrant with functional groups of the particles. This well evidenced that if the particles could be considered as impermeable ($D=0$), it is not true for their solubility. Increase of S could also be related to the progressive uncovering of active sorption sites in the polymer matrix as a consequence of particle addition and to the creation of specific sites at the interface particle/polymer matrix that favour the sorption of molecular penetrant [Sadhegi et al., Suzuki et al.(2005)].

For the diffusivity coefficient, the expected behaviour is a decrease due to the restriction of the motion of molecular penetrant and the creation of a more tortuous path caused by the presence of the particles [Sadhegi et al. (2009), Suzuki et al.(2005)]. Kim et al. (2001) showed that, in poly(amide-6-b-ethylene oxide), in spite of the presence of agglomerated particles, the tortuosity effect still led to a decrease of the diffusivity coefficient. Besides an increase in the crystallinity of the composite with the incorporation of particles could act as an obstacle for the diffusion of the molecular penetrant and then led to a decrease of the diffusivity coefficient. The opposite phenomenon could also happen. Sadhegi et al. (2008), seeking to understand the increase of the permeability in polyvinyl acetate with the addition of particles, made the assumption that the diffusivity coefficient could increase either due to a reduction of the packing density of the composite which provide further open structures for the diffusion of CO_2 or due to a reduction of the impermeable crystalline region in composites which could boost the diffusion of CO_2 . The latter effect was also demonstrated by Kono et al (2007) and Ahn et al. (2008). The diffusivity could also remain constant with the addition of impermeable particles

[Muller et al. (2009)]. Due to bad adhesion or compatibility particles/polymer matrix, the creation of interconnected cavities/channels could be formed at the interface particles/polymer matrix and thus led to an increase of the diffusivity coefficient [Suzuki et al. (2005), Kim (2001), Cong et al. (2007)].

In summary, although a decrease of the relative permeability P/P_0 should be observed with the addition of impermeable particles due to a decrease of the diffusivity and solubility coefficient whatever the particle nature or shape and the kind of molecular migrant, but sometimes an increase of P/P_0 occurred. This evolution could be generally explained by an increase of S while D decrease in accordance with tortuosity principle, even if both S and D increase could be observed in some cases. Non-monotonic changes of P/P_0 , in peculiar, decrease of P/P_0 following by an increase for higher particle volume fraction, could be ascribed to an increase of S that could, from a threshold value of particle volume fraction, counteracts the decrease of D (and vice et versa).

5. Conclusion

The recently-measured values of O_2 , CO_2 and H_2O permeability in agro-, bio- and synthetic-based composites have been comprehensively reviewed with emphases on the link between their microstructures and their barrier performance. From this analysis it concluded that the shape of the particle had a great influence on the modulation of the relative permeability (P/P_0); while spherical and cylindrical particles lead to both increase and decrease of P/P_0 , the platelet particles mainly lead to a decrease P/P_0 . In any event, the addition of impermeable particles in a polymer matrix is expected to decrease the permeability by both a decrease of the

solubility and diffusivity coefficient due to the diminution of specific area for the sorption of gases and vapours and the formation of a more tortuous path respectively. To explain the deviation of the permeability, structural aspects, related to both the particle nature, size and shape and the composite processing techniques, have been discussed. Good dispersion or exfoliation of the particles should lead to a tortuosity effect, responsible of the decrease of the permeability. However in some cases, the particles tended to agglomerate upset that tortuosity effect by the creation of specific channel for a faster permeation of the molecular penetrant. Another reason to an unexpected behaviour of the permeability is changes in the polymer matrix behaviour which came along with for example an increase of the diffusivity coefficient due to a decrease of the polymer chain packing density. One additional phenomena which favour the increase of the permeability with the incorporation of particles is the creation of specific sites for the sorption of the molecular penetrant. To complete this study, it should be pointed out that not only the particle shape played a role on the modulation of the permeability but also the composites processing techniques which will results in various composite structures exhibiting different impact on the mass transfer properties of gases and vapours.

Table 1: Characteristics of the spherical particles-based composites of the publication quoted in this article; information about the nature, the size and the modification of the particles, and overview of the composites processing and applications

Publication	Particle	Matrix	Size before/ after process	Chemical modification	Process	Film thickness	Molecular penetrant	Application
Ahn et al. (2008)	Silica particle	Polysulfone (PSF)	11.1-13.3 /	Trimethylsilyl	Solution / Casting	60 - 80 μm	Oxygen/ Carbon dioxide	Membrane application
Bracho et al. (2012)	Silica particle	Poly(propylene)	20 and 100nm /	Tetraethoxysilane	Melt mixing / Thermopressing	1000 μm	Water vapour	General engineering application
				Trimethylchlorosilane Dimethyloctylchlorosilane				
Cong et al. (2007)	Silica particle	Brominated Poly(2,6-diphenyl-1,4-phenylene oxide)	10nm /	Unmodified	Sol-gel / Solution casting	50 - 90 μm	Carbon dioxide	Membrane application
				Trimethylsilyl Triphenylsilyl				
Cornelius et al. (2002)	Silica particle	Poly(amide)		Tetraethoxysilane	Sol gel / Solution casting	80 μm	Oxygen / Carbon dioxide	Membrane application
				Phenyltrimethoxylane Methyltrimethoxysilane				
Cornelius et al. (2002)	Silica particle	Poly(amide)		Tetramethoxysilane	Sol gel / Solution casting	80 μm	Oxygen / Carbon dioxide	Membrane application
				Phenyltrimethoxylane Methyltrimethoxysilane				
Dougnac et al. (2010)	Silica particle	Poly(propylene)	10-150nm /	Tetraethoxysilane	Sol gel / Melt mixing / Pressing	5000 μm	Oxygen	General engineering application
Hu et al. (1997)	Titanium dioxide particle	Poly(amide imide)		Unmodified	Sol-gel / Solution casting	15 -17 μm	Oxygen / Carbon dioxide	Membrane application
Iwata et al. (2002)	Silica particle	Poly(acrilonitrile)	/ 56.7nm	Tetraethoxysilane	Sol gel / Solution casting	60 - 110 μm	Oxygen	Membrane application
Joly et al. (1999)	Silica particle	Poly(amide Poly(1,4-oxdiphenylene pyromellitimide)	/ 50-150nm	Tetramethoxysilane	Solution / Casting	25 - 30 μm	Oxygen / Carbon dioxide	Membrane application
Kim et al. (2001)	Silica particle	Poly(amide-6-b-ethylene oxide)	/ 33 and 517nm	Tetraethoxysilane	Sol-gel / Solution casting		Oxygen / Carbondioxide	Membrane application
Kong et al. (2002)	Titanium dioxide particle	Poly(amide)	/ 10nm	Unmodified	Sol-gel / Solution casting		Oxygen	Membrane application
Kono et al. (2007)	Silica particle	Poly(1-chloro-2-phenylacetylene)	13 nm /	Trimethylsilyl	Solution / Casting	80 - 120 μm	Oxygen / Carbon dioxide	Membrane application
		Poly[1-phenyl-2-(4-trimethylsilyl)phenylacetylene] Poly[1-(trimethylsilyl)-1-propyne]						

Publication	Particle	Matrix	Size before/ after process	Chemical modification	Process	Film thickness	Molecular penetrant	Application
Mateucci et al. (2008)	Titanium dioxide particle	1,2 Poly(butadiene)	< 50nm / 9(+/-)4nm	Unmodified	Solution / Casting	180 - 220 μ m	Carbon dioxide	Membrane application
Moghadam et al. (2011)	Titanium dioxide particle	Poly(imide)	3 nm /	Unmodified	Solution / Casting	80 - 120 μ m	Oxygen / Carbon dioxide	Membrane application
Patel et al. (2003)	Silica particle	Poly(ethylene glycol)	12nm /	Methacrylate	Solution / Casting	40 - 200 μ m	Oxygen / Carbon dioxide	Membrane application
Patel et al. (2004)	Silica particle	Crosslinked Poly(ethylene glycol)	12nm /	Methacrylate	Solution / Casting	40 - 200 μ m	Carbon dioxide	Membrane application
Rafiq et al. (2012)	Silica particle	Poly(sulfone) Poly(imide)	/ <100nm	Tetraethoxysilane 3-amino- propyltrimethoxysilane	Solution / Casting	150 μ m	Carbon dioxide	Membrane application
Romero et al. (2011)	Silica particle	Poly(etherimide)		Tetraethoxysilane 3-amino- propyltrimethoxysilane	Solution / Casting	25 - 70 μ m	Oxygen / Carbon dioxide	Membrane application
Sadhegi et al. (2008)	Silica particle	Poly(ethylene vinyl acetate)		Tetraethoxysilane	Sol-gel / Solution casting		Oxygen / Carbon dioxide	Membrane application
Sadeghi et al. (2009)	Silica particle	Poly(benzimidazole)		Tetraethoxysilane 3-glycidyl/oxi- propyltrimethoxysilane	Sol-gel / Solution casting	40 μ m	Carbon dioxide	Membrane application
Sadeghi et al. (2011)	Silica particle	Poly(ether-based polyurethane)		Tetraethoxysilane 3-glycidyl/oxi- propyltrimethoxysilane	Sol-gel / Solution casting	100 μ m	Oxygen / Carbon dioxide	Membrane application
Sadeghi et al. (2013)	Silica particle	Polycaprolactone-based polyurethane		Tetraethoxysilane 3-glycidyl/oxi- propyltrimethoxysilane	Sol-gel / Solution casting	100 μ m	Oxygen / Carbon dioxide	Membrane application
Semsarzadeh et al. (2013)	Silica particle	Polyurethane		Tetraethoxysilane / Polyvinyl alcohol	Sol-gel / Solution casting	120 μ m	Oxygen / Carbon dioxide	Membrane application
Suzuki et al. (2005)	Silica particle	Poly(imide)		Tetraethoxysilane	Sol-gel / Solution casting		Oxygen / Carbon dioxide	Membrane application
Takahashi et al. (2006)	Silica particle	Poly(etherimide)	18-26nm / 11-13nm / 25-31nm /	Methyl Trimethylsilyl Polydimethylsiloxane	Solution / Casting and Melt processing / Compression moulding	50 - 70 μ m / 200 - 300 μ m	Oxygen / Carbon dioxide	Membrane application

Publication	Particle	Matrix	Size before/ after process	Chemical modification	Process	Film thickness	Molecular penetrant	Application
Takahashi et al. (2006)	Silica particle	Poly(etherimide)		3-amino-propyltrimethoxysilane	Solution Casting and Melt processing / Compression moulding	30 - 50 μm / 200 μm	Oxygen / Carbon dioxide	Membrane application
Ulutun et al. (1996)	Silica particle	Poly(vinyl chlorure)		Unmodified	Melt-mixing / Thermopressing	300 - 500 μm	Water vapour	Membrane application
Vassilou et al. (2007)	Silica particle	Isostatic poly(propylene)	12nm /	Unmodified	Melt mixing / Thermopressing	45 - 55 μm	Oxygen	Membrane application
Vladimirov et al. (2006)	Silica particle	Isostatic poly(propylene)	12nm /	Unmodified	Melt mixing / Thermopressing	45 - 55 μm	Oxygen	Membrane application
Yu et al. (2011)	Silica particle	Poly(sulfone)	— / 16nm / 12nm	Hydroxyl Trimethylsilyl	Solution / Casting	50 nm	Carbon dioxide	Membrane application
Zhou et al. (2009)	Titanium dioxide particle	Whey protein	< 20nm /	Unmodified	Solution / Casting	50 μm	Water vapour	Packaging application
Zhu et al. (2007)	Silica particle	Poly(vinyl chlorure)	25nm /	3-(Trimethoxysilyl)-propyl methacrylate	Melt mixing / Compression moulding	450 - 550 μm	Oxygen / Water vapour	General engineering application
Zoppi et al. (2000)	Silica particle	Poly(ethylene oxide-b-amide-6)		Tetraethoxysilane	Sol-gel / Solution casting		Oxygen / Carbon dioxide	Membrane application
Zoppi et al. (2000)	Titanium dioxide particle	Poly(ethylene oxide-b-amide-6)		Tetraethoxysilane	Sol-gel / Solution casting		Oxygen / Carbon dioxide	Membrane application

Table 2: Characteristics of the cylindrical particles-based composites of the publication quoted in this article; information about the nature, the size and the modification of the particles, and overview of the composites processing and applications

Publication	Particle	Matrix	Size before/after process	Chemical modification	Process	Film thickness	Molecular migrant	Application
Azeredo et al. (2009)	Cellulose fibre	Mango puree	Length 82.6 ± 4.3 nm Diameter 7.2 ± 0.3 nm	Unmodified	Solution / Casting	29 μ m	Water vapour	Packaging application
Azeredo et al. (2010)	Cellulose fibre	Chitosan	Length 98.1 ± 4.7 nm Diameter 8.0 ± 3.4 nm	Unmodified	Solution / Casting	29 μ m	Water vapour	Packaging application
Bessadok et al. (2009)	Alpha fibre	Unsaturated polyester resin	Average diameter 13 μ m /	Unmodified Maleic anhydride Acrylic acid Styrene	Melt mixing / Thermopressing	400 - 500 μ m	Water vapour	General engineering application
Bilbao-Sainz et al. (2011)	Cellulose fibril Eucalyptus sulphite wood pulp Oxidized cellulose fibril Softwood cellulose fibre Cellulose whisker Microcrystalline cellulose	Hydroxypropyl methyl cellulose	Diameter 35 ± 9 nm Diameter 67 ± 34 nm Length 301 ± 67 nm Diameter 28 ± 9 nm	Unmodified TEMPO sodium bromide Unmodified	Solution / Casting	1150 μ m	Water vapour	Packaging application
Chang et al. (2010)	Cellulose particle	Wheat starch	Diameter $50 - 100$ nm /	Unmodified	Solution / Casting		Water vapour	Packaging application
Cong et al. (2007)	Carbon nanotube	Brominated poly(2,6-diphenyl-1,4-phenylene oxide)	Length $0.1 - 1$ μ m Diameter $0.8 - 1.2$ nm Length $0.5 - 50$ μ m Diameter $40 - 60$ nm	Unmodified	Solution / Casting	50 - 80 μ m	Carbon dioxide	Membrane application
Dias et al. (2011)	Eucalyptus cellulose fibre	Rice flour	Length $1 - 1.3$ nm /	Unmodified	Solution / Casting		Water vapour	General engineering application
Dogan et al. (2007)	Microcrystalline cellulose	Hydroxypropyl methyl cellulose	Average size $0.5 - 3$ μ m	Unmodified	Solution / Casting		Water vapour	Packaging application
Espino Perez et al. (2013)	Cellulose whisker	Poly(lactic acid)	Length 243.9 ± 48.5 nm Diameter 9.4 ± 2.5 nm	n-octadecyl isocyanate	Solution / Casting	40 - 120 μ m	Oxygen / Water vapour	General engineering application
Fama et al. (2009)	Wheat bran fibre	Cassava starch	Length $75 - 125$ μ m	Unmodified	Solution / Casting	30 - 50 μ m	Water vapour	Packaging application
Fendler et al. (2007)	Cellulose fibre	High Density Polyethylene	Length 60 μ m Width 20 μ m	Maleic anhydride grafted polyethylene (PE-MA)	Melt mixing / Compression moulding	100 μ m	Oxygen	Packaging application
Follain et al. (2013)	Cellulose nanocrystal	Poly(ϵ -caprolactone)		Long-chain isocyanate	Solution / Casting	300 - 400 μ m	Water vapour	General engineering application

Publication	Particle	Matrix	Size before/after process	Chemical modification	Process	Film thickness	Molecular migrant	Application
Georges et al. (2012)	Bacterial cellulose nanocrystal	Food gelatin	/Length 290 ± 130 nm Diameter 20 ± 5 nm	Unmodified	Solution / Casting		Water vapour	Packaging application
Ismail et al. (2011)	Carbon nanotube	Poly(ethersulfone)	Average inner and outer diameter 3.5 – 15 nm	3-aminopropyl-triethoxysilane (APTES)	Solution / Casting		Oxygen / Carbon dioxide	Membrane application
Kim et al. (2006)	Carbon nanotube	Poly(imide siloxane)	Diameter 1.4 ± 0.2 nm	Acid treatment	Solution / Casting		Oxygen / Carbon dioxide	Membrane application
Kim et al. (2007)	Carbon nanotube	Poly(sulfone)	Average diameter 1.2 nm	Wet-oxidation Acid treatment	Solution / Casting		Oxygen / Carbon dioxide	Membrane application
Mondal et al. (2008)	Carbon nanotube	Poly(urethane)	Diameter 2 – 15 nm Length 1 – 10 µm	Aniline solution diluted in DMF	Solution / Casting	90 µm	Water vapour	General engineering application
Muller et al. (2009)	Cellulose fibre	Starch	Length 1.2 mm Diameter 0.1 mm	Unmodified	Solution / Casting	100 - 150 µm	Water vapour	Packaging application
Murali et al. (2010)	Carbon nanotube	Poly(ether-block-amide)	Length 5 - 15 µm Diameter 10 - 20 nm	Unmodified	Solution / Casting	15 - 20 µm	Oxygen / Carbon dioxide	Membrane application
Pantani et al. (2013)	ZnO particle	Poly(lactic acid)	Length around 100 nm Diameter 15 - 30 nm	Unmodified	Melt compounding / Compression moulding	150 µm	Water vapour	Packaging application
Paralikar et al. (2008)	Cellulose nanocrystal	Poly(vinyl alcohol) Crosslinked Poly(acrylic acid)	Length 50 - 200 nm Diameter 5 - 10 nm	Unmodified Free acid	Solution / Casting	10 µm	Water vapour	Membrane application
Pradhan et al. (2012)	Carbon nanotube	Poly(acrilonitrile)	Length 0.1 - 10 µm Diameter 10 - 15 nm	Sulphuric and nitric acid	Free emulsion polymerization / Thermopressing	500 µm	Oxygen	General engineering application
Sanchez-Garcia et al. (2008)	Cellulose fibre	Poly(lactic acid) Poly(hydroxybutyrate-co-valerate) Poly(caprolactone)	Average length 60 µm Average width 20 µm	Sodium hypochloride (NaClO) 2,2,6,6-tetramethyl-1-piperidinyloxy radical (TEMPO) Sodium bromide (NaBr)	Solution / Casting	100 µm	Water vapour	Packaging application
Sanchez-Garcia et al. (2010)	Carbon nanofibre Carbon nanotube	Polyhydroxybutyrate-co-valerate Poly(caprolactone)	Length 1 - 10 µm Diameter 5 - 20 nm Length 50 - 100 µm Diameter 70 - 200 nm	Unmodified Unmodified	Solution / Casting	100 µm	Oxygen	Packaging application
Sanchez-Garcia et al. (2010)	Cellulose whisker	Poly(Lactic acid)	Length 60 - 160 nm Thickness 10 - 20 nm	Unmodified	Solution casting		Oxygen / Water vapour	Packaging application
Sanchez-Garcia et al. (2010)	Cellulose whisker Cellulose fibre	Hybrid Carrageenan	Length 25 - 50 nm Diameter 5 nm Length 50 - 150 µm Diameter 10 - 30 µm	Unmodified Unmodified	Solution / Casting	50 µm	Water vapour	Packaging application

Publication	Particle	Matrix	Size before/after process	Chemical modification	Process	Film thickness	Molecular migrant	Application
Saxena et al. (2009)	Cellulosic whisker	Oat spelt xylan	Length 150 - 200 nm	Sulphuric acid	Solution / Casting	89 - 93 µm	Water vapour	General engineering application
	Softwood fibre		Width < 20 nm					
Sreekumar et al. (2011)	Sisal fiber	Isophthalic polyester resin	Length 30 mm	Unmodified	Melt mixing / Compression moulding		Water vapour	General engineering application
Yu et al. (2009)	ZnO-carboxymethylcellulose sodium	Glycerol plasticized-pea starch	Length 30 – 40 nm	Unmodified	Solution / Casting		Water vapour	General engineering application

Table 3: Characteristics of the platelet particles-based composites of the publication quoted in this article; information about the nature, the size and the modification of the particles, and overview of the composites processing and applications

Publication	Particle	Matrix	Size before/ after process	Chemical modification	Process	Film thickness	Molecular penetrant	Application
Abdollahi et al. (2013)	Montmorillonite	Alginate	Average length: 300nm Average diameter: 40nm /	Unmodified	Solution / Casting		Water vapour	Packaging application
Alboofetieh et al. (2013)	Montmorillonite	Sodium alginate		Unmodified	Solution / Casting	40 - 60 µm	Water vapour	Packaging application
Alena et al. (2013)	Montmorillonite	Linear low density polyethylene Poly(chlorure vinyl)		Unmodified				
				Methyl bis-2- hydroxyethyl tallow ammonium Dimethyl, hydrogenated tallow, 2-ethylhexyl quaternary ammonium Methyl, dehydrogenated tallow ammonium	Extrusion / roll-pressing	100 µm	Oxygen / Carbon dioxide / Water vapour	Packaging application
Alexandre et al. (2009)	Montmorillonite	Poly(amide 12)	/ Thickness: 2-6nm	Methyl bis-2- hydroxyethyl tallow ammonium	Melt processing / Compression moulding	200 - 250µm	Water vapour	Membrane application
Ali et al. (2011)	Montmorillonite	Starch / Poly(vinyl alcohol)		Unmodified	Solution / Casting		Water vapour	Packaging application
Angelier et al. (2005)	Waxy maize starch nanocrystals	Natural rubber	Thickness: 6-8nm Length: 40-60nm Width: 15-30nm/ Aspect ratio 16	Unmodified	Solution / Casting	200 - 1000 µm	Oxygen / Water vapour	General engineering application
Bae et al. (2009)	Montmorillonite	Fish gelatin		Unmodified	Solution / Casting		Oxygen / Water vapour	Packaging application
Balanchandrin et al. (2010)	Montmorillonite	Nitrile rubber		Dimethyl dehydrogenated tallow ammonium	Melt processing / Compression moulding	2000 µm	Oxygen	General engineering application
Bharadwaj et al. (2002)	Montmorillonite	Polyester resin		Methyl bis-2- hydroxyethyl tallow ammonium chlorid	Melt processing / Compression moulding		Oxygen	General engineering application
Chaiko et al. (2005)	Montmorillonite	Paraffin wax	10-20nm /	1-hydroxydodecane-1,1-diphosphate ammonium salt	Melt processing	50 µm	Oxygen	General engineering application
Chang et al. (2001)	Montmorillonite	Poly(imide)		Dodecylamine ammonium salt Hexadecylamine ammonium salt	Solution / Casting	10 - 15 µm	Oxygen / Water vapour	General engineering application
				Methyl bis-2- hydroxyethyl tallow ammonium Hexadecylamine	Solution / Casting	10 - 15 µm	Oxygen	Packaging application
Chien et al. (2006)	Montmorillonite	Poly(vinyl acetate)	/ Aspect ratio 320	Dodecyltrimethyl ammonium bromide-montmorillonite	Soap free emulsion polymerization / Casting	150 µm	Water vapour	General engineering application

Publication	Particle	Matrix	Size before/ after process	Chemical modification	Process	Film thickness	Molecular penetrant	Application
Chivrac et al. (2010)	Montmorillonite	Wheat starch		Organo-modification	Melt processing / Compression moulding		Water vapour	Packaging application
Choi et al. (2004)	Montmorillonite	Poly(urethane)		Organofier UE400	Solution / Spin coating	30 - 50 μm	Oxygen	General engineering application
Choi et al. (2011)	Montmorillonite	Poly(propylene)		Dimethyl di(hydrogenated tallowalkyl) quaternary ammonium	Melt-compounding / Injection moulding	600 - 800 μm	Oxygen	Packaging application
Dash et al. (2013)	Silicon carbide	Starch	50nm /	Unmodified	Solution / Thermopressing	500 μm	Oxygen	Packaging application
Duan et al. (2013)	Montmorillonite	Poly(lactic acid)	Average thickness:1.6nm Average length:80nm	Methyl bis-2- hydroxyethyl tallow ammonium chlorid	Melt processing / Compression moulding	600 μm	Water vapour	Packaging application
Dunkerley et al. (2010)	Montmorillonite	Poly(styrene)		Dimethyl di(hydrogenated tallowalkyl) quaternary ammonium	Solution spraying	60 - 270 μm	Oxygen	Packaging application
Echeverria (2014)	Montmorillonite	Soy protein isolate		Unmodified	Solution / Casting	75 - 90 μm	Water vapour	Packaging application
Fashi et al. (2011)	Montmorillonite	Poly(amide 6)	Average particle size 8 μm /Aspect ratio 210	Organo-modification	Melt processing / Compression moulding	150 μm	Oxygen	Packaging application
Fortunati et al. (2012)	Cellulose nanocrystals	Poly(lactic acid)	Length:100-200nm Width: 5- 10nm /	Unmodified Acid phosphate ester of ethoxylated nonyphenol	Solution - Casting	150 - 250 μm	Oxygen / Water vapour	Packaging application
Gain et al. (2004)	Montmorillonite	Poly(ϵ -caprolactone)		Unmodified Methyl bis-2- hydroxyethyl tallow ammonium	Melt blending - In situ polymerization / Compression moulding	100 μm	Carbon dioxide	General engineering applications
Gatos et al. (2007)	Fluorohectorite	Hydrogenated acrylonitrile butadiene rubber	/ Aspect ratio 200	Synthetic fluorohectorite Synthetic fluorohectorite / Octadecylamine	Melt mixing / Thermopressing	1000 μm	Oxygen	General engineering application
	Montmorillonite		/ Aspect ratio 100	Quaternary ammonium salt / Quaternary ammonium salt / Octadecylamine				
Ghasemi et al. (2012)	Montmorillonite	Poly(ethylene terephthalate)		Methyl bis-2- hydroxyethyl tallow ammonium	Melt processing / Casting	25 - 90 μm	Oxygen	Packaging application
Guo et al. (2013)	Montmorillonite	Fish gelatin		Unmodified	Solution / Casting	300 μm	Water vapour	Packaging application
Herrera-Alonso et al. (2010)	Montmorillonite	Poly(n-butylacrylate)	/Average particle diameter 140nm	[2-(Acryloyloxyethyl)-trimethylammonium	Emulsion polymerization / Casting	180 - 240 μm	Oxygen / Carbon dioxide	Membrane application

Publication	Particle	Matrix	Size before/ after process	Chemical modification	Process	Film thickness	Molecular penetrant	Application
Herrera-Alonso et al. (2010)	Montmorillonite	Poly(n-butylacrylate)		[2-(Acryloyloxyethyl)-trimethylammonium	In-situ polymerization / Casting	180 - 240 μm	Oxygen / Carbon dioxide	Membrane application
Host et al. (2007)	Montmorillonite	Poly(propylene)		Quaternary ammonium salt	Melt-mixing / Injection moulding	140 - 200 μm	Oxygen	General engineering application
Hotta et al. (2004)	Montmorillonite	Linear low density polyethylene		Dimethylbis(hydrogenated tallow) ammonium Hexadecyltrimethylammonium bromide	Melt processing / Compression moulding	150 μm	Oxygen / Carbon dioxide	General engineering application
Huang et al. (2008)	Montmorillonite	Poly(imide)		Ammonium bromide 4,4'-oxydianiline Hexadecyltrimethylammonium bromide / 4,4'-oxydianiline	Solution / Casting / Thermal imidization	60 μm	Oxygen / Water vapour	Membrane application
Ito et al. (2010)	Montmorillonite	Poly(amide 6)		12-aminolauric acid ammonium salt	Extrusion / Compression moulding	200 μm	Oxygen	General engineering application
Jacquelot et al. (2005)	Montmorillonite	High and low density polyethylene		Dimethyl tallow benzyl ammonium	Melt processing / Compression moulding	150 μm	Oxygen / Carbon dioxide	General engineering application
Kasirga et al. (2012)	Montmorillonite	Chitosan	Mix nano- / micro- <100nm to 2μm	Unmodified	Solution / Casting		Oxygen / Water vapour	Packaging application
Katiyar et al. (2010)	Montmorillonite Laureate hydroxide	Poly(L-lactic acid)		Dimethyl, hydrogenated tallow, 2-ethylhexyl quaternary ammonium Unmodified	Extrusion / Rolling compression	400 μm	Oxygen / Water vapour	Packaging application
Ke et al. (2005)	Montmorillonite	Poly(ethylene terephthalate)		Organo-modification	Melt mixing - In situ polymerization / Thermopressing	25 μm	Oxygen	Packaging application
Kisku et al. (2012)	Boron nitride	Chitosan		Unmodified	Solution / Thermopressing	500 μm	Oxygen	Packaging application
Kisku et al. (2014)	Silicon carbide	Cellulose	70nm /	Unmodified	Solution / Thermopressing	500 μm	Oxygen	Packaging application
Kim et al. (2005)	Montmorillonite	Epoxy resin		Quaternary alkylamine Quaternary ammonium salt Octadecylamine	Solution / Casting	1000 - 3000 μm	Water vapour	General engineering application
Koh et al. (2008)	Montmorillonite	Poly(lactic acid)		Octadecyl ammonium chloride Dimethyl di(hydrogenated tallowalkyl) quaternary ammonium Methyl bis-2- hydroxyethyl tallow ammonium chlorid	Solution / Casting	25-40 μm	Oxygen / Carbon dioxide	Membrane application

Publication	Particle	Matrix	Size before/ after process	Chemical modification	Process	Film thickness	Molecular penetrant	Application
Kristo et al. (2007)	Starch crystals	Pullulan	Thickness: 6-8nm	Unmodified	Solution / Casting	69-75 μm	Water vapour	General engineering application
Kumar et al. (2010)	Montmorillonite	Soy protein isolate		Unmodified	Melt processing / Casting		Water vapour	Packaging application
Kumar et al. (2010)	Montmorillonite	Soy protein isolate		Dimethyl di(hydrogenated talloalkyl) quaternary ammonium / Methyl bis-2-hydroxyethyl tallo ammonium	Melt processing / Casting		Water vapour	Packaging application
Lan et al. (1994)	Montmorillonite	Poly(imide)		Polyamic acid	Solution - Casting	25 μm	Carbon dioxide	General engineering application
Lavorina et al. (2010)	Montmorillonite	Chitosan		Unmodified	Solution / Casting	115 - 125 μm	Water vapour	Packaging application
Lee et al. (2005)	Montmorillonite	High density polyethylene		Octadecylamine	Melt processing / Compression moulding	50 μm	Carbon dioxide	General engineering application
Lee et al. (2008)	Montmorillonite	Poly(methyl acrylate-co-methyl methacrylate)		Unmodified	Soap free emulsion polymerization / Casting	200 μm	Water vapour	General engineering application
Lee et al. (2010)	Montmorillonite	Soy protein		Unmodified	Solution / Casting	90 μm	Water vapour	Packaging application
Liang et al. (2012)	Montmorillonite	Poly(ether sulfone)	/ Aspect ratio 7.4 - 20	Unmodified	Solution / Casting	21 - 27 μm	Carbon dioxide	Membrane application
Luecha et al. (2010)	Montmorillonite	Zein		Methyl dihydroxy ethyl hydrogenated tallo ammonium	Solution / Casting / Blown - Extrusion	40 - 80 μm	Water vapour	Packaging application
Masclaux et al. (2010)	Montmorillonite	Native potato starch		Unmodified	Solution / Casting	50 μm	Oxygen	General engineering application
Meera et al. (2012)	Montmorillonite	Natural rubber		Octadecyl ammonium chloride	Melt processing / Compression moulding	1000 μm	Oxygen / Carbon dioxide	Membrane application
Merinska et al. (2011)	Montmorillonite	Poly(ethylene)		Methyl bis-2-hydroxyethyl tallo ammonium / Dimethyl, hydrogenated tallo, 2-ethylhexyl quaternary ammonium / Methyl, dehydrogenated tallo ammonium	Extrusion / Thermopressing	50 μm	Oxygen / Carbon dioxide / Water vapour	Packaging application
Messersmith et al. (1995)	Montmorillonite	Poly(ϵ -caprolactone)		Organo-modification / Protonated amino acid	Solution / Casting	200 μm	Water vapour	General engineering application

Publication	Particle	Matrix	Size before/ after process	Chemical modification	Process	Film thickness	Molecular penetrant	Application
Mittal et al. (2007)	Montmorillonite	Poly(propylene)		1-decyl-2-methyl-3-octadecylimidazolium bromide	Melt processing/ Compression moulding	100 µm	Oxygen	General engineering application
Mittal et al. (2007)	Montmorillonite	Poly(propylene)		Dimethyldioctadecylammonium bromide	Melt processing/ Compression moulding	100 µm	Oxygen	General engineering application
Monsivais Barron et al. (2013)	Montmorillonite	High density polyethylene		Dimethyl di(hydrogenated tallowalkyl) quaternary ammonium Quaternary ammonium salt	Melt-compounding / Thermopressing	100 µm	Oxygen	Packaging application
Müller et al. (2012)	Montmorillonite	Cassave starch		Unmodified Methyl bis-2-hydroxyethyl tallow ammonium	Melt processing/ Compression moulding	350 - 550 µm	Water vapour	General engineering application
Nazarenko et al. (2007)	Montmorillonite	Poly(styrene)	Thickness: 1nm Length: 80-300nm	Unmodified Octadecyldimethyl betaine Vinylbenzyl dimethyldodecylammonium chloride	Melt processing/ Compression moulding		Oxygen	General engineering application
Osman et al. (2005)	Montmorillonite	Linear high density polyethylene		Octadecyltrimethylammonium chloride Dioctadecyldimethylammonium bromide Methyltrioctadecylammonium bromide Tetraoctadecylammonium bromide	Melt processing/ Compression moulding	60 µm	Oxygen	General engineering application
Osman et al. (2007)	Montmorillonite	Poly(propylene)		Octadecyltrimethylammonium Dimethyldioctadecylammonium Methyltrioctadecylammonium Benzylhexadecyldimethylammonium Docosyltriethylammonium	Melt processing / Compression moulding	100 µm	Oxygen	Packaging application
Picard et al. (2007)	Montmorillonite	Poly(amide 6)		Dihydroxy methyl tallow quaternary ammonium	Melt processing / Compression moulding	75 - 85 µm	Oxygen / Water vapour	General engineering application
Picard et al. (2011)	Montmorillonite	Poly(lactic acid)	/ Aspect ratio 2.4	Dihydroxy methyl tallow quaternary ammonium	Melt processing / Compression moulding	100 µm	Oxygen	General engineering application
Ray et al. (2003)	Montmorillonite	Poly(lactic acid)		Organically modified synthetic fluorine mica	Melt processing / Compression moulding	300 µm	Oxygen	Packaging application

Publication	Particle	Matrix	Size before/ after process	Chemical modification	Process	Film thickness	Molecular penetrant	Application
Rhim et al. (2006)	Montmorillonite	Chitosan		Unmodified Dimethyl, hydrogenated tallow, 2-ethylhexyl quaternary ammonium	Solution / Casting	60 - 70 μm	Water vapour	Packaging application
Rhim et al. (2009)	Montmorillonite	Poly(L-lactide)		Unmodified Dimethyl di(hydrogenated tallowalkyl) quaternary ammonium Bis-(2-hydrox- yethyl)methyl (hydrogenated tallowalkyl) quaternary ammonium	Solution / Casting	80 μm	Water vapour	Packaging application
Rhim et al. (2011)	Montmorillonite	Food grade Agar		Unmodified	Solution / Casting		Water vapour	Packaging application
Sanchez et al. (2007)	Montmorillonite	Blend (80%wt)PHB / (20%wt)PCL		Organophilic surface modified kaolinite	Melt processing / Compression moulding	100 - 700 μm	Oxygen	Packaging application
Sanchez et al. (2009)	Montmorillonite	Poly(hydroxybutyrate-covalerate) Poly(ϵ -caprolactone) Poly(lactic acid)		Organo-modification	Solution / Casting	100 μm	Oxygen / Water vapour	Packaging application
Shah et al. (2006)	Montmorillonite	Low density polyethylene Sodium ionomer of poly(ethylene-co-methacrylic acid)		Dimethyl di(hydrogenated tallow) ammonium	Melt processing / Blown processing	25.4 - 76.2 μm	Oxygen / Carbon dioxide / Water vapour	Packaging application
Slavutsky et al. (2014)	Montmorillonite	Brea gum		Unmodified	Solution / Casting		Oxygen / Carbon dioxide / Water vapour	Packaging application
Sothornvit et al. (2009)	Montmorillonite	Whey protein		Unmodified Dimethyl di(hydrogenated tallowalkyl) quaternary ammonium Bis-(2-hydrox- yethyl)methyl (hydrogenated tallowalkyl) quaternary ammonium	Solution / Casting	150-190 μm	Water vapour	Packaging application
Sothornvit et al. (2010)	Montmorillonite	Whey protein		Bis-(2-hydrox- yethyl)methyl (hydrogenated tallowalkyl) quaternary ammonium	Solution / Casting	170 - 210 μm	Water vapour	Packaging application
Strawhecker et al. (2000)	Montmorillonite	Poly(vinyl alcohol)		Unmodified	Solution / Casting	89 μm	Water vapour	General engineering application

Publication	Particle	Matrix	Size before/after process	Chemical modification	Process	Film thickness	Molecular penetrant	Application
Sun et al. (2008)	α -zirconium phosphate	Epoxy resin	Thickness: 1nm Length: 100nm - 1 μ m	Polyoxyalkyleneamine Tetra-n-butyl ammonium hydroxide	Solution / Casting	1000 μ m	Oxygen	General engineering application
Swain et al. (2013)	Boron nitride	Cellulose	70nm /	Unmodified	Solution / Thermopressing	5000 μ m	Oxygen	Packaging application
Rodriguez Marin et al. (2013)	Montmorillonite	Rice flour Banana flour		Unmodified Citric acid Citric acid / Sulphuric acid	Solution / Casting	180 μ m	Water vapour	Packaging application
Tang et al. (2008)	Montmorillonite	Corn starch Wheat starch Potato starch		Unmodified Onium ion modified MMT	Melt processing / Casting		Water vapour	Packaging application
Theilen et al. (2005)	Montmorillonite	Poly(L-lactide)		Dimethyl, hydrogenated tallow, 2-ethylhexyl quaternary ammonium	Melt processing / Blown processing	75 μ m	Oxygen / Water vapour	Packaging application
Tsai et al. (2009)	Montmorillonite	Poly(methyl methacrylate)	/ Aspect ratio 100-150	Organo-modification	In situ free radical polymerization / casting	100 -115 μ m	Oxygen	Membrane application
Tsai et al. (2010)	Montmorillonite	Poly(methyl methacrylate)		Organo-modification	In situ polymerization / casting		Oxygen	Membrane application
Tunc et al. (2006)	Montmorillonite	Wheat gluten	Particle size distribution: 5-10 μ m	Unmodified	Solution - Casting	200 μ m	Oxygen / Carbon dioxide / Water vapour	Packaging application
Villaluenga et al. (2007)	Montmorillonite	Isotactic polypropylene		Unmodified Octadecyl ammonium chloride	Melt processing / Compression moulding	100-170 μ m	Oxygen	Membrane application
Wang et al. (2004)	Rectorite	Styrene butadiene rubber	/ Aspect ratio 20	Unmodified	Melt-compounding / Thermopressing	1000 μ m	Oxygen	General engineering application
Xu et al. (2002)	Montmorillonite	Poly(urethane urea) segmented block copolymers		Octadecyl ammonium chloride	Solution / Casting	250 μ m	Water vapour	General engineering application
Yeh et al. (2006)	Montmorillonite	Epoxy resin		Tetradecyltrimethyl-ammonium chloride	Solution / Casting	250 μ m	Oxygen / Water vapour	Membrane application
Zehetmeyer et al. (2012)	Montmorillonite	Poly(propylene)		Octadecyl ammonium chloride	Melt-compounding / Thermopressing	25 μ m	Oxygen / Water vapour	Packaging application
Zhang et al. (2012)	Magnetic iron oxide Fe ₃ O ₄	Zein	Long diagonal size: 200nm Height: 20nm /	Amphiphilic oleic acid	Solution / Casting	600 - 1300 μ m	Oxygen / Water vapour	Packaging application
Zhong et al. (2007)	Montmorillonite	Ethylene vinyl acetate Low density polyethylene High density polyethylene		Dimethyl di(hydrogenated tallowalkyl) quaternary ammonium	Melt processing / Blown processing		Oxygen	General engineering application

Publication 2**State of the art and beyond, on multi-scale modelling of structure
& mass transfer relationships in nanocomposite materials**

Caroline Wolf, Valérie Guillard, Nathalie Gontard

ABSTRACT: *Modelling mass transfer properties of nanocomposite which mostly result from the dispersion of impermeable nanoparticles in permeable polymer matrixes have been discussed with a special emphasis on how the shape of the particles (e.g. spherical, cylindrical and platelet nanoparticles) is handled in the models. Analytical and numerical models available in the literature have been reviewed. The convenience of a given model to consider the geometrical complexity of the structure, such as the in-situ particle aspect ratio, particle dispersion and orientation, has been examined in terms of model definition and on the basis of validity conditions; existence (quantity and quality) of experimental model validation was also considered. The prediction of selected analytical tortuosity-based models were then compared to a large panel of experimental data (more than 700 permeability values) among those collected in a previous work [Wolf et al. (forthcoming (a))]. The suitability of the listed models to predict the observed decrease of permeability was discussed according to the shape of the particles; it was concluded that the numerical simulations were more reliable for the prediction of mass transfer in nanocomposites since they could take into consideration the complex structure of these materials and address the lack of data of the tortuosity-based model related to the structure.*

KEYWORDS : Modelling, Nanocomposites, Particle shape, Structure & mass transfer relationships, Permeability

1. Introduction

Since the past twenty years, wide-ranging of research activities have been dedicated to the development of nanocomposite materials consisting of two phases; continuous polymeric matrix and dispersed particles of nano-sized. These particles are mostly of inorganic nature (e.g. silicate layers, carbon nanotubes, silica nanoparticles) but could also be of organic nature (e.g. cellulose-based reinforcements, starch crystals). Nanoparticles are introduced in polymeric matrices to enhance their mechanical thermal and barrier properties towards gas and vapours [Ray et al. (2003)]. Considering this last category of functional properties, the impermeable particles act by creating a tortuous pathway that increases the distance to be covered by the diffusing molecule. This last feature is particularly applied in the food packaging field where high barrier properties can be required, for example to protect sensitive food against oxidation [Azeredo et al. (2009), Silvestre et al. (2011)]. The most appropriate nanoparticles shape for this role being platelets, the impact of clays on the diffusion and/or on the permeation properties has been extensively studied [Xu et al. (2006), Choudalakis et al. (2009), Kumar et al. (2011) and Mittal et al. (2013)]. Most of the reviews on the topic dealt mainly with the predictive modelling of nanocomposites barrier properties and listed the different available models with confrontation to a set of experimental data judiciously chosen for its marked effect of platelets addition on the nanocomposite permeability (i.e. a decrease of P/P_0 as a function of filler volume fraction). On a recent paper tried the impact of the particle shape (spheres, cylinders or platelets) on the relative variation of barrier properties was deciphered by an exhaustive collection and analysis of the literature experimental data [Wolf et al. forthcoming (a)]. Collecting more than 700 permeability values confirmed that platelets were globally more efficient than

spheres and cylinders to decrease the relative permeability of nanocomposites toward O_2 , CO_2 and H_2O (only these migrants investigated). However, it was noted that a decrease of the permeability of the nanocomposite compare to the neat matrix was not systematically achieved by addition of platelets. Indeed non-significant variation or sometimes unexpected increases, of the relative permeability were related to the heterogeneous structure obtained after processing: lack of particles dispersion, occurrence of agglomeration phenomena, and creation of an interphase at the particle/polymer interface. Experimentally, a nanostructure, optimally targeted towards high barrier property is ascribed to the nature of the raw materials (compatibility of polymer matrix and particles), and to processing conditions (e.g. physical dispersion of the particles within the polymer). To increase and to propose predictive modelling approach of the nanocomposite permeability, mathematical modelling has emerged for more than 50 years and was recently upgraded via the development of numerical approach (figure 2). All these modelling approaches are based on the hypothesis that mass transfer in the composite materials obeys to Fick's law and that the impact of the structure on the permeability coefficient could be entirely represented by means of geometrical input parameters. Therefore, all modelling approaches tried to predict the permeability of the composite (P) from the permeability of the polymer matrix (P_0), and from different additional factors related to the structure of the composites such as for example the particle volume fraction, the mean size aspect ratio of the particles, the in-situ particle dispersion (regular or random arrangement) and orientation towards the flux direction.

In front of the huge effect of the addition of platelet shaped particles on the composite permeability, most of the modelling approaches have focus on the

prediction of mass transport properties of platelets based-materials (e.g. considered as infinite ribbons or lamellae, or as flakes or disks, etc.); such as for instance the studies of the group of Cussler [Cussler et al. (1988), Falla et al. (1996) and Derocher et al. (2005)]. Among platelet shape, some authors focused precisely on polymer-layered silicate nanocomposites [Bharadwaj et al. (2001), Xu et al. (2006), Sorrentino et al. (2007) and Choudalakis et al. (2009)]. Compare to platelets, the impact of spherical or cylindrical particles on composite permeability has conducted to less modelling development, only one model for cylinders and three for spheres against more than 12 for platelets.

Historically, these models derived from other fields of science such as the prediction of dielectric properties in composites and nanocomposite materials [Maxwell et al. (1873), Higushi et al. (1958)] and were further adapted for the prediction of the permeability on the basis that both properties behaved in the same manner. A little later on, Barrer and Petropoulos (1961) proposed a first calculation of the diffusivity of membranes in which a second, permeable phase is dispersed in regular arrangement. Therefore, they took into account the diffusivity of the dispersed phase in their calculation, but their approach could be easily extrapolated to impermeable particles by considering that the diffusivity of the dispersed phase was null. In the same time, Nielsen and co-workers (1967) first introduced the concept of tortuosity in a mathematical expression of the relative permeability of the nanocomposite related to the permeability of the polymer matrix. Starting from this work, several other analytical tortuosity-based models have been derived. Last developments in the field were the numerical 2D and 3D models based in majority on the use of Finite Difference Method (FEM) [Greco et al. (2013, 2014) or Finite Volume Method [Minelli et al. (2009, 2011)].

The objective of this paper is to list and analysis the analytical tortuosity-based models available in the literature in terms of conditions of use, applicability and validity. Three types of particles were for the first time considered together: spheres, cylinders and platelets. A comparison of the prediction done by the most quoted models with an exhaustive set of data of the literature on O₂, CO₂ and H₂O permeability, collected in a previous work [Wolf et al. forthcoming (a)] was then carried out which was never done previously. This will permit to confront the models to the variability of the results obtained for agro-, bio- or synthetic polymers and different nature and shape of particles. A special emphasis was put on the examination of the limitations of these models to well predict the experimental data. Then in a last step, the more recent numerical approaches were presented and discussed with an emphasis on multi-scale modelling approach.

2. Basics on mass transfer

Mass transfer in a homogeneous polymer matrix is supposed to obey to Fick's law which related the flux (J) to the gradient of concentration through a proportionality coefficient, (D):

$$J = -D \left(\frac{\partial c}{\partial x} \right) \quad [1]$$

where D is a kinetic or mobility parameter which characterizes the mobility of molecular species as they diffuse through the materials.

Henry's law gives the correspondence between the concentration (c) and the partial pressure (p) for dilute system:

$$c = S \times p \quad [2]$$

where S is the solubility coefficient, a thermodynamic parameter which characterizes the number of molecular species sorbed onto and into the material.

By combining equations (1) and (2), the first Fick's law could be expressed for a monodirectional flux through a plane sheet film as follows:

$$J = \frac{D S (p_1 - p_2)}{h} \quad [3]$$

where p_1 and p_2 are the pressure on the two sides of the film and h is the thickness of the film.

Mass transfer phenomena in the polymer matrix film could be then represented by a solution-diffusion mechanism described by the three coefficients i.e. solubility (S), diffusivity (D) and permeability (P). The permeability coefficient combines the effects of diffusion and solubility:

$$P = D \times S \quad [4]$$

Providing that several assumptions are required, mass transfer phenomena in the nanocomposites could be described by the same mechanism of solution-diffusion than in the neat polymer [Barrer et al. (1961)]. The assumptions made are thus:

- first, the polymer matrix intrinsic properties are not affected by the presence of the nanoparticles;
- second, the nanoparticles/polymer matrix interactions are strong enough to avoid free volume creation at the interphase nanoparticles/polymer matrix.

Considering that nanoparticles are impermeable, the solubility of the nanocomposite could be predicted by knowing the solubility in the neat polymer matrix (S_0) and the particle volume fraction (ϕ). Thereby, gas solubility of a polymer-based composite can be expressed as:

$$S = (1 - \phi) \times S_0 \quad [5]$$

Then, considering that nanoparticles act as an obstacle for the migration of molecular species that have to follow a more tortuous path to diffuse through the nanocomposites, diffusion coefficient is decreased and can be expressed as:

$$D = \frac{D_0}{\tau} \quad [6]$$

where D and D_0 are the diffusion coefficient of the neat polymer matrix and of the nanocomposites and τ is the tortuosity as defined in figure 1.

The permeability of the nanocomposite deduced from equation (4) becomes:

$$P = \frac{1 - \phi}{\tau} \times P_0 \quad [7]$$

where P and P_0 are the permeability coefficient of the neat polymer matrix and of the composite.

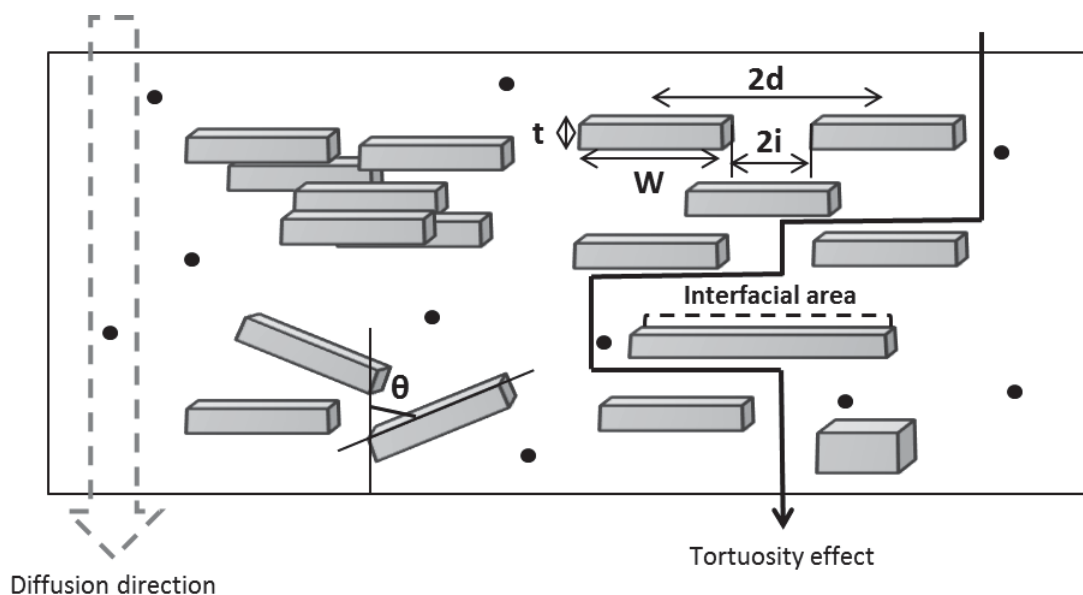


Figure 1: Representation of the tortuosity effect through nanoplatelets-based composites

According to equation 7, the predominant parameters in the modulation of the permeability in nanocomposites system are the tortuosity and the nanoparticles volume fraction. It is indeed obvious that for higher ϕ and τ , the permeability of the nanocomposite decreases. Considering that in most of the systems, especially the nanocomposites containing layered-silicates, the particle volume fraction is usually low (less than 1 vol%), the decrease of permeability relies mainly on the tortuosity, which appears to be the main degree of freedom to modulate the barrier properties of the nanocomposites. But, contrary to the volume fraction of nanoparticles, which is supposed to be perfectly characterizable, the tortuosity is a more arbitrary concept. Actually the tortuosity factor is defined as the ratio of the distance a molecular penetrant must travel to diffuse through a film when nanoparticles are present to the distance it must pass through without particles (i.e. thickness of the film). This factor is expressed as the contribution and the resistance introduced by an average number of particles to the diffusion of molecular specie. The purpose in all the modelling approaches attempted in the past, was to propose the most accurate

estimation of this parameter. Nielsen et al. (1957) and later on Cussler et al. (1988), two of the initial authors who proposed tortuosity-based models for the prediction of the permeability in composites, first attempted to express tortuosity from the geometrical characteristic of the nanocomposites in the case of regular arrangement of parallel platelets (infinite ribbon). In these simplified conditions of size (particles identical in size), dispersion (regular) and orientation (orthogonal to the flux), this tortuosity factor was related to the in-situ size aspect ratio of the particles.

3. General overview of available analytical tortuosity-based model for permeability prediction

3.1. History, evolutions, principles and conditions of validity of tortuosity-based models

A list as exhaustive as possible of the analytical tortuosity based-models is proposed in Table 1 and 2. Models in table 1 are dedicated to nanoplatelets while those in table 2 to spheres and cylinders nanoparticles. In table 1, the presented models are classified considering their increasing complexity as regard the alignment (regular or random) and the orientation (perpendicular to the flux or not) as described previously. In table 1 and table 2 every model was represented by the mathematical expression of the tortuosity factor with the list of the parameters required for a simulation, its condition of validity, its number of citations taken from the WOS and its experimental validation with precision if it has been realised by the authors of the model themselves or other teams.

Table 1: Description of different tortuosity-based models for platelet-based composites implemented on the basis of geometrical inputs with their conditions of validity and model validation if achieved

Model	Geometry	Tortuosity factor	Condition validity	Time quoted (from ISI Web of Science)	Experimental validation	Comparison with numerical models prediction
Regular arrangement of parallel nanoparticles oriented perpendicular to the diffusion/permeation direction						
Nielsen Nielsen (1957)	Rectangular platelets with infinite length, finite width and thickness	[A] $1 + \left(\frac{\alpha}{2}\right) \phi$	$\phi \leq 0,1$		Experimental validation Gatos et al. (2007) Sun et al.(2008), Picard et al. (2011), Gashemi et al.(2012), Duan et al. (2013), No experimental validation Hotta et al. (2004) Balachandran et al. (2012) Calculation of the aspect ratio Bharadwaj et al. (2002), Ray et al. (2003), Kim et al. (2005), Chaiko et al.(2005), Shah et al. (2006), Nazarenko et al. (2007), Herrera-Alonso et al. (2010), Meera et al. (2012), Duan et al. (2013),	Gusev et al. (2001) Minelli et al. (2011)
Aris Aris (1986)	Rectangular platelets with finite width and thickness	[B] $1 + \frac{\frac{\alpha \phi}{\pi} \left(\frac{\pi - \alpha \phi}{\alpha - \phi} \right) \ln \left(\frac{\pi}{\alpha - \phi} \right) + \frac{\left[\frac{\alpha \phi (\pi - \alpha \phi)^2}{(\alpha - \phi)^2} \right] \ln \left(\frac{\pi - \alpha \phi}{\alpha - \phi} \right)}{\left[\frac{\alpha \phi (\pi - \alpha \phi)^2}{(\alpha - \phi)^2} \right] + \frac{\alpha \phi (\pi - \alpha \phi)}{\alpha - \phi}}$	$\phi \leq 0,1$	27		Gusev et al. (2001) Swannack et al. (2005) Goodyer et al. (2007)
Cussler Cussler et al. (1988)	Rectangular platelets with infinite length, finite width and thickness	[C] $1 + \frac{\mu \alpha^2 \phi^2}{4(1-\phi)}$ [D] $1 + \frac{\alpha \phi}{\sigma}$	$\phi \leq 0,1$ $\alpha \phi < 1$ $\mu = 1$ $\phi \leq 0,1$ $\alpha \phi > 1$	255	Validation by the authors 1st version: validation with electrical conductance 2nd version: co-Silicone-PC-rmica/vermulite Calculation of the aspect ratio Chaiko et al. (2005), Nazarenko et al. (2007) Meera et al. (2012)	Gusev et al. (2001) Minelli et al. (2011)
Falla Falla et al. (1996)	Rectangular platelets with infinite length, finite width and thickness	[E] $1 + \frac{\alpha^2 \phi^2}{1-\phi} + \frac{\alpha \phi}{\sigma} + \frac{\alpha \phi}{\pi(1-\phi)} \ln \left(\frac{\pi \alpha^2 \phi}{\sigma(1-\phi)} \right)$	$\phi \leq 0,1$	77		Goodyer et al. (2009) Minelli et al. (2009)
Moggridge Moggridge et al. (1996)	Hexagonal platelets	[F] $1 + \frac{\mu \alpha^2 \phi^2}{4(1-\phi)}$	$\phi \leq 0,1$ High α $\mu = 2/27$	42	Validation by the authors PVA-rmica PC-rmica	

Model	Geometry	Tortuosity factor	Condition validity	Time quoted (from ISI Web of Science)	Experimental validation	Comparison with numerical models prediction
Random lateral and longitudinal positioning of parallel nanoparticles oriented perpendicular to the diffusion/permeation direction						
Brydges Brydges et al. (1975)	Rectangular platelets with finite width and thickness	$1 + \frac{\alpha^2 \phi^2}{1-\phi} \gamma(1-\gamma)$ [G]	$\phi \leq 0.1$ $\alpha > 100$ $\gamma < 1$	28	Validation by the authors Epoxy-glass fibre	
Yang Yang et al. (2004)	Rectangular platelets with infinite length, finite width and thickness	$1 + \frac{\mu \alpha^2 \phi^2}{4(1-\phi)}$ [H]	$\phi \leq 0.1$ $\mu = 1/2$	48		
Lape Lape et al. (2004)	Monodisperse sized platelets Polydisperse sized platelets	$\left(1 + \frac{\alpha \phi}{3}\right)^2$ [I] $\left[1 + \frac{\phi}{3 \alpha \sum_i n_i R_i} \sum_i n_i R_i^2\right]^2$ [J]	$\phi \leq 0.1$ $\phi \leq 0.1$	109	Validation by the authors Silicone rubber+graphite PVA+mica Experimental validation Picard et al. (2007)	Minelli et al. (2011)
Fredrickson and Bicerano Fredrickson et al. (1999)	Disks	$4 \frac{\left(1 + \frac{\alpha \phi}{2n} \left(\frac{\sigma \phi}{2n} + 0.1245 \left(\frac{\alpha \phi}{2n} \right)^2\right)\right)^2}{\left(2 + \frac{\alpha \phi}{2n} \left(\frac{\sigma \phi}{2n}\right)\right)}$ [K]	$\alpha \phi \leq 1$	142	Experimental validation Sun et al. (2008) Gashemi et al. (2012) Xu et al. (2001) Calculation of the aspect ratio	Gusev et al. (2001) Minelli et al. (2011) Greco et al. (2014)
Gusev and Lusti Gusev et al. (2001)	Disks	$\exp\left[-\left(\frac{\alpha \phi}{x_0}\right)^\beta\right]$ [L]	Least-square parameters $x_0 = 3.47$ $\beta = 0.71$	149	Experimental validation Sun et al. (2008), Gashemi et al. (2012) Osman et al. (2005) Calculation of the aspect ratio	
Random lateral and longitudinal positioning of parallel nanoparticles with random orientation according to the diffusion/permeation direction						
Bharadwaj Bharadwaj (2001)	Rectangular platelets with finite width and thickness	$1 + \frac{\alpha^2}{2} \left(S + \frac{1}{2}\right) \phi$ [M] $S = \frac{1}{2} (3 \cos^2 \theta - 1)$	$\phi \leq 0.1$	386	Experimental validation Chien et al. (2008) No experimental validation Alexandre et al. (2009), Faslihi et al. (2011) Calculation of the aspect ratio Meera et al. (2012)	Bhumia et al. (2012) Greco et al. (2013) Greco et al. (2014)

ϕ : volume fraction

α : aspect ratio

σ : slit aspect ratio

μ : geometric factor

γ : stacking parameter

R : ribbon width

Table 2: Description of different tortuosity-based models for spherical and cylindrical-based composites implemented on the basis of geometrical inputs with their conditions of validity and model validation if achieved

Model	Geometry	Tortuosity factor	Condition validity	Time quoted (from ISI Web of Science)	Experimental validation	Comparison with numerical models prediction
Maxwell Maxwell (1873)	Isotropic spheres dispersed in a continuous phase	$1 + \frac{\phi}{2} [N]$	$\phi \leq 0,1$	60	No model validation Cornelius et al. (2002), Patel et al. (2003), Takahashi et al.(2006), Ahn et al. (2008), Sadhegi et al. (2013)	Greco et al. (2013)
Bruggeman Petropoulos et al. (1985)	Isotropic spheres dispersed in a continuous phase	$\frac{(1-\phi)}{(1-\phi)^{3/2}} [O]$	$\phi \leq 0,2$	60	No model validation Matteucci et al. (2008)	
Higushi Higushi (1957)	Random suspension of isotropic spheres in a continuous phase	$\frac{(1-\phi)}{\left(1 - \frac{6\phi}{4+2\phi - K_H(1-\phi)}\right)} [P]$	$\phi \leq 0,1$	28	No model validation Sadhegi et al. (2009), Sadhegi et al.(2013) Model validation Sadhegi et al. (2009), Sadhegi et al. (2011)	
Strutt-Rayleigh Strutt (1892)	Dilute suspension of cylinders aligned to the surface	$1 + \phi [Q]$	$\phi \leq 0,1$			

The conditions of validity refer to the maximum volume fraction of particles that the model could consider for a reliable prediction of the relative permeability P/P_0 . In the case of platelets, this maximum particle volume fraction depends on the in-situ aspect ratio of the particle. Therefore, in table 1, the condition of validity is sometimes given as the product of ϕ with α . It is admitted that $\phi\alpha \ll 1$ corresponds to a dilute regime of concentration for the particle in an oriented disk composite, i.e. disks are spaced by a mean distance that exceeds the disk radius. On the contrary, $\phi\alpha \gg 1$ corresponds to a semi-dilute regime where the disks are strongly overlapping due to their great aspect ratio [Choudalakis et al. (2009)]. In the case of spheres and cylinders, the maximum particle volume fraction is defined under the assumption that the flux pattern around one particle is not affected by the presence of neighbour particles.

3.1.1. Chronology of the modelling theories

Before the 20th century, models developed were dedicated to the prediction of electro-magnetic properties in polymers filled with spherical particles, cylindrical and ellipsoidal particles. A little later on, some of these models, such as the Maxwell model [Maxwell (1873)], the Bruggeman model [Petropoulos et al. (1985), Bouma et al. (1997)] or the Strutt model [Strutt (1892)], were extended to predict mass transfer properties in nanocomposites with the postulate that as electro-magnetic properties, the permeability was affected only by the particle volume fraction. However, these “mono-parameter” models were restrictive to composites containing spherical, cylindrical or ellipsoidal particles (table 2) and could not be extrapolated to other type of particle shapes, especially with the emergence, in the 50s, of nanocomposite filled with platelets (e.g. nanoclay).

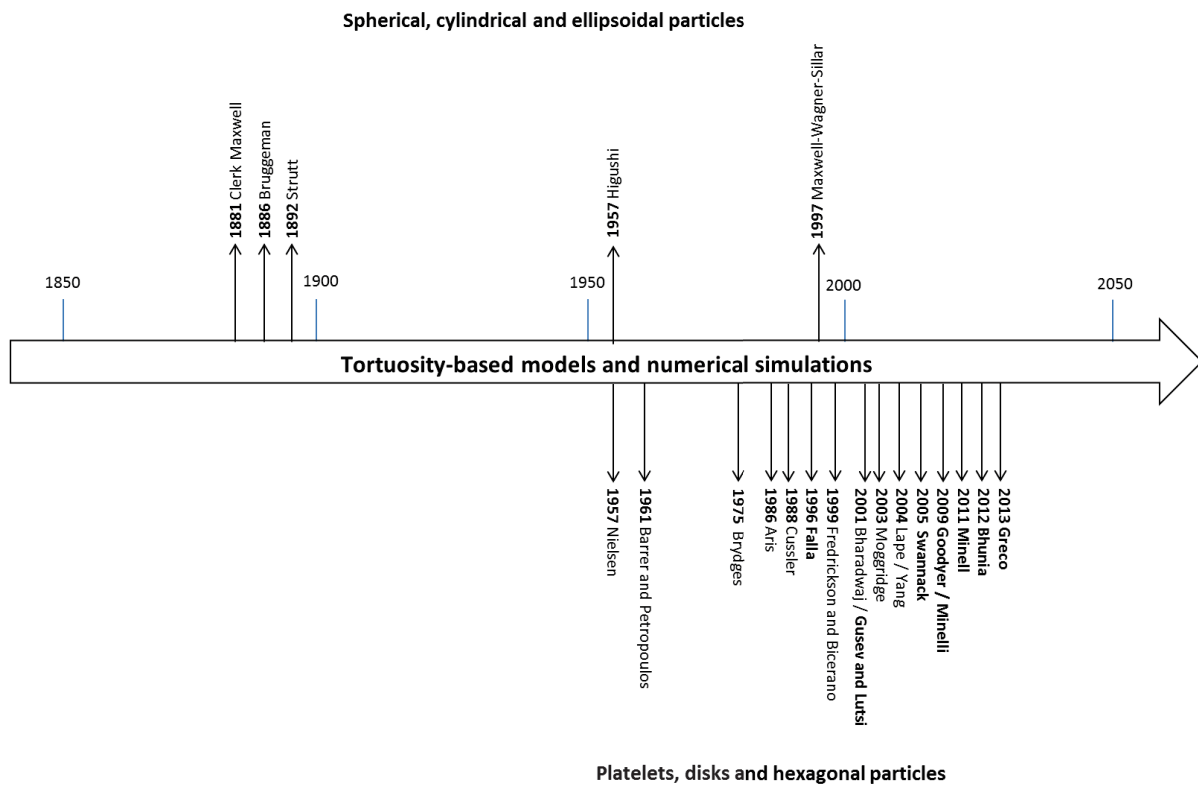


Figure 2: Spatial-temporal axis representing the chronology of development of the main analytical tortuosity-based models and more recently numerical simulations applied for the prediction of mass transfer in composite materials according to the shape of the particles

Further chronological developments were then dedicated to the prediction of permeability into nanocomposites containing nanoplatelets. Increasing complexity in the geometry (figure 3) was considered in those successive developments:

- **regular arrangement of parallel nanoplatelets or flakes** [Nielsen (1967), Barrer et al. (1961), Aris et al. (1986), Cussler et al. (1988), Falla et al. (1996)]. Most of the aforementioned theories assumed that the platelets were aligned like long ribbons of finite thickness d and width W and infinite length. Only the finite thickness and width were visible in the section plane transverse to the diffusion direction in the nanocomposite. Infinite particle length justified that diffusion was considered as two-dimensional. Alternatively, some theories have

considered further finite flakes and three-dimensional diffusion but always in regular platelets arrangement [Moggridge et al. (2003)]. The same equation than that of Cussler (equation C in table 1) was proposed by Moggridge et al. (2003) except a corrective factor, $2/27$, added in the formula to take into account the specific platelet shape (equation F in table 1);

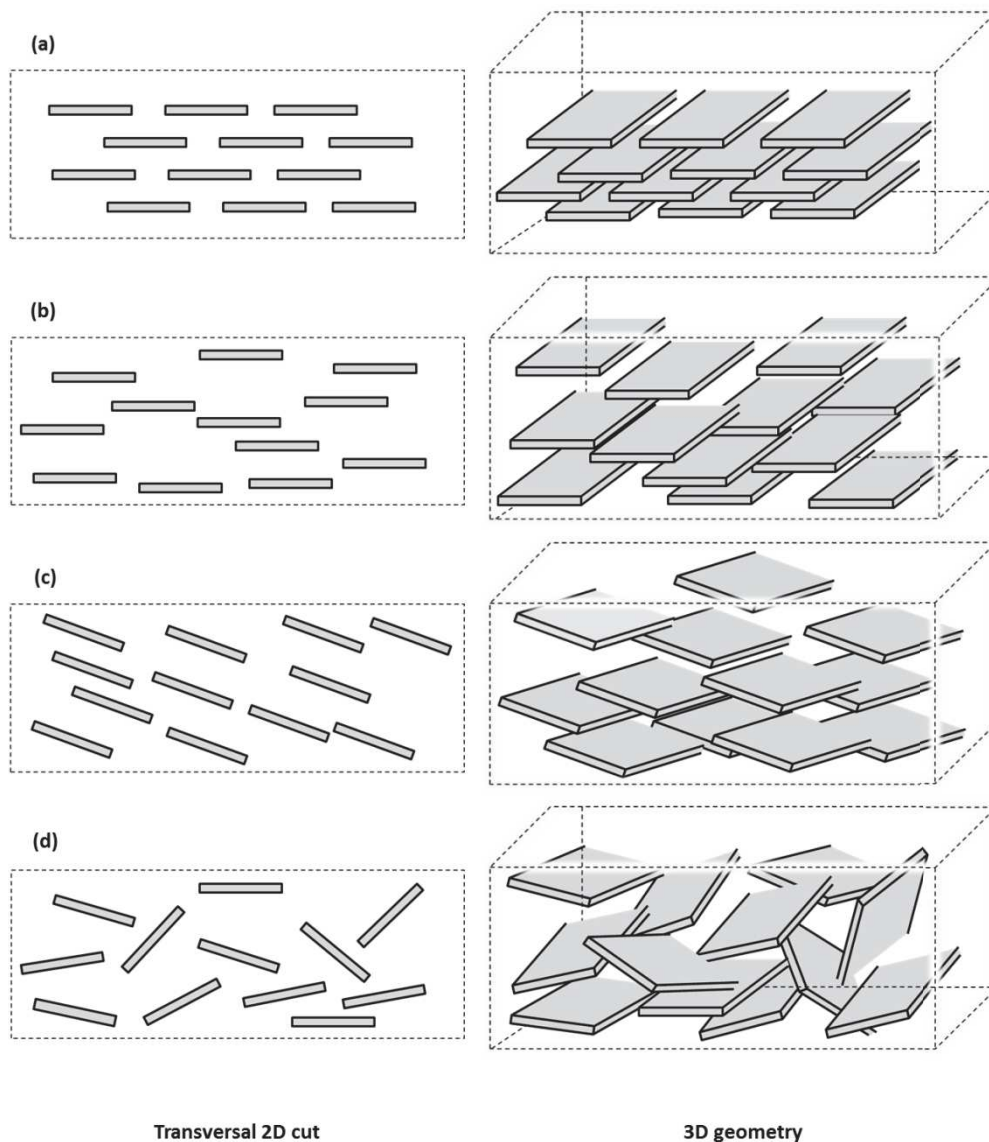


Figure 3: Example of possible arrangement of schematic platelet particles into 2D and 3D nanocomposite structures considered in analytical tortuosity-based models; the particle should be considered as either lamellae or ribbon (with finite/infinite length L), or hexagonal or disk flakes. (a) regular arrangement of parallel particles / (b) random spatial positioning of parallel particles / (c) random spatial positioning of same orientated particles / (d) random spatial positioning of randomly orientated particles

- **random spatial positioning of parallel nanoplatelets or flakes** [Aris et al. (1986) Brydges et al. (1975); Cussler et al. (1988), Lape et al. (2004)]. Brydges et al. (1975) first considered the case of deviation from the periodicity of the alignment by introducing a stacking parameter (γ), defining the horizontal offset of each ribbon layer with respect to the layer underneath it. Cussler and co-workers, themselves, enriched their modelling approach by examining the case of randomly positioned parallel platelets. Indeed the chief limitation of their initial theory (equation C in table 1) was the assumption that the flakes were regularly spaced. Hence, in an upgrading of their theory, they assumed that the flakes could be randomly spaced and introduced the geometrical parameter (μ) equal to $\frac{1}{2}$ in order to take into account this randomly arrangement.

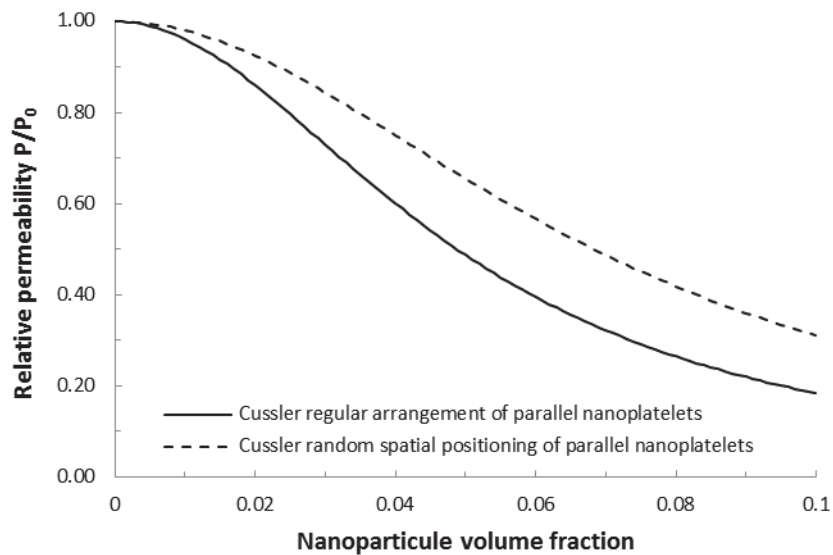


Figure 4: Prediction of Cussler model (equation C) for regular (solid line) and random spatial positioning (equation H) (dash line) of parallel nanoplatelets as function of particle volume fraction for a mean aspect ratio value equal to 20.

As shown in figure 4, the hypothesis of regular or random arrangement of the platelets significantly changes the prediction of the relative permeability of the nanocomposite by the Cussler model. A higher decrease of P/P_0 was obtained when the nanoplatelets were regularly positioned compare to when they were randomly positioned. Keeping in mind that the platelets played the role of obstacle for the diffusion of molecular species through a composite material, when the particles are randomly positioned, area without particles should be considered as favourable channel for the diffusion of the molecular species. Face to the importance of taking into account the spatial arrangement of the particle; several other authors have considered the case of random spatial positioning such as Fredrickson et al. (1999) who proposed a model for the prediction of the diffusion coefficient in composites containing randomly arranged, impermeable disks oriented perpendicularly to the diffusion flux. In the same objective of analysis the impact of random spatial positioning, Gusev et al. (2001) developed a 3D computational model for the prediction of the permeability in a random array of parallel circular disks;

- **random spatial positioning of randomly orientated nanoplatelets or flakes.** The case of random orientation was first considered by [Bharadwaj et al. (2001)] who proposed a modified form of the Nielsen's equation in order to take into account the angle of orientation (θ) of the platelets with the surface of diffusion. In their theory, they modified Nielsen equation to relate the dependence of the tortuosity factor on the mean orientation of the sheets in a continuous manner by introducing the order parameter (S). On the same basis, Dunkerley et al. (2010) proposed a progression of all existing tortuosity-based models, developed for parallel platelets, with a more generalized

mathematical relation of the tortuosity factor taking into account the average angle of orientation of the platelet (table 1). This approach permitted to use former models for the case of randomly oriented particles-based composites. Maksimov et al (2008) proposed an empirical relation for the prediction of the permeability in nanocomposites with randomly (3D) oriented platelets. Although several models have been proposed for the random orientation of the particles, the work of Bharadwaj (386 in the WOS, table 1) remains definitively the most quoted one even if numerical simulations permit nowadays to consider geometries with arbitrarily oriented lamellae [Bhunia et al. (2012), Greco et al. (2013)].

More recently (2005-2014), numerical models, based for example on Finite Element Method (FEM) or Finite Volume Method (FVM) have been developed in order to take into account more complex geometries. The first step of these models study was to compare their prediction to those obtained by the analytical tortuosity-based models, therefore, in relative simplified geometries. For example, Minelli et al. (2011) showed that their model prediction was proven to be fairly close to the prediction of Lape model [Lape et al. (2004)] in the case of geometrical configuration for which it was originally proposed (random spatial positioning of parallel nanoplatelets). Greco et al. (2014) showed that their model prediction was in good agreement with that of Bharadwaj model [Bharadwaj et al. (2001)] for non-oriented particles ($S=0$ in equation M, table 1). Once these models were validated in the case of simplified geometries, they could be used to represent and model the case of more heterogeneous geometries. It is the case for (Greco & Maffezzoli, 2013; Greco, 2014) who used their FEM model to simulate the diffusion into polymer nanocomposites in 2D and 3D geometries based on a random distribution of non-interpenetrating

impermeable lamellae with an arbitrary average orientation angle for each platelet (case d in Figure 3).

As listed in Table 1 and 2, different parameters were used to calculate the relative permeability ratio in the nanocomposite. In the models for spheres and cylinders and the number of input parameters is very low in case of spheres and cylinders and mostly limited to the volume fraction (table 2). Aside the particle volume fraction (ϕ) which was used in all models whatever the geometry of the nanoparticles, the size aspect ratio is one the more important parameter. In the specific case of platelets, theories of increasing complexity have necessitated the introduction of several other input parameters to describe the specific geometry of platelets such as the aspect ratio (α) of the particle, the slit aspect ratio (σ), a geometric factor (μ) introduced by Cussler et al. (1988), as explained above, to describe the arrangement (random or regular) of the nanoparticles, a stacking parameter (γ) introduced by Brydges et al. (1975), (S) an orientation parameter introduced by Bharadwaj et al. (2001).

3.1.2. Role of the “in-situ” aspect ratio of the particles

All the aforementioned platelet-based tortuosity models included a key player: the size aspect ratio of the particles added into the polymer matrix. The aspect ratio of a sphere is unity but for nanoplatelets it could reach more than 100 [Publication 1]. Hence at this stage the concept of “native” and “in-situ” aspect ratio should be distinguished, the former corresponding to the size of the particle before its incorporation in the polymer matrix while the latter corresponds to the aspect ratio of the particle after its incorporation in the polymer. Besides the “native” aspect ratio is usually known while the “in-situ” one is not. The efficiency of the dispersion of

nanoparticles within a polymer matrix depends on the affinity of the particle for the matrix and of the elaboration strategy [Publication 1]. In case of lack of particle dispersion, spherical or cylindrical particles could agglomerate leading to an apparent “bigger” particle in the material than the native one. Therefore the in-situ aspect ratio of the particle is higher than that of the native one. The same phenomenon occurs with platelets and is related to their exfoliation. From a practical point of view, complete exfoliation of platelets remains difficult to achieve, especially at high volume fraction. Therefore the actual “in-situ” aspect ratio is much lower than the “native one” and the efficiency of the nanostructure on the reduction of permeability is usually less than that predicted by the tortuosity-based models using the “native” aspect ratio.

As already mentioned above, in the case of spherical and cylindrical particles, the in situ size aspect ratio does not intervene in the predictive models. However, several studies listed in Publication 1 have observed that agglomeration phenomena strongly impacted the resulting permeability of the nanocomposite. Improvement of the predictive modelling approach should be carried out in a next future to take into account the in situ arrangement of cylinders and spheres.

3.1.3. Experimental validation of the models

When a model is developed, a validation step is needed in order to validate the efficiency of the model to predict, for example in the case of tortuosity-based model, the permeability of composite materials.

Some authors validated their model in the same paper where the model was presented as for example, Moggridge et al (1996) who validated their model with two particles/polymer matrix system, i.e. a PVA/mica and a PC/mica system. Other ones, such as Cussler et al. (1988) validated their model afterward [Eitzelmann et al. (1996)] on a silicone-PC/vermullite system. Although Nielsen and Bharadwaj models have not been validated by the authors themselves, they have been used later on by several authors (table1) and principally for identification of the aspect ratio. Bharadwaj et al. (2002) did not manage to validate his theory himself because of unexpected trouble in the processing of his nanocomposite. Indeed due to montmorillonite aggregation within the polyester matrix he investigated, the experimental data of permeability did not follow the same trend than the predicted one, if he considered only one single value for the size aspect ratio. This well-illustrated the limits of the developed theories to depict real cases and especially the particle polydispersity of size.

3.1.3. Impact of the polydispersity of size aspect ratio, dispersion and orientation

Almost all the models above assumed particles of uniform size. Ones of the first authors who examined the effect of the particle size polydispersity (effect of coexistence of several widths in the material) were Lape et al. (2004) (equation I and J). On the basis of their experimental and modelling works on mica particles/poly(vinyl alcohol) they showed that larger flakes played a key role on the permeability decrease if compared to small ones. Moreover, they pointed out that a greater polydispersity resulted in better barrier property. Afterwards, Picard et al. (2007) proposed an extension of the Lape model in order to consider both the polydispersity of the width and the thickness of the particles. Their model was proved

more appropriate than the Lape one for the cases of high loading of particles where due to insufficient exfoliation, there was a distribution in the values of the aspect ratio.

In such analytical models, polydispersity of width and/or length parameters, could be represented either by a continuous distribution of sizes, e.g. Gaussian, if known, or by a discrete function, sum of the respective contribution of several classes or fractions (i) of same size to the overall size aspect ratio, such as for example:

$$\sum_{i=1}^m n_i \frac{w_i}{t_i} \quad [8]$$

where w_i and t_i are the width and the thicknesses of the fractions (i) of the platelets.

In 2D/3D numerical approached, the real polydispersity of size could be considered since each particle could be individually drawn and considered in the geometry (see for example definition of geometry in commercial COMSOL software). Some equation of distribution could be required to generate, through reconstruction algorithm, the observed geometry. In all cases, the difficulty is to gain the information on this polydispersity from experimental observations which is as for the in-situ size aspect ratio, tricky to analyze.

Polydispersity of in-situ particle orientation was also detected; some analytical models have considered the orientation of the particle in the matrix but only acknowledge an average orientation [(Bhardawaj et al. (2001), Dunkerley et al. (2010) Maksimov et al. (2008)]. It is obvious in figure 5 that the decrease of the relative permeability is function of the particle as evaluated by using the Bharadwaj model. When several orientations are coexisting in a nanocomposite, the real curve relating their impact on the prediction of the relative permeability lies somewhere between the two extrema of the Bharadwaj simulations ($S=-1/2$ et $S=1$). The higher

decrease of the permeability is observed for perpendicularly to the diffusion flux oriented particles ($S=1$), which corresponded to the orientation related to the maximum effect of the tortuosity. On the opposite, the decrease in permeability is the lowest for platelets oriented parallel to the flux. To represent the polydispersity of the orientation, i.e. a random orientation, Bharadwaj proposed an intermediate case with $S=0$. The coexistence in the material of different zones with their own particles orientation could not be considered by using this model. Only numerical approach permits to depict such complex case of polydispersity of orientation.

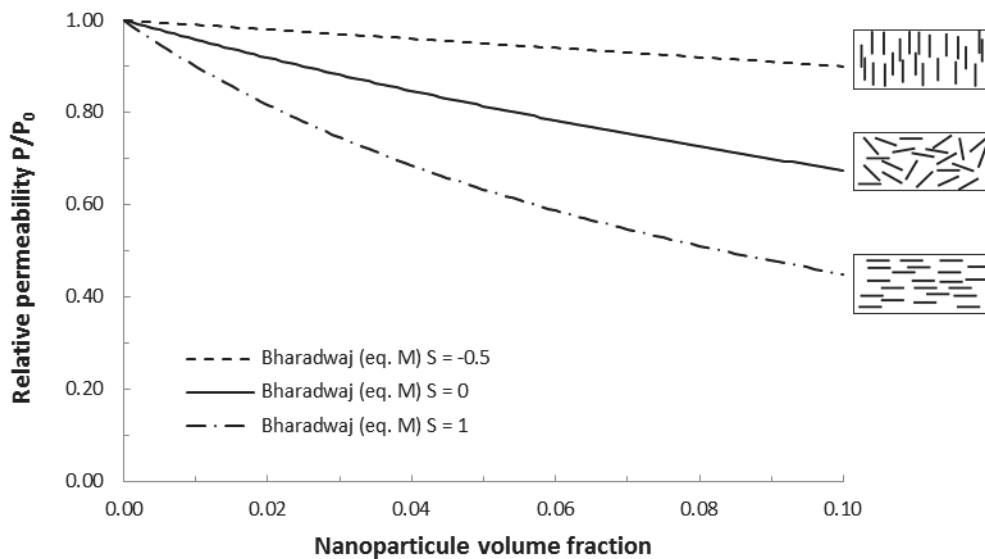


Figure 5: Predictions of Bharadwaj models according to the orientation of the particles as function of particle volume fraction for a mean aspect ratio value equal to 20.

3.1.4. Comparison of models' prediction: impact of particle shape and arrangement

To corroborate the impact of the particle shape on the prediction of the relative permeability, a comparison of different model predictions from table 1 and 2 is given in figure 6.

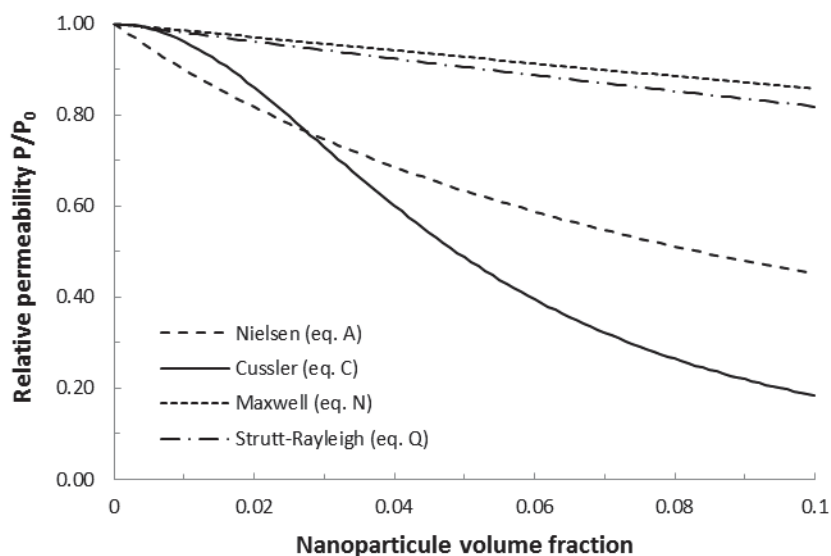


Figure 6: Predictions of Nielsen, Cussler, Maxwell and Strutt-Rayleigh models as function of particle volume fraction for a mean aspect ratio value equal to 20.

As anticipated, the impact of spherical or cylindrical particles on the decrease of the relative permeability, represented by the Maxwell and the Strutt-Rayleigh models respectively, was much lower than that of platelets, represented by the Nielsen and Cussler models respectively, for an aspect ratio equal to 20. Even if Strutt-Rayleigh model predictions are lower than that of Maxwell model they follow the same trend as function of particle volume fraction. Besides, when the aspect ratio was considered equal to 1, Nielsen model converged toward Maxwell model; nevertheless the consideration of such a low value of aspect ratio did not sound very realistic for platelets. In Maxwell (equation N in table 2) and Strutt-Rayleigh (equation Q in table 2) equation, the relative permeability was related to the particle volume fraction only; therefore, high particle volume fractions were required to achieve a significant decrease of the relative permeability. The very limited number of models available for spherical and cylinder particles prevented us to study in a constructive and instructive manner the reliability of predictive modelling in nanocomposites with spherical and cylindrical particles.

In figure 6, it was shown that the decrease of the permeability predicted from both Nielsen (equation A in table 1) and Cussler (equation B in table 2) models developed for platelet-based composites did not display the same tendency. This discrepancy was previously observed. Choudalakis et al. (2009) in their review on the permeability of polymer/clay nanocomposites proposed a comparison of the predictions of most of the models listed in table 1 for three different aspect ratio ($\alpha=10$, $\alpha=100$ and $\alpha=1000$) (simulations not reproduced here). Main conclusions that could be picked up from this comparison are that (1) high discrepancies lie between the simulations of the different models tested (Nielsen, Cussler for regular arrangement, Fredrickson & Bicerano and Gusev & Lusti) especially for $\alpha =10$ and $\alpha =100$; and (2) for $\alpha =1000$, simulations tend to converge at particle volume fraction higher than 6 vol%.

In the comparison made by Choudalakis et al. (2009), the Nielsen and Cussler models were for regular arrangement of ribbon and that of the Fredrickson & Bicerano and Gusev & Lusti ones for random arrangement of disks. Nevertheless this difference on the basements of each theory did not suffice to explain the high discrepancy observed between simulations. These authors concluded that the comparison of the models was not straightforward because the definition of the aspect ratio of the platelets sometimes diverge from one theory to another and must be adapted when disks instead of ribbons are considered. They advised therefore to use the product of the aspect ratio (α) by the particle volume fraction (φ) as the significant parameter. Nevertheless, even for the two simplest theories, Nielsen and Cussler, a divergence of more than 20% was noticed for $\varphi=0.06$; Nielsen prediction being lower than that of Cussler. This analysis pointed out that the choice of a theory is not so easy and that, for a given geometry, different models could be alternatively chosen leading to different results.

After this comparison between models themselves, next part of the present work will be dedicated to the comparison of the model predictions with experimental data collected from the literature.

3.2. Comparison of the model's prediction with an experimental set of data taken from the literature

In figure 7, the predictions of the most used model (Nielsen, Maxwell, Strutt) and the most quoted (Cussler, Bharadwaj) quoted models listed in table 1 and 2 for spherical, cylindrical and platelets were compared to a set of data collected in a previous work [Publication 1]. Seeing that no tortuosity-based models predicted an increase of the permeability with the addition of impermeable particles, all the experimental relative permeability (P/P_0) value higher than 1 were neglected, i.e. almost half of the data in case of spherical and cylindrical-based nanocomposites. As explained in a previous work [Wolf et al. (forthcoming (a))] the incorporation of impermeable particles within a permeable matrix should lead to a decrease of the permeability; however, it has been demonstrated for some researches that an increase of the permeability occurred. This evolution was hypothetically explained by (1) particle agglomeration in the polymeric matrix which created specific channel favourable to the diffusion of the molecular species, (2) formation of an interphase at the interface particles/polymer matrix which exhibit different barrier properties mainly due to changes of the polymer properties induced by the particle (free volume, crystallinity, etc) or (3) sorption of the molecular diffusing species at the surface of the particles because of the presence of available specific sites for their sorption. Hence in the following, only the decrease of the relative permeability was taken into account for the comparison with the model prediction.

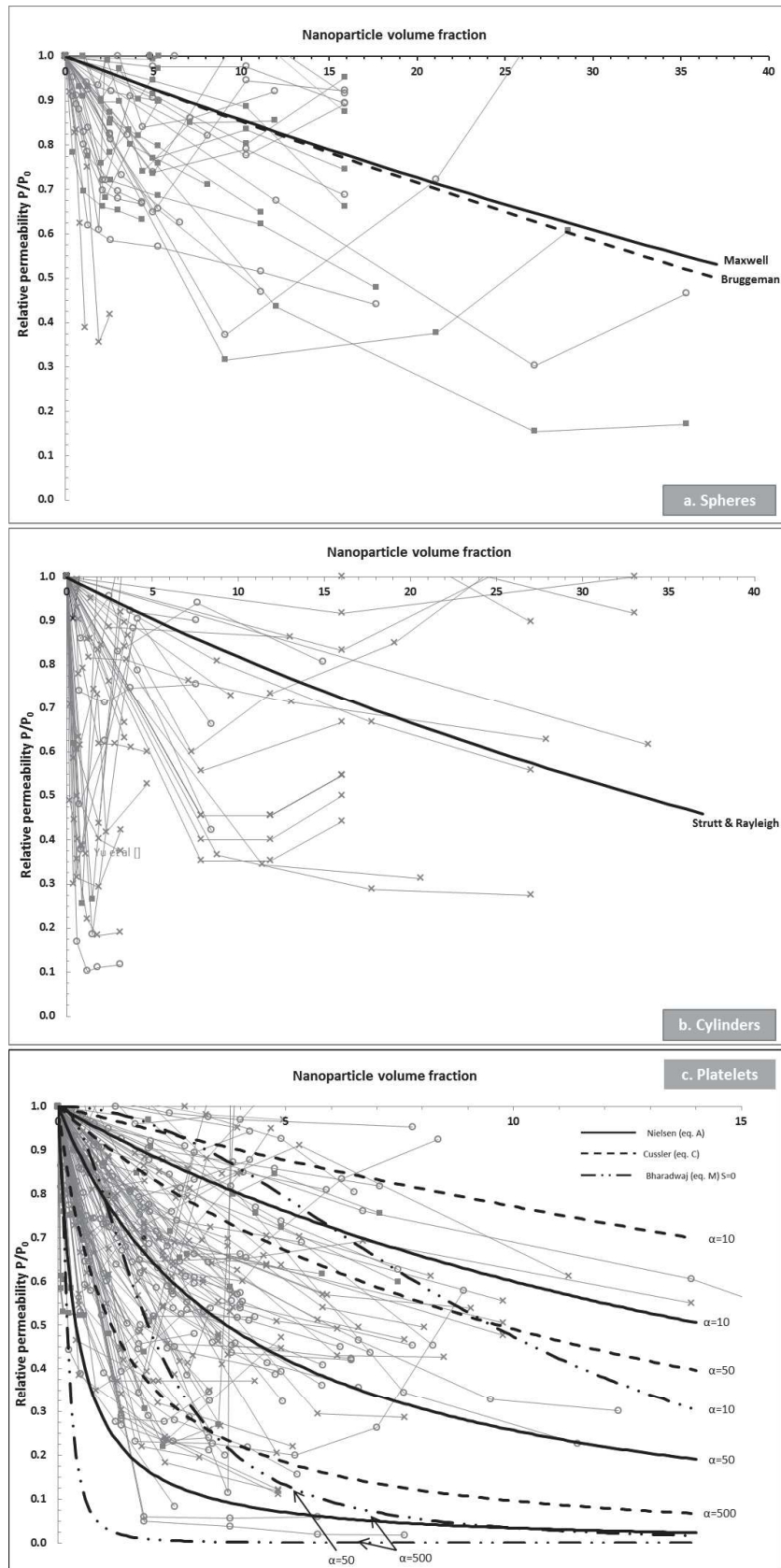


Figure 7: Representation of the model prediction and comparison with the set of permeability data gathered in [Wolf et al. (forthcoming (a))] according to the shape of the particles; (a) spherical, (b) cylindrical and (c) platelets particles

For spherical and cylindrical particles, the model predictions showed huge discrepancies with the experimental data. As already mentioned, there are only few models for spherical and cylindrical-based nanocomposites and they only considered a single input parameter, the filler volume fraction. Consequently some authors tried to predict the properties of cylinder-based nanocomposites with tortuosity-based model initially developed for platelets-based composites. For example Svagan et al. (2009) showed that Strutt model could not predict the relationship between the moisture diffusivity and the nanofibres (e.g. cylindrical particles) content; therefore they applied Aris model for the prediction of the diffusivity. As shown in figure 7, with such model predictions, very high loading of particle (>0.1 vol%) are required to achieve a significant but low decrease of the relative permeability (less than 20% of decrease for 0.1 vol% with the Maxwell model) which definitively did not match the experimental data and did not represent the disparity of the experimental permeability data. For cylindrical based-nanocomposites, much deeper initial decrease of the relative permeability was obtained experimentally than with the Strutt and Rayleigh model. In figure 7 a and b, experimental P/P_0 rapidly decrease and/or after a given particle volume fraction (approximately below 10 vol%) increased again. The tortuosity-based models of Table 2 are simply unable to represent the non-monotonic variations of experimental P/P_0 with the volume filler fraction often observed in spherical and cylindrical-based nanocomposites.

For platelet particles, all the range of experimental data could be covered by the predictions of the most famous models (Nielsen, Cussler and Bharadwaj) for aspect ratio in the range of 10 to 500. For a given set of data it is unlikely that a model prediction will match the data for a given aspect ratio. As for spherical and

cylindrical particles, the non-monotonic behaviour of P/P_0 as a function of ϕ could not be represented by the models because they correspond to a failure in the tortuosity concept (e.g. due to agglomeration phenomena). Among all the data collected on platelet-based nanocomposites, a large number of them display this non-monotonic behaviour with a small increase of P/P_0 after a threshold value of ϕ . From these observations it seemed very complicated to reach a general conclusion of availability of predictive models to predict P/P_0 in the case of platelets. It is doubtlessly highlighted that, among all, and in the case of monotonic decrease of P/P_0 , the reliable prediction of the nanocomposite permeability is a matter of the aspect ratio representation.

In the following, it was therefore decided to focus on one set of experimental data in order to analyse the prediction of the different models of table 1 and provide general guidelines on the choice of a predictive model for P/P_0 .

3.2.1. Choice of the tortuosity-based model adapted to one permeability set of data

Shah et al. (2006) have characterized the oxygen, carbon dioxide and nitrogen permeability of a montmorillonites/low density polyethylene process through melt-mixing and film-blowing. They observed a monotonic decrease of their experimental P/P_0 (figure 8). They measured the in-situ aspect ratio by using a methodology they developed [Vermogen et al. (2007)] and found values between 10 and 30; for the following discussion, the mean aspect ratio would be taken equal to 20. From their work, we decided to compare the prediction of different tortuosity-based models for a mean fixed aspect ratio. In their paper, there was no information on the dispersion state (regular or not) and orientation of the platelets. It is likely that platelets were

randomly placed and oriented in the material. Nevertheless, in the following, all type of models were considered for comparison with their data, for regular (Nielsen and Cussler) or random arrangement (Yang, Fredrickson & Bicerano, Gusev & Lutsi) of particle oriented perpendicularly to the flux direction and for random orientated particles (Bharadwaj). In figure 8a, it has been shown that the model prediction failed for all considered models; Fredrickson model prediction was the closest to the experimental permeability data. Large discrepancies were noted between the 6 model predictions tested. Shah et al. (2006) reached the same conclusion by using the Nielsen model on their data. They explained the discrepancy as the results of the assumptions built into the permeability model and the problems associated with the calculation of the particle aspect ratio from TEM micrographs. They then decided to adjust the Nielsen model on their experimental data in order to identify a more reliable value of alpha: the decrease of the relative permeability could not be described with one value of aspect ratio; they found a range of predicted aspect ratio from 80 to 140 against 10 to 30 as determined experimentally. At volume fraction equal to 0.5 and 1.4 vol% the value of the aspect ratio was approximately equal to 140 and 80 respectively. The decrease of the aspect ratio could be attributed to agglomeration phenomena.

Doing the same, we decided to fit all the above models to the experimental data, in order to identify the aspect ratio value (figure 8b). All models succeeded in fitting the experimental data of Shah et al. (2006) with more discrepancy for Cussler and Yang models than the other model but aspect ratio could however be identified and equal to 72, 51, 73, 87, 143 and 217 for Nielsen (eq. A), Cussler (eq. C), Yang (eq. H), Fredrickson (eq. K), Gusev (eq. L) and Bharadawaj (eq. M) respectively. All these

values were very far from the experimental size aspect ratio experimentally measured.

In some cases, the model prediction matched the experimental data. Indeed, Picard et al. (2011) and Chien et al. (2008) studied permeability of oxygen and water vapour respectively of montmorillonite/polylactide and montmorillonites/poly(vinyl acetate) composites respectively. Both groups of authors have characterized the in-situ aspect ratio in order to be able to apply and compare their experimental data to a model prediction. Experimentally, with the investigation of microscopy pictures, they found aspect ratio equal to 24 and 300 respectively. By comparison with the identified aspect ratio value, by fitting the Bharadwaj model to their data, they found a value of 24 and 327 for Picard et al. (2011) and Chien et al. (2008) respectively which are very close to the experimental ones. In the same approach, Angellier-Coussy et al. (2013) found a good match between their experimental data of water vapour diffusivity in montmorillonites/wheat gluten nanocomposite with the Bharadwaj model for a mean aspect ratio of 23.

This analysis highlighted that the application of a theory for the prediction of one set of experimental data is not so easily done. The characterization of the in-situ aspect ratio is not so surely accessible and most of the time, the model chosen is fitted and the aspect ratio is identified. Besides the decrease of the permeability may not only be governed by a tortuosity factor but also by additional structural effects; this will be discussed in the following.

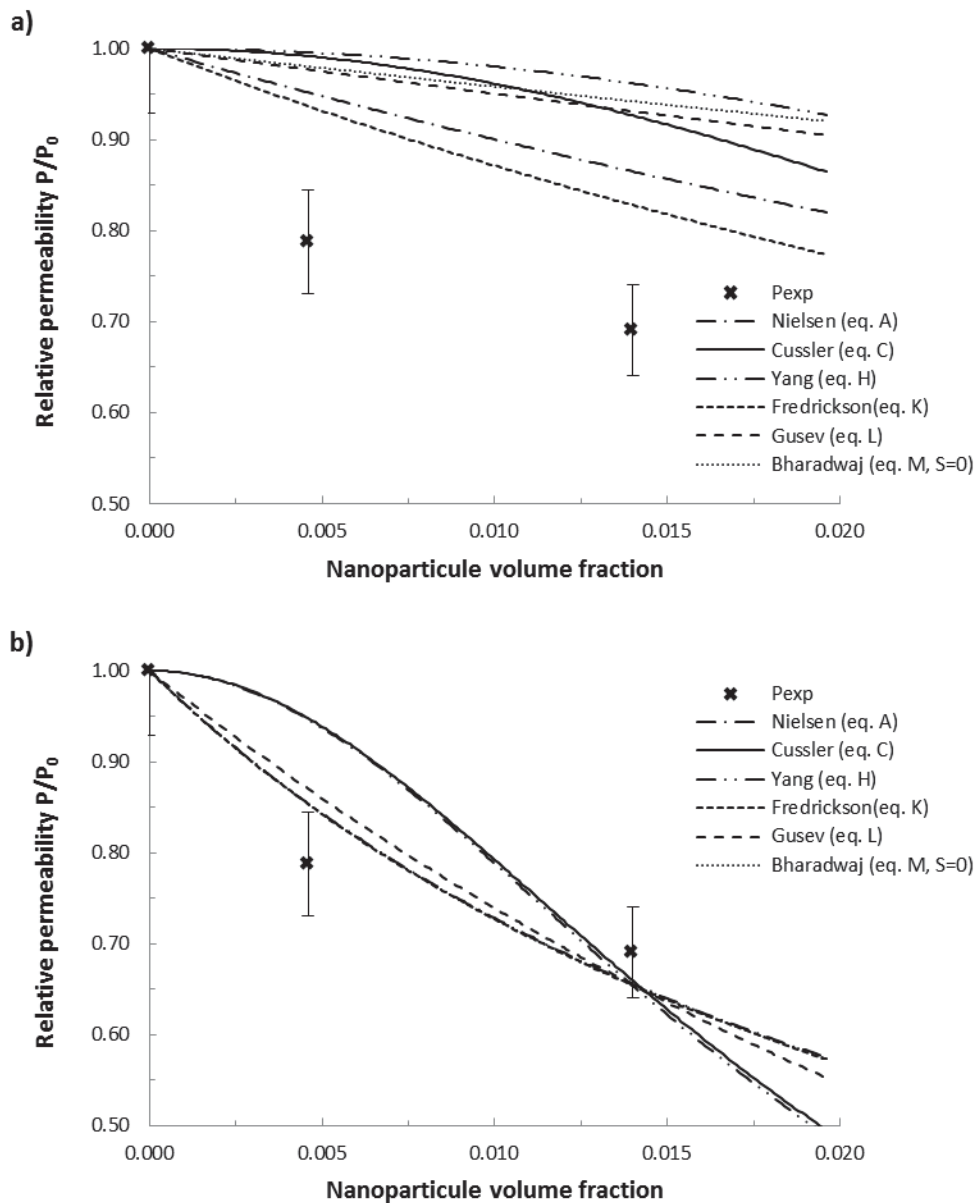


Figure 8: Representation of model prediction (from table 1) and oxygen experimental permeability data (Shah et al. (2006)); (a) model predictions with a mean aspect ratio equal to 20 and (b) models prediction with fitted aspect ratio

3.2.2. Limitations of the analytical tortuosity-based models

The geometrical input parameters of the tortuosity-based models are often very difficult to reach. One of the most important parameter is the aspect ratio; a lot of work as already been dedicated to the in-situ characterization of this parameter [Vermogen et al. (2007), Angellier-Coussy et al. (2013)]. Indeed, to allow a correct interpretation of the size of the particles within the polymer matrix, intensive pictures

analysis need to be achieving in order to get a mean aspect ratio of the particles. To overcome this difficulty, and as shown in the above section, models are often used with arbitrary chosen values of alpha or even fit on the experimental data to identify the aspect ratio value. For example Osman et al. (2005) have validated Gused & Lusti model for an aspect ratio arbitrary taken between 50 and 150 in aligned disk and in misaligned disk particles without experimentally studying the average aspect ratio obtained in montmorillonites/polyethylene nanocomposites. Chaiko et al. (2005) in their study, identified the aspect ratio values by using fit of the Nielsen and Cussler models and found values equal to 3000-9500 and 240-250. Although Cussler aspect ratio values were in the range of experimental characterized aspect ratio values, Nielsen aspect ratio values did not sound very realistic and were well beyond the expected value. An easy shortcut is thus to conclude that the Cussler model is more adapted to the Nielsen one in the study of Chaiko et al. (2005). In the same way, Meera et al. (2012) identified aspect ratio values from experimental permeability in montmorillonite/natural rubber nanocomposites with Nielsen, Cussler and Bharadwaj model; they also found different aspect ratio values. Other authors succeeded in measuring the experimental aspect ratio and to validate the theory they chose [Picard et al. (2011), and Chien et al. (2008)]. These findings let think that, in some cases, the aspect ratio would be not the only key parameter for obtaining an accurate prediction of P and that additional phenomena would counteract and provoke failure of the tortuosity-based theories.

Another point is the presence of empirical fitting parameter as in Higushi model with K_H , an experimental constant for a given migrant. For example, Sadhegi et al. validated Higushi model on two systems, a silica nanoparticles/polybenzimidazole (PBI) (2009) and a silica nanoparticles/polyurethane (PU) (2011) composite systems

for the permeation of nitrogen. The fitted parameter $K_H(N_2)$ was different according to the composite systems, equal to 3.8 and 3.58 in PBI and PU respectively. Furthermore, in PU systems, these parameters were found to vary also according to the migrant (oxygen, carbon dioxide and methane) ranging from 2.6 to 3.58.

In addition to the difficulty to experimentally assess the mean aspect ratio and other model input parameter that must, therefore, be identified from experimental data, numerous case of non-validation of the models could be explained due to changes of the nanocomposite structure which are not taken into account by the predictive models. Alexandre et al. (2009) and Balachandran et al. (2012) have shown discrepancies between experimental and predicted permeability from a particle volume fraction of 3 vol% in montmorillonite/poly(amide) and 4 vol% in montmorillonites/nitrile rubber. Alexandre et al. (2009) explained this evolution by an increase of the permeability from 3 vol% due to the decrease of the crystalline volume fraction in the nanocomposites and the clay/polymer matrix interface contribution which permit the sorption of water vapour molecular species. On their side, Balanchandran et al. (2012) justified the deviation between experimental and predicted permeability values with the presence of particles agglomerates within the polymer matrix which lead to coexistence of multiple particle aspect ratio in the same time in the material that was not defined by Nielsen model. The problem of coexistence of multiple particle aspect ratio could be easily overcome by taking into account the polydispersity of size as done by Lape et al. (2004) and Picard et al. (2007). Of course this required to know the polydispersity distribution (see discussion above).

As regard the modification of polymer matrix with the addition of particles, the formation of an interphase at the interface particles/polymer matrix could prevent the use of the tortuosity-based model because of a likely change of mass transfer properties in this specific area. The creation of an interphase between particle and matrix was already observed in mixed matrix membrane used for gas separation. In such type of material, where particles could be porous one such as zeolite, sieve, etc ..., interphase could be representative of interfacial voids, area with rigidified polymer chain layer or region where pores of the particle were blocked [Vinh-Thang et al. (2013)]. In order to take into account this interphase in their predictive model of membrane performance, based on permeability, some authors in the field have introduced a third constituents in addition to the continuous and dispersed phases, the interphase that has its own geometrical and mass transfer properties [Gonzo et al. (2006), Hashemifard et al. (2010), Mahajan et al. (2000), Pal et al. (2008), Vinh-Tang 2013)]. As far as we knew, this approach was never attempted in the field of packaging science for nanocomposite with impermeable particles.

4. Toward a multi-scale modelling of the structure / mass transfer properties relationship

4.1. Modelling at different scales: an overview

Theory and modelling method can be categorized into four groups (figure 9), depending on the time and the length scale on which there are defined [Gubbins et al. (2010)]. The first group, the electronic level of description, in which the matter is regarded as made up of fundamental particles such as electrons, protons, etc... is described by quantum mechanics. The second group, the atomistic level of

description in which the matter is made up of atoms whose behaviour obeys to the laws of statical mechanics. The third and the fourth groups are the mesoscale and the continuum level in which the matter is regarded as composed of beds of matter in the former and as a continuum medium respectively in the latter. In the continuum level, the recognized macroscopic (or phenomenological) laws, such as Fick's law for mass flow can be applied. The electronic scale requires no experimental input, only the knowledge of all the species involved in the phenomena. The atomistic scale is described by methods such as Monte Carlo or molecular dynamics simulation enabling systems of thousands and millions of atoms to be studied over time intervals of nanoseconds. The mesoscale is described by methods based on coarse graining and are extended in time and space if compared to the atomistic scale; systems of in the range of 100 nanometers to 100 micrometres to be studied over time intervals of micron and micro seconds.

The continuum scale, compared to the other scales, is not limited in terms of length and time scales and is rigorously based on macroscopic observations. In this level the physical, chemical and mechanical law are based on conservation laws which assume that the matter is a continuum that can be subdivided in space and time. Continuum methods for physical problems on mass transfer can be based on analytical or numerical solutions of the constitutive equation governing diffusion (Fick's law). This law is the basis of all the aforementioned theories (§ 3). One of the commonly methods for numerically solving these equations is the finite element method [Hughes (1987)].

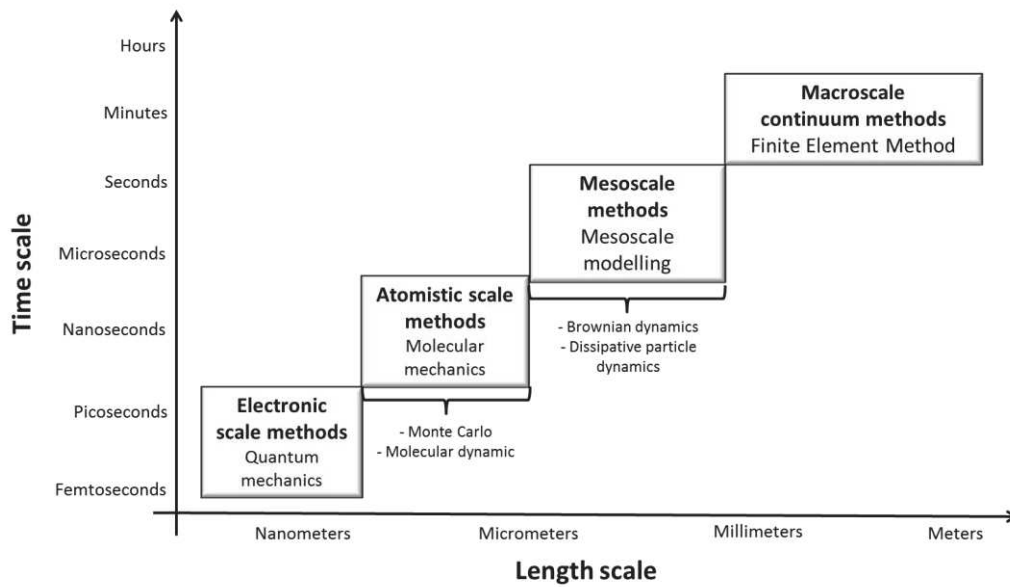


Figure 9: Theory and simulation scales from nanoscale to macroscale

The most common approach to reach a computational solution, in continuum methods, is to discretize the space so that the unknown functions, such as the concentration which varies continuously in the system is now represented by discrete values at lattice points. The differential problem becomes then an algebraic one which can be easily solved. In the continuum methods, the phenomenological coefficients that derive from atomic or subatomic properties such as diffusion coefficients must be obtained separately, either from experiment or from calculation performed at a lower scale such as molecular dynamics. Diffusion or permeability coefficients could be also determined using one of the above theories (see § 3). Usually, input parameters are directly identified from experimental data by fitting of the model to these data. Therefore, calculations at the continuum scale require extensive experimental input.

4.2. Modelling of the structure / mass transfer properties: current issues in polymer nanocomposite research

One of the most important issues in computational materials research is the multi-scale simulation, namely the bridging of length and time scales, and the linking of computational methods to predict macroscopic properties and behaviour from fundamental molecular processes [Charpentier et al. (2002)]. Currently, multi-scale modelling approach is based on simulations realized at the nano- and molecular scale, simulations supporting a mesoscale simulation step aimed at bridging the gap between the discontinuous nano-scale structure and the continuum macroscale models ; itself used as the basis for macroscale simulations of effective material properties where structural elements are observed at lower scales [Scocchi et al. (2007)].

Computational materials science based on multiscale approach is very promising in the domain of the nanoscience and especially on the modelling of the structure and properties relationships in nanostructures materials [Fermaglia et al. (2009), Jancar et al. (2010)]. Indeed, Jancar et al. (2010) reported that there has been a considerable interest in the utilisation of reliable models capable of bridging the gap between macroscale mechanical and barrier properties of nanocomposites, and their nanoscale structural variables. Besides, Fermaglia et al. (2009) reported that a general good agreement in the comparison of the simulation with experimental literature data of mechanical properties and morphologies is obtained and that multiscale modelling was an appropriate tool for the design of new structure responding to materials property's needs. In conclusion, multiscale simulation can be defined as enabling technology of science and engineering that links phenomena, models, and information between various scales of complex systems. However,

despite the tremendous advance made in the modelling of structural, thermal, mechanical and transport properties of the materials at macroscopic level, such as for example the use of finite element analysis of complicated structures, there remains crucial uncertainty about how to predict macroscopic properties of industrial interest, related to the performance of the materials.

Currently multiscale modelling of structure and mass transfer relationships is achieved for the prediction of macroscopical properties from structural information gained at the microscale. The founding work in that field was that of Falla et al. in 1996 that used Monte Carlo simulations for modelling the diffusivity in 2D nanocomposites filled with flakes. Their work was extended to 3D structures by Swannack et al. (2005) and by Gusev et al. (2001) for disks. More recently, interest of Finite Element Method (FEM) was explored by Goodyer et al. (2007, 2009) for 3D modelling of mass transfer properties in nanocomposites filled with impermeable particles. Minelli et al. (2011) did the same using finite volume algorithm (a method derived of FEM). All the aforementioned computational modelling attempts were done for platelets perfectly perpendicular to the direction of the flux for comparison purpose with tortuosity based models. Bhunia et al. (2012) first introduced the effect of the orientation in its 2D finite element model, followed by Greco and co-workers (2013 and 2014) who worked on 2D and 3D models based on random distribution and orientation of non-interpenetrating impermeable lamellae. These numerical models were generally compared and found more powerful than analytical tortuosity based models such as that of Bharadwaj (Bharadwaj, (2001)).

5. Conclusion

Modelling of mass transport properties of nanocomposite systems resulting from the dispersion of impermeable nanoparticles in permeable polymer matrixes have been widely discussed in this article with a special emphasis on the shape of the particles (e.g. spherical, cylindrical and platelet nanoparticles). From this analysis it should be drawn that spherical and cylindrical particles tortuosity-based models for the prediction of mass transfer properties were most of the time re-used from other fields of science and they are fewer than platelets-based models. More recently, the latter models were developed considering the particle volume fraction, the particle shape (ribbons, flakes, lamellae,...) and the aspect ratio, and the dispersion and the orientation of the particle in-situ the polymer matrix. The particle volume fraction and the aspect ratio are the main parameters; while the volume fraction is easily experimentally characterizable, the aspect ratio needs tough microscopy pictures analysis. According to the shape of the particles it has been demonstrated that the prediction of platelets-based models lead to better enhancement of the permeability than the spherical and the cylindrical particles tortuosity-based models. Numerical simulation, initially developed to take into account the geometrical complexity of the nanocomposites, such a as particle orientation or agglomeration have proven to be promising tool for the design of new materials whose properties are influenced by the structure at the nanoscale.

PERSPECTIVES

Through the analysis of the studies dealing with nano-impermeable particle based-composites designed for general engineering, membrane and packaging applications, it appears that the permeability can be modulated within a broad range. Indeed the nature, size and shape of the particles, the matching particles/polymer matrix and the structuration of the composites have an influence on the evolution of the permeability. Although until now, most of the studies were conducted in the objective of seeking a decrease of the permeability of gases and vapours with the addition of impermeable particles, a lot of studies have revealed that permeability was not decreased and in some cases, was even increased in the composites compare to that of the neat matrix, especially in the case of cylinders and spheres. Besides, some non-monotonic variations were noted in the case of platelets. These unexpected behaviours experimentally observed were related mainly to inhomogeneous dispersion of the particles in the matrix which was itself linked to lack of affinity between the particle and the matrix causing particles agglomeration, interphase, cracks etc.

Of course these peculiar behaviours were not represented at all by the tortuosity-based models that all predict a decrease of permeability in the composite compare to that of the neat polymer. According to the shape of the particles, it has been shown that the predictions of platelets tortuosity-based models lead to better enhancement of the permeability than the spherical and the cylindrical particles tortuosity-based models. While the main parameters of these models are the particle volume fraction and aspect ratio, the latter parameter is hardly experimentally

characterizable due to tough microscopy picture analysis work. The prediction of these models has thence been considered as a tool for identifying of the aspect ratio of the composites.

One of the main conclusions arising of this extensive state of the art is that particles were always considered as impermeable. Therefore, particles never participate to the overall mass transfer which, in practice, is not always the case, especially when vegetal fibres are used as filler. Through the lack of experimental data and predictive modelling of mass transfer properties of composite with permeable particles, the next part of this manuscript will be devoted to this type of material. In this purpose, deeper experimental and modelling investigation on the structure and the mass transfer properties of these bi-phasic permeable materials was conducted with a special emphasis on the characterizing of mass transport within the individual particle which was never attempted up to now. This exercise was realised on water vapour as diffusing molecule and on wheat straw fibres/biopolyester system as composite material. As regard to the analytical tortuosity-based models discussed in the first part, it will not be possible to achieve prediction of the permeability in bi-phasic permeable composites with these models. Some existing analytical biphasic models will be tested and a numerical model based on finite element method will be developed to predict and describe water vapour transfer in WSF/PHBV composites.

CHAPTER 2: In depth understanding of mass transfer and development of a 2D numerical model for the prediction of these properties into composites filled with permeable particles



Publication 3

Water vapour sorption and diffusion in wheat straw fibres and impact on mass transfer in PHBV based bio-composites

Caroline Wolf, Nathalie Gontard, Ghizzi Da Silva Gabriela, Valérie Guillard

ABSTRACT: *The contribution of matrix and vegetal fibrous constituents to the transfer properties of composites was deciphered by investigating water vapour sorption (S) and diffusion (D) of poly(3-hydroxybutyrate-co-3-hydroxyvalerate) (PHBV) matrix, grinded wheat straw fibres (WSF) and resulting composites containing 10 wt% and 20 wt% WSF at 20°C. A peculiar interest has been devoted to the key point of accurate WSF water vapour diffusion assessment, which was performed on single pieces of fibre, and to the study of water interactions in PHBV, WSF and WSF-based composites. The increase of WSF percentage led to an increase of the water vapour sorption isotherm of composites, which was attributed to the high water vapour sorption of WSF if compared to the neat PHBV matrix. As expected, water vapour D in WSF was much higher than in PHBV. However, in all composites, D was always lower than in WSF and PHBV. The main discussed hypothesis to explain this unexpected behaviour, are the changes of structure and properties of the WSF particle once embedded in the polymer matrix and the representativeness of water vapour diffusion, which is difficult to assess on this type of individual constituent.*

KEYWORDS : Particle shape, Nanocomposites, Structure & mass transfer relationships, Permeability

1. Introduction

Composites are materials consisting of at least two non-miscible constituents with different properties, whose synergism creates properties unavailable from individual single constituents. Due to increasing environmental concerns, a great attention has been paid during the last decade, to the study of manufacture, structure and properties of biocomposites composed of bio-mass based matrix and fibres [Mukherjee et al. (2011)]. For example poly(3-hydroxybutyrate-co-3-hydroxyvalerate) (PHBV) is considered to be a good alternative for non-biodegradable synthetic polymers because it is an environmental friendly material issued from renewable resources and moreover biodegradable. Its production is now possible from liquid effluents of food industry [[Albuquerque et al. (2012), Duque et al. (2014), Carvahlo et al. (2013)]. However its high manufacturing costs are still hampering the market growth of this material. Provided they are highly compatible with the matrix, vegetal fibres are attractive for their high strength, low environmental and economic cost and non-food origins. The incorporation of cheap fillers such as wheat straw fibres (WSF) in the PHBV matrix was already considered to overcome the drawback of PHBV cost [Faruk et al. (2012)]. A potentially undesirable effect of introducing vegetal fibres in a polymer matrix is the higher water sensibility of the resulting composites. Moisture transfer in the bio-composite could lead to a substantial alteration of the material functional properties, especially under usage conditions, due to an accelerated degradation of the constituents in the presence of water molecules [Cho et al. (2010), Mannberg et al. (2014)]. On other hand, in the field of food packaging applications, fresh and respiring foods such as fruits and vegetables or cheeses need to be packed with materials presenting sufficiently high moisture and gases transfer [Cagnon et al. (2013), Gontard et al. (2010)].

Recently, WSF have been specifically studied for their ability to increase composite permeability in order to fit the requirements of respiring fresh food produces. In the case of PHBV matrix, the incorporation of up to 20 wt% of WSF in PHBV polymer matrix was proved to modulate mass transfer properties of the composite while maintaining its mechanical properties [Berthert et al (2014)]. Whether needed or not, moisture sensitivity and transfer in bio-composites containing vegetal fibres is important and a good knowledge of the impact of each constituents on the water transfer in composites is required to design materials which are tailored to the targeted applications. A significant number of publications have already been devoted to the study of liquid water transfer in biocomposites and constituting biopolymers and fibres. For example, after immersion in liquid water, Srubar III et al. (2012) demonstrated that due to the presence of hydrophilic wood fibres both the water content at equilibrium and the identified liquid diffusion coefficient increased in the PHBV-based composites. However, in literature, transfer properties of water in its vapour form, were very little discussed for fibres-based bio-composites, and especially the impact of individual constituents. Corradini et al. (2013) showed the same trend of vapour and liquid water absorption increase for PHBV and green coconut fibres based composites. However the comparison between liquid water and water vapour transfer is difficult because of the qualitative and quantitative differences of physical phenomena involved (e.g. loss of soluble substances from constituents in liquid water which does not occur in the presence of water vapour). In many usage conditions, foods packaging materials are not in contact with aqueous liquid but exposed to different humidity of solid foods and external atmosphere during its life cycle.

In order to improve the knowledge of moisture transfer in composite materials, the present study aims at deciphering water vapour transfer mechanisms in a PHBV/WSF bio-composite, which was previously developed for food packaging applications using a thermal processing representative of industrial shaping conditions. For a better understanding of the behaviour of the composite, the water vapour sorption and water vapour diffusion of PHBV containing two different percentages of WSF, were experimentally evaluated and discussed in relationship with their physical-chemical characteristics and with the sorption and diffusion properties of the individual PHBV and wheat straw constituents. A specific effort was dedicated to a better evaluation of the diffusion properties of the fibres constituent.

2. Experimental

2.1. Materials

Commercial poly(3-hydroxybutyrate-co-3-hydroxyvalerate) (PHBV) was supplied by Tianan under the reference Y1000P with HV content 3%. Wheat straw (*Triticum aestivum* cv. Apache) was provided by Fernand Meaux (Saint Jean du Salés, Aveyron, France), harvested in 2007 and was ground to obtain wheat straw fibres. The wheat straw fibres (WSF) were impact-milled at a size of 100-150 μm and the median diameter of the fibre is around 62 μm using a process previously developed [Ghizzi D. Silva et al. (2012)] and recently re-use [Berthet et al. (forthcoming)].

2.2. Preparation of the PHBV and the PHBV-based composites

PHBV and PHBV-based composites with 10 wt% and 20 wt% fibre weight fraction (PHBV10 and PHBV20) were prepared by extrusion using a lab-scale twin-screw extruder (Eurolab from ThermoFisher Scientific). After extrusion, the obtained pellets were dried in an oven at 60 °C for at least 8 h. Then, the compounds were heated 5 min at 170 °C between two Teflon-coated plates and then thermo-moulded for 5 min at 150 bar and 170 °C with a heated hydraulic press (PLM 10 T, Techmo, Nazelles, France) to obtain films [Berthet et al. (2014)].

2.3. Sample preparation and conditioning

Before water sorption experiments, PHBV and PHBV-based composite films were respectively cut into discs of 0.8 cm diameter and stored at 0% RH on P₂O₅ at room temperature for at least 10 days before use. Native wheat straw fibres were prepared for sorption experiment with a first perpendicular cut to its height in order to obtain a cylinder of 0.5 mm height, which was in turn cut itself vertically by its middle. The resulting half cylinder was then easily mechanically flattened into a square piece of approximately 0.5 × 0.5 cm² by putting it underweight (around 200 N.m⁻² during 1 week) as described in figure 1. Wheat straw fibres were prepared in such conditions in order to characterize their water vapour sorption and to identify water vapour diffusivity coefficients.

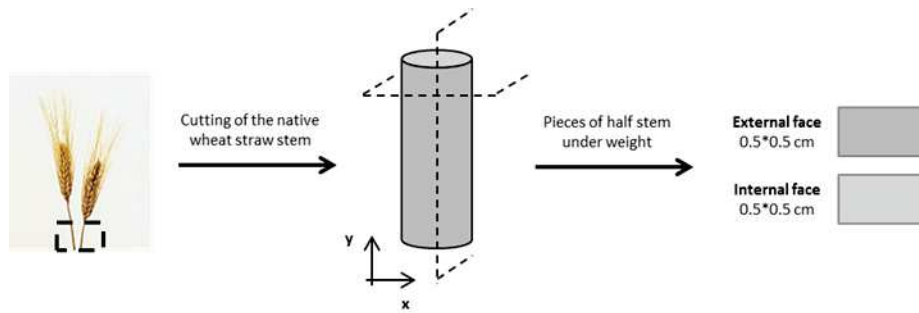


Figure 1: Explanation of the cutting procedure for the preparation wheat straw fibre films for DVS experiment

2.4. Characterization of the WSF, PHBV and PHBV-based composites

The apparent density of the dry films was calculated at room temperature from the ratio of the weight of dry matter to the corresponding volume of total material; the films were dried in an oven 24 h at 105 °C. The thickness of the films was measured using a micrometer (Braive Instruments, Chécy, France) in a dry state.

The real weight and volume particle fractions were determined by ash content analysis; measurements were performed using a Thermolyse 6000 device from Furnace, at a temperature of 190 °C during 2 hours. The samples, with a mass in the range between 2 and 5 g, were heated in quartz incineration pans. After two hours in the oven, the pans were put in a desiccator at room temperature under dry CaCl₂ during 30 minutes before weighting. The exact weight filler fraction (w) was calculated from the respective inorganic residue at 900 °C as:

$$w = \frac{R_{composite} - R_{matrix}}{R_{filler} - R_{matrix}} \quad [1]$$

where $R_{composite}$, R_{matrix} and R_{filler} are the inorganic residue of the PHBV-based composites, PHBV and WSF. Then the real volume filler fractions (ϕ) were calculate with the following equation:

$$\Phi = \frac{\frac{W}{\rho_{filler}}}{\frac{W}{\rho_{filler}} + \frac{1-W}{\rho_{matrix}}} \quad [2]$$

where ρ_{filler} and ρ_{matrix} are respectively the WSF and PHBV density and w the exact weight fraction of WSF previously measured.

Differential scanning calorimetry (DSC) were performed using a thermo-modulated calorimeter (Q200 modulated DSC, TA Instruments, New Castle, USA) on PHBV and PHBV-based composites dry material. The weight samples of the DSC sample were between 6 and 9 g. The samples were placed in open aluminium pan which were immediately hermetically sealed. Sample were first heated from 40 °C to 190 °C with a ramp rate of 50 °C.min⁻¹ in order to erase the thermal history of the sample. The sample were then cooled with a cooling rate of 10 °C.min⁻¹ to -40 °C and after heated with heating rate of 10 °C.min⁻¹ to 190 °C using N₂ as the purging gas. The crystallization temperature (T_c), melting temperature (T_m), melting enthalpy (ΔH_f) and enthalpy of crystallization (ΔH_c) were determined from the DSC curves. The crystallinity of the PHBV was calculated with the following equations:

$$\chi_c = \frac{\Delta H_f(PHBV)}{\Delta H^{\circ}(PHBV)} * \frac{100}{w_{PHBV}} \quad [3]$$

where $\Delta H^{\circ}(PHBV)$ is the enthalpy of melting per gram of 100% crystalline (146 J.g⁻¹) [Avella et al. (2000)], and w_{PHBV} the weight fraction of PHBV in the composite.

2.5. Microscopic observations

Internodes, nodes and leaves were humidified for 2 days at 4°C with deionised water under vacuum in a desiccator. 50 and 100 µm thick transverse sections were prepared with a vibratome Microcut H1200 (Bio-Rad, UK). These fresh sections were observed in a stereomicroscope MVX 10 (Olympus, JP) equipped to observe fluorescence (Optical objective x1.6, optical zooms x1 and x2).

2.6. Moisture sorption kinetics of WSF, PHBV and PHBV-based composites

Water vapour sorption experiments were carried out at 20 °C over a wide range of water activities (a_w) from 0 to 95% relative humidity using a controlled atmosphere microbalance apparatus (Surface Measurement System Ltd., London, UK) described in previous publications [Guillard et al. (2003)]. The tested samples, in the form of flat films, were first equilibrated at 0% relative humidity in a desiccator containing P_2O_5 for at least 8 days. The samples were then put into the microbalance in quartz sample pan and re-equilibrated at 0% relative humidity for a time frame of 24 h to establish a dry mass (M_d). The samples were exposed to different relative humidity by a continuous air stream of a specific relative humidity. Mass equilibrium was reached at each humidity level by measuring the percent of mass change with respect to time ($dm/dt < 0.002$) for WSF or by imposing a time frame for each relative humidity step for PHBV and PHBV-based composites. Once the equilibrium was achieved, the experiment proceeded to the next programmed humidity stage. The values of water content at each equilibrium were used to build the sorption isotherm. The moisture content at equilibrium (X) was calculated as follows:

$$X = \frac{M_w - M_d}{M_d} \quad [4]$$

where M_w (g) is the mass of the wet sample at equilibrium state and M_d (g) the dry mass. All adsorption tests were performed at least three times to verify the repeatability of the measurement.

2.7. Modelling of water vapour sorption isotherm

2.7.1. Sorption models

Water sorption isotherm equations are convenient for predicting water sorption properties and allowed to provide further information on the interaction of water vapour with the materials according to the water vapour activity. In the literature several models [Al-Muhtsabe et al. (2004)] have been proposed for the description of water vapour sorption but in the case of water vapour sorption in polymer matrixes and composites the most used sorption models were GAB and Park models. GAB model considers that water molecules condense layer by layer on adsorption surfaces such as external surfaces, specific sites or internal surfaces of cavities or pores:

$$X = \frac{X_m \cdot C_g \cdot K \cdot a_w}{(1 - K \cdot a_w)(1 - K \cdot a_w + C_g \cdot K \cdot a_w)} \quad [5]$$

where X is the water content at equilibrium as calculated by equation 4, X_m is the monolayer of water content, C_g is the Guggenheim constant and K is the constant relative to the adsorption energies of second and subsequent layers which lie

somewhere between the monolayer adsorption energy and the pure adsorptive liquefaction energy [Quirijns et al. (2005)].

Park model corresponds to a multi-sorption mode which could be divided in three steps. The first step, at low water activities, describes the Langmuir physical absorption assuming a first monolayer of water molecules adsorbed at the surface of sorption specific sites. The second step, at medium water activities, related to Henry's law, represents random adsorption by dissolution and diffusion of the water molecules inside the materials. And finally the third step, at higher water activities, represents water clustering phenomenon. The corresponding equation can be written as follows:

$$X = \frac{A_L \cdot b_L \cdot a_w}{1 + b_L \cdot a_w} + k_H \cdot a_w + K_a \cdot a_w^n \quad [6]$$

with A_L the Langmuir capacity constant, b_L the Langmuir affinity constant, k_H the Henry's solubility coefficient, K_a the equilibrium constant for the clustering reaction and n the mean number of water molecules per cluster. The mathematical models were fitted to the experimental water vapour isotherm using the GRG nonlinear solver from Excel 2010. In order to evaluate the fit of each model to the experimental data, the regression coefficient (R^2) and mean relative percentage of deviation modulus (E) were determined. The mean relative percentage of deviation modulus is one of the most used criteria to evaluate quality of model fitting in scientific publications dealing with water sorption; a modulus value below 10% is usually an indicator for a good fit [Lomauro et al. (1985)].

2.7.2. Water interactions in WSF, PHBV and PHBV-based composites

Two theories have been investigated and applied in order to quantify the water interactions in WSF, PHBV and PHBV-based composites. Zimm and Lundberg [Zimm et al. (1956)], based on statistical mechanics, have developed a theory to determine the degree of clustering defined under the name of clustering function which is defined as the ratio of the clustering integral ($G_{w,w}$) to the partial molecular volume of water (V_w) and was calculated from the equation of the water vapour sorption isotherm.

$$\frac{G_{w,w}}{V_w} = -(1 - \Phi_w) \left[\frac{\partial \left(\frac{a_w}{\Phi_w} \right)}{\partial a_w} \right] - 1 \quad [7]$$

where ϕ_1 and a_1 are the water volume fraction and activity. Negative values of the clustering function ($G_{w,w}/V_w < -1$) indicate that water vapour molecules are dissolved randomly in the polymer and positive values ($G_{w,w}/V_w > 1$) indicate that the concentration of water vapour near a given water molecule is greater than the average concentration of water vapour molecules in the polymer. Besides, the quantity $G_{w,w} \cdot \phi_w / V_w$ represent the mean number of water vapour molecules in excess in the neighbourhood of a given molecules. The mean cluster size is defined as:

$$MCS = 1 + \frac{\Phi_w G_{w,w}}{V_w} \quad [8]$$

ENSIC model [Favre et al. (1996)], based on a probabilistic and a mechanistic approach, has been developed in order to describe different types of molecular interactions in solvent-polymer systems. The model considers the probability of insertion of one molecule in a polymer matrix containing only the polymer and the previously sorbed molecules. The parameters taken into account in this model are the affinity between the non-polymeric molecule and the polymer (k_p) or the previously sorbed molecules (k_s). The increase of sorbed solvent molecule number (dn_s) due to an increase of the pressure (dP) in the gaseous phase can be related as:

$$dn_s = (k_p n_p + k_s n_s) \left(\frac{dP}{P_0} \right) \quad [9]$$

where n_s and n_p represents the solvent and the polymer cell number in the polymer. The relation is verified on the basis that the volume change in the polymer is negligible with the addition a solvent molecule. Assuming the gas phase as ideal, integration of equation 9 lead to the following expression:

$$\Phi_w = \frac{e^{(k_s - k_p) a_w} - 1}{(k_s - k_p) / k_p} \quad [10]$$

where ϕ_w and a_w are the water volume fraction and activity.

ENSIC equation was fitted to the average values of experimental water vapour sorption isotherm comprising three replicates for PHBV and PHBV-based composites and six replicates for WSF.

2.8. Effective moisture diffusivity identification

Effective moisture diffusivity values at different water activities were identified for WSF, PHBV and PHBV-based composites from moisture sorption kinetics measured using the DVS apparatus. The material samples, in the form of flat films, used in the DVS apparatus were thin enough for the water vapour diffusion to be considered as one-dimensional in the axial direction. The procedure, used in this study for the identification of the diffusivity coefficient (D_{eff}), was the same than that developed and presented by Guillard et al. [Guillard et al. (2003)] and successfully applied to starch based-films [Chivrac et al. (2010)] and to wheat gluten-based films [Guillard et al. (2013)]. The moisture sorption kinetic within the samples, assuming that the film did not swell, that the diffusivity coefficient remained constant for a given water activity stage, that the flux was equal to zero at the interface sample/DVS pan and that the film surface was instantaneously equilibrated at the surrounding a_w , could be modelled using the following equation [Crank (1975)]:

$$\frac{M_t}{M_\infty} = 1 - \sum_{n=0}^{\infty} \frac{8}{(2n+1)^2\pi^2} \exp\left(\frac{-D_{eff}(2n+1)^2\pi^2 t}{4l^2}\right) \quad [11]$$

where M_t (g.g(dry basis)⁻¹) denotes the total amount of water vapour which has entered the film at time t , M_∞ (g.g(dry basis)⁻¹) the quantity of water vapour content after an infinite time and l the film thickness (m).

3. Results and discussion

3.1. Water vapour sorption isotherms of PHBV, WSF and resulting PHBV-based composites

Water vapour sorption isotherm curves of WSF, PHBV and WSF-based composite films were obtained from water vapour sorption kinetics using a controlled atmosphere microbalance (DVS). Water vapour sorption isotherms of WSF and PHBV films (figure 2a) clearly highlighted the fact that the WSF films are more hydrophilic than the PHBV films; at a water activity equal to 0.95 the water content in WSF films was approximately 36 fold higher if compared to PHBV films. Water vapour sorption results were coherent with the only previous published result on moisture sorption of PHBV [Miguel et al. (1999)], which found in PHBV (8% HV), at 30 °C, a moisture content of $3.5 \times 10^{-3} \text{g.g}_{(\text{dry basis})}^{-1}$ at 50% RH and $7.0 \times 10^{-3} \text{g.g}_{(\text{dry basis})}^{-1}$ at 95%RH, against $2.05 \pm 0.47 \times 10^{-3} \text{g.g}_{(\text{dry basis})}^{-1}$ and $5.43 \pm 1.05 \times 10^{-3} \text{g.g}_{(\text{dry basis})}^{-1}$ for our PHBV (3%HV) at the same water activities but at a temperature of 20°C. Both studies (Miguel et al. and the present one) showed that the moisture sorption as function of relative humidity of PHBV film was almost linear until 80% RH and then exhibited a slightly higher slope at higher water activity.

Determination of water vapour sorption isotherms either on bulk or on single cut pieces of fibres, did not lead to any significant difference between the curves, as expected; figure 2a represents the average of all data obtained. The water vapour sorption isotherm of WSF curve displayed a sigmoidal evolution which was characteristic of hydrophilic materials and corresponded to type II of the sorption modes from Brunauer classification [Brunauer et al. (1940)]. This sigmoid shape was already presented in previous publications from the literature for different fibres of

various botanical species; agave fibres [Bessadok et al. (2009)], cellulose whisker [Belbekouche et al. (2011)], flax fibres [Alix et al. (2009)], [Gouanvé et al. (2006)] and could be described as multi-stages sorption. The present outcome highlighted the hydrophilic character of WSF which might be due to the presence of hydrophilic groups, such as hydroxyl groups of cellulose [Bessadok et al. (2009)] especially at the surface of the fibres or polar sites or micro-voids in materials [Follain et al. (2013)].

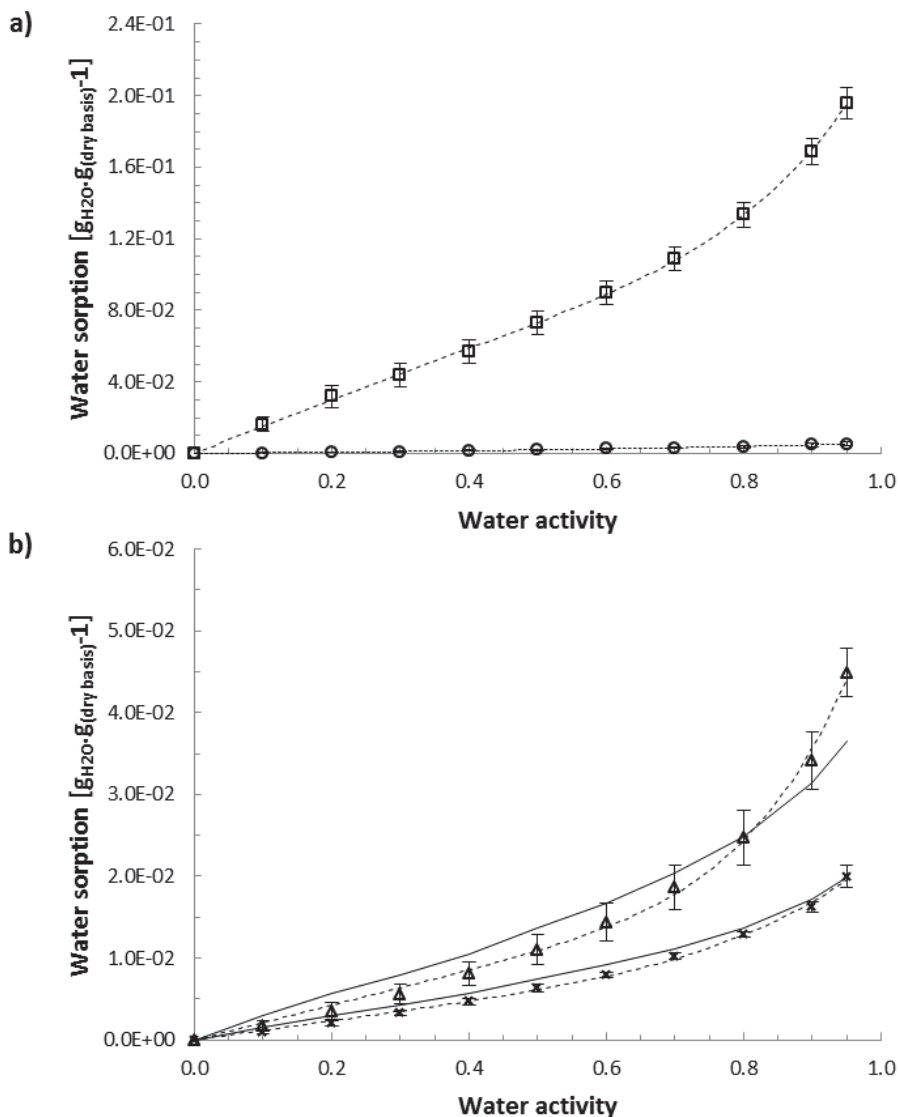


Figure 2: Water vapour sorption isotherms of PHBV (circle) and WSF (square) with the fitting of GAB equation (5) for PHBV and the fitting of Park equation (6) for WSF (dotted line) (2a), and (2b) water vapour sorption isotherm of PHBV10 (cross) and PHBV20 (triangle) with the fitting of Park (6) equation for PHBV10 and PHBV20 (dotted line), and prediction of the rule of mixture (solid line)

Water vapour sorption isotherms of resulting composites, PHBV10 and PHBV20 were shown in figure 2b and displayed the same sigmoid shape than WSF; curves with less pronounced upturns at higher water activities. As expected, the hydrophilic nature of WSF play a major role on water vapour sorption behaviour of composites as shown by the increase of water vapour content in the composites compared to neat PHBV, over the whole range of water activity. As anticipated, this effect is more pronounced at 20% WSF than 10%. These observations are in good agreement with previously published observations on water vapour sorption in poly(ϵ -caprolactone) (PCL)/cellulose nanocrystals composite [Follain et al. (2013)]. In order to further understand the contribution of each constituent, PHBV and WSF, the rule of mixtures (equation 12) was applied to predict water vapour sorption in the composite from the water vapour sorption of PHBV and WSF.

$$X_c = w_f X_f + w_p X_p \quad [12]$$

where X_c is the water vapour content in the PHBV-based composites, w_f and w_p the weight fraction of WSF and PHBV, and X_f and X_p the water vapour content of WSF and PHBV at each water activity in the range from 0 to 0.95.

Resulting plots were illustrated in figure 2b for both PHBV10 and PHBV20. In a general way, the rule of mixture permitted to approximate the water vapour sorption of the composite but most often overestimated water vapour sorption. A significant discrepancy between calculated and experimental curves shape is observed, especially for 20% WSF with an overestimation at RH lower than 80% and an underestimation for higher relative humidity. This means that the rule of mixture failed on representing the sigmoidal part of the sorption isotherm at high RH related to

fibres intrinsic properties. The water vapour sorption behaviour of composites can be concluded to not result from a simple addition of the contribution of each single constituent, which suggests that processing constituents into a composite could therefore modify their individual water vapour sorption behaviour.

3.2. Modelling of water vapour sorption isotherms of PHBV, WSF and resulting PHBV-based composites

Water vapour sorption could be considered as complex mechanism in PHBV-based composites. In order to clarify this mechanism, sorption models were applied to reach a better understanding of water vapour sorption at different water activity stages and a deeper insight on water interactions. Hence, GAB (equation 5) and Park (equation 6) were fitted to the average values of experimental water vapour sorption isotherm comprising three replicates for PHBV and PHBV-based composites and six replicates for WSF. Results are shown in figure 2 and identified parameters in table 1 with regression coefficient (R^2) and mean relative percentage of deviation modulus (E). GAB and Park models both fit experimental sorption data, with satisfying R^2 (all higher than 0.99) and E (all below 8%) values with, however a very slight advantage to the GAB model.

Table 1: GAB and Park fitting parameters which were identified from the water vapour sorption isotherm of the neat polymer matrix (PHBV), wheat straw fibres (WSF) and PHBV-based composites (PHBV10, PHBV20) at 20°C

Samples	GAB parameters					PARK parameters						
	X_m	C_g	K	R^2	E (%)	A_L	b_L	k_H	K_a	n	R^2	E (%)
PHBV	0.004	1.388	0.571	0.999	2.26	0.033	0.034	0.002	0.003	3.262	0.998	2.85
WSF	0.065	4.090	0.736	1.000	1.37	0.259	0.345	0.068	0.091	6.151	1.000	1.78
PHBV10	0.007	2.227	0.748	0.998	4.63	0.068	0.070	0.007	0.011	5.026	0.998	6.50
PHBV20	0.009	2.652	0.850	0.999	4.76	0.079	0.083	0.015	0.034	6.714	0.997	7.87

From the GAB model, the first part of the isotherm, was described essentially by the parameters X_m (water content at the monolayer) and C_g (adsorption energy of the first layers of adsorbed water); the values obtained for the composite lied logically between the values of the individual constituents (PHBV and WSF). For the last part of the isotherm, the K value was predominant by representing the adsorption energy of the second and subsequent water molecules layers. The values of K for the composite were higher than the K of WSF and pure PHBV. As previously suggested with the rule of mixture, the sorption in the composite at high a_w was confirmed to be a “non-additivity” result of each individual constituent property.

For the Park model, the parameters A_L and b_L were much lower for PHBV than WSF, indicating that the hydrophobic PHBV constituent did not own many specific sites for water vapour sorption compared to the hydrophilic WSF constituent. As anticipated the addition of WSF in PHBV results in an increase of the parameters A_L and b_L in PHBV-based composites, which however still remained lower than the WSF parameter, these two parameters representing specific hydrophilic groups able to absorb superficial water vapour molecules. The parameter k_H which described the random water vapour molecules dissolution in the materials based on Henry's law, was higher in PHBV-based composites than in PHBV and might be interpreted as the creation, by WSF presence, of specific sites for the adsorption of water vapour molecules. The parameter K_a and n , representing the formation of water clusters at high water activity, increased for WSF-based composites in comparison with PHBV. It is interesting to note that the parameter n , which is related to the cluster size (number of clustered water molecules), is higher for the 20%WSF composite (6.714) than for the individual constituents PHBV (3.262) and WSF (6.151). Large size clusters formation could be favoured by interfacial phenomena between polymer matrix and fibres.

Since water clustering can have a great influence on the water vapour transport properties [29], the clustering of water vapour molecules was more in depth investigated.

To this purpose Zimm-Lundberg's theory of water clustering in polymer and the engaged species induced clustering (ENSIC) model have been used to determine the extent of water vapour clustering in PHBV, WSF-based composites and WSF. From the Zimm-Lundberg's theory, the clustering function ($\frac{G_{w,w}}{V_w}$) and the mean cluster size (MCS) have been calculated using GAB and PARK fitting parameters for the representation of the sorption isotherm equation for respectively PHBV, WSF and PHBV/WSF composites. Significant water clustering started at water vapour activity equal to zero in PHBV, at a water activity of respectively 0.2 and 0.3 for PHBV10 and PHBV20 and 0.6 for WSF. This pointed out that PHBV formed water clusters as soon as relative humidity increased in its surrounding atmosphere confirming its hydrophobicity: due to the lack of sorption sites in PHBV, water interacted with itself.

According to figure 3, and confirming the results obtained with the Park model, water vapour molecules aggregates appeared to be larger in PHBV20 than in PHBV10, and larger in PHBV10 than in PHBV. Contrary to what it was expected through Park n parameter, WSF displayed the lowest mean cluster size with the Zimm-Lundberg's theory.

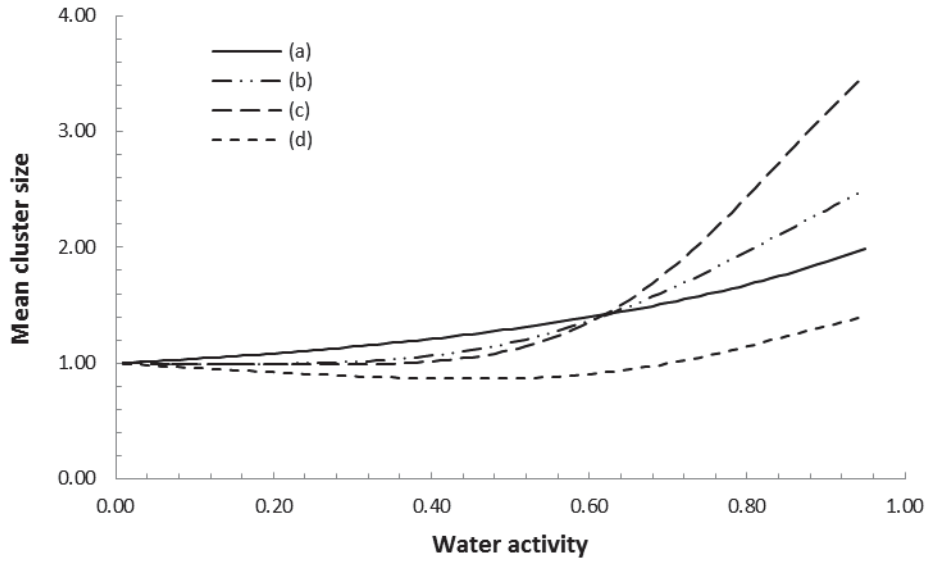


Figure 3: Application of the Zimm and Lundberg's theory (equation 8) to evaluate the mean cluster size of PHBV (a), PHBV10 (b), PHBV20 (c) and WSF (d) as function of the water vapour activity at 20°C

Water vapour clustering was also investigated with the ENSIC theory to evaluate the water-water (k_s) and water-material interactions (k_p) and resulting k_s/k_p ratio was calculated in PHBV, WSF and PHBV-WSF composites. According to the results shown in table 2, the k_s/k_p ratio was much lower in WSF (12.64) than in PHBV10 and PHBV20, and much lower than in PHBV.

Table 2: ENSIC fitting parameters, which were identified from the water vapour sorption isotherm of the neat polymer matrix (PHBV), wheat straw fibres (WSF) and PHBV-based composites (PHBV10, PHBV20) at 20°C

Sample	ENSIC parameters				
	k_p	k_s	R^2	E	k_s/k_p
PHBV	0.002	1.661	0.995	6.98	705.69
WSF	0.104	1.321	0.991	9.08	12.64
PHBV10	0.007	1.880	0.994	5.92	260.15
PHBV20	0.009	2.759	0.988	13.26	299.48

According Park, Zimm & Lundberg and ENSIC theories, developed under various hypotheses, the results were not consistent to predict in which materials water clustering would be the more important. In any case, it was highlighted that water clustering phenomena occurred in PHBV, WSF and WSF-composites with greater or lesser extent. Water vapour clustering could have an impact on water vapour mass transfer, even in the composites, by modulating the diffusivity coefficient.

3.2. Effective water vapour diffusivity

The effective moisture diffusion coefficients (D_{eff}) of PHBV, WSF-based composites and WSF were identified at 20°C from the water sorption kinetics by using equation 11. As the model used was not strictly representative of the various mechanisms of water transport prevailing in PHBV and WSF films, the identified diffusion coefficient was considered as an effective diffusivity. According to figure 4, water vapour diffusivity could be considered as constant in PHBV and WSF-based composites in the whole range of water vapour activity. In WSF, water vapour diffusivity first increased and then decreased until water vapour activities of respectively 0.3 and 0.95. This phenomenon was already observed by Gouanvé et al. (2006) in flax fibres and could be explained by a first increase of water vapour diffusivity due to an increase of the molecular mobility and then a decrease due to the formation of water clusters in WSF whose size was large enough to behave similarly as bulk liquid water [Modesti et al. (2004)] at higher water activity. However in our study while D_{eff} decreased from $a_w > 0.6$, the mean cluster size in WSF did not significantly increase. The decrease of D_{eff} should be attributed to other phenomena.

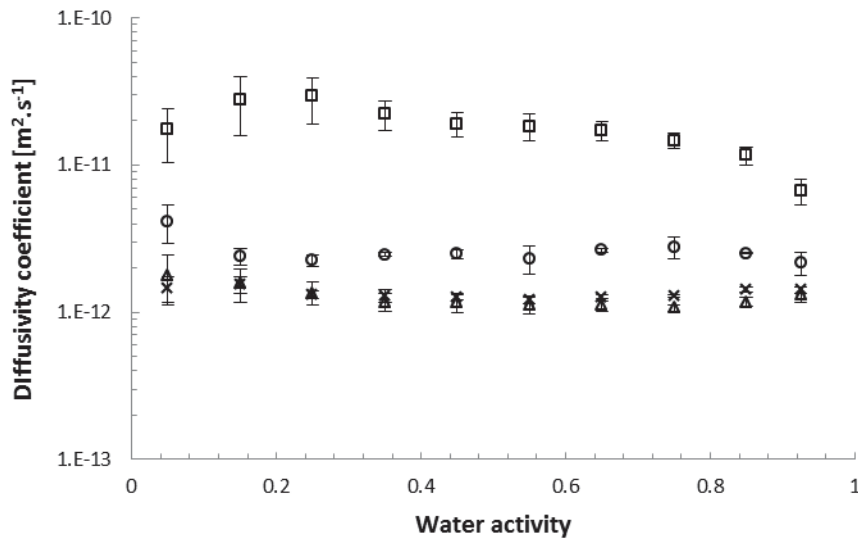


Figure 4: Effective water vapour diffusivity of PHBV (circle), PHBV 10 (cross), PHBV20 (triangle) and WSF (square) identified with equation (11)

In comparison with water vapour diffusivity in other natural fibre species (table 3), D_{eff} in the WSF was lower. It should be mentioned that the methodology used in all these published studies are different from the current one. In all previously published data of diffusion in vegetal fibres, experimental data were mostly obtained on an amount of numerous fibres, which could be as such, or shaped by different processes (compression, aqueous casting, dry laying...). Whatever the method used, the sample always contain a significant amount of air, and is more representative of a mixture of air and fibres, than of fibres alone. A higher water vapour diffusion coefficient could be explained by the presence of air, which could favour the overall water transport and thus increase the apparent diffusivity through the contribution of water vapour diffusion in the continuous gas phase (for instance water vapour diffusivity in the air equal to $2.2 \times 10^{-5} m^2.s^{-1}$).

Table 3: Water vapour diffusivity coefficients of different vegetal fibres, which were determined from water vapour sorption experiments performed on large piles of numerous fibres (data from the literature). Only the last one (present study) was obtained by testing a single piece of wheat straw

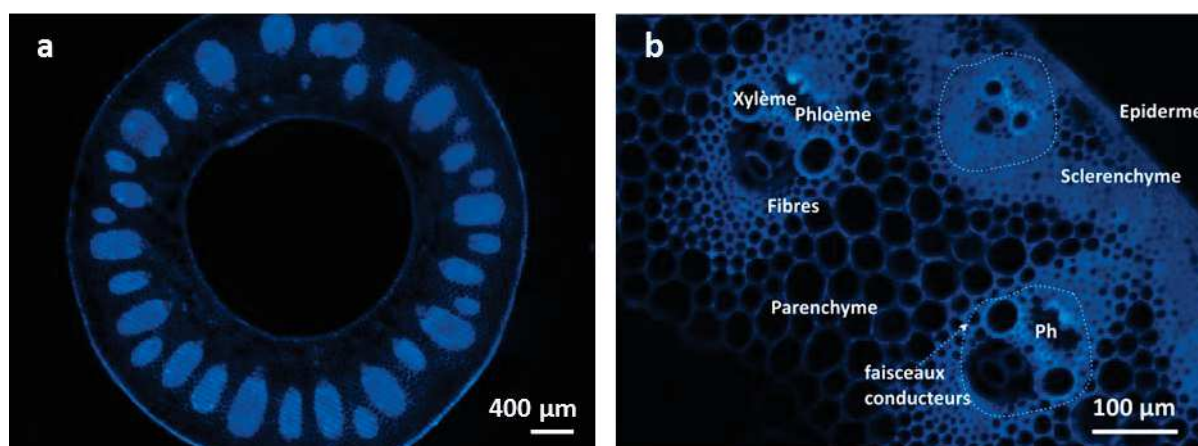
Samples	Diffusivity coefficient ($m^2.s^{-1}$)	Experimental conditions	Environment	References
Sisal cellulose whisker films	First half sorption $D_1 = 12.60 \times 10^{-8}$	Dynamic gravimetric water vapour sorption balance (DVS)	25°C, 80%RH	Belbekouche (2011) (from graphical lecture)
	Second half sorption $D_2 = 1.58 \times 10^{-8}$			
Sisal microfibrillated cellulose films	First half sorption $D_1 = 2.51 \times 10^{-8}$	Gravimetric water vapour sorption in a climatic chamber	24°C, 80%RH	Céline (2011)
	Second half sorption $D_2 = 0.50 \times 10^{-8}$			
Hemp fibre bundles	0.02×10^{-8}	Gravimetric water vapour sorption in a climatic chamber	24°C, 80%RH	Céline (2011)
Jute fibre bundles	0.04×10^{-8}			
Flax fibre bundles	0.02×10^{-8}			
Sisal fibre bundles	0.01×10^{-8}			
Agave fibres	First half sorption $D_1 = 0.46 \times 10^{-8}$	Dynamic gravimetric water vapour sorption balance (IGA)	25°C, 75%RH	Bessadok (2009)
	Second half sorption $D_2 = 2.24 \times 10^{-8}$		25°C, 84%RH	
	First half sorption $D_1 = 0.29 \times 10^{-8}$	Dynamic gravimetric water vapour sorption balance (IGA)		
	Second half sorption $D_2 = 1.60 \times 10^{-8}$			
Nonwovens flax fibres films	1.26×10^{-8}	Dynamic gravimetric water vapour sorption balance (DVS)	25°C, 80%RH	Alix (2009) (from graphical lecture)
Flax fibre fibres	First half sorption $D_1 = 79.40 \times 10^{-8}$ Second half sorption $D_2 = 179.00 \times 10^{-8}$	Dynamic gravimetric water vapour sorption balance (DVS)	20°C, 75%RH 20°C, 85%RH	This study

Although D_{eff} was higher in WSF than in PHBV, the addition of WSF in PHBV lead to unexpectedly lower D_{eff} in PHBV10 and PHBV20 if compared to D_{eff} in PHBV. A reason to this change could be related to a change in the PHBV properties, such as an increase of crystallinity. Crystals act as obstacles, and slow down the diffusion of water molecules. From the DSC measurements (table 4) it could be asserted that the addition of WSF in PHBV matrix did not have a significant impact on the crystallinity rate which stayed constant whatever the WSF content. Therefore, the unexpected trend of D_{eff} in the composite would not be linked to PHBV changes but more probably to WSF structural change once the filler is embedded in the polymer matrix.

Table 4: Characteristics of the neat polymer matrix (PHBV), wheat straw fibres (WSF) and composites (PHBV10, PHBV20)

Sample	Density (g.cm ⁻³)		Particle fraction (%)		T _c (°C)	Crystallinity	
	Experimental density	Calculated density	Weight fraction	Volume fraction		ΔH _m (J.g ⁻¹)	χ _c (%)
PHBV	1.12 ± 0.01				122.55 ± 0.08	101.67 ± 0.87	69.64 ± 0.60
WSF	1.69 ± 0.03*						
PHBV10	1.13 ± 0.03	1.16 ± 0.02	7.58 ± 1.44	5.14 ± 0.98	118.60 ± 0.04	92.05 ± 0.24	68.22 ± 0.18
PHBV20	1.16 ± 0.02	1.20 ± 0.02	16.30 ± 1.69	11.40 ± 1.20	116.11 ± 0.05	81.21 ± 0.54	66.45 ± 0.44
PHBV30	1.18 ± 0.04	1.25 ± 0.02	26.85 ± 2.31	19.52 ± 1.72	115.34 ± 0.14	72.30 ± 0.39	67.70 ± 0.37

Hence the identification of water vapour diffusivity on a piece of flat WSF and not on a single milled WSF might not reflect the same D_{eff} than in single milled WSF. Indeed as shown in figure 5a-b, the structure of a piece of WSF exhibit specific porous guide beam, such as phloem, xylem and perivascular fibres which could accelerate the diffusion of water vapour if compared the structure of single milled WSF. Hence, D_{eff} in single milled WSF dispersed in the PHBV polymer matrix could exhibit a lesser water vapour diffusivity coefficient and might be lower than D_{eff} in PHBV.

**Figure 5:** Fluorescence microscopy observation of a WSF node (3a) and internode (3b) cross sections [Ghizzi D. Silva, PhD work (2011)]

4. Conclusion

Investigating water vapour mass transfer properties of PHBV, WSF-based composites and WSF was proposed through the study of water vapour sorption and diffusion. From the water vapour sorption isotherm, it was noticed that the hydrophilic character of WSF predominantly contributed to the water vapour sorption in WSF-based composites which presented the sigmoidal shape. Contribution of both PHBV and WSF to the composite water sorption isotherm did not follow the rule of mixture, revealing the existence of other effects contributing to water vapour sorption, such as water vapour clustering, change in sorption properties of each individual component when put together in a composite structure. Based on Park, Zimm Lundberg and ENSIC theories, it was demonstrated that water clustering occurred in all materials but was not conclusive due divergence between the theories. Concomitantly, although the water vapour diffusivity coefficient was higher in the WSF than in PHBV, D_{eff} in the composites was always lower than in the PHBV. This peculiar phenomenon could be explained by the structural differences between single milled WSF and flat piece of WSF, used for the identification of D_{eff} . On that account D_{eff} in single milled WSF might be lower than D_{eff} in flat piece of WSF, and lower than D_{eff} in the PHBV. The evolution of D_{eff} in the composite could thus be understandable. In this perspective future research study should focus on a methodology to identify D_{eff} in single milled WSF dispersed in PHBV polymer matrix either through experimental or modelling works.



Publication 4

Prediction of water vapour permeability in biocomposites using theoretical models

Caroline Wolf, Nathalie Gontard, Valérie Guillard

ABSTRACT: *Water vapour permeability (P) of poly(3-hydroxybutyrate-co-3-hydroxyvalerate) (PHBV) matrix, grinded wheat straw fibres (WSF) and resulting PHBV-based composites containing 10 wt%, 20 wt% and 30 wt% of WSF was investigated. The increase of WSF percentage in PHBV led to an increase of the water vapour P of the composites, which was attributed to the high water vapour P of the WSF particles, estimated, due to technical limitations for the characterization of their P , from the product of its water vapour diffusivity coefficient (D) and its solubility coefficient (S). For predicting PHBV-based composite P from constituents' P , available models for bi-phasic materials were critically analysed, applied and compared to experimental P of the different composites. All models with and without fitting parameters successfully predicted the experimental data up to a WSF content of 20 wt%. The failure of all models in predicting the high P of composite containing 30 wt% of WSF was attributed to a deterioration of the barrier properties of the matrix at high WSF content.*

KEYWORDS : Fibres, Polymer-matrix composites, Transport properties, Modelling; water vapour permeability

1. Introduction

In the past few years, composite materials came out to be suitable structures for the design of food packagings [Azeredo et al. (2009), Arora et al. (2010), Silvestre et al. (2011), Rhim et al. (2013)]. Hence a lot of researches, in both industrial and academic fields, have been carried out in order to broaden the knowledge on composites manufacturing, structures and properties. With regard to the global growing conscience linked to the misuse of non-biodegradable petroleum-based plastics, biopolymers [Syracusa et al. (2008)] and biocomposites [Johansson et al. (2012)] could be good alternatives. However, the biopolymers and biocomposites should exhibit the same mechanical, thermal and barrier properties than the synthetic ones. For example poly(3-hydroxybutyrate-co-3-hydroxyvalerate) (PHBV), an eco-friendly biopolyester, offers good barrier properties against water vapour transmission, similar to those of conventional thermoplastic of moderate hydrophobicity such as PVC and PET [Miguel et al. (1999), Cava et al. (2006)]. Indeed mass transfer properties are of major importance in the field of food packaging as regard to food preservation and conservation. A lot of publications have already dealt with the experimental study of water vapour mass transfer in biopolymer-based composites [Rhim et al. (2009), Sanchez-Garcia et al. (2010), Katiyar et al. (2011), Fortunati et al. (2012)] but only a few on water vapour transfers in vegetal fibres-based biocomposites. Among the rare studies on water vapour transfer on fibres-based composite, Alix et al. (2008) and Pardo-Ibanez et al. (2014) have studied the importance of fibres transfer properties (flax for Alix et al. and keratin for Pardo-Ibanez et al.), of fibres distribution in the polymer matrix and of fibres effect on matrix characteristics (such as crystallinity), on final biocomposites water vapour sorption and permeability properties.

In contrast with permeable fibres based composite, numerous papers have been published on assessment and modelling of mass transfer properties of composite containing impermeable nano-particles [Choudalakis et al. (2009), Nazarenko et al. (2007), Picard et al. (2007), Alexandre et al. (2009)]. In theory, incorporation of impermeable particles in a polymer matrix lead to a decrease of the permeability due to an increase of the path length that the penetrant molecule needs to follow, i.e. a tortuosity effect due to the presence of the particles. Nevertheless when these particles are permeable, these models are no more useable for the prediction of barrier properties because they did not take into account the permeability of the particles. For predicting the permeability in particulate composites (for separative membrane applications) with two permeable phases, mathematical models initially developed for the prediction of dielectrics [Maxwell (1873)], thermal and mechanical [Lewis et al. (1970), Nielsen et al. (1973)] properties in bi-phasic materials were adapted to the prediction of permeability in particulate composites with two permeable phases, [Gonzo et al. (2006), Pal et al. (2008), Aroon et al. (2010), Petsi et al. (2012)].

In order to improve the knowledge and prediction of water vapour transport in bi-phasic composite materials, and favour their applications as food packaging, the present study aims at providing a better understanding of water vapour permeability in the promising WSF-based composites. In this perspective, an analysis of available models for predicting properties of bi-phasic permeable composites was carried out and the ability of these models to predict the impact of particle volume fraction on water vapour permeability of PHBV/WSF biocomposites were discussed based on experimental data.

2. Theory on analytical biphasic models

Since the 1990s a lot of experimental studies have been carried out in the membrane area and especially in composites due to their high technological potential in terms of barrier properties [Koros et al. (2013), George et al. (2001)]. These membranes exhibited heterogeneous structures consisting in the dispersion of inorganic particles in a polymer matrix and were used in many applications such as H₂ separation, O₂/N₂ separation, natural gas separation such as removing of CO₂, vapours separation and dehydration of air [Hwang et al. (2011)]. Indeed these materials were very effective in that field because they allowed good gas separation and the access to high selectivity; one of the major objectives in membrane sciences. In order to avoid systematic experimental characterization of each new composite materials, need of mathematical modelling approach has emerged for prediction of permeability in composites. From analogy between electrical/thermal conductivity properties and permeability properties, models have been proposed to predict the effective permeability of composites. Petropoulos et al. in 1985 was one of the first authors who reviewed these theoretical approaches and compared the models to experimental gas permeability values in polymer blends. Afterwards Aroon et al. (2012) proposed a review on the study of gas separation efficiency of mixed matrix membranes by discussing the different predictive models according to the nature of the particle and by addressing particle/polymer matrix interfacial defects. Besides Gonzo et al. (2006) and Pal et al. (2008) have listed some models and Petsi et al. (2012) have developed a new numerical computational model for the prediction of effective permeability in mixed matrix membranes. Hashemifard et al. (2010) discussed the gas permeabilities, such as oxygen, carbon dioxide, nitrogen and methane in these membranes filled zeolites NaA and NaX with using theoretical models and the results

were compared with the published experimental data; they demonstrated Felske model Felske et al. (2004), which take into consideration the interphase particles/polymer matrix, provided the better agreement with experimental data.

The models, gathered in table 1, related the effective permeability of the composite P_{eff} as function of the permeability of the polymer matrix P_c which is considered as the continuous phase, the permeability of the particles P_d which is considered as the dispersed phase and at least the volume fraction of the particles ϕ_d . Most of these models directly depicted the permeability of the composite as function of the volume fraction of particles but other models needed first to be numerically solved before obtaining the permeability of the composite as function of the particle volume fraction as explained in the previous section [Banhegyi et al. (1986), Bouma et al. (1997), Pal et al. (2008)]. Some other models could also have additional fitting parameters such as the maximum volume packing of the particles ϕ_m [Lewis et al. (1970), Nielsen et al. (1973), Pal et al. (2008)], the percolation threshold constant ϕ_t , a shape factor, n , related to the geometry of the particle [Banhegyi et al. (1986), Bouma et al. (1997)] or even a fully empirical constant K_H [Higushi et al. (1958)].

The first well-known models applied for the prediction of material properties, such as mechanical, thermal and barrier properties, were the series (equation A) and parallels (equation B) models. In the case of mass transfer and whatever the shape of the particles, spherical or ellipsoids, the values predicted by these two models were usually considered as respectively the minimum and the maximum values of the effective permeability. In case of a dilute dispersion of spheres or ellipsoids, fully oriented along the axis of the diffusion direction, the permeability of the composite membrane could be expressed with the Maxwell-Wagner-Sillars equation

(equation C). In equation C, the parameter n represented the shape factor of the particle and took different values according to the geometry of the particles; for prolate ellipsoids, i.e. the longest axis of the ellipsoid is directed along the diffusion direction $0 \leq n \leq 1/3$, for spherical particle $n = 1/3$, for oblate ellipsoids, i.e. the shortest axis of the ellipsoids is directed along the diffusion direction $1/3 \leq n \leq 1$. For spherical particle, when $n=1/3$, equation C could be rewritten and simplified as equation D. The so-called Maxwell model has been widely used in membrane applications for the prediction of permeability in bi-phasic systems. However, its used is restricted to filler volume fraction lower than about 20% under the assumption that the flux pattern around one particle was not affected by the presence of neighbour particles [Maxwell (1873), Banhegyi et al. (1986), Bouma et al. (1997)]. Like the Maxwell model, the Böttcher model (equation E) and the Higushi model (equation F) were used for the prediction of permeability properties in composites at low particle volume fraction with random dispersion of spheres. The parameter K_H in Higushi model was treated as an empirical constant and assigned to a value of 0.78 by Higushi himself on the basis of experimental data. The Bruggeman model (equation G) was particularly appropriate for the prediction of composite permeability when there were small differences between the matrix and the particle permeability and, contrary to the Higushi and the Maxwell model, for higher particle loading higher than 20% [Bruggeman (1935), Banhegyi et al. (1986), Bouma et al. (1997)].

Based on the percolation theory (equation H), Chiew et al. (1983) have proposed an extension of the Maxwell model represented by (equation I, J) in Table 1. The second term ($3\beta\phi_d$) of the equation represented the interaction between particles and the polymer matrix and the third term ($K\phi_d^2$) the interaction between the particles themselves. Instead of applying the percolation theory to describe the maximum

volume concentration of particles, another possibility is to use the theory of the maximum packing volume of particles represented by the parameter ϕ_m , which is function of the particle size distribution, shape and aggregates. Lewis-Nielsen model (equation K) and Pal model (equation L) gave accurate prediction of the effective permeability of the composite until the maximum packing volume fraction of particles.

The aforementioned models assumed ideal contact between the particles and the matrix, i.e. a well-defined interface. But in some cases, the interphase polymer/particles presented defects as for example interfacial void space between the two phases due to bad adhesion between polymer and particles. Besides polymer matrix changes has been observed when the polymer molecules in direct contact with the particle surface became more rigidified in comparison to the bulk polymer molecules [Chung et al. (2007), Cong et al. (2007)]. In order to take into account the presence of defected interphase in composites, several authors have tried to propose more complex model to predict the effective permeability of the composites. For example, Mahajan et al. (2002), working on a zeolite/polyimide system, have put in evidence the existence of an interphase particles-polymer matrix. Confirming this, by applying the Maxwell model on their results, they observed some deviations between modelled and experimental data at high particles contents even if they obtained a satisfactory prediction at low particles contents up to 15vol% [Mahajan et al. (2000)] As a consequence, they proposed an extension to the Maxwell model by considering the existence of a third phase, i.e. an interphase, a polymer region near the particle/polymer matrix interface owing its own permeability value [Mahajan et al. (2002)]. In the present case, the authors assumed that the interphase displayed a reduced permeability compare to that of the neat

polymer due to chain immobilization in the interphase. Other authors have focussed on the prediction of permeability in multi-phase composites, with at least three phases [Pal et al. (2008), Felske et al. (2004), Shariati et al. (2011)].

The experimental determination of the permeability of the dispersed phase, i.e. the particle in the case of composites, and if necessary, that of the interphase particle/polymer could hinder the prediction of permeability in composites with these last models. To overcome this difficulty, the models have often been fit to the experimental data by adjusting the ratio P_d/P_c [Gonzo et al. (2006)] and the permeability at the interphase [Pal et al. (2008)] considered therefore, as fitting parameters. In some rare studies, the permeability of the dispersed phase has been successfully experimentally measured, either on native inorganic materials before being milled in zeolites [Mahajan et al. (2002)] or on native vegetal material before being milled in fibres [Wolf et al. (forthcoming (c))]. However, the aforementioned studies remain some rare cases for this kind of determination.

Table 1: Analytical bi-phasic models for the prediction of the permeability in composite materials with permeable particles

Model	Geometry of the system	Geometrical input parameters	Fitting parameters	Mathematical equation	Additional equations	Validity of the model	Reference
Series model	Suspension of spheres	ϕ_d : particle volume fraction ϕ_c : matrix volume fraction		$\frac{1}{P_{eff}} = \frac{\phi_d}{P_d} + \frac{\phi_c}{P_c}$ [A]			Petropoulos (1985)
Parallels model				$P_{eff} = \phi_d P_d + \phi_c P_c$ [B]			Petropoulos (1985)
Maxwell-Wagner-Sillars	Dilute suspension of ellipsoids	ϕ_d : particle volume fraction	n : related to the geometry of the particle	$P_{eff} = P_c \left[\frac{n P_d + (1-n) P_c + (1-n) \phi_d (P_d - P_c)}{n P_d + (1-n) P_c - n \phi_d (P_d - P_c)} \right]$ [C]		$0 < \phi_d < 0.2$ $0 < \phi_d < \phi_m$	Maxwell (1983), Banhegyi (1986), Bouma (1997)
Maxwell	Dilute suspension of spheres	ϕ_d : particle volume fraction		$P_{eff} = P_c \frac{1+2\beta\phi_d}{1-\beta\phi_d}$ [D]	$\beta = \frac{P_d - P_c}{P_d + 2P_c}$	$0 < \phi_d < 0.2$ $0 < \phi_d < \phi_m$	Maxwell (1983), Banhegyi (1986), Bouma (1997)
Böttcher	Random suspension of spheres	ϕ_d : particle volume fraction		$\left(1 - \frac{P_c}{P_{eff}}\right) \left(\frac{P_d}{P_c} - 2 \frac{P_{eff}}{P_c}\right) = 3\phi_d \left(\frac{P_d}{P_c} - 1\right)$ [E]		Low ϕ_d	Petropoulos (1985)
Higushi	Random suspension of spheres	ϕ_d : particle volume fraction	K_H : empirical constant	$P_{eff} = P_c \left[1 + \frac{3\phi_d \beta}{(1-\phi_d \beta - K_H(1-\phi_d \beta^2))} \right]$ [F]	$\beta = \frac{P_d - P_c}{P_d + 2P_c}$	Low ϕ_d	Higushi (1957)
Bruggeman	Dilute and random suspension of spheres	ϕ_d : particle volume fraction		$\left(\frac{P_{eff}}{P_c} - \frac{P_d}{P_c}\right) \left(\frac{P_{eff}}{P_c}\right)^{-1/3} = 1 - \phi_d$ [G]		High ϕ_d $0 < \phi_d < \phi_m$	Bruggeman (1935)
Percolation theory	Suspension of spheres	ϕ_d : particle volume fraction ϕ_c : percolation threshold		$P_{eff} = P_d (\phi_d - \phi_c)^t$ [H]		Low ϕ_d	Chiew (1983) Gonzo (2006)
Chiew-Glandt	Random suspension of spheres	ϕ_d : particle volume fraction		$P_{eff} \approx P_c (1 + 3\beta\phi_d + 3(\beta\phi_d)^2 + O(\phi_d^3))$ [I]	$K = a + b \phi_d^{3/2}$	Low ϕ_d	Chiew (1983)
Modified Chiew-Glandt	Random suspension of spheres			$P_{eff} = P_c (1 + 3\beta\phi_d + K\phi_d^2 + O(\phi_d^3))$ [J]	$a = -0.002254 - 0.123112\beta + 2.93656\beta^2 + 1.690\beta^3$ $b = -0.0039298 - 0.803494\beta - 2.16207\beta^2 + 6.48296\beta^3 + 5.27196\beta^4$	Low ϕ_d	Chiew (1983)
Lewis-Nielsen	Dilute suspension of particles	ϕ_d : particle volume fraction	ϕ_m : maximum packing volume of particles	$P_{eff} = P_c \left[\frac{1+2\left(\frac{P_d}{P_c}-1\right)\phi_d}{1-\left(\frac{P_d}{P_c}-1\right)\phi_d\psi} \right] \phi_d \psi$ [K]	$\psi = 1 + \left(\frac{1-\phi_d}{\phi_m^2}\right) \phi_d$	$0 < \phi_d < \phi_m$	Lewis (1970) Nielsen (1973)
Pal	Dilute suspension of particles	ϕ_d : particle volume fraction	ϕ_m : maximum packing volume of particles	$\left(\frac{P_{eff}}{P_c}\right)^{1/3} \left[\frac{\left(\frac{P_d}{P_c}-1\right)}{\left(\frac{P_d}{P_c}-\frac{P_{eff}}{P_c}\right)}\right] = \left(1 - \frac{\phi_d}{\phi_m}\right)^{-\phi_m}$ [L]		$0 < \phi_d < \phi_m$	Pal (2007)

3. Experimental

3.1. Materials

Commercial poly(3-hydroxybutyrate-co-3-hydroxyvalerate) (PHBV) was supplied by Tianan under the reference Y1000P with HV content 3%. Wheat straw (*Triticum aestivum* cv. Apache) was provided by Fernand Meaux (Saint Jean du Salés, Aveyron, France), harvested in 2007 and was ground to obtain wheat straw fibres. The wheat straw fibres (WSF) were impact-milled at a size of 100-150 μm and the median diameter of the fibre is around 62 μm using a process previously developed by [Ghizzi D. Silva et al. (2012)] and re-use recently by [Berthet et al. (2014)].

3.2. Materials and film preparation

PHBV and PHBV-based composites with 10 wt%, 20 wt% and 30 wt% fibre weight fraction (PHBV10 and PHBV20) were prepared by extrusion using a lab-scale twin-screw extruder (Eurolab from ThermoFisher Scientific). After extrusion, the obtained pellets were dried in an oven at 60 °C for at least 8 h. Then, the compounds were heated 5 min at 170 °C between two Teflon-coated plates and then thermo-moulded for 5 min at 150 bar and 170 °C with a heated hydraulic press (PLM 10 T, Techmo, Nazelles, France) to obtain films [Berthet et al. (2014)].

3.3. Optical microscopy

Optical microscopy observations of PHBV20 cross-sections were performed on thin samples (cuts of approximately 3 μm) obtained after the cut with a microtome of composite samples previously embedded in Technovit ® hydroxyethylmethacrylate resin. A Leica MacroFluo Leica Z6 APO 16:1 was used for the observations.

3.4. Water vapour permeability

Experimental water vapour permeability ($WVP(\text{exp})$) were gravimetrically determined at 20 °C for a relative humidity difference of 100% using a modified ASTM procedure [Gontard et al. (1993)]. The samples (discs of 33 mm diameter) were hermetically sealed (with Teflon seals) in a glass permeation cell containing distilled water. The permeation cells were placed in a desiccator containing P_2O_5 , thus obtaining a relative humidity (RH) gradient equal to 100% (assuming that the relative humidity on P_2O_5 is negligible). The water vapour transfer through the exposed film area (8.55 cm^2) was measured from the cell weight loss as a function of time. The cells were weighed using a four-digit balance every 48 hours over a 20 days period after a steady-state vapour flow had been reached. Six samples of each type of film were tested and the water vapour permeability ($\text{mol}\cdot\text{m}^{-1}\cdot\text{s}^{-1}\cdot\text{Pa}^{-1}$) was calculated from the following equation:

$$WVP(\text{exp}) = \frac{\theta \times l}{A \times \Delta P} \quad [1]$$

where θ is the slope of the weight loss versus time ($\text{g}\cdot\text{s}^{-1}$), l is the film thickness at equilibrium measured at the end (m), A is the area of exposed film (m^2), and ΔP is the water vapour pressure differential across the film at 20°C and $\Delta P = 2338 \text{ Pa}$.

The calculated water vapour permeability (WVP_{calc}) was obtained by the following relation:

$$WVP_{calc} = S_{calc} \times D_{eff} \quad [2]$$

The solubility coefficient (S_{calc}) was calculated from the water sorption isotherm measured in [Wolf et al. (forthcoming (c))] by using the relation previously established by Bourlieu et al (2006):

$$S_{calc} = \frac{\rho_{film}}{M \cdot p_w} \left(\frac{X_1 - X_2}{aw_1 - aw_2} \right) \quad [3]$$

where X_1 is the moisture content ($g \cdot g_{(dry \ basis)}^{-1}$) of the film at aw_1 and X_2 the moisture content ($g \cdot g_{(dry \ basis)}^{-1}$) at aw_2 , ρ is the film density ($g \cdot m^{-3}$) and p_w the saturated water vapour pressure (Pa) at a constant temperature (20 °C).

The effective diffusivity coefficient (D_{eff}) was taken from previous work [Wolf et al. (forthcoming (c))] It was determined from transient water vapour sorption kinetic. A D_{eff} value was obtained for each RH step experimentally assayed. For each material, PHBV, WSF and PHBV-based composites, D_{eff} was averaged on the whole range of water activity from 0 to 0.95.

3.5. Numerical implementation of the analytical bi-phasic models

Equation D, F and K were implemented in Excel 2010 for the identification of the fitting parameters n , kH and ϕ_m respectively. Fitting in Excel was carried out by using the GRG nonlinear solver (table3).

Equation E, G and K, were numerically solved on Matlab software. The equation was rewritten in order to get a polynomial equation of degree 2 for equation E and of degree 3 for equation G and K, with P_{eff}/P_c as polynomial indefinite. The real and positive root of the polynome was calculated for each filler content. The identification of parameter on Matlab software was done using a Levenberg-Marquardt method for equation K (table 3).

The identification either in Excel or in Matlab was performed from the experimental relative permeability values by minimizing the root mean square of the deviation between simulated and experimental results. In order to evaluate the goodness of the fit of each model to the experimental data, the RMSE value was determined for Excel and Matlab identification.

4. Results and discussion

4.1. Water vapour permeability experimental data

The water vapour permeability of PHBV, PHBV10, PHBV20 and PHBV30 were experimentally determined at 20°C from a modified ASTM method for a 0-100% relative humidity (RH) gradient. The relative water vapour permeability, i.e. the ratio of the permeability of PHBV10, PHBV20 and PHBV30 to PHBV as function of the particle volume fraction were reported in figure 1 and the absolute values of water vapour permeability were reported in table 2.

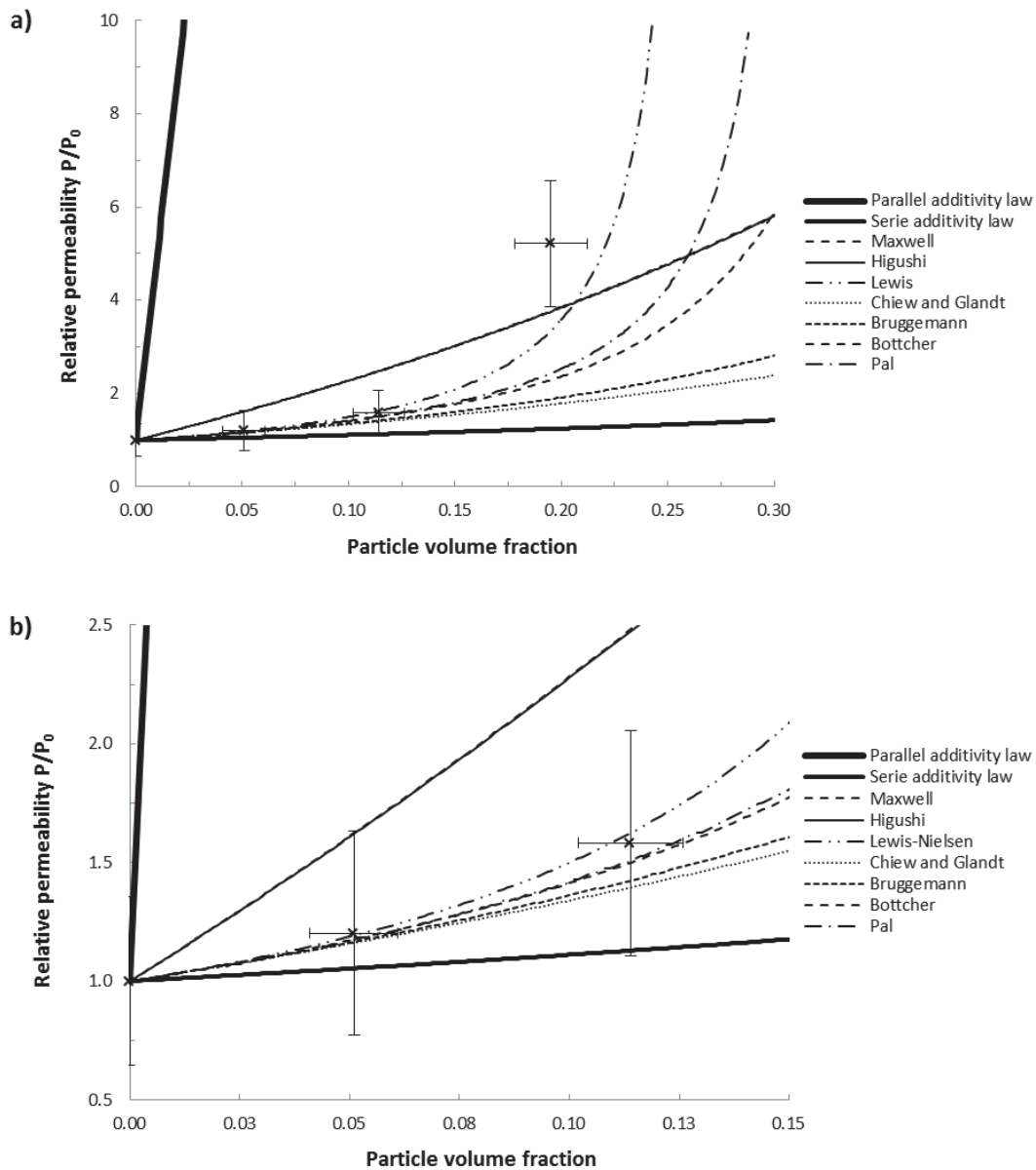


Figure 1: Prediction of the relative permeability as function of particle volume fraction with analytical (quoted in table 1) for the first set of data up to 19.52 vol% until 30 vol% (a) and until 15 vol% (b)

Table 2: Characteristics of polymer matrix (PHBV), wheat straw fibres (WSF) and PHBV-based composites (PHBV10, PHBV20) at 20 °C

Sample	Solubility coefficient from DVS ($\text{mol}\cdot\text{m}^{-3}\cdot\text{Pa}^{-1}$)	Diffusivity coefficient from DVS ($\text{m}^2\cdot\text{s}^{-1}$)	Experimental water vapour permeability WVP(exp) ($\text{mol}\cdot\text{m}^{-1}\cdot\text{s}^{-1}\cdot\text{Pa}^{-1}$)	Calculated water vapour permeability ^(c) WVP(calc) ($\text{mol}\cdot\text{m}^{-1}\cdot\text{s}^{-1}\cdot\text{Pa}^{-1}$)
PHBV	$1.583 \pm 0.280 \times 10^{-01}$ (a)	$2.615 \pm 0.351 \times 10^{-12}$	$1.096 \pm 0.257 \times 10^{-12}$	$0.414 \pm 0.092 \times 10^{-12}$
WSF	$90.656 \pm 3.498 \times 10^{-01}$ (b)	$18.395 \pm 3.78 \times 10^{-12}$		$1.668 \pm 0.349 \times 10^{-10}$
PHBV10	$6.068 \pm 0.282 \times 10^{-01}$ (b)	$1.344 \pm 0.288 \times 10^{-12}$	$1.317 \pm 0.334 \times 10^{-12}$	$0.816 \pm 0.179 \times 10^{-12}$
PHBV20	$1.512 \pm 0.107 \times 10^{-00}$ (b)	$1.283 \pm 0.259 \times 10^{-12}$	$1.735 \pm 0.283 \times 10^{-12}$	$1.940 \pm 0.416 \times 10^{-12}$

As expected an increase of the permeability as function of particle volume fraction was observed; 1.20 ± 0.43 , 1.58 ± 0.47 , and 5.22 ± 1.36 fold higher in PHBV10, PHBV20 and PHBV30. From Publication 1, it was found that the water vapour sorption and diffusion in WSF was 36 and 7 times higher than in PHBV respectively. Hence, WSF provided the main contribution in the overall mass transfer of the composites.

However the standard deviation of the experimental data for the composites was very high and overlapped for PHBV, PHBV10 and PHBV20. This result could be explained by the heterogeneity of the composites, i.e. the size, the shape, the dispersion and the orientation of the wheat straw particles within the polymer matrix as revealed by optical microscopy pictures in figure 2.

Indeed during the process of composites, wheat straw fibres might not be well-dispersed and during film forming the distribution of wheat straw fibres within the film would not be homogeneous resulting in samples with heterogeneous repartition and content of fibres. This was supported by the ash content results which served to precisely determine the filler volume fraction from the inorganic residue mass. From ash content determination presented in [Wolf et al. (forthcoming (c))], the exact filler volume weight fraction was found equal to 7.5 ± 1.44 wt%, 16.30 ± 1.69 wt% and 26.85 ± 2.31 wt% equivalent to 5.14 ± 0.98 vol%, 11.40 ± 1.20 vol% and 19.52 ± 1.72 vol% for PHBV10, PHBV20 and PHBV30 respectively. For all weight fractions, the exact filler content (estimated from a representative mass of material 2-5 g) was lower than the expected experimental filler content and was subjected to high standard deviation underlining the heterogeneity of the samples [Wolf et al. (forthcoming (c))].

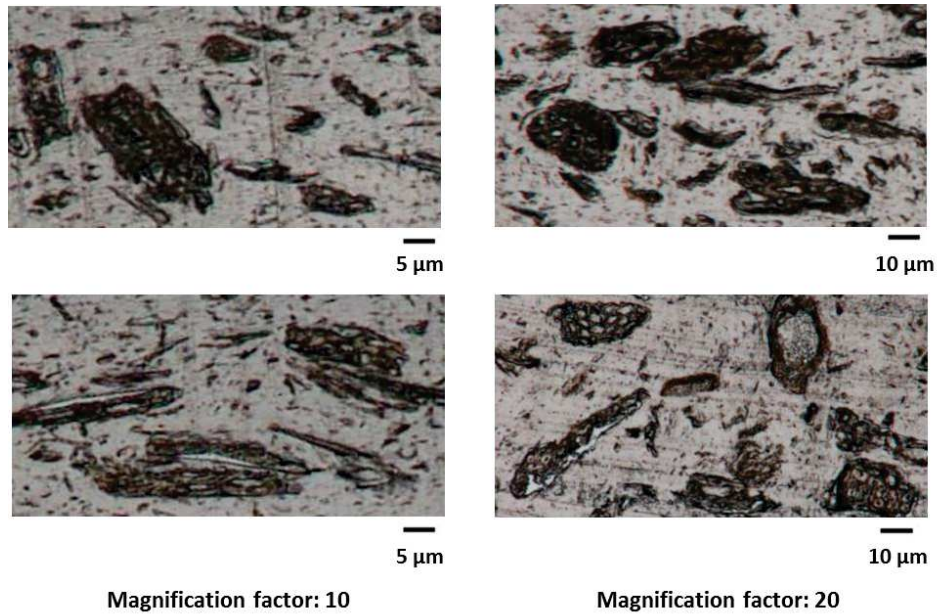


Figure 2: Optical microscopy observations at 10 and 20 magnification of PHBV20 composites cross-section cutting

In order to use the predictive permeability models previously quoted, the permeability of the wheat straw fibre was needed but was not directly experimentally accessible. Considering the solution-diffusion mechanism, $P=D \times S$, the permeability ($WVP(\text{calc})$) in the particle has been calculated as the multiplication of the solubility and diffusivity coefficient. This relation could be applied on the assumption that the addition of WSF in PHBV matrix would not have an influence on the polymer matrix. The solubility was calculated using equation 3 from the water sorption isotherm previously determined on a piece of wheat straw [Wolf et al. (forthcoming (c))]. D_{eff} was taken in the same previous work, was averaged on the whole range of water activity and was found equal to $18.395 \pm 3.78 \times 10^{-12} \text{ m}^2 \cdot \text{s}^{-1}$.

In the same way the $WVP(\text{calc})$ in neat PHBV and PHBV-based composite were calculated for a 0-95% RH difference for further comparison with $WVP(\text{exp})$. All results were gathered in Table 2. $WVP(\text{calc})$ and $WVP(\text{exp})$ were not significantly different for PHBV-based composite while $WVP(\text{calc})$ of PHBV was significantly lower (around

two times) than the corresponding WVP(exp). This discrepancy for neat PHBV could be ascribed to the uncertainty relying on the D_{eff} and S determination for this polymer. Indeed, the high hydrophobicity of the polymer has hampered the accurate determination of the water sorption kinetics (measured using a controlled Cahn microbalance). Indeed, the mass uptake by the PHBV for each RH step imposed by the balance to the material to build the sorption curve was too low and thus in the limit of sensitivity of the balance.

In the literature, Crétois et al. (2014) and Fabra et al. (2014) have found water vapour permeability equal to $4.99 \pm 0.20 \times 10^{-14}$ and $3.88 \pm 0.39 \times 10^{-13} \text{ mol.m}^{-1}.\text{s}^{-1}.\text{Pa}^{-1}$ respectively at 25°C and 0-100%RH on the same neat PHBV materials also processed through melt-compounding and compression moulding. The discrepancies in the values could arise from the different method of water vapour permeability characterization; home built apparatus with a permeation cell [Crétois et al. (2014)] or cup method [Fabra et al. (2014)]. However the values was higher than our for both WVP(exp) at 20 °C and 0-100%RH and WVP(calc) at 20 °C and 0-95%RH. Zembouai et al. (2013) have found a water permeability equal to $1.28 \times 10^{-13} \text{ mol.m}^{-1}.\text{s}^{-1}.\text{Pa}^{-1}$ at 23 °C and 0-50%RH for film prepared through melt-mixing and compression moulding, and water vapour permeability characterized with the cup cell method. Although the relative humidity gradient across the film was not the same, this value was more in agreement with ours.

The WVP(calc) for the piece of wheat straw was 100 fold higher than that of neat PHBV. This confirmed that the WSF particles were much more permeable than the PHBV matrix and that they highly contributed to the overall mass transport in the composite material and especially when fibres volume fractions increased. In the

following $WVP(\text{calc})$ in the WSF (namely P_d in the models) and $WVP(\text{exp})$ in PHBV (namely P_c) were considered in the biphasic models for the prediction of the permeability in WSF-based composites.

4.2. Predicting permeability in PHBV-based composites with analytical biphasic models

Once all the input parameters were determined, i.e. the permeability in the polymer matrix (P_c), the permeability in the wheat straw fibres (P_d), the polymer volume fraction (ϕ_c) and the particle volume fraction (ϕ_d), all the models from table 1 were tentatively used to predict the experimental permeability of the composite as function of particle volume fraction; resulting plots were represented in figure 2. Among all the models used, only the series and parallels laws (equation A,B) and Chiew and Glandt model (equation J) could be applied without any adjustment while Maxwell, Higushi and Lewis-Nielsen models (equation C,G, K) required the fit of at least one parameter, n , k_H or ϕ_m , namely the shape factor, an empirical parameter and the maximum packing volume for the particles. Contrary to the aforementioned models (Maxwell, Higushi and Lewis-Nielsen) which are explicit relationships, Bruggeman (equation E), Böttcher (equation F) and Pal (equation L) models required a numerical solving on Matlab software.

As expected, series and parallels models were positioned at the extremes of the graph in figure 1, parallel model predicting the highest ratios while the series model the lowest ones. However the prediction of permeability from the series model was better and located in the bottom of the standard deviation error bars for the PHBV, PHBV10 and PHBV20 experimental permeability values. In fact and after optical

microscopy pictures investigation (figure 2) of the composite structures, the particles seemed to be oriented perpendicularly to the diffusion flux and thus the series model was more appropriate for the prediction of the permeability than the parallels ones. The prediction of permeability from Chiew and Glandt, Bruggeman, and Böttcher models, without any adjustments of any parameters, were in good agreement with the experimental data until a wheat straw fibres content of 11.40 vol%. At higher loading there were discrepancies between the prediction of the permeability of PHBV30 with the models and the experimental relative permeability values; the predicted values at 19.52 vol% was 34%, 36% and 44% lower than the experimental value for Chiew and Glandt, Bruggeman and Böttcher models respectively.

Maxwell, Higushi and Lewis-Nielsen models were then used and for this purpose, n , K_H and ϕ_m were identified from the fit of the model to the experimental permeability values. As expected, the fit on the whole set of experimental data failed confirming the change in WVP behaviour between 11.40 vol% and 19.52 vol%. Therefore, the fit of these models was carried out in two steps: first fit on experimental data up to 19.52 vol% and second fit with all the data up to 11.40 vol%; all the resulting fitting parameters were gathered in table 3. The prediction of Higushi and Maxwell models were quasi equivalent as evidenced by the superposition of the curves in figure 2. The fitting parameter in Higushi model was the empirical constant K_H equal to 0.78 in the initial model building. In the case of the present fits, K_H was found equal to 0.78 and 0.14 for respectively the first and second set of data. This result was not a proof that the prediction was better for the first set of data because the 0.78 value had no geometrical or physical meaning. Indeed in another previous study [Sadhegi et al. (2011)], Sadhegi et al. used the Higushi model for the prediction of gas permeability in membranes made up of silica nanoparticles/polyether-based polyurethane and in

their system, the value of K_H was comprised between 2 and 3 according to the gas nature. The K_H value might be more related to the nature of the migrant than the geometry of the particle.

The fitting parameter in Maxwell model was, as presented previously, a constant related to the geometry of the particles. In the present case, the fit of the first set of data was obtained for n equal to 0.08 while the fit of the second set of data gave a n value equal to 0.29. In line with the optical microscopy observations and previous work of [Berthet et al. (forthcoming)], the wheat straw fibres used in this study exhibited spherical and cylinder shape with an average diameter of 62 μm and a mean aspect ratio of 2. The two fits of Maxwell model with the corresponding identified n values confirmed that globally the WSF particles were not spherical but rather ellipsoidal (n comprised between 0 and 1/3). However, a steep change of this shape factor occurred between 11.40 vol% and 19.52 vol% which remained at present unexplained.

As the Maxwell model, the Lewis-Nielsen model considered a geometrical parameter, the maximum volume packing fraction of particles ϕ_m . As previously stated by Petropoulos et al. (1985), the maximum volume packing in the case of spherical particles system is equal to 0.64 and in cylinder particles system equal to 0.79. In the present case, the fit of the first set of data was obtained for ϕ_m equal to 0.36 while the fit of the second set of data was obtained for ϕ_m equal to 0.46.

Pal model, as Lewis-Nielsen was fitted to the experimental data using the maximum volume packing fraction of particles. Hence, the fit of the first set of data was obtained for ϕ_m equal to 0.31 while the fit of the second set of data was obtained for ϕ_m equal to 0.22. Even if, the Lewis-Nielsen and Pal models considered the same geometrical parameter, the resulting identified ϕ_m value differed from one model to

the other (Table 3). Moreover the evolution of the fitting parameter did not follow the same trend, for the Lewis-Nielsen model an increase of ϕ_m value between the first to the second fit while for the Pal model a decrease of ϕ_m value between the first to second fit was decreased. The representative of this ϕ_m parameter remained questionable in the case of our biocomposites.

Table 3: Resulting fitting parameters from the prediction of the permeability in bi-phasic material with analytical model for the first set of data up to 19.52 vol% and the second set of data up to 11.40 vol%

Model	First set of data	Second set of data
	Fitting up to 19.52vol% of particle (PHBV30)	Fitting up to 11.40vol% of particle (PHBV20)
Maxwell (equation C)	0.08	0.29
Higushi (equation F)	0.78	0.14
Lewis-Nielsen (equation K)	0.36	0.46
Pal (equation L)	0.31	0.22

Most of the models from table 1, with or without fitting parameters, well-predicted the experimental water vapour permeability data for PHBV10 and PHBV20 but clearly underestimated the WVP value of PHBV30. The first hypothesis for such discrepancies could arise from the fact that these analytical models did not take into account structural heterogeneities, such as various particle shapes and sizes, different particle state of dispersion and orientation. It is easily understandable that high filler contents (30wt% for instance) favoured the occurrence of heterogeneities in the composite structure that hampered the prediction of the permeability by the analytical biphasic models. The second hypothesis could derive from the existence of a particle/polymer matrix interphase, i.e. creation of interfacial voids, area of rigidification and/or change of the crystallinity of the polymer matrix, which exhibit different barrier properties than both PHBV and WSF. This interphase would be much more important in the case of high filler content (> 20wt%). In such cases predictive

models [Pal et al. (2008), Mahajan et al. (2002), Felske et al. (2004), Shariati et al. (2011)] which considered the interphase as a third constituent, should be preferred for the prediction of the water vapour permeability. Nevertheless, it is experimentally difficult to get a right idea of the area and properties of this interphase.

5. Conclusion

The incorporation of WSF in PHBV polymer matrix lead to an increase of water vapour permeability in WSF-based composite and more especially in PHBV filled with WSF up to 19.52 vol% in accordance with the hydrophilic character of the WSF. Prediction of permeability by using analytical bi-phasic models required to known permeability of the continuous phase (polymer matrix) and, trickier, that of the dispersed phase. An estimation of the P_d in WSF was done from the product of D by S and confirmed the contribution of WSF to the overall water vapour transfer in the composite; P_d of WSF was 100 folds higher than that of the neat matrix PHBV. Prediction of permeability by using analytical bi-phasic models necessitated in most cases the adjustment of at least one parameter. Only three models were applied as they stand; predictive modelling of P by these three models was successful only up to a loading 11.40 vol% of WSF in WSF-based composites. When the volume fraction of particles was higher than 11.40 vol%, structural changes could occur and disrupted the barrier properties. Furthermore the fit of the other kinds of models gave the same conclusion: the value of the fitting parameter changed between 11.40 vol% and 19 vol% with no physical meaning.

PERSPECTIVES

Within the objective to elucidate the role of the vegetal fibre in the overall water vapour transfer of a composite material (WSF/PHBV), water vapour transfers (e.g. water vapour solubility, diffusivity and permeability) have been characterized in the permeable particles (WSF), the polymer matrix (PHBV) and the resulting WSF/PHBV composites. A dedicated experimental strategy has been used to explore the water vapour transfer in the WSF particles. The structure has been explored through optical microscopy and it can be concluded that the structure of the WSF/PHBV composites present particle size and particle shape heterogeneity. Bi-phasic model, with or without fitting parameters, failed in the prediction of permeability in the WSF/PHBV composites for the entire range of filler volume fraction investigated (from 0 to 30 wt%). The reason for this failure was ascribed to the heterogeneity of the structure. Along with, we noted that the permeability of the particle, required as input in the analytical bi-phasic model was based on an estimation based on the diffusivity and solubility value measured on a piece of wheat straw material and not on the embedded particle. These values may be not representative of the mechanisms that prevail in the particle placed in-situ in the polymer. From this starting point and in order to encounter this complex problem, a new numerical modelling approach has been proposed in order to predict global macroscopic mass transfer in biphasic-permeable composites from structural information gained at the microscopic scale.



Publication 5**A numerical model for predicting mass transfer in bio-composites: assessment of the permeable particles impact on the water vapour properties**Caroline Wolf, Nathalie Gontard, Valérie Guillard

ABSTRACT: A model based on Finite Element Method (FEM) has been developed to predict water vapour flux in composite materials containing fibre-type particles and to analyse its modulation according to the particle shape, size and volume fraction. Morphology of the permeable particle was modelled considering either, spherical, ellipsoidal and platelet shapes and its mean aspect ratio (α) has been varied considering realistic values (from $\alpha = 1$ to 100). Input parameters for mass transfer properties, water vapour diffusivity and solubility for each constituent of the composite, were taken from a previous work for poly(3-hydroxybutyrate-co-3-hydroxyvalerate) (PHBV) as continuous phase and wheat straw fibres (WSF) as dispersed phase [Wolf et al. (forthcoming (c))]. Impact of particle shapes was first investigated and it was determined that for a lower than 4 the modelled shape of the particle had no influence on the measured flux through the composite for a given volume fraction ($\phi_{vol} = 5\%$). Comparison of the present numerical model with existing analytical one of the literature (Maxwell model) was then performed and has revealed a strong discrepancy between the two predictions probably related to different hypothesis in the building of each model as regard the geometry considered. In a third step, the numerical model was tentatively validated for a PHBV/WSF biocomposite containing 20 wt% of WSF and by comparison with experimental water vapour permeability. This validation step has revealed that the model was very sensitive to the water vapour diffusivity of the particle, which could not be determined directly on the WSF particle but only on a macroscopic piece of wheat straw. Value gained on this macroscopic sample could not be extrapolated to WSF particle dispersed in the PHBV matrix and therefore, diffusivity of WSF particle value must be identified by adjusting predicted water vapour permeability to the measured one.

KEYWORDS: Numerical modelling, Finite Element Method, Water vapour flux, Geometry composites, Permeable dispersed phase

1. Introduction

In the last ten years a serious interest has been devoted to the modelling of mass transfer properties of composite materials and more particularly of their permeability toward gases and vapours. This last parameter is very important in the food packaging field because it determines the ability of the packaging material to regulate the transfer of gases (O_2/CO_2) and vapours such as water vapour in the food/packaging system and thus, the preservation of food quality during storage [Guillaume et al. (2011), Cagnon et al. (2013)]. Composites materials are obtained with the addition of at least two non-miscible constituents with different properties, whose synergism creates properties unavailable from individual single constituents. A lot of work has been carried out on the incorporation of nano-sized particles either inorganic (e.g. clays) or organic (e.g. starch nanowhiskers) in either synthetic polymer matrix [Alexandre et al. (2000), Ray et al. (2003), Mittal (2009)] or biopolymer [Ray et al. (2005), Sorrentino et al. (2007), Arora et al. (2010)] leading to the elaboration of nanocomposites. Incorporation of (nano)particles in a continuous polymer phase permits to significantly modulated the mass transfer properties of the resulting composite and makes this strategy very attractive for the food packaging field. For example, incorporation of impermeable nanoparticle such as nanoclays in a polymer matrix could lead to a significant decrease of the permeability of the nanocomposite compare to that of the neat matrix (review 1) while incorporation of permeable particles (e.g. vegetal fibres) could deeply increase the permeability of the composite [Wolf et al. (forthcoming (a))]. Indeed, the design of new tailored composite structures corresponding to the food requirements as regard to mass transfer properties is very crucial [Azeredo et al. (2009)].

A lot of work has been carried out on modelling of mass transfer properties in nanocomposites containing impermeable particles. Some analytical, tortuosity-based models [Nielsen (1957), Cussler et al. (1988)] were developed in the past and then, used to predict permeability of nanocomposites displaying well dispersed and/or exfoliated nanostructure with more or less success [Wolf et al. (forthcoming (b))]. However, these models could not be used for predicting permeability in bi-phasic material where the particle significantly contributes to the overall mass transport, as for example natural fibre-based composite. Some analytical bi-phasic models have been extrapolated from other science field, such as electrics and thermo-mechanics, for the prediction of mass transfer through bi-phasic membranes containing permeable particles [Maxwell (1873), Lewis et al. (1970)] but they have never been used in the field of packaging except one rare study [Wolf et al. (forthcoming (d))]. It is worth noticing that the study of mass transfer properties of composite materials in packaging science is almost a blank field from a modelling as well as an experimental point of view.

For predicting the overall permeability of the composite, existing analytical bi-phasic models required to know the respective permeability of each component which is not so evident to experimentally access for the particle. Once this first bottleneck is unlocked, the second one is related to the shape of the particle which must be specifically characterized and considered homogenous and constant in the entire composite. Except for perfectly spherical particles, the shape parameter is not often known and it should thus be identified by fitting the analytical bi-phasic model to experimental data, represented by the evolution of the relative permeability P/P_0 as a function of filler content [Wolf et al. (d)]. This feature prevents the use of these models for predictive modelling of permeability and considerably restricts their

interest as explicative modelling to reach a good understanding of the impact of particle dimensions (shape and size) on the composites mass transfer properties.

To overcome the limitations of current analytical approaches and develop more mechanistic and explicative modelling approach, numerical model could be convenient. The pioneering work in that field was that of Falla et al. in 1996 who used Monte Carlo simulations for modelling 2D regular arrangement of impermeable flakes in a matrix. Their work was extended to 3D structures by Swannack et al. (2005) and to randomly placed particles by Gusev et al. (2001). More recently, interest of Finite Element Method (FEM), a numerical technique used to find approximate solutions for differential equations, was explored by Goodyer et al. (2007, 2009) for 3D modelling of mass transfer properties in nanocomposites filled with impermeable particles. Minelli et al. (2011) did the same using finite volume algorithm (a method derived of FEM) and studied in addition to their predecessors, effect of platelet shape and filler loading on the effective coefficient of diffusion. All the aforementioned computational modelling attempts were done for platelets perfectly perpendicular to the direction of the flux. Bhunia et al. (2012) first introduced the effect of the orientation in its 2D finite element model, followed by Greco and co-workers (2013 and 2014) who worked on 2D and 3D models based on random distribution and orientation of non-interpenetrating impermeable lamellae. These numerical models were generally compared and found more powerful than analytical tortuosity based models such as that of Bharadwaj [Bharadwaj et al. (2001)] because particles with different orientation could be considered simultaneously while only a mean particle orientation could be dealt with at the same time for analytical model such as that of Bharadwaj, represented by one constant parameter. Nevertheless, in all the aforementioned studies, particles were

always impermeable. Such type of numerical approaches was, as far as we knew, never applied to composites containing permeable particles that hugely contribute to the overall mass transport. However, such approach would permit to solve the complex mathematics of transport phenomena by taking into account the property of both the continuous (e.g. polymer matrix) and the dispersed phase (e.g. particle) and by defining precisely the particle morphological (e.g. shape, size, volume fraction) and its dispersion (e.g. regular or random arrangement, agglomeration, orientation).

In practice, this implies to know precisely the mass transport properties of each component, in that case, solubility and diffusivity as well as the partition between particle and matrix. As for previously developed FEM models, the geometry of the composite represented by the polydispersity of the particle shape and the size (e.g. polydispersity of the aspect ratio), the state of dispersion of the particles must be known. If it is not the case, hypothesis on the structure of the materials should be done. One main advantage of FEM modelling approach is that successive hypothesis on the structure could be emitted, tested, validated or not until the right one was reached.

In this context, the objective of this paper was to propose a 2D numerical model to describe and predict mass transport into composite materials where particle were permeable and widely contributed to the overall mass transport. This model was applied to biocomposites made of poly(3-hydroxybutyrate-co-3-hydroxyvalerate) (PHBV) as continuous phase and wheat straw fibres (WSF) as dispersed phase and for water vapour as diffusing molecule. WSF particles being hydrophilic, they participated a lot to the water vapour flux if compared to the hydrophobic PHBV

matrix, and as a consequence, water vapour permeability of biocomposites increased as a function of filler content [Wolf et al. (d)]. The implementation of the 2D FEM model will be first presented. Then, second, the model will be used to (1) theoretically investigate the effect of particle shape and size, volume fraction and positioning in the neat matrix on the simulated water vapour flux, (2) compare the numerical simulation to analytical ones performed using the Maxwell model from the literature and (3) validate numerical simulations in the PHBV/WSF biocomposites by comparison with experimental water vapour permeability data.

2. Mathematical modelling and simulation

The numerical Finite Element Method (FEM) model has been developed in 2D using the Transport of Diluted Species physics interface of the Chemical Reaction Engineering module included in the COMSOL Multiphysics 4.3b software.

2. 1. Definition of the geometry

The composite film structures were drawn within the COMSOL interface and were composed of two domains; the matrix ($\Omega_{\text{matrix},1}$) and the particle ($\Omega_{\text{particle},2}$) as represented in figure 5. Various particle shapes (spheres, ellipsoids, platelets) and sizes (aspect ratio α) could be represented. To go further in the definition of the geometry, random or oriented and aligned distribution of the particles were achieved in the composites. In order to minimise computational cost, modelling was restricted to 1000 μm of length for the material and 300 μm of thickness.

2.2. Governing equation

The un-steady water vapour diffusion in composite materials was described by Fick's transport equation in both the matrix ($i=1$) and the particle domains ($i=2$):

$$\frac{\partial c_i}{\partial t} + \nabla \cdot (D_i \cdot \nabla c_i) = 0, \text{ in } \Omega_{\text{matrix}} \text{ and } \Omega_{\text{particle}} \quad [1]$$

where D_1 and D_2 ($\text{m}^2 \cdot \text{s}^{-1}$) were respectively the diffusivity coefficient in the matrix and the particle domains and c_1 and c_2 ($\text{mol} \cdot \text{m}^{-3}$) respectively the water vapour concentration in the matrix and the particle domains. The transport could be considered as diffusion-governed, i.e. penetrant diffuse through the thickness of the composite materials (L) due to concentration differences between the upper and the lower boundary of the film.

2.3. Boundary conditions

The diffusion mechanism was based on the fact that diffusion occurred through the permeable domains of the composite materials from the upper bound ($\partial\Omega_{\text{in,m/p}}$) to the lower bound ($\partial\Omega_{\text{out,m/p}}$).

The upper bound ($\partial\Omega_{\text{in,m/p}}$) and the lower bound ($\partial\Omega_{\text{out,m/p}}$) boundary conditions were defined as follow:

$$\begin{cases} c_{\text{in}} = c_{\text{in}_i} \\ c_{\text{out}} = 0 \end{cases} \text{ at } \partial\Omega_{\text{in,m/p}} \text{ and } \partial\Omega_{\text{out,m/p}} \quad [2]$$

where c_{in_i} was the concentration of water vapour at the upper surface of the material obtained for a fixed relative humidity, RH.

The composite films were considered as planar sheet and the lateral flux at the bound ($\partial\Omega_{axl,m/p}$ and $\partial\Omega_{axr,m/p}$) could be neglected:

$$(-D_i \nabla c_i) \cdot \mathbf{n} = 0 \text{ at } \partial\Omega_{axl,m/p} \text{ and } \partial\Omega_{axr,m/p} \quad [3]$$

where \mathbf{n} is the normal vector to the boundary.

The boundary condition at the interface matrix/particle was defined as follow:

$$(-D_2 \nabla c_2) \cdot \mathbf{n} = M(K \cdot c_1 - c_2) \quad [4]$$

where K was the dimensionless partition coefficient calculated as follows:

$$K = \frac{c_{1eq}}{c_{2eq}} \quad [5]$$

and M the water vapour stiff-spring velocity ($\text{m}\cdot\text{s}^{-1}$) which was supposed equal to 10^3 . Stiff-spring equilibrium boundary condition [Comsol tutorial (2011)] has already been used for calculating fluxes in membrane [Shehni et al (2011)] and food packaging [Cerisuelo et al (2013)] and was used in this study in order to concurrently encounter concentration discontinuities and to allow continuous flux at the interface matrix/particle and more generally flux continuity across the composite film.

2.4. Initial conditions

The initial water vapour concentration in each domain, matrix (Ω_{matrix}) and particle (Ω_{particle}), was assumed to be constant:

$$c_{ini} = c_{ini_i} \text{ in } \Omega_{\text{matrix}} \text{ and } \Omega_{\text{particle}} \quad [6]$$

2.5. Numerical implementation and calculations

The mesh used for this study was free triangular elements and was refined manually, by changing the size of the mesh for each geometry, to get a mesh independent solution (figure 5b). The time of simulation, linked to the refining of the mesh was taken into account but the main parameter considered was the convergence of the model. The solver Paradiso was used because it is preferable for 2D modelling of diffusion law, and combined to a backward differentiation formula (BDF) used to determine the time steps calculation. The solver was ran with a relative tolerance, an absolute tolerance and an initial time stepping respectively equal to 0.01, 0.001 and 0.01. One result of simulation is shown in figure 5c.

2.6. Calculation of model output

The model validation was achieved with the comparison of experimental PHBV/wheat straw fibre permeability and that calculated from the flux coming from the output of the FEM simulation:

$$P = \frac{N \times L}{p_2 - p_1} \quad [7]$$

where H the thickness of the film, P the water vapour permeability ($\text{mol} \cdot \text{m}^{-1} \cdot \text{s}^{-1} \cdot \text{Pa}^{-1}$) and p_1 and p_2 the water vapour pressure across the film.

3. Materials and experimental modelling parameters determination

The numerical model was applied to a PHBV/WSF biocomposites, where vapour diffusivity and water vapour concentration were determined in both PHBV and WSF. Water vapour diffusivity and concentrations was also determined in the composite PHBV/(20 wt%)WSF for the experimental validation step. Most of the data used in the current paper were taken from a previous work [Wolf et al. (c)] and were recalculated in line with the objective of the 2D numerical simulation. Details on the composite processing and obtaining of the data required for calculated the model input parameters were briefly recalled in the following.

3.1. Materials and composite preparation (film processing)

Commercial poly(3-hydroxybutyrate-co-3-hydroxyvalerate) (PHBV) was supplied by Tianan under the reference Y1000P with HV content 3%. Wheat straw (*Triticum aestivum* cv. Apache) was provided by Fernand Meaux (Saint Jean du Salés, Aveyron, France), harvested in 2007 and was ground to obtain wheat straw fibres. The wheat straw fibres (WSF) were impact-milled at a size of 100-150 μm and the median diameter of the fibre is around 62 μm using a process previously developed by [Ghizzi D. Silva et al. (2012)] and re-use recently by [Berthet et al. (2014)]. PHBV and PHBV/(20 wt%)WSF composites (PHBV20) were prepared by extrusion and film thermo-pressing [Berthet et al. (forthcoming)]. All the samples were stored at 0% RH on P_2O_5 at room temperature for at least 10 days before use.

3.2. Calculation of input parameters

3.2.1. Water vapour concentrations in matrix and particles

Initial and boundary condition for each domain (matrix and particle), namely water concentration, were determined from the water vapour sorption isotherm. This water vapour sorption isotherm was obtained from dynamical water vapour sorption experiments carried out at 20 °C over a wide range of water activities (from 0 to 95% relative humidity) using a controlled atmosphere microbalance apparatus (DVS) (Surface Measurement System Ltd., London, UK). The moisture content at equilibrium ($\text{g.g}_{(\text{dry basis})}^{-1}$) at a given temperature was calculated as follows:

$$X = \frac{M_w - M_d}{M_d} \quad [8]$$

where M_w (g) is the mass of the wet sample at equilibrium state and M_d (g) the dry mass.

For the purpose of numerical simulations in COMSOL, the moisture content at equilibrium (X) was converted in water vapour concentration (mol.m^{-3}) using the following expression:

$$c = \frac{X}{M_{H_2O}} \times \rho \quad [9]$$

where M_{H_2O} is the water molar mass (g.mol^{-1}) and ρ the material density (g.m^{-3}). The material densities were equal to 1.11 ± 0.006 , 1.156 ± 0.021 and $1.692 \pm 0.031 \text{ g.cm}^{-3}$ for respectively PHBV, PHBV20 and WSF [Wolf et al. (c)].

3.2.2. Water vapour partition at particle / matrix interface

As regard to the internal boundary condition at the interface particle/matrix, the parameter K , which relates the relationship between the water concentration in the particle (c_2) and that in the matrix (c_1), is required. To calculate that, the equations of water sorption isotherm for both components, matrix and particle, were used. GAB equation (equation 10) and Park model (equation 11) were applied with respect to previous findings [Wolf et al. (c)] for modelling water vapour sorption isotherm of PHBV and WSF respectively.

Both equations provide an expression of water vapour concentration as function of water vapour activity. They were then used to graphically represent the evolution of c_2 a function of c_1 for a_w values from 0 to 0.95 (results not shown) resulting in straight lines for a_w values between 0.15 and 0.25, between 0.45 and 0.55, between 0.65 and 0.75 and 0.90 and 1 which slopes corresponded to K values at a_w equal to 0.2, 0.5, 0.7 and 0.95 (table 1).

$$c_1 = \frac{X_m \cdot C_g \cdot K \cdot a_w}{(1 - K \cdot a_w)(1 - K \cdot a_w + C_g \cdot K \cdot a_w)} \times \frac{\rho}{M_{H_2O}} \quad [10]$$

$$c_2 = \left(\frac{A_L \cdot b_L \cdot a_w}{1 + b_L \cdot a_w} + k_H \cdot a_w + K_a \cdot a_w^n \right) \times \frac{\rho}{M_{H_2O}} \quad [11]$$

3.2.3. Effective moisture diffusivity

Effective moisture diffusivity values at different water activity were identified for PHBV and WSF using DVS moisture sorption experiments. The procedure of identification was already submitted by Wolf et al. (c), the identification was achieved on four relative humidity steps. All the inputs parameters were gathered in table 1 and figure 2.

Table 1: Experimental initial and boundary modelling input parameters (20°C)

Gradient of relative humidity (%RH)	Mean relative humidity (%RH)	Initial conditions		Boundary conditions		
		Diffusivity coefficient $\Omega_{\text{matrix}} (1)$ ($\text{m}^2 \cdot \text{s}^{-1}$)	Diffusivity coefficient $\Omega_{\text{particle}} (2)$ ($\text{m}^2 \cdot \text{s}^{-1}$)	Upper boundary concentration at $\partial\Omega_{\text{in,m/p}}$ $\Omega_{\text{matrix}} (1)$ ($\text{mol} \cdot \text{m}^{-3}$)	Upper boundary concentration at $\partial\Omega_{\text{in,m/p}}$ $\Omega_{\text{particle}} (2)$ ($\text{mol} \cdot \text{m}^{-3}$)	Partition coefficient K (dimensionless)
0 - 20%	15	$2.39 \pm 0.41 \times 10^{-12}$	$27.71 \pm 0.34 \times 10^{-12}$	40.84	2777.22	67.63
0 - 50%	45	$2.49 \pm 0.15 \times 10^{-12}$	$18.99 \pm 0.30 \times 10^{-12}$	120.72	6817.41	56.36
0 - 70%	65	$2.65 \pm 0.08 \times 10^{-12}$	$17.14 \pm 0.36 \times 10^{-12}$	193.83	10050.89	51.88
0 - 95%	92.5	$2.16 \pm 0.34 \times 10^{-12}$	$6.91 \pm 0.76 \times 10^{-12}$	332.91	18326.10	55.11

All parameters were determined in [Wolf et al. (c)]

3.3. Experimental validation

Water vapour permeability (WVP) of the composite material containing 20 wt% of WSF presented in Publication 4 was used to validate the numerical simulation. This experimental water vapour permeability (WVP(exp)) gravimetrically determined at 20 °C for a relative humidity difference of 0-100% using a modified ASTM procedure was compared to the calculated one by using equation 7.

As it was previously demonstrated that this experimental value did not completely match the theoretical value obtained via product of the diffusivity coefficient (D) by the solubility coefficient (S), a calculated water vapour permeability (WVP(calc))

was estimated by using the aforementioned relationship ($WVP(\text{calc})=D*S$). As D and S were known for each a_w step investigated in the DVS, the $WVP(\text{calc})$ was estimated for different relative humidity steps, namely 0-20, 0-50, 0-70 and 0-95%. Resulting $WVP(\text{calc})$ are gathered in table 2.

Table 2: Water vapour solubility, diffusivity and calculated permeability coefficient of PHBV20 at 20°C

Gradient of relative humidity (%RH)	Mean relative humidity (%RH)	Solubility coefficient ($\text{mol.m}^{-3}.\text{Pa}^{-1}$)	Diffusivity coefficient ($\text{m}^2.\text{s}^{-1}$)	Permeability coefficient $WVP(\text{calc})$ ($\text{mol.m}^{-1}.\text{s}^{-1}.\text{Pa}^{-1}$)
0 - 20%	15	1.15×10^{-1}	1.56×10^{-12}	1.79×10^{-13}
0 - 50%	45	2.98×10^{-1}	1.16×10^{-12}	3.47×10^{-13}
0 - 70%	65	4.68×10^{-1}	1.12×10^{-12}	5.24×10^{-13}
0 - 95%	92.5	12.10×10^{-1}	1.32×10^{-12}	15.90×10^{-13}

All parameters were determined in [Wolf et al. (c)]

4. Results and discussion

4.1. Modelling results: effect of particles size shape, fraction and positioning

The numerical model solved using COMSOL Multiphysics® software succeeded in predicting the evolution with time (24 hrs) of the water vapour flux through the composite material of 300 μm thickness in less than 10 min of computation time (on Intel® Core™ I7 CPU at 2.7 GHz, 8GB RAM). The composite considered contains various amount of permeable WSF. These particles were more sensitive to water than the neat matrix as revealed by the observation of water sorption isotherms in figure 1, therefore they highly contributed to the overall mass transport. The water vapour flux in the composite was then always higher than that in the neat matrix in all the configurations studied in the following.

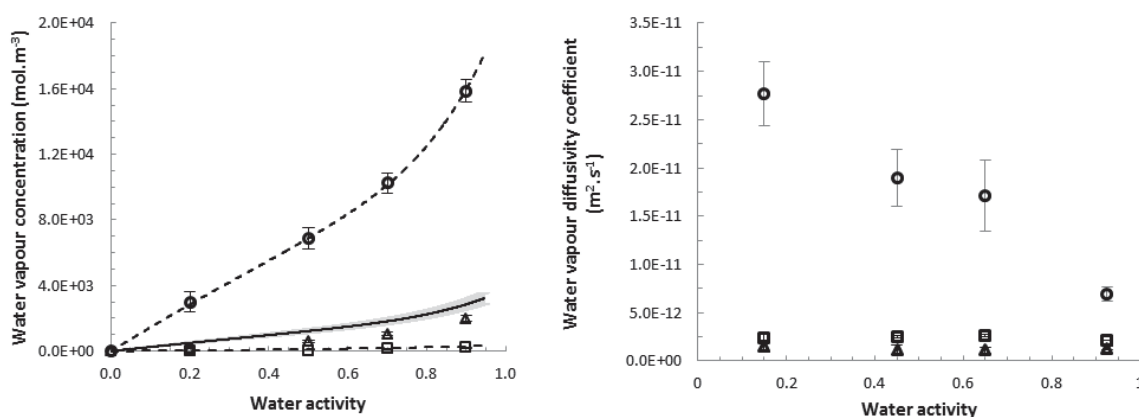


Figure 1: Representation of water vapour sorption isotherm and water vapour diffusivity coefficient in PHBV (square), WSF (circle) and PHBV20 (triangle) as function of water activity (from [Wolf et al. (c)] at 20°C)

The results obtained from the finite element simulation were first exploited in order to compare the water vapour flux in composites exhibiting various particles sizes and shapes (represented by the aspect ratio named α), and filler fractions (φ) and positioning in the matrix; the results are shown in figure 2.

The relative flux, N_{eff}/N_0 , with N_{eff} the effective flux in the composites and N_0 the flux in the polymer matrix, in spherical and platelets-based composites with particles displaying a mean aspect ratio (α) of 1 were first examined as function of particle fraction and positioning in the matrix. For simplification purpose, only one single particle was considered in the geometry as previously done by Minelli et al. (2011). The relative flux values in spherical and platelets-based composites were not significantly different whatever the position of the particle in the polymer, either in contact with the top or the bottom of the film or centred in the film. Even when the aspect ratio increased for the platelet from 20 to 100, the relative flux value did not change according to the position of the particles.

N_{rel}/N_0	$\phi = 0.01$		$\phi = 0.025$		$\phi = 0.05$		$\phi = 0.1$	
	Diagram	Value	Diagram	Value	Diagram	Value	Diagram	Value
$\alpha = 1$		8.82		17.54		28.18		47.12
		7.47		15.38		25.10		43.12
		7.47			33.51		66.17	
$\alpha = 1$		7.46		15.73		26.54		41.44
		8.16		16.56		26.03		41.44
		32.79		65.17		102.85		156.56
$\alpha = 20$		39.79		71.55		106.46		156.56
		60.30		111.68		170.13		251.54
		68.75		117.94		172.21		249.45
$\alpha = 100$		93.73		165.95		247.36		355.91
		101.83		170.13		246.32		367.39

Figure 2: Representation of the relative flux for various particles shapes (spheres, platelets) exhibiting different aspect ratio in the range from 1 to 100 and positioned differently in the polymer matrix, either in contact with the upper and/or lower bound or centred in the polymer matrix

For platelets, the effect of simultaneous increase of the particle fraction and of the aspect ratio was investigated on the relative flux N_{eff}/N_0 (figure 3). Particle fraction ranged from 1 to 10 vol% and mean aspect ratio of the particle from 1 to 100 on the basis of previous values found in the literature [Wolf et al. (a)]. The relative flux was enhanced with increasing particle aspect ratio and filler fraction. For example, N_{eff}/N_0 increased from 7.5 to 41 at $\alpha=1$ and increased from 94 to 356 at $\alpha=100$ as ϕ increased from 0.01 to 0.1, representing a 5.5 and 3.8 fold higher value of the relative flux at $\alpha=1$ and $\alpha=100$ respectively. For a given filler fraction, for example $\phi=0.01$, the relative flux increases 13 times (from 7.5 to 94) when the aspect ratio is multiplied by 100. In the particular case of $\phi=0.1$, for $\alpha=100$, the flux value was around ten times higher than in the case of $\alpha=1$ (figure 2). The effect of increasing aspect ratio was even higher than that of increasing filler content.

The increase of the relative flux with an increase of particle fraction was easily comprehensible; indeed by taking into account that the particle was more permeable than the matrix, an increase of particle filler fraction, i.e. filler surface in the 2D, FEM representation, lead logically to an increase of the flux value of the composite. As regard to the effect of increasing mean aspect ratio, for a given filler fraction, it could be related to the higher specific front line of exchange between the particle and the matrix when a is high. For example at $\phi=0.01$ the surface of particle is equal to $1.00 \times 10^{-9} \text{ m}^2$ and the perimeter for the particle at $\alpha=1$ and $\alpha=100$ were equal to $1.26 \times 10^{-4} \text{ m}$ and $6.39 \times 10^{-4} \text{ m}$ and respectively. The higher perimeter at $\alpha=100$ promoted the diffusion of water vapour molecules and explained the increase of the relative flux value, which was approximately ten times higher. In figure 2 this effect was well represented in the case of spheres. At $\phi=0.1$, when ten spheres were dispersed instead of a single one, representing the same particle

surface but a perimeter of 1.12×10^{-3} m instead of 3.54×10^{-4} m for a single, big sphere, the relative flux was 1.5 times higher for the dispersion of ten spheres.

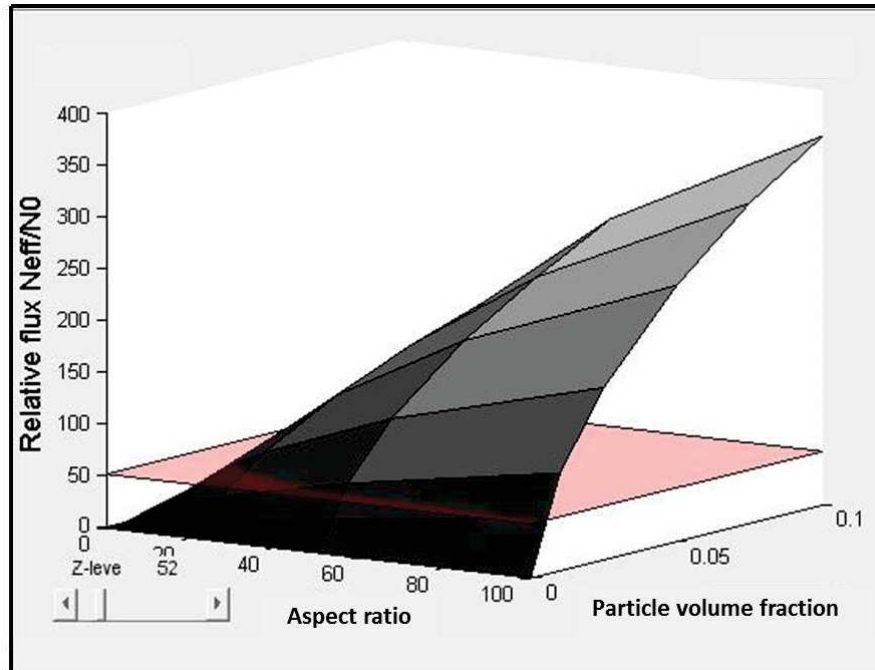


Figure 3: Influence of the particle fraction (ϕ) and particle aspect ratio (α) on the relative flux N_{eff}/N_0 in platelets-based composites

According to the coefficient of variation obtained on the experimental measurement of water vapour flux which was estimated to be around 50% [Publication 4], the relative flux value became significantly higher when it exceeded 50. Although for $\alpha=1$ the value of N_{eff}/N_0 was not significantly different up to 10wt% of particles, for $\alpha=100$ the N_{eff}/N_0 value was higher than 50 even at very low loading ($\phi=0.01$). At $\phi=0.05$ and at $\alpha=1$, N_{eff}/N_0 is equal to around 26, at $\alpha=4$ it exceeded 50 and at $\alpha=20$ N_{eff}/N_0 is equal to around 105 (figure 2). Hence there is a dividing line among the couples (α, ϕ) : on one side of this line, given the values of (α, ϕ) , the increase of N_{eff}/N_0 value is not significant (e.g. for low size aspect ratio or low filler fraction) and on the other side, the increase of N_{eff}/N_0 value is significantly higher than 50. This line is given in figure 3 by the intercept between the plan of $N_{\text{eff}}/N_0=50$ and the response surface.

4.2. Modelling results: comparison of the numerical model with the Maxwell model

In a second step, the numerical model proposed in the current study was compared with the prediction of an analytical bi-phasic model of the literature, the Maxwell model. The Maxwell model [Maxwell (1873)] allowed to calculate the permeability of a composite material by taking into account the permeability of both permeable particle and the one of the matrix, the filler volume fraction and a shape factor, n , representing the morphology of the particle:

$$P_{\text{eff}} = P_c \left[\frac{n P_d + (1-n) P_c + (1-n) \Phi_d (P_d - P_c)}{n P_d + (1-n) P_c - n \Phi_d (P_d - P_c)} \right] \quad [12]$$

with P_{eff} , P_c , P_d the permeability of the composite, the matrix and the particle and Φ_d the volume fraction of particles. Of course, if the particle is impermeable the same model could be used and therefore, $P_d=0$.

This model was already successfully used in a previous work to fit experimental water vapour permeability in PHBV/WSF composites [Wolf et al. (d)] for filler fraction ranging from 0 to 20 vol%. The fit of the model with the adjustment of the parameter n was in good agreement with experimental data until a particle weight fraction of 11.5vol%. In this paper, for comparison purpose with the numerical model and to simplify the geometry, the parameter n was considered equal to 1/3, i.e. for the case of spherical particles according to [Maxwell (1873)]. Then the permeability P_{eff} of the composite was calculated for increasing Φ_d by using P_c and P_d equal to 4.10×10^{-13} and $1.65 \times 10^{-10} \text{ mol.m}^{-1}.\text{s}^{-1}.\text{Pa}^{-1}$ respectively (Table 1).

In the numerical model, some spherical particles will be considered to be in agreement with the Maxwell model for $n=1/3$. These particles were well aligned and dispersed in the matrix. The upper and lower boundaries were fixed at respectively 95% and 0% of relative humidity corresponding to one of the conditions of table 1. The output of the model was a water vapour flux. For comparison with the Maxwell model, the calculated flux was converted into a permeability value by using equation 7.

The relative permeability P_{eff}/P_0 obtained from the FEM simulations and those predicted by the Maxwell model were plotted together against the particle fraction in figure 4. Two case studies were investigated: (1) case of permeable particles with P_d equal to the permeability value of WSF piece and (2) case of impermeable particles ($P_d=0$). From figure 5 it was shown that the prediction of the Maxwell model matched to the prediction of the FEM model in the case of impermeable particles.

Similar good agreement between FEM simulation and Maxwell model in the case of impermeable lamellae was already reported by Greco and Maffezzoli (2013). However for permeable particles, high discrepancies were found and deviation was observed between the FEM simulation values and the Maxwell model. For instance, at low particle fraction, $\phi=0.01$, P_{eff}/P_0 was higher than 10, against 1.03 for the P_{eff}/P_0 predicted by the Maxwell model, and therefore was not displayed in the graph (figure 4).

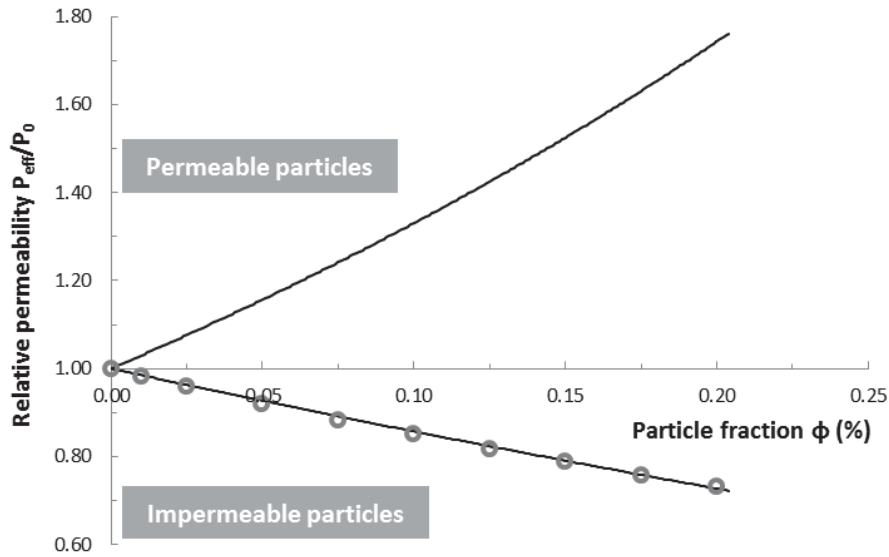


Figure 4: Comparison of relative permeability P_{eff}/P_0 estimated from Maxwell model for permeable and impermeable particles (straight line) and the FEM simulation from this study (circle) as function of particle volume fraction (ϕ)

This high discrepancy between the predictions of the FEM model and that of the Maxwell model could be ascribed to differences in the main hypothesis used in model basements. The Maxwell model even with $n=1/3$ may not fully represent permeability of a composite with spherical particles dispersed in a continuous phase as done in the trial of figure 4.

4.3. Model validation

Third step of this study was to experimentally validate the proposed numerical model. To do that, predicted water vapour permeability value in a PHBV20 composite was compared to that experimentally measured equal to $1.74 \times 10^{-12} \text{ mol.m}^{-1}.\text{s}^{-1}.\text{Pa}^{-1}$ at 0-100%RH. The experimental mean aspect ratio of the particle was found equal to 2 [Berthet et al. (2014)]. According to the aforementioned results, for this aspect ratio and the filler content equal to 11.40 vol% investigated, the shape of the particle drawn in the FEM geometry has no significant impact on the result.

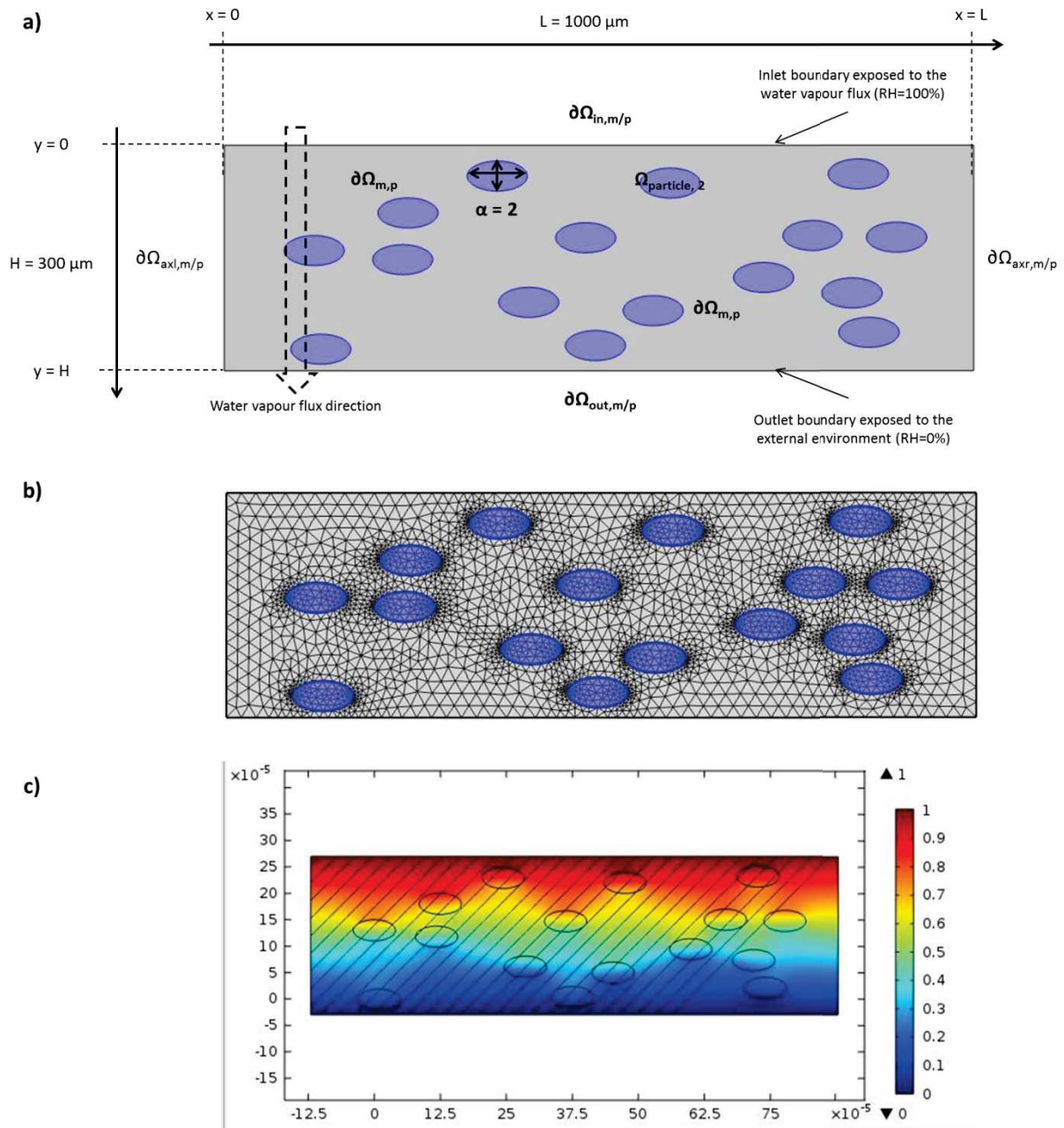


Figure 5: Representation of (a) the geometry of the composite with the domains, initial & boundary conditions and the experimental conditions, (b) the associated meshed computational geometry and (c) dimensionless concentration and streamline profile of water vapour in randomly dispersed ellipsoid-based composites

Therefore, spheres ($\alpha=1$) and ellipsoid particles ($\alpha=2$) were chosen to represent the WSF particle shape. The polydispersity of the particle size was neglected. Numerical simulations were carried out at four different upper boundary relative humidities (0-20%, 0-50%, 0-70% and 0-95%) with input parameters given in table 1 and in six different composite structures exhibiting various arrangements of non-

interpenetrating particle, (a) well-aligned particles, (b) particles in alternating gridlines and (c) random dispersion of particles (figure 5). The estimated permeability value after FEM simulation was deduced from the flux value with equation 7 and compared to the experimental water vapour permeability (WVP(exp)) and the calculated water vapour permeability (WVP(calc)). All the results are shown in figure 6 together with a schematized representation of the FEM geometry.

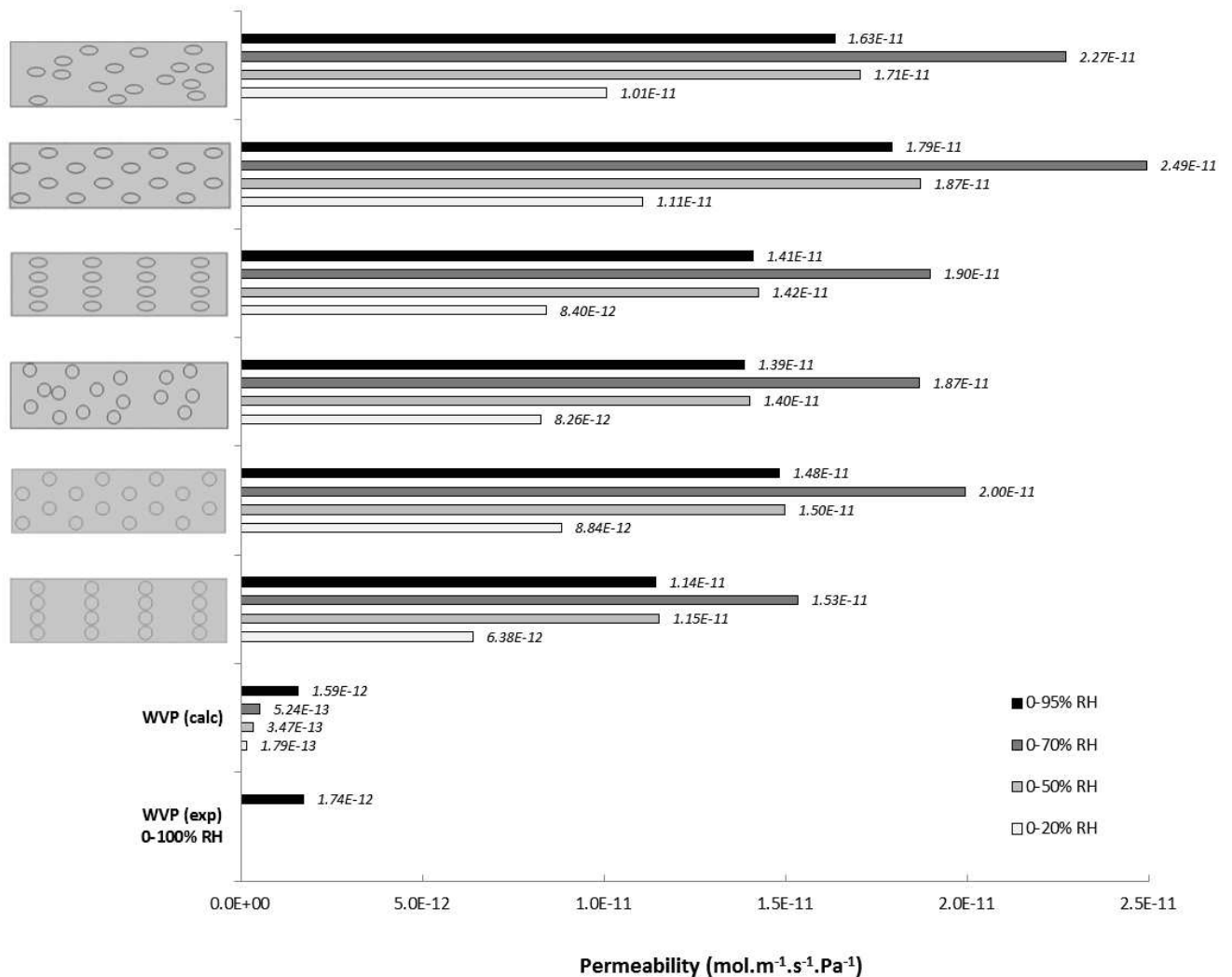


Figure 6: Comparison of FEM simulation permeability results in spherical and ellipsoidal particles-based composite loaded with 11.40 vol% particles and WVP(exp) of PHBV20 at 20 °C and WVP(calc) of PHBV20 calculated from D(PHBV20) and S(PHBV20) at 20 °C and at different relative humidity (0-20, 0-50, 0-70, 0-95 %RH)

At first sight, the numerical model considerably overestimated the WVP(exp), determined for 0-100% RH; experimental permeability value was almost ten times lower than the numerical one. If we considered the WVP(calc), calculated using the product of diffusivity with solubility obtained in the composite material (table 2), we noted that the value calculated for 0-95% RH, which is the closest representative of the conditions encountered during experimental WVP test was in agreement with the WVP(exp) one. This WVP(calc) was consequently around 10 times lower than that predicted by the numerical model whatever the RH step considered 0-20, 0-50, 0-70 and 0-95%.

Moreover, WVP(calc) values monotonically increased with an increase of relative humidity step while the numerical value first increased for 0-20% to 0-70% and decreased for 0-95% RH. Contrary to WVP(calc), which was estimated using D and S for the PHBV20 composite, numerical predicted permeability value was calculated using the FEM model by using D and S for each individual component, i.e. matrix and particle. Therefore, the FEM simulations covered (of) the variations of D and S for each individual component. For instance, at high relative humidity, WSF exhibited a lower water vapour diffusivity coefficient compare to that obtained for lower RH. This decrease in D counteracted the high solubility of WSF. In the composite, the diffusivity value did not vary according to relative humidity (table 2) and did not cover this specific behaviour of the WSF explaining why WVP(calc) and numerical predicted permeability values did not vary in the same trend as a function of RH step investigated.

The overestimation of the numerical model could be ascribed to (1) modification of matrix properties when used in the composite material and/or (2) change in particle properties when included in the PHBV. Indeed, addition of particles could lead to modification of the polymer matrix (e.g. change in crystallinity, in polymer free volume, etc). The water vapour sorption properties of the composite were relevant with the predicted one from those of the neat PHBV and the pure WSF using mixture rule [Wolf et al. (c)]. Therefore sorption properties of each component seemed to be not modified in the composite. One first hypothesis would be that the D of the PHBV would be modified in the composite. Besides the addition of particles did not change the crystallinity of the PHBV polymer matrix, one parameter which could induce changes in the barrier properties of the polymer. In the light of the aforementioned features, we can conclude that $D(\text{PHBV})$ was not significantly modified by addition of WSF particles. A second hypothesis to interpret the overestimation of the numerical model compared to experimental values could be explained by a significant change of the water vapour diffusivity coefficient of the WSF when embedded in the matrix. Indeed the $D(\text{WSF})$ was identified on a piece of wheat straw material considered as a planar film and not on a single fibre embedded in PHBV polymer matrix. Thus WSF was able to swell in all directions during dynamical water vapour sorption and was not under mechanical constraints as the single fibres in-situ in the PHBV polymer matrix.

In order to estimate a more realistic diffusivity value for the embedded WSF particle, the numerical model for 0-20% and 0-95% RH step and a composite structure represented by a random dispersion of ellipsoids was fitted to the WVP(calc). The identified diffusivity coefficient was found to be equal to $0.41 \times 10^{-12} \text{ m}^2\cdot\text{s}^{-1}$ compared to 27.71×10^{-12} and $0.57 \times 10^{-12} \text{ m}^2\cdot\text{s}^{-1}$ compared to $6.91 \times 10^{-12} \text{ m}^2\cdot\text{s}^{-1}$ respectively.

The water vapour diffusivity of an embedded WSF particle would be thus respectively 68 and 12 times lower than the experimental value measured on a piece of wheat straw depending on the relative humidity step (RH). The two identified diffusivity values did not vary a lot according to the RH step whereas those identified through water sorption experiments could differ from a factor 4. Hence, this tendency would confirm that the embedded WSF particle in the matrix would not be able to swell a lot through water sorption.

5. Conclusion

This study presented a new FEM model for the multi-scale description and prediction of structure/mass transfer relationship for composites containing permeable particles. This model was confronted to experimental measurement of water vapour flux and permeability data in a PHBV20 composite material. Results have shown a relatively strong dependence of the relative flux on the particle fraction and aspect ratio for couples of (ϕ, a) above given threshold values. The application of the model pointed out the experimental difficulty to characterize mass transfer properties in the permeable particle; for example, in the case of vegetal fibres, such as the WSF investigated in the current work, the diffusivity value measured on a piece of wheat straw was not representative of the diffusion in an embedded WSF particle. The FEM model developed in this study was more relevant than analytical model such as the Maxwell model for the prediction of barrier properties for composite structures where the distribution of particles in the polymer matrix could be relatively more complex compared to ordered structures and where mass transfer properties (e.g. diffusivity and solubility) should be taken into consideration in both component polymer matrix and particles. The developed 2D model could be seen as premise work waiting for

the generation of 3D composite structures based on experimental observation in future research. 3D FEM model would be reliably used in food packaging applications for the design and the development of packaging films.

PERSPECTIVES

Considering a hydrophobic biopolyester (PHBV) and hydrophilic wheat straw fibers (WSF), two composite constituents exhibiting totally opposite behaviour as regard water vapour, the convergence of the model was even ensured under continuous flux assumption at the interface particles/polymer matrix. While it has been demonstrated that the water vapour properties in piece of WSF were different than that of single WSF embedded in PHBV polymer matrix, the crystallinity of the PHBV matrix was assessed to be unchanged with the addition of WSF in PHBV. However, it has been recently demonstrated by Berthet et al. (2014) that the crystallinity decreased with the incorporation of WSF in PHBV through WAXS experiments. Thus with the objective to reach a validation level of the numerical models with PHBV/WSF composite systems, each constituent should be first well-characterized in-situ the composites.

CONCLUDING REMARKS AND GENERAL DISCUSSION

Despite the growing interest of composite structures for the design of tailor-made materials responding to the requirement of food product in terms of barrier properties, the understanding of mass transfer through composite materials remained a challenge for the future. On one hand due to experimental hindrance the three-dimensional structure characterization of composite materials and the characterization of barrier properties of permeable particles still remained difficult, and on the other hand due to a lack of efficient modelling approach. This PhD project was centred on the investigation of mass transfer of gases and vapours in nano- and micro-composites containing impermeable or permeable particles (impact of type, shape and size etc.) and on the development of a numerical 2D modelling of the structure/mass transfer relationships in composite materials

First part of this work was expended on the study of existing data of the literature on gases and vapours permeabilities in nano- and micro-composites and to the review of current predictive modelling approaches of these permeabilities. O₂, CO₂ and H₂O permeabilities in nano- and micro-composites with different kind of particles (inorganic and organic such as cellulose nanowhiskers), and various particle shapes (e.g. spherical, cylindrical and platelets). Scientific publications were listed and their results were compared and discussed in order to elucidate the role of the particle shape and size on the composite permeability value. In all the references collected, the nanoparticles added were considered impermeable and were added to modulate and mainly to decrease the permeability of the composite compare to that of the neat matrix. According to the shape of the particles; for spherical and cylindrical particles the permeability could either increase or decrease with the incorporation of impermeable particles. However, when platelet particles were considered, only an overall decrease of the permeability was observed and

sometimes the decrease was non-monotonic, i.e. a decrease and after that, for high filler content, an increase of the relative permeability of the composite. In the case of platelets, the high permeability reduction could be explained by the creation of a more tortuous pathway for the diffusing molecular species. But the modulations of the barrier properties, especially the enhancement of these barrier properties which is the main target when impermeable nanoparticles are added, were tremendously related to the structure of the composites. In fact, when the structure of the composite exhibited good particle dispersion, the decrease of the permeability was larger than in the case of mixture of well-dispersed and agglomerated particles. This feature was also demonstrated with the application of the tortuosity-based models for the prediction of the permeability of composites. When the particles were well-dispersed, the predictions of the models were sometimes in good agreement with the experimental data. However in case of particles agglomeration, the models were in limit of their validity conditions and discrepancies appeared between predicted and experimental permeability. Actually dispersion strongly depends on the chemical modification of the particle surface and on the optimization of the composite processing techniques which have been of great importance in order to reach well-dispersed particles within the polymeric matrix. Other tortuosity-based model limitations on the use include the difficulty to experimentally evaluate the in-situ aspect ratio of the particles, thus in most of the cases, the models help in the identification of this geometrical parameter. In general the geometrical hypothesis used for the development of the models are oversimplified and do not represent the heterogeneous structural reality of the composites, i.e. the polydispersity of the particle shape, size, dispersion and orientation. Moreover it is very complicated to choose the accurate tortuosity-based model for the prediction of mass transfer of one specific set of experimental permeability data; the application of several

theories is realizable but their predictions do not converge towards the same results, except for high filler content, due to the too simplistic basic premises of the models. Finally few models are available for the prediction of mass transfer properties in spherical and cylindrical based composites; they also do not allow predicting an increase of the permeability of the composites, frequently observed in experimental work.

In the literature a lot of study dealt with impermeable particles, and only rare studies were found dealing with permeable particles such as vegetal fibres. In the case of water vapour transfer, vegetal fibre such as wheat straw fibres could no longer be considered as impermeable. As regard predictive modelling of permeability of composites filled with permeable particles that hugely contribute to the overall mass transfer, and as far as we know, no scientific researches were carried on that topic in the packaging field at the beginning of that work. Therefore the second part of this PhD work was thus dedicated to the study of mass transfer in a composite material with permeable particles and to the development of a numerical model to predict mass transfer in such systems.

Due to obvious technical bottlenecks, because of the size and shape of the particle that limit its handling and disposal in diffusion and permeation cells, water vapour sorption, diffusion and permeability could not be assayed on one single milled WSF. Consequently the water vapour sorption experiment has been explored on a piece of native WSF, which did not exhibit the same structure than single milled WSF. If compared to poly(3-hydroxybutyrate-co-3-hydroxyvalerate) (PHBV) polymer matrix, the sorption in WSF was around 40 times higher and it has therefore been proven that WSF improved the water vapour permeability of the resulting WSF/PHBV

biocomposites due to their hydrophilic character. Although the experimental water vapour transfer in WSF was not representative of the embedded particle, it permitted to determine the solubility coefficient and the diffusivity coefficient to access the permeability coefficient of WSF necessary for the application of bi-phasic model for the prediction of the permeability in bi-phasic permeable composites. From the model prediction, it has first been highlighted that almost half of the models required the fitting of at least one parameter to the experimental data (e.g. evolution of P/P_0 as a function of filler fraction). Once fitted to the experimental data, these models of course satisfactory represented the data with a given uncertainty but could not be extrapolated. However, they showed inconclusive findings and discrepancies with experimental permeability values at higher particle content (>10 vol%). Similarly for model which did not required any adjustment, differences between experimental and predicted permeability of the composites appeared at higher particle content. As consequence, the use of analytical bi-phasic model was not suitable to our heterogeneous composite structures. In this sense, the development of a new 2D modelling approach has been proposed for the prediction of barrier properties in bi-phasic permeable composite based on finite element method. The model allowed the calculation of barrier properties (e.g. from a flux value in the composite) in relation with the structural parameters of the particles dispersed in the polymeric phase. The model was built by considering initial and boundary concentrations and diffusivity coefficients in both the matrix and the particles with simplified and realistic 2D geometry (e.g. random dispersion of ellipsoids) of the composite structures. COMSOL Multiphysics was used for the approximate calculation of the flux within the drawn composite structure. The model was implemented with mass transfer input parameters obtained experimentally for water vapour. The simulation results indicated that the composite flux increased with both an increase of the volume

fraction and aspect ratio. However at low particle volume fraction (e.g. around ϕ less than 2.5 vol%) and low aspect ratio (e.g. α around 5) the increase of the flux was not significant considering the experimental uncertainty obtained on a measure of water vapour flux. A trial of model validation was performed on a random dispersion of ellipsoids with different gradient of relative humidity across the composite film (for example 0-95%RH) with experimental input at 0-95% relative humidity. The predicted permeability value in the composite was approximately ten times higher than the experimental one. According to the rule of mixture, the prediction of the sorption in composites was in good agreement with the experimental sorption in WSF/PHBV composites and thus the initial and boundary conditions were confirmed in PHBV and WSF. Notwithstanding as said before, the WSF water vapour diffusivity coefficient was identified on a piece of native wheat straw and not on a single WSF. Once embedded in the PHBV matrix the milled WSF probably encountered mechanical constraints that prevent them to swell during water absorption as in the sorption experiment perform on a piece of wheat straw. This feature likely led to a modification of the diffusivity of water vapour of the WSF once in the composite structure. Confirming that, identification of, the diffusivity coefficient of water during the numerical simulation gave value 12 times lower than the experimental one, i.e. equal $0.57 \times 10^{-12} \text{ m}^2 \cdot \text{s}^{-1}$ against $6.91 \times 10^{-12} \text{ m}^2 \cdot \text{s}^{-1}$ as calculated from the product of $D \times S$ measured in the piece of wheat straw. This result showed the difficulty encounter for the characterization of mass transfer in a single milled particle. Indeed in order to improve the precision of the measure, it could be useful to develop a technology to monitor the mass transfer in-situ in the particle after its inclusion in the matrix.

While it has been proven that numerical simulation granted successful prediction of mass transfer in composites made up with constituents exhibiting totally opposite behaviour as regard water vapour transfer properties for example, the convergence of the model could still be ensured by defining continuous flux condition at the interface particle/polymer matrix. To reach the next level, by developing a 3D numerical model to predict mass transfer in bi-phasic composites by mimicking the realistic 3D structure, a complete characterization of the composite structure will be needed with the dispersion and the orientation of the particles in three dimensions.



REFERENCES

- Abdollahi, M., Alboofetileh, M., Rezaei, M., & Behrooz, R.**, *Comparing physico-mechanical and thermal properties of alginate nanocomposite films reinforced with organic and/or inorganic nanofillers*, *Food Hydrocolloids*, 32 (2013), 416–424
- Abdul Khalil, H. P. S., Bhat, a. H., & Ireana Yusra, a. F.** (2012). Green composites from sustainable cellulose nanofibrils: A review. *Carbohydrate Polymers*, 87 (2012), 963–979
- Abdul Khalil, H. P. S., Bhat, I. U. H., Jawaid, M., Zaidon, Hermawan, D., & Hadi, Y. S.**, Bamboo fibre reinforced biocomposites: A review. *Materials & Design*, 42 (2012), 353–368
- Abdulkhani, A., Hojati Marvast, E., Ashori, A., Hamzeh, Y., & Karimi, A. N.**, Preparation of cellulose/polyvinyl alcohol biocomposite films using 1-n-butyl-3-methylimidazolium chloride. *International journal of biological macromolecules*, 62 (2013), 379–86
- Ahn, J., Chung, W.-J., Pinnau, I., & Guiver, M. D.**, Polysulfone/silica nanoparticle mixed-matrix membranes for gas separation, *Journal of Membrane Science*, 314 (2008), 123–133
- Akil, H.M., Omar, M. F., Mazuki, M., Safiee, S., Ishak, Z. M., & Abu Bakar**, Kenaf fiber reinforced composites: A review, *Materials & Design*, 32 (2011), 4107–4121.
- Akil, Hazizan M, Cheng, L. W., Mohd Ishak, Z., Abu Bakar, & Abd Rahman, M.**, Water absorption study on pultruded jute fibre reinforced unsaturated polyester composites. *Composites Science and Technology*, 69(2009), 1942–1948
- Alboofetileh, M., Rezaei, M., Hosseini, H., & Abdollahi, M.**, Effect of montmorillonite clay and biopolymer concentration on the physical and mechanical properties of alginate nanocomposite films, *Journal of Food Engineering*, 117 (2013), 26–33
- Albuquerque, M. G. E., Adiutori, R., Trindade, N. M. P., Carmo, I. T. D., Oliveira, C. S. S., Pardelha, F., & Reis, M. A. M.**, BIOBASED FEEDSTOCK VALORISATION THROUGH POLYHYDROXYALKANOATE PRODUCTION: FROM EXCESS CHEESE WHEY TO ECO-EFFICIENT BIOPLASTICS *Environmental, Engineering and Management Journal*, 11 (2012)
- Alena, K., Dagmar, M., Francois, G. J., & Miroslav, S.**, Polymer/Clay Nanocomposites and Their Gas Barrier Properties, *Polymer Composites*, (2013), 1–7
- Alexandre, B., Langevin, D., Médéric, P., Aubry, T., Couderc, H., Nguyen, Q. T., ... Marais, S.**, Water barrier properties of polyamide 12/montmorillonite nanocomposite membranes: Structure and volume fraction effects, *Journal of Membrane Science*, 328(2009), 186–204
- Alexandre, M., & Dubois, P.**, Polymer-layered silicate nanocomposites : preparation, properties and uses of a new class of materials, *Materials Science and Engineering*, 28(2000), 1–63
- Ali, S. S., Tang, X., Alavi, S., & Faubion, J.**, Structure and physical properties of starch/poly vinyl alcohol/sodium montmorillonite nanocomposite films, *Journal of agricultural and food chemistry*, 59(2011), 12384–95
- Alix, S., Lebrun, L., Marais, S., Philippe, E., Bourmaud, Baley, C., & Morvan, C.**, Pectinase treatments on technical fibres of flax: Effects on water sorption and mechanical properties, *Carbohydrate Polymers*, 87(2012), 177–185
- Alix, S., Lebrun, L., Morvan, C., & Marais, S.**, Study of water behaviour of chemically treated flax fibres-based composites: A way to approach the hydric interface, *Composites Science and Technology*, 71(2011), 893–899
- Alix, S., Marais, S., Morvan, C., & Lebrun, L.**, Biocomposite materials from flax plants: Preparation and properties, *Composites Part A: Applied Science and Manufacturing*, 39(2008), 1793–1801

- Alix, S., Philippe, E., Bessadok, A., Lebrun, L., Morvan, C., & Marais, S.**, Effect of chemical treatments on water sorption and mechanical properties of flax fibres, *Bioresource technology*, 100(2009), 4742–4749
- Al-Muhtaseb, H., McMinn, W. M., & Magee, T. R.**, Water sorption isotherms of starch powders. *Journal of Food Engineering*, 61(2004), 297–307
- Al-Saleh, M. H., & Sundararaj, U.**, Review of the mechanical properties of carbon nanofiber/polymer composites. *Composites Part A: Applied Science and Manufacturing*, 42 (2011), 2126–2142
- Anadão, P., Sato, L. F., Montes, R. R., & De Santis, H. S.**, Polysulphone/montmorillonite nanocomposite membranes: Effect of clay addition and polysulphone molecular weight on the membrane properties, *Journal of Membrane Science*, 455 (2014), 187–199
- Andrews, R., & Weisenberger, M.**, Carbon nanotube polymer composites, *Current Opinion in Solid State and Materials Science*, 8 (2004), 31–37
- Angellier, H., Molina-Boisseau, S., Lebrun, L., & Dufresne, A.**, Processing and Structural Properties of Waxy Maize Starch Nanocrystals Reinforced Natural Rubber, *Macromolecules*, 38 (2005), 3783–3792
- Angellier-Coussy, H., Gastaldi, E., Da Silva, F. C., Gontard, N., & Guillard, V.**, Nanoparticle size and water diffusivity in nanocomposite agro-polymer based films. *European Polymer Journal*, 49 (2013), 299–306
- Angellier-coussy, H., Guillard, V., Guillaume, C., & Gontard, N.**, Role of packaging in the smorgasbord of action for sustainable food consumption, *Agro FOOD Industry Hi Tech*, 24 (2013), 15–19
- Aris, R.**, On a problem in hindered diffusion, *Archive for Rational Mechanics and Analysis*, 95(1986), 83–91
- Aroon, M. a., Ismail, a. F., Matsuura, T., & Montazer-Rahmati, M. M.**, Performance studies of mixed matrix membranes for gas separation: A review, *Separation and Purification Technology*, 75 (2010), 229–242
- Arora, A., & Padua, G. W.**, Review : Nanocomposites in Food Packaging, *Journal of food science*, 75 (2010), 43–49
- Avella, M., La Rota, G., Martuscelli, E., & Raimo, M.**, Poly(3-hydroxybutyrate-co-3-hydroxyvalerate) and wheat straw fibre composites: thermal, mechanical properties and biodegradation behaviour, *Journal of Materials Science*, 35 (2000), 829–836.
- Avella, Maurizio, De Vlieger, J. J., Errico, M. E., Fischer, S., Vacca, P., & Volpe, M. G.**, Biodegradable starch/clay nanocomposite films for food packaging applications, *Food Chemistry*, 93 (2005), 467–474
- Azeredo, Henriette M.C. De.**, Nanocomposites for food packaging applications, *Food Research International*, 42 (2009), 1240–1253
- Azeredo, Henriette M C, Mattoso, L. H. C., Avena-Bustillos, R. J., Filho, G. C., Munford, M. L., Wood, D., & McHugh, T. H.**, Nanocellulose reinforced chitosan composite films as affected by nanofiller loading and plasticizer content, *Journal of food science*, 75 (2010), 1–7
- Azeredo, Henriette M C, Mattoso, L. H. C., Wood, D., Williams, T. G., Avena-Bustillos, R. J., & McHugh, T. H.**, Nanocomposite edible films from mango puree reinforced with cellulose nanofibers, *Journal of food science*, 74 (2009), 31–35
- Azizi Samir, M. A. S., Alloin, F., & Dufresne, A.**, Review of recent research into cellulosic whiskers, their properties and their application in nanocomposite field, *Biomacromolecules*, 6 (2005), 612–26

- Bae, H. J., Park, H. J., Hong, S. I., Byun, Y. J., Darby, D. O., Kimmel, R. M., & Whiteside, W. S.,** Effect of clay content, homogenization RPM, pH, and ultrasonication on mechanical and barrier properties of fish gelatin/montmorillonite nanocomposite films, *LWT - Food Science and Technology*, 42(2009), 1179–1186
- Balachandran, M., & Bhagawan, S. S.** (2012), Mechanical, thermal and transport properties of nitrile rubber (NBR) - nanoclay composites, *Journal of Polymer Research*, 19(2012), 9809
- Banhegyi, G.,** Comparison of electrical mixture rules for composites, *Colloid & Polymer Science*, 264 (1986), 1030–1050
- Barrer, R. M., & Petropoulos, J. H.,** Diffusion in heterogeneous media: lattice and parallelepipeds in a continuous phase. *Journal of Applied Physics*, 12 (1961), 691–697
- Bedane, A. H., Huang, Q., Xiao, H., & Eić, M.,** Mass transfer of water vapor, carbon dioxide and oxygen on modified cellulose fiber-based materials, *Nordic Pulp and Paper Research Journal*, 27(2012), 409–417
- Belbekhouche, S., Bras, J., Siqueira, G., Chappey, C., Lebrun, L., Khelifi, B., ... Dufresne, A.,** Water sorption behavior and gas barrier properties of cellulose whiskers and microfibrils films, *Carbohydrate Polymers*, 83 (2011), 1740–1748
- Bendahou, A., Kaddami, H., Espuche, E., Gouanvé, F., & Dufresne, A.,** Synergism Effect of Montmorillonite and Cellulose Whiskers on the Mechanical and Barrier Properties of Natural Rubber Composites, *Macromolecular Materials and Engineering*, 296 (2011), 760–769
- Berthel, M.A.,** Sustainable biocomposites for food packaging issued from food industry by-products: Structure-properties relationships, PhD research work (2014)
- Bessadok, Langevin, D., Gouanvé, F., Chappey, C., Roudesli, S., & Marais, S.,** Study of water sorption on modified Agave fibres, *Carbohydrate Polymers*, 76 (2009), 74–85
- Bessadok, Marais, S., Roudesli, S., Lixon, C., & Métayer, M.,** Influence of chemical modifications on water-sorption and mechanical properties of Agave fibres, *Composites Part A: Applied Science and Manufacturing*, 39 (2008), 29–45
- Bessadok, Roudesli, S., Marais, S., Follain, N., & Lebrun, L.,** Alfa fibres for unsaturated polyester composites reinforcement: Effects of chemical treatments on mechanical and permeation properties, *Composites Part A: Applied Science and Manufacturing*, 40 (2009), 184–195
- Bharadwaj, R. K.,** Modeling the Barrier Properties of Polymer-Layered Silicate Nanocomposites, *Macromolecules*, 34 (2001), 9189–9192
- Bharadwaj, R. K., Mehrabi, a. R., Hamilton, C., Trujillo, C., Murga, M., Fan, R., ... Thompson, a. K.,** Structure–property relationships in cross-linked polyester–clay nanocomposites, *Polymer*, 43 (2002), 3699–3705
- Bhunia, K., Dhawan, S., & Sablani, S. S.,** Modeling the oxygen diffusion of nanocomposite-based food packaging films, *Journal of food science*, 77 (2012), 29–38
- Bilbao-Sainz, C., Bras, J., Williams, T., Sénechal, T., & Orts, W.,** HPMC reinforced with different cellulose nano-particles, *Carbohydrate Polymers*, 86 (2011), 1549–1557
- Bledzki, A. K., & Gassan, J.,** Composites reinforced with cellulose based fibres, *Progress in Polymer Science*, 24 (1999), 221–274
- Bordes, P., Pollet, E., & Averous, L.,** Nano-biocomposites: Biodegradable polyester/nanoclay systems, *Progress in Polymer Science*, 34 (2009), 125–155

- Boukhoulda, B. F., Adda-Bedia, E., & Madani, K.**, The effect of fiber orientation angle in composite materials on moisture absorption and material degradation after hygrothermal ageing, *Composite Structures*, 74 (2006), 406–418
- Bouma, R. H. B., Checchetti, Chidichimo, G., & Drioli, E.**, Permeation through a heterogeneous membrane: the effect of the dispersed phase, *Journal of Membrane Science*, 128 (1997), 141–149
- Bourlieu, C., Guillard, V., Powell, H., Vallès-Pàmies, B., Guilbert, S., & Gontard, N.**, Performance of lipid-based moisture barriers in food products with intermediate water activity, *European Journal of Lipid Science and Technology*, 108 (2006), 1007–1020
- Bracho, D., Dougnac, V. N., Palza, H., & Quijada, R.**, Functionalization of Silica Nanoparticles for Polypropylene Nanocomposite Applications, *Journal of Nanomaterials*, 2012, 1–8
- Bruggeman, D. A.**, Effective medium approximations, *Annals of Physics*, 24 (1935), 635–664
- Brunauer, S., Deming, L. S., Deming, W. E., & Teller, E.**, On a Theory of the van der Waals Adsorption of Gases, *Journal of American Chemical Society*, 62 (1940), 1723–1732
- Brydges, W. T., Gulati, S. T., & Baum, G.**, Permeability of glass ribbon-reinforced composites, *Journal of Materials Science*, 10 (1975), 2044–2049
- Cabedo, L., Giménez, E., Lagaron, J. M., Gavara, R., & Saura, J. J.**, Development of EVOH-kaolinite nanocomposites. *Polymer*, 45 (2004), 5233–5238
- Carvalho, G., Oehmen, A., Albuquerque, M. G. E., & Reis, M.**, The relationship between mixed microbial culture composition and PHA production performance from fermented molasses. *New biotechnology* (2013)
- Casariego, A., Souza, B. W. S., Cerqueira, M., Teixeira, J., Cruz, L., Díaz, R., & Vicente**, Chitosan/clay films' properties as affected by biopolymer and clay micro/nanoparticles' concentrations, *Food Hydrocolloids*, 23 (2009), 1895–1902
- Cava, D., Gimenez, E., Gavara, R., & Lagaron, J. M.**, Comparative Performance and Barrier Properties of Biodegradable Thermoplastics and Nanobiocomposites versus PET for Food Packaging Applications, *Journal of Plastic Film and Sheeting*, 22 (2006), 265–274
- Célino, A., Fréour, S., Jacquemin, F., & Casari, P.** (2013). Characterization and modeling of the moisture diffusion behavior of natural fibers. *Journal of Applied Polymer Science*, 130 (2013), 297–306. doi:10.1002/app.39148
- Cerisuelo, J.P., Muriel-Galet, V., Bermúdez, J. M., Aucejo, S., Catalá, R., Gavara, R., & Hernández-Muñoz, P.**, Mathematical model to describe the release of an antimicrobial agent from an active package constituted by carvacrol in a hydrophilic EVOH coating on a PP film. *Journal of Food Engineering*, 110 (2012), 26–37
- Cerisuelo, Josep Pasqual, Bermúdez, J. M., Aucejo, S., Catalá, R., Gavara, R., & Hernández-Muñoz, P.**, Describing and modeling the release of an antimicrobial agent from an active PP/EVOH/PP package for salmon. *Journal of Food Engineering*, 116 (2013), 352–361
- Chaiko, D. J., & Leyva, A.**, Thermal Transitions and Barrier Properties of Olefinic Nanocomposites. *Chemistry of Materials*, 17 (2005), 13–19
- Chang, J.H., An, Y.U.K., & Sur, G.S.**, Poly (lactic acid) Nanocomposites with Various Organoclays . I . Thermomechanical Properties , Morphology , and Gas Permeability, *Journal of Polymer Science Part B: Polymer Physics*, 41 (2002), 94–103.
- Chang, J., Park, K. N. Cho, D., & Yang, H. S.**, Preparation and Characterization of Polyimide Nanocomposites With Different, *Polymer Engineering & Science*, 41 (2001), 1514–1520.

- Chanprateep, S.**, Current trends in biodegradable polyhydroxyalkanoates. *Journal of bioscience and bioengineering*, 110 (2010), 621–32
- Charpentier, J.-C.** (2002). The triplet "molecular processes–product–process" engineering: the future of chemical engineering ? *Chemical Engineering Science*, 57 (2002), 4667–4690
- Chen, B., & Evans, J. R. G.** (2005). Thermoplastic starch–clay nanocomposites and their characteristics. *Carbohydrate Polymers*, 61 (2005), 455–463
- Chien, A., Lee, Y., & Lin, K.**, Crosslinkable Poly (vinyl acetate)/ Clay Nanocomposite Films Cast from Soap-Free Emulsion-Polymerized Latices, *Journal of Applied Polymer Science*, 109 (2008), 355–362
- Chiew, Y. C., & Glandt, E.**, The Effect of Structure on the Conductivity of a Dispersion, *Journal of colloid and interface science*, 94 (1983), 90–104.
- Chivrac, F., Angellier-Coussy, H., Guillard, V., Pollet, E., & Avérous, L.** (2010), How does water diffuse in starch/montmorillonite nano-biocomposite materials? *Carbohydrate Polymers*, 82 (2010), 128–135
- Chivrac, F., Pollet, E., & Avérous, L.** (2009), Progress in nano-biocomposites based on polysaccharides and nanoclays, *Materials Science and Engineering: R: Reports*, 67 (2009), 1–17
- Cho, S.-W., Gällstedt, M., & Hedenqvist, M.**, Properties of Wheat Gluten/Poly(lactic acid) Laminates, *Journal of Agricultural and Food Chemistry*, 58 (2010), 7344–7350
- Choi, R.-N., Cheigh, C.-I., Lee, S.-Y., & Chung, M.-S.**, Preparation and properties of polypropylene/clay nanocomposites for food packaging, *Journal of food science*, 76 (2011), 62–67
- Choi, W. J., Kim, S. H., Jin Kim, Y., & Kim, S. C.**, Synthesis of chain-extended organifier and properties of polyurethane/clay nanocomposites, *Polymer*, 45 (2004), 6045–6057
- Choudalakis, G., & Gotsis, D.**, Permeability of polymer/clay nanocomposites: A review. *European Polymer Journal*, 45 (2009), 967–984
- Chow, C., Xing, X., & Li, R.**, Moisture absorption studies of sisal fibre reinforced polypropylene composites, *Composites Science and Technology*, 67 (2007), 306–313
- Chung, T.-S., Jiang, L. Y., Li, Y., & Kulprathipanja, S.**, Mixed matrix membranes (MMMs) comprising organic polymers with dispersed inorganic fillers for gas separation, *Progress in Polymer*, 32 (2007), 483–507
- Cong, H, Radosz, M., Towler, B., & Shen, Y.**, Polymer–inorganic nanocomposite membranes for gas separation, *Separation and Purification Technology*, 55 (2007), 281–291
- Cong, Hailin, Hu, X., Radosz, M., & Shen, Y.**, Brominated Poly(2,6-diphenyl-1,4-phenylene oxide) and Its Silica Nanocomposite Membranes for Gas Separation, *Industrial & Engineering Chemistry Research*, 46 (2007), 2567–2575
- Cong, Hailin, Zhang, J., Radosz, M., & Shen, Y.** (2007). Carbon nanotube composite membranes of brominated poly(2,6-diphenyl-1,4-phenylene oxide) for gas separation, *Journal of Membrane Science*, 294 (2007), 178–185
- Cornelius, C. J., & Marand, E.**, Hybrid silica-polyimide composite membranes : gas transport properties. *Journal of Membrane Science*, 202 (2002), 97–118
- Cornelius, C. J., & Marand, E.**, Hybrid inorganic ± organic materials based on a 6FDA ± 6FpDA ± DABA polyimide and silica : physical characterization studies. *Polymer*, 43 (2002), 2385–2400

- Corradini, E., Ferreira, F. C., & Rosa, M. F.**, Absorção de Água, Solubilidade em Água, Propriedades Mecânicas e Morfológicas de Compósitos de Glúten de Milho e Poli (hidroxibutirato-co-valerato) (PHBV) Reforçados com Fibras de Coco Verde. *Polimeros*, 23 (2014), 807–813.
- Cosoli, P., Fermeglia, M., Ferrone, M., Posocco, P., S., P., & Scocchi, G.**, New materials from multiscale modelling procedures: properties prediction and customisation of polymeric nanocomposites. *Chemical Engineering Transactions*, 11 (2007), 89–94.
- Crank, J.** The mathematics of diffusion. (C. Press, Ed.) (2nd ed Oxf., p. 414). U.K., (1975)
- Crétois, R., Follain, N., Dargent, E., Soulestin, J., Bourbigot, S., Marais, S., & Lebrun, L.**, Microstructure and barrier properties of PHBV/organoclays bionanocomposites, *Journal of Membrane Science*, 467 (2014), 56–66
- Cussler, E. L., Hughes, S. E., Ward, W. J., & Aris, R.**, Barrier Membranes. *Journal of Membrane Science*, 38 (1988), 161–174
- Dash, S., & Swain, S. K.**, Synthesis of thermal and chemical resistant oxygen barrier starch with reinforcement of nano silicon carbide. *Carbohydrate polymers*, 97 (2013), 758–63
- De Moraes, M. A., & Beppu, M. M.**, Biocomposite membranes of sodium alginate and silk fibroin fibers for biomedical applications. *Journal of Applied Polymer Science*, 130 (2013), 3451–3457
- De Moura, M. R., Avena-Bustillos, R. J., McHugh, T. H., Krochta, J. M., & Mattoso, L. H. C.**, Properties of novel hydroxypropyl methylcellulose films containing chitosan nanoparticles, *Journal of food science*, 73 (2008), 31–37
- Derocher, J., Gettelfinger, B., Wang, J., Nuxoll, E., & Cussler, E.**, Barrier membranes with different sizes of aligned flakes, *Journal of Membrane Science*, 254 (2005), 21–30
- Di, Y., Iannac, S., Sanguigno, L., & Nicolais, L.**, Barrier and Mechanical Properties of Poly(caprolactone) / organoclay Nanocomposites, *Macromolecular Symposia*, 228 (2005), 115–124
- Dias, A. B., Müller, C. M. O., Larofonda, F. D. S., & Laurindo, J. B.**, Mechanical and barrier properties of composite films based on rice flour and cellulose fibers, *LWT - Food Science and Technology*, 44 (2011), 535–542
- Dogan, N., & McHugh, T. H.**, Effects of microcrystalline cellulose on functional properties of hydroxy propyl methyl cellulose microcomposite films, *Journal of food science*, 72 (2007), 16–22
- Doroudiani, S., Chaffey, C. E., & Kortschot, M. T.**, Sorption and diffusion of carbon dioxide in wood-fiber/polystyrene composites. *Journal of Polymer Science Part B: Polymer Physics*, 40 (2002), 723–735
- Dougnac, V.N, Alamillo, R., Peoples, B. ., & Quijada, R.**, Effect of particle diameter on the permeability of polypropylene/SiO₂ nanocomposites, *Polymer*, 51 (2010), 2918–2926
- Du, A., Koo, D., Theryo, G., Hillmyer, M. a., & Cairncross, R.**, Water transport and clustering behavior in homopolymer and graft copolymer polylactide, *Journal of Membrane Science*, 396 (2012), 50–56
- Duan, Z., Thomas, N. L., & Huang, W.**, Water vapour permeability of poly(lactic acid) nanocomposites, *Journal of Membrane Science*, 445 (2013), 112–118
- Dunkerley, E., & Schmidt, D.**, Effects of Composition, Orientation and Temperature on the O₂ Permeability of Model Polymer/Clay Nanocomposites, *Macromolecules*, 43 (2010), 10536–10544

- Duque, A. F., Oliviera, C. S. S., Carmo, I. T. D., Gouveia, A. R. Gouveia, Pardelha, F., Ramos, A. M., & Reis, M. A. M.**, Response of a three-stage process for PHA production by mixed microbial cultures to feedstock shift: impact on polymer composition, *New Biotechnology*, 31 (2014), 276–288
- Echeverría, I., Eisenberg, P., & Mauri, A. N.**, Nanocomposites films based on soy proteins and montmorillonite processed by casting, *Journal of Membrane Science*, 449 (2014), 15–26
- Eitzman, D. M., Melkote, R. R., & Cussler, E. L.**, Barrier membranes with tipped impermeable flakes, *AIChE Journal*, 42 (1986), 2–9
- Espino-Pérez, E., Bras, J., Ducruet, V., Guinault, A., Dufresne, A., & Domenek, S.**, Influence of chemical surface modification of cellulose nanowhiskers on thermal, mechanical, and barrier properties of poly(lactide) based bionanocomposites, *European Polymer Journal*, 49(2013), 3144–3154
- Fabra, M. J., Lopez-Rubio, A., & Lagaron, J. M.**, High barrier polyhydroxyalcanoate food packaging film by means of nanostructured electrospun interlayers of zein, *Food Hydrocolloids*, 32 (2013), 106–114
- Falla, W. R., Mulski, M., & Cussler, E. L.**, Estimating diffusion through flake-filled membranes, *Journal of Membrane Science*, 119 (1996), 129–138
- Famá, L., Gerschenson, L., & Goyanes, S.**, Starch-vegetable fibre composites to protect food products. *Carbohydrate Polymers*, 75 (2009), 230–235
- Faruk, O., Bledzki, A. K., Fink, H.-P., & Sain, M.**, Biocomposites reinforced with natural fibers: 2000–2010. *Progress in Polymer Science*, 37 (2012), 1552–1596
- Fasihi, M., & Abolghasemi, M. R.**, Oxygen Barrier and Mechanical Properties of Masterbatch- Based PA6 / Nanoclay Composite Films, *Journal of Applied Polymer Science*, 125 (2011), 2–8
- Favre, E., Nguyen, Q. T., & Nrel, J.**, The engaged species induced clustering (ENSIC) model : a unified mechanistic approach of sorption phenomena in polymers. *Journal of Membrane Science*, 117 (1996), 227–236
- Felske, J. D.**, Effective thermal conductivity of composite spheres in a continuous medium with contact resistance, *International Journal of Heat and Mass Transfer*, 47 (2004), 3453–3461
- Fendler, A., Villanueva, M. P., Gimenez, E., & Lagarón, J. M.**, Characterization of the barrier properties of composites of HDPE and purified cellulose fibers, *Cellulose*, 14 (2007), 427–438
- Fermeglia, M., & Pricl, S.**, Multiscale molecular modeling in nanostructured material design and process system engineering, *Computers & Chemical Engineering*, 33 (2009), 1701–1710
- Follain, N., Belbekhouche, S., Bras, J., Siqueira, G., Marais, S., & Dufresne, A.**, Water transport properties of bio-nanocomposites reinforced by *Luffa cylindrica* cellulose nanocrystals, *Journal of Membrane Science*, 427 (2013), 218–229
- Fortunati, E., Peltzer, M., Armentano, I., Torre, L., Jiménez, a, & Kenny, J. M.**, Effects of modified cellulose nanocrystals on the barrier and migration properties of PLA nano-biocomposites. *Carbohydrate polymers*, 90 (2012), 948–956
- Fredrickson, G. H., & Bicerano, J.**, Barrier properties of oriented disk composites, *The Journal of Chemical Physics*, 110 (1999), 2181–2188
- Fujishima, A., Rao, T. N., & Tryk, D. A.**, Titanium dioxide photocatalysis, *Journal of Photochemistry and Photobiology C: Photochemistry Reviews* 1, 1(2000), 1–21

- Gain, O., Espuche, E., Pollet, E., Alexandre, M., & Dubois, P.**, Gas barrier properties of poly(ϵ -caprolactone)/clay nanocomposites: Influence of the morphology and polymer/clay interactions, *Journal of Polymer Science Part B: Polymer Physics*, 43 (2005), 205–214
- Gatos, K. G., & Karger-Kocsis, J.**, Effect of the aspect ratio of silicate platelets on the mechanical and barrier properties of hydrogenated acrylonitrile butadiene rubber (HNBR)/layered silicate nanocomposites, *European Polymer Journal*, 43 (2007), 1097–1104
- George, J., Sreekala, M. S., & Thomas, S.**, A review on interface modification and characterization of natural fiber reinforced plastic composites. *Polymer Engineering & Science*, 41 (2001), 1471–1485. doi:10.1002/pen.10846
- George, S. C., & Thomas, S.**, Transport phenomena through polymeric systems, *Progress in Polymer Science*, 26 (2001), 985–1017
- Ghadimi, A., Sadrzadeh, M., Shahidi, K., & Mohammadi, T.**, Ternary gas permeation through a synthesized PDMS membrane: Experimental and modeling, *Journal of Membrane Science*, 344 (2009), 225–236
- Ghasemi, H., Carreau, P. J., Kamal, M. R., & Tabatabaei, S. H.**, Properties of PET/Clay Nanocomposite Films, *Polymer Engineering & Science*, 52 (2012), 420–430
- Ghizzi D Silva**, Fractionnement par voie sèche de la biomasse ligno-cellulosique : Broyage poussé de la paille de blé et effets sur ses bioconversions, PhD research work (2011)
- Ghizzi D Silva, G., Couturier, M., Berrin, J.-G., Buléon, A., & Rouau, X.**, Effects of grinding processes on enzymatic degradation of wheat straw, *Bioresource technology*, 103 (2012), 192–200
- Giannelis, E. P.**, Polymer-layered silicate nanocomposites: Synthesis, properties and applications. *Applied Organometallic Chemistry*, 12 (1998), 675–680
- Gontard, N., Guilbert, S., & Cuq, J. L.**, Water and Glycerol as Plasticizers Affect Mechanical and Water Vapor Barrier Properties of an Edible Wheat Gluten Film, *Journal of Food Science*, 58 (1993), 206–211
- Gonzo, E. E.**, Estimating correlations for the effective thermal conductivity of granular materials, *Chemical Engineering Journal*, 90 (2002), 299–302
- Gonzo, E. E., Parentis, M. L., & Gottifredi, J. C.**, Estimating models for predicting effective permeability of mixed matrix membranes. *Journal of Membrane Science*, 277 (2006), 46–54
- Goodyer, C. E., & Bunge, A. L.**, Numerical simulations compared against experimental results for barrier membranes with lithographically printed flakes, *Journal of Membrane Science*, 306 (2007), 196–208
- Goodyer, C. E., & Bunge, A. L.**, Comparison of numerical simulations of barrier membranes with impermeable flakes, *Journal of Membrane Science*, 329 (2009), 209–218
- Gorrasi, G., Pantani, R., Murariu, M., & Dubois, P.**, PLA/Halloysite Nanocomposite Films: Water Vapor Barrier Properties and Specific Key Characteristics, *Macromolecular Materials and Engineering*, 299 (2014), 104–115
- Gorrasi, G., Tortora, M., Vittoria, V., Galli, G., & Chiellini, E.**, Transport and mechanical properties of blends of poly(ϵ -caprolactone) and a modified montmorillonite-poly(ϵ -caprolactone) nanocomposite, *Journal of Polymer Science Part B: Polymer Physics*, 40 (2002), 1118–1124
- Gorrasi, G., Vittoria, V., Murariu, M., Ferreira, A. D. S., Alexandre, M., & Dubois, P.**, Effect of filler content and size on transport properties of water vapor in PLA/calcium sulfate composites, *Biomacromolecules*, 9 (2008), 984–990. doi:10.1021/bm700568n

- Gouanvé, F., Marais, S., Bessadok, A., Langevin, D., & Métayer, M.**, Kinetics of water sorption in flax and PET fibers, *European Polymer Journal*, 43 (2007), 586–598
- Gouanvé, F., Marais, S., Bessadok, A., Langevin, D., Morvan, C., & Métayer, M.**, Study of water sorption in modified flax fibers, *Journal of Applied Polymer Science*, 101 (2006), 4281–4289
- Grazia De Angelis, M., & Sarti, G. C.**, Solubility and Diffusivity of Gases in Mixed Matrix Membranes Containing Hydrophobic Fumed Silica: Correlations and Predictions Based on the NELF Model, *Industrial & Engineering Chemistry Research*, 47 (2008), 5214–5226
- Greco**, Simulation and modeling of diffusion in oriented lamellar nanocomposites, *Computational Materials Science*, 83 (2014), 164–170
- Greco, A., & Maffezzoli, A.**, Two-dimensional and three-dimensional simulation of diffusion in nanocomposite with arbitrarily oriented lamellae, *Journal of Membrane Science*, 442 (2013), 238–244
- Gubbins, K. E., & Moore, J. D.**, Molecular Modeling of Matter : Impact and Prospects in Engineering, *Industrial & Engineering Chemistry Research*, 49 (2010), 3026–3046
- Guilherme, M. R., Mattoso, L. H. C., Gontard, N., Guilbert, S., & Gastaldi, E.**, Synthesis of nanocomposite films from wheat gluten matrix and MMT intercalated with different quaternary ammonium salts by way of hydroalcoholic solvent casting, *Composites Part A: Applied Science and Manufacturing*, 41 (2010), 375–382
- Guillard, V., Broyart, B., Bonazzi, C., Guilbert, S., & Gontard, N.**, Moisture Diffusivity in Sponge Cake as Related to Porous Structure Evaluation and Moisture Content, *Journal of food science*, 68 (2003), 555–562.
- Guillard, Valérie, Chevillard, A., Gastaldi, E., Gontard, N., & Angellier-Coussy, H.**, Water transport mechanisms in wheat gluten based (nano)composite materials, *European Polymer Journal*, 49 (2013), 1337–1346
- Gunning, M. a., Geever, L. M., Killion, J. a., Lyons, J. G., & Higginbotham, C. L.**, Mechanical and biodegradation performance of short natural fibre polyhydroxybutyrate composites. *Polymer Testing*, 32 (2013), 1603–1611
- Guo, J., Li, X., Mu, C., Zhang, H., Qin, P., & Li, D.**, Freezing–thawing effects on the properties of dialdehyde carboxymethyl cellulose crosslinked gelatin-MMT composite films. *Food Hydrocolloids*, 33 (2013), 273–279
- Gusev, A., & Lusti, H.**, Rational design of nanocomposites for barrier applications. *Advanced Materials*, 13 (2001), 1641–1643
- Hashemifard, S. A., Ismail, A. F., & Matsuura, T.**, Prediction of gas permeability in mixed matrix membranes using theoretical models. *Journal of mem*, 347 (2010), 53–61
- He, Z., Pinnau, I., Morisato, A., Road, W., & Park, M.**, Nanostructured poly (4-methyl-2-pentyne)/ silica membranes for gas separation. *Desalination*, 146 (2002), 11–15.
- Herrera-Alonso, J. M., Marand, E., Little, J. C., & Cox, S. S.**, Transport properties in polyurethane/clay nanocomposites as barrier materials: Effect of processing conditions, *Journal of Membrane Science*, 337 (2009), 208–214
- Herrera-Alonso, J. M., Sedlakova, Z., & Marand, E.**, Gas barrier properties of nanocomposites based on in situ polymerized poly(n-butyl methacrylate) in the presence of surface modified montmorillonite, *Journal of Membrane Science*, 349 (2010), 251–257

- Herrera-Alonso, J. M., Sedláková, Z., & Marand, E.**, Gas transport properties of polyacrylate/clay nanocomposites prepared via emulsion polymerization, *Journal of Membrane Science*, 363 (2010), 48–56
- Higushi, W. I.**, A new relationship for the dielectric properties of two- phase mixtures, *Journal of Physical Chemistry*, 62 (1958), 649–653
- Horst, F., Tuckart, W., Blanco, L. Del, Failla, M. D., & Quinzani, L. M.**, Effect of Clay Concentration on the Wear Behavior and Permeability of Polypropylene / Clay Nanocomposites, *Journal of Applied Polymer Science*, 125 (2012), 495–502
- Hotta, S., & Paul, D. R.**, Nanocomposites formed from linear low density polyethylene and organoclays, *Polymer*, 45 (2004), 7639–7654
- Hu, Q., Marand, E., Dhingra, S., Fritsch, D., & Wen, J.**, Poly (amide-imide)/ TiO₂ nano-composite gas separation membranes " Fabrication and characterization. *Journal of Membrane Science*, 135 (1997), 65–79.
- Huang, C., Jang, G., Chang, K., Hung, W., & Yeh, J.**, High-performance polyimide – clay nanocomposite materials based on a dual intercalating agent system, *Polymer International*, 57 (2008), 605–611
- Hwang, S.-T.**, Fundamentals of membrane transport, *Korean Journal of Chemical Engineering*, 28 (2010), 1–15
- Imam, S. H., Cinelli, P., Gordon, S. H., & Chiellini, E.**, Characterization of Biodegradable Composite Films Prepared from Blends of Poly(Vinyl Alcohol), Cornstarch, and Lignocellulosic Fiber, *Journal of Polymers and the Environment*, 13 (2005), 47–55
- Ismail, A. F., Rahim, N. H., Mustafa, A., Matsuura, T., Ng, B. C., Abdullah, S., & Hashemifard, S.**, Gas separation performance of polyethersulfone/multi-walled carbon nanotubes mixed matrix membranes, *Separation and Purification Technology*, 80 (2001), 20–31
- Ito, M., & Nagai, K.**, Thermal Aging and Oxygen Permeation of Nylon-6 and Nylon-6 / Montmorillonite Composites, *Journal of Applied Polymer Science*, 118 (2010), 928–935
- Iwata, M., Adachi, T., Tomidokoro, M., Ohta, M., & Kobayashi, T.**, Hybrid Sol – Gel Membranes of Polyacrylonitrile – Tetraethoxysilane Composites for Gas Permselectivity, *Journal of Applied Polymer Science*, 88 (2003), 1752–1759
- Jacquelot, E., Espuche, E., Gérard, J.-F., Duchet, J., & Mazabraud, P.**, Morphology and gas barrier properties of polyethylene-based nanocomposites, *Journal of Polymer Science Part B: Polymer Physics*, 44 (2006), 431–440
- Jancar, J., Douglas, J. F., Starr, F. W., Kumar, S. K., Cassagnau, P., Lesser, a. J., ... & Buehler, M. J.**, Current issues in research on structure–property relationships in polymer nanocomposites, *Polymer*, 51 (2010), 3321–3343
- Jawaid, M., & Abdul Khalil, H. P. S.**, Cellulosic/synthetic fibre reinforced polymer hybrid composites: A review, *Carbohydrate Polymers*, 86 (2011), 1–18
- Johansson, C., Bras, J., Mondragon, I., Nechita, P., Plackett, D., Simon, P., & Aucejo, S.**, RENEWABLE FIBERS AND BIO-BASED MATERIALS FOR PACKAGING APPLICATIONS – A REVIEW OF RECENT DEVELOPMENTS. *BioResources*, 7 (2012), 2506–2552
- John, M., & Thomas, S.**, Biofibres and biocomposites, *Carbohydrate Polymers*, 71 (2008), 343–364
- Joliff, Y., Belec, L., & Chailan, J. F.**, Modified water diffusion kinetics in an unidirectional glass/fibre composite due to the interphase area: Experimental, analytical and numerical approach. *Composite Structures*, 97 (2013), 296–303

- Joliff, Y., Belec, L., Heman, M. B., & Chailan, J. F.**, Experimental, analytical and numerical study of water diffusion in unidirectional composite materials – Interphase impact. *Computational Materials Science*, 64 (2012), 141–145
- Joly, C., Smaihi, M., Porcar, L., & Noble, R. D.**, Polyimide-Silica Composite Materials: How Does Silica Influence Their Microstructure and Gas Permeation Properties?, *Chemistry of Materials*, 11(1999), 2331–2338
- Jordan, J., Jacob, K. I., Tannenbaum, R., Sharaf, M. a., & Jasiuk, I.** (2005), Experimental trends in polymer nanocomposites—a review, *Materials Science and Engineering: A*, 393 (2005), 1–11
- Kasirga, Y., Oral, A., & Caner, C.**, Preparation and Characterization of Chitosan / Montmorillonite-K10 Nanocomposites Films for Food Packaging Applications, *Polymer composites*, 33 (2012), 1874–1882
- Katiyar, V., Gerds, N., Koch, C. B., Risbo, J., Hansen, H. C. B., & Plackett, D.**, Melt Processing of Poly (L-Lactic Acid) in the Presence of Organomodified Anionic or Cationic Clays, *Journal of Applied Polymer Science*, 122 (2011), 112–125
- Ke, Z., & Yongping, B.**, Improve the gas barrier property of PET film with montmorillonite by in situ interlayer polymerization, *Materials Letters*, 59 (2005), 3348–3351
- Kim, J. H., & Lee, Y. M.**, Gas permeation properties of poly(amide-6-b-ethylene oxide)–silica hybrid membranes, *Journal of Membrane Science*, 193 (2001) 209–225
- Kim, J., Hu, C., Woo, R., & Sham, M.**, Moisture barrier characteristics of organoclay/epoxy nanocomposites, *Composites Science and Technology*, 65 (2005), 805–813
- Kim, S., Chen, L., Johnson, J. K., & Marand, E.**, Polysulfone and functionalized carbon nanotube mixed matrix membranes for gas separation: Theory and experiment, *Journal of Membrane Science*, 294 (2007), 147–158
- Kim, S., Pechar, T. W., & Marand, E.**, Poly(imide siloxane) and carbon nanotube mixed matrix membranes for gas separation, *Desalination*, 192 (2006), 330–339
- Kim, J. K., May, Y. W.**, Engineered interfaces in fibre reinforced composites, Elsevier Science. (1998)
- Kisku, S. K., Dash, S., & Swain, S. K.**, Dispersion of SiC nanoparticles in cellulose for study of tensile, thermal and oxygen barrier properties, *Carbohydrate polymers*, 99 (2014), 306–10
- Kisku, S. K., & Swain, S. K.**, Study of Oxygen Permeability and Flame Retardancy Properties of Biodegradable Polymethylmethacrylate / Starch Composites, *Polymer composites*, 33 (2012), 79–84
- Kong, Y., Du, H., Yang, J., Shi, D., & Wang, Y.**, Study on polyimide / TiO₂ nanocomposite membranes for gas separation, *Desalination*, 146 (2002), 49–55
- Kono, T., Hu, Y., Masuda, T., Tanaka, K., Priestley, R. D., & Freeman, B. D.**, Effect of Fumed Silica Nanoparticles on the Gas Permeation Properties of Substituted Polyacetylene Membranes, *Polymer Bulletin*, 58 (2006), 995–1003
- Koros, W.J., & Fleming, G. K.**, Membrane-based gas separation, *Journal of Membrane Science*, 83 (1993), 1–80
- Kristo, E., & Biliaderis, C.**, Physical properties of starch nanocrystal-reinforced pullulan films, *Carbohydrate Polymers*, 68 (2007), 146–158

- Kumar, P., Sandeep, K. P., Alavi, S., & Truong, V. D.**, A review of experimental and modeling techniques to determine properties of biopolymer-based nanocomposites, *Journal of food science*, 76 (2011), 2–14
- Kumar, P., Sandeep, K. P., Alavi, S., Truong, V. D., & Gorga, R. E.**, Preparation and characterization of bio-nanocomposite films based on soy protein isolate and montmorillonite using melt extrusion, *Journal of Food Engineering*, 100 (2010), 480–489
- Kumar, P., Sandeep, K. P., Alavi, S., Truong, V. D., & Gorga, R. E.**, Effect of type and content of modified montmorillonite on the structure and properties of bio-nanocomposite films based on soy protein isolate and montmorillonite, *Journal of food science*, 75 (2010), 46–56
- Lan, T., Kaviratna, P. D., & Pinnavaia, T. J.**, On the Nature of Polyimide-Clay Hybrid Composites, *Chemical Materials*, 6 (1994), 573–575.
- Lange, J., & Wyser, Y.**, Recent innovations in barrier technologies for plastic packaging : a review, *Packaging Technology and Science*, 16 (2003), 149–158
- Lape, N. K., Nuxoll, E. E., & Cussler, E. L.**, Polydisperse flakes in barrier films. *Journal of Membrane Science*, 236 (2004), 29–37
- Lau, K., Gu, C., & Hui, D.**, A critical review on nanotube and nanotube/nanoclay related polymer composite materials, *Composites Part B: Engineering*, 37(2006), 425–436
- Lebaron, P. C., Wang, Z., & Pinnavaia, T. J.**, Polymer-layered silicate nanocomposites : an overview, *Applied Clay Science*, 15 (1999), 11–29
- Lee, C. H., Hwang, S. Y., Sohn, J. Y., Park, H. B., Kim, J. Y., & Lee, Y. M.**, Water-stable crosslinked sulfonated polyimide–silica nanocomposite containing interpenetrating polymer network, *Journal of Power Sources*, 163 (2006), 339–348
- Lee, C.-H., Chien, A.-T., Yen, M.-H., & Lin, K.-F.**, Poly(methyl acrylate-co-methyl methacrylate)/montmorillonite nanocomposites fabricated by soap-free emulsion polymerization, *Journal of Polymer Research*, 15 (2008), 331–336
- Lee, J., & Kim, K. M.**, Characteristics of Soy Protein Isolate-Montmorillonite Composite Films, *Journal of Applied Polymer Science*, 118 (2010), 2257–2263
- Lee, J.-H., Jung, D., Hong, C.-E., Rhee, K. Y., & Advani, S. G.**, Properties of polyethylene-layered silicate nanocomposites prepared by melt intercalation with a PP-g-MA compatibilizer, *Composites Science and Technology*, 65 (2005), 1996–2002
- Lei, Y., Wu, Q., Clemons, C. M., Yao, F., & Xu, Y.**, Influence of Nanoclay on Properties of HDPE / Wood Composites, *Journal of Applied Polymer Science*, 106 (2007), 3958–3966
- Lewis, T., & Lewis, L.**, Dynamic mechanical properties of particulate-filled composites, *Journal of Applied Polymer Science*, 14 (1970), 1449–1471
- Lewis, T., & Nielsen, L.**, Dynamic mechanical properties of particulate-filled composites, *Journal of Applied Polymer Science*, 14 (1970), 1449–1471
- Li, J.-F., Xu, Z.-L., Yang, H., Yu, L.-Y., & Liu, M.**, Effect of TiO₂ nanoparticles on the surface morphology and performance of microporous PES membrane, *Applied Surface Science*, 255 (2009), 4725–4732
- Liu, Y., & Kumar, S.**, Polymer/Carbon nanotube nano composite fibers-a review. *ACS applied materials & interfaces*, 6 (2014), 6069–87

- Lotti, C., Isaac, C. S., Branciforti, M. C., Alves, R. M. V., Liberman, S., & Bretas, R. E. S.**, Rheological, mechanical and transport properties of blown films of high density polyethylene nanocomposites, *European Polymer Journal*, 44 (2008), 1346–1357
- Lu, C., & Mai, Y.-W.**, Permeability modelling of polymer-layered silicate nanocomposites, *Composites Science and Technology*, 67 (2007), 2895–2902
- Luecha, J., Sozer, N., & Kokini, J. L.**, Synthesis and properties of corn zein/montmorillonite nanocomposite films, *Journal of Materials Science*, 45 (2010), 3529–3537
- Mahajan, R., & Koros, W. J.**, Mixed Matrix Membrane Materials With Glassy Polymers . Part 1, *Polymer Engineering and Science*, 42 (2002), 1420–1431
- Mahajan, R., & Koros, W. J.**, Mixed Matrix Membrane Materials With Glassy Polymers . Part 2, *Polymer Engineering and Science*, 42 (2002), 1432–1441
- Mahajan, Rajiv, & Koros, W. J.**, Factors Controlling Successful Formation of Mixed-Matrix Gas Separation Materials, *Industrial & Engineering Chemistry Research*, 39 (2000), 2692–2696
- Maksimov, R. D., Gaidukov, S., Zicans, J., & Jansons, J.**, Moisture permeability of a polymer nanocomposite containing unmodified clay, *Mechanics of Composite Materials*, 44 (2008), 505–514
- Mannberg, P., Nyström, B., Wallström, L., & Joffe, R.**, Service life assessment and moisture influence on bio-based composites, *Journal of Materials Science*, 49 (2014), 5265–5270
- Marais, S., Gouanvé, F., Bonnesoeur, A., Grenet, J., Poncin-Epaillard, F., Morvan, C., & Métayer, M.**, Unsaturated polyester composites reinforced with flax fibers: effect of cold plasma and autoclave treatments on mechanical and permeation properties, *Composites Part A: Applied Science and Manufacturing*, 36 (2005), 975–986
- Marcovich, N., Reboredo, M., & Aranguren, M.**, Moisture diffusion in polyester–woodflour composites. *Polymer*, 40 (1999), 7313–7320
- Matteucci, S., Kusuma, V. A., Swinnea, S., & Freeman, B. D.**, Gas permeability, solubility and diffusivity in 1,2-polybutadiene containing brookite nanoparticles. *Polymer*, 49 (2008), 757–773
- Maxwell, J. C.** (1873). *Treatise on Electricity and Magnetism*, (Oxford Uni.). London.
- Meera, A. P., P, S. T., & Thomas, S.**, Effect of Organoclay on the Gas Barrier Properties of Natural Rubber Nanocomposites. *Polymer Composites*, 33 (2012), 524–531
- Merinska, D., Kubisova, H., Kalendova, a., Svoboda, P., & Hromadkova, J.**, Processing and Properties of Polyethylene/Montmorillonite Nanocomposites. *Journal of Thermoplastic Composite Materials*, 25 (2011), 115–131
- Messersmith, P. B.**, Synthesis and Barrier Properties of Poly (ϵ -caprolactone)-Layered Silicate Nanocomposites, *Journal of Polymer Science Part A: Polymer Chemistry*, 33 (1995), 1047–1057
- Miguel, O., & Irwin, J. J.**, Water Transport Properties in Poly (3-hydroxybutyrate) and Poly (3-hydroxybutyrate-co-3-hydroxyvalerate) Biopolymers, *Journal of Applied Polymer Science*, 73 (1999), 455–468
- Minelli, M., Baschetti, M. G., & Doghieri, F.**, Analysis of modeling results for barrier properties in ordered nanocomposite systems, *Journal of Membrane Science*, 327 (2009), 208–215
- Minelli, M., Baschetti, M. G., & Doghieri, F.**, A comprehensive model for mass transport properties in nanocomposites, *Journal of Membrane Science*, 381 (2011), 10–20

- Mittal, V.**, Mechanical and Gas Permeation Properties of Compatibilized Polypropylene – Layered Silicate Nanocomposites, *Journal of Applied Polymer Science*, 107 (2007), 1350–1361
- Mittal, V.**, Polymer Layered Silicate Nanocomposites: A Review, *Materials*, 2(3), 992–1057
- Mittal, V.**, Modelling and Prediction of Barrier Properties of Polymer Layered Silicate Nanocomposites, *Polymer & Polymer composites*, 21 (2013), 509–518.
- Modesti, M., Dall’Acqua, C., Lorenzetti, a, & Florian, E.**, Mathematical model and experimental validation of water cluster influence upon vapour permeation through hydrophilic dense membrane, *Journal of Membrane Science*, 229 (2004), 211–223
- Modi, S., Koelling, K., & Vodovotz, Y.**, Assessment of PHB with varying hydroxyvalerate content for potential packaging applications, *European Polymer Journal*, 47 (2011), 179–186
- Moggridge, G. ., Lape, N. K., Yang, C., & Cussler, E.**, Barrier films using flakes and reactive additives, *Progress in Organic Coatings*, 46 (2003), 231–240
- Moghadam, F., Omidkhah, M. R., Vasheghani-Farahani, E., Pedram, M. Z., & Dorosti, F.**, The effect of TiO₂ nanoparticles on gas transport properties of Matrimid5218-based mixed matrix membranes, *Separation and Purification Technology*, 77 (2011), 128–136
- Mohan, T. P., & Kanny, K.**, Water barrier properties of nanoclay filled sisal fibre reinforced epoxy composites. *Composites Part A: Applied Science and Manufacturing*, 42 (2011), 385–393
- Mohanty, a. K., Misra, M., & Hinrichsen, G.**, Biofibres, biodegradable polymers and biocomposites: An overview, *Macromolecular Materials and Engineering*, 276-277 (2000), 1–24
- Mondal, S., & Hu, J. L.**, Microstructure and Water Vapor Transport Properties of Functionalized Carbon Nanotube-Reinforced Dense- Segmented Polyurethane Composite Membranes, *Polymer Engineering & Science*, 48 (2008), 1718–1724
- Monsiváis-Barrón, a. J., Bonilla-Rios, J., Ramos de Valle, L. F., & Palacios, E.**, Oxygen permeation properties of HDPE-layered silicate nanocomposites. *Polymer Bulletin*, 70 (2013), 939–951
- Moradi Shehni, P., Amooghin, A. E., Ghadimi, A., Sadrzadeh, M., & Mohammadi, T.**, Modeling of unsteady-state permeation of gas mixture through a self-synthesized PDMS membranes, *Separation and Purification Technology*, 76 (2011), 385–399
- Mukherjee, T., & Kao, N.**, PLA Based Biopolymer Reinforced with Natural Fibre: A Review, *Journal of Polymers and the Environment*, 19 (2011), 714–725
- Müller, Carmen M.O., Laurindo, J. B., & Yamashita, F.**, Effect of cellulose fibers addition on the mechanical properties and water vapor barrier of starch-based films, *Food Hydrocolloids*, 23 (2009), 1328–1333
- Murali, R. S., Sridhar, S., Sankarshana, T., & Ravikumar, Y. V. L.**, Gas Permeation Behavior of Pebax-1657 Nanocomposite Membrane Incorporated with Multiwalled Carbon Nanotubes, *Industrial & Engineering Chemistry Research*, 49 (2010), 6530–6538
- Muralidharan, M. N., Kumar, S. A., & Thomas, S.**, Morphology and transport characteristics of poly(ethylene-co-vinyl acetate)/clay nanocomposites, *Journal of Membrane Science*, 315 (2008), 147–154
- Nazarenko, S., Meneghetti, P., Julmon, P., Olson, B. G., & Qutubuddin, S.**, Gas Barrier of Polystyrene Montmorillonite Clay Nanocomposites: Effect of Mineral Layer Aggregation, *Journal of Polymer Science Part B: Polymer Physics*, 45 (2007), 1733–1753

- Nielsen, L.**, Thermal Conductivity of Particulate-Filled Polymers, *Journal of Applied Polymer Science*, 17 (1973), 3819–3820
- Nielsen, L. E.**, Models for the permeability of filled polymer systems, *Journal of Macromolecular Science Part A*, 1 (1967), 929–942.
- Osman, M. a., Mittal, V., Morbidelli, M., & Suter, U. W.**, Epoxy-Layered Silicate Nanocomposites and Their Gas Permeation Properties, *Macromolecules*, 37 (2004), 7250–7257
- Osman, M. a., Mittal, V., & Suter, U. W.**, Poly(propylene)-Layered Silicate Nanocomposites: Gas Permeation Properties and Clay Exfoliation, *Macromolecular Chemistry and Physics*, 208 (2007), 68–75
- Osman, M. a., Rupp, J. E. P., & Suter, U. W.**, Gas permeation properties of polyethylene-layered silicate nanocomposites, *Journal of Materials Chemistry*, 15 (2005) 1298–1304
- Pal, R.**, New models for thermal conductivity of particulate composites, *Journal of Reinforced Plastics and Composites*, 26 (2007), 643–651
- Pal, R.**, Permeation models for mixed matrix membranes, *Journal of Colloid and Interface Science*, 317 (2008), 191–198
- Pantani, R., Gorrasi, G., Vigliotta, G., Murariu, M., & Dubois, P.**, PLA-ZnO nanocomposite films: Water vapor barrier properties and specific end-use characteristics, *European Polymer Journal*, 49 (2013), 3471–3482
- Paralikar, S. A., Simonsen, J., & Lombardi, J.**, Poly(vinyl alcohol)/cellulose nanocrystal barrier membranes, *Journal of Membrane Science*, 320 (2008), 248–258
- Pardo-Ibáñez, P., Lopez-Rubio, A., Martínez-Sanz, M., Cabedo, L., & Lagaron, J. M.**, Keratin-polyhydroxyalkanoate melt-compounded composites with improved barrier properties of interest in food packaging applications, *Journal of Applied Polymer Science*, 131 (2014), 1–10
- Patel, N.P., Miller, a. C., & Spontak, R. J.**, Highly CO₂-Permeable and Selective Polymer Nanocomposite Membranes, *Advanced Materials*, 15 (2003), 729–733
- Patel, Nikunj P., Aberg, C. M., Sanchez, A. M., Capracotta, M. D., Martin, J. D., & Spontak, R. J.**, Morphological, mechanical and gas-transport characteristics of crosslinked poly(propylene glycol): homopolymers, nanocomposites and blends, *Polymer*, 45 (2004), 5941–5950
- Pavlidou, S., & Papaspyrides, C. D.**, A review on polymer-layered silicate nanocomposites, *Progress in Polymer Science*, 33 (2008), 1119–1198
- Petersen, K., Væggemose Nielsen, P., Bertelsen, G., Lawther, M., Olsen, M. B., Nilsson, N. H., & Mortensen, G.**, Potential of biobased materials for food packaging, *Trends in Food Science & Technology*, 10 (1999), 52–68
- Petersson, L., & Oksman, K.**, Biopolymer based nanocomposites: Comparing layered silicates and microcrystalline cellulose as nanoreinforcement, *Composites Science and Technology*, 66 (2006), 2187–2196
- Petropoulos, J.**, A Comparative study of Approaches Applied to the Permeability of Binary Composite Polymeric Materials, *Journal of Polymer Science: Polymer Physics Edition*, 23 (1985), 1309–1324
- Petsi, A. J., & Burganos, V. N.**, Interphase layer effects on transport in mixed matrix membranes. *Journal of Membrane Science*, 421-422 (2012), 247–257

- Picard, E., Vermogen, a, Gerard, J., & Espuche, E.**, Barrier properties of nylon 6-montmorillonite nanocomposite membranes prepared by melt blending: Influence of the clay content and dispersion state Consequences on modelling, *Journal of Membrane Science*, 292 (2007), 133–144
- Picard, Emilie, Espuche, E., & Fulchiron, R.**, Effect of an organo-modified montmorillonite on PLA crystallization and gas barrier properties, *Applied Clay Science*, 53 (2011), 58–65
- Plackett, D., Anturi, H., Hedenqvist, M., Ankerfors, M., Ga, M., & Lindstro, T.**, Physical Properties and Morphology of Films Prepared from Microfibrillated Cellulose and Microfibrillated Cellulose in Combination with Amylopectin, *Journal of Applied Polymer Science*, 117 (2010), 3601–3609
- Pradhan, A. K., & Swain, S. K.**, Electrical Conductivity and Oxygen Permeability of Polyacrylonitrile / Multiwalled Carbon Nanotubes Composites, *Polymer Composites*, 33 (2012), 1114–1119
- Quirijns, E. J., Van Boxtel, A. J. B., Van Loon W.K.P. & Van Straten, G.**, Sorption isotherms, GAB parameters and isosteric heat of sorption, *Journal of the Science of Food and agriculture*, 85 (2005), 1805–1814
- Rafiq, S., Man, Z., Maulud, A., Muhammad, N., & Maitra, S.**, Separation of CO₂ from CH₄ using polysulfone/polyimide silica nanocomposite membranes, *Separation and Purification Technology*, 90 (2012), 162–172
- Ray, S.**, International Journal of Food The Potential Use of Polymer-Clay Nanocomposites in Food Packaging The Potential Use of Polymer-Clay Nanocomposites in Food Packaging, *International Journal of Food Engineering*, 2 (2006), 1–11
- Ray, S. S., Yamada, K., Okamoto, M., Ogami, A., & Ueda, K.**, New Polylactide / Layered Silicate Nanocomposites. 3. High-Performance Biodegradable Materials, *Chemical Materials*, 15 (2003), 1456–1465
- Rhim, J.-W.**, Effect of clay contents on mechanical and water vapor barrier properties of agar-based nanocomposite films, *Carbohydrate Polymers*, 86 (2011), 691–699
- Rhim, J.-W., Hong, S.-I., & Ha, C.-S.**, Tensile, water vapor barrier and antimicrobial properties of PLA/nanoclay composite films, *LWT - Food Science and Technology*, 42 (2009), 612–617
- Rhim, J.-W., Hong, S.-I., Park, H.-M., & Ng, P. K. W.**, Preparation and characterization of chitosan-based nanocomposite films with antimicrobial activity, *Journal of agricultural and food chemistry*, 54 (2006), 5814–5822
- Rhim, J.-W., Park, H.-M., & Ha, C.-S.**, Bio-nanocomposites for food packaging applications, *Progress in Polymer Science*, 38 (2013), 1629–1652
- Rodríguez-Marín, M.L., Bello-Pérez, L.A., Yee-Madeira, H., Zhong, Q., & González-Soto, R.A.**, Nanocomposites of rice and banana flours blend with montmorillonite: partial characterization, *Materials science & engineering. C, Materials for biological applications*, 33 (2013), 3903–3908
- Romero, A. I., Parentis, M. L., Habert, A. C., & Gonzo, E. E.**, Synthesis of polyetherimide/silica hybrid membranes by the sol-gel process: influence of the reaction conditions on the membrane properties, *Journal of Materials Science*, 46 (2011), 4701–4709
- Rouse, J.**, Diffusion of vapors, *Journal of American Chemical Society*, 69 (1947), 1068–1073.
- Sadeghi, M., Khanbabaei, G., Dehaghani, A. H. S., Sadeghi, M., Aravand, M. a., Akbarzade, M., & Khaffi, S.**, Gas permeation properties of ethylene vinyl acetate-silica nanocomposite membranes, *Journal of Membrane Science*, 322 (2008), 423–428
- Sadeghi, M., Mehdi Talakesh, M., Ghalei, B., & Shafiei, M.**, Preparation, characterization and gas permeation properties of a polycaprolactone based polyurethane-silica nanocomposite membrane, *Journal of Membrane Science*, 427 (2013), 21–29

- Sadeghi, M., Semsarzadeh, M. A., Barikani, M., & Pourafshari Chenar, M.,** Gas separation properties of polyether-based polyurethane–silica nanocomposite membranes, *Journal of Membrane Science*, 376 (2011), 188–195
- Sadeghi, M., Semsarzadeh, M. A., & Moadel, H.,** Enhancement of the gas separation properties of polybenzimidazole (PBI) membrane by incorporation of silica nano particles, *Journal of Membrane Science*, 331(2009), 21–30
- Sánchez-García, M. D., Hilliou, L., & Lagarón, J. M.,** Morphology and water barrier properties of nanobiocomposites of κ /I-hybrid carrageenan and cellulose nanowhiskers, *Journal of agricultural and food chemistry*, 58 (2010), 12847–57
- Sanchez-Garcia, M.D. & Lagaron, J. M.,** Novel Clay-Based Nanobiocomposites of Biopolyesters with Synergistic Barrier to UV Light, Gas, and Vapour, *Journal of Applied Polymer Science*, 118 (2010), 188–99.
- Sanchez-Garcia, M.D., Gimenez, E., & Lagaron, J. M.,** Novel PET Nanocomposites of Interest in Food Packaging Applications and Comparative Barrier Performance With Biopolyester Nanocomposites, *Journal of Plastic Film and Sheeting*, 23 (2007), 133–148
- Sanchez-Garcia, M.D., Gimenez, E., & Lagaron, J. M.,** Morphology and barrier properties of solvent cast composites of thermoplastic biopolymers and purified cellulose fibers, *Carbohydrate Polymers*, 71 (2008), 235–244
- Sanchez-Garcia, M.D., Lagaron, J. M., & Hoa, S. V.,** Effect of addition of carbon nanofibers and carbon nanotubes on properties of thermoplastic biopolymers, *Composites Science and Technology*, 70 (2010), 1095–1105
- Sanchez-Garcia, Maria D., & Lagaron, J. M.,** On the use of plant cellulose nanowhiskers to enhance the barrier properties of polylactic acid, *Cellulose*, 17 (2010), 987–1004
- Sanchez-Garcia, Maria D., Lopez-Rubio, A., & Lagaron, J. M.,** Natural micro and nanobiocomposites with enhanced barrier properties and novel functionalities for food biopackaging applications, *Trends in Food Science & Technology*, 21 (2010), 528–536
- Saxena, A., & Ragauskas, A. J.,** Water transmission barrier properties of biodegradable films based on cellulosic whiskers and xylan, *Carbohydrate Polymers*, 78 (2009), 357–360
- Scocchi, G., Posocco, P., Danani, A., Pricl, S., & Fermeglia, M.,** To the nanoscale, and beyond!, *Fluid Phase Equilibria*, 261(2007), 366–374
- Semsarzadeh, M. A., & Ghalei, B.,** Preparation, characterization and gas permeation properties of polyurethane–silica/polyvinyl alcohol mixed matrix membranes, *Journal of Membrane Science*, 432 (2013), 115–125
- Shah, R. K., Krishnaswamy, R. K., Takahashi, S., & Paul, D. R.,** Blown films of nanocomposites prepared from low density polyethylene and a sodium ionomer of poly(ethylene-co-methacrylic acid), *Polymer*, 47 (2006), 6187–6201
- Shariati, A., Omidkhan, M., & Pedram, M. Z.,** New permeation models for nanocomposite polymeric membranes filled with nonporous particles, *Chemical Engineering Research and Design*, 90 (2011), 563–575
- Sheffel, J. A., & Tsapatsis, M.,** A model for the performance of microporous mixed matrix membranes with oriented selective flakes. *Journal of Membrane Science*, 295 (2007), 50–70
- Sheffel, J. A., Tsapatsis, M., & Stefan, M.,** A semi-empirical approach for predicting the performance of mixed matrix membranes containing selective flakes, *Journal of Membrane Science*, 326 (2009), 595–607

- Silvestre, C., Duraccio, D., & Cimmino, S.,** Food packaging based on polymer nanomaterials, *Progress in Polymer Science*, 36 (2011), 1766–1782
- Sinha Ray, S., & Okamoto, M.,** Polymer/layered silicate nanocomposites: a review from preparation to processing, *Progress in Polymer Science*, 28 (2003), 1539–1641
- Sinha Ray, S., Yamada, K., Okamoto, M., & Ueda, K.,** Biodegradable Polylactide/Montmorillonite Nanocomposites. *Journal of Nanoscience and Nanotechnology*, 3 (2003), 503–510
- Sinharay, S., & Bousmina, M.,** Biodegradable polymers and their layered silicate nanocomposites: In greening the 21st century materials world, *Progress in Materials Science*, 50 (2005), 962–1079
- Siqueira, G., Bras, J., & Dufresne, A.,** Cellulosic Bionanocomposites: A Review of Preparation, Properties and Applications. *Polymers*, 2 (2010), 728–765
- Siracusa, V., Rocculi, P., Romani, S., & Rosa, M. D.,** Biodegradable polymers for food packaging: a review, *Trends in Food Science & Technology*, 19 (2008), 634–643
- Slavutsky, A. M., Bertuzzi, M. A., Armada, M., García, M. G., & Ochoa, N. A.,** Preparation and characterization of montmorillonite/brea gum nanocomposites films, *Food Hydrocolloids*, 35 (2014), 270–278
- Smaihi, M., Schrotter, J.-C., Lesimple, C., Prevost, I., & Guizard, C.,** Gas separation properties of hybrid imide–siloxane copolymers with various silica contents, *Journal of Membrane Science*, 161 (1999), 157–170
- Sorrentino, Andrea, Gorrasi, G., & Vittoria, V.,** Potential perspectives of bio-nanocomposites for food packaging applications, *Trends in Food Science & Technology*, 18 (2007), 84–95
- Sothornvit, R., Hong, S.-I., An, D. J., & Rhim, J.-W.,** Effect of clay content on the physical and antimicrobial properties of whey protein isolate/organo-clay composite films, *LWT - Food Science and Technology*, 43 (2010), 279–284
- Sothornvit, R., Rhim, J.-W., & Hong, S.-I.,** Effect of nano-clay type on the physical and antimicrobial properties of whey protein isolate/clay composite films, *Journal of Food Engineering*, 91 (2009), 468–473
- Sreekumar, P. A., Albert, P., Unnikrishnan, G., Joseph, K., & Thomas, S.,** Mechanical and Water Sorption Studies of Ecofriendly Banana Fiber-Reinforced Polyester Composites Fabricated by RTM, *Journal of Applied Polymer Science*, 109 (2008), 1547–1555
- Srithep, Y., Ellingham, T., Peng, J., Sabo, R., Clemons, C., Turng, L.-S., & Pilla, S.,** Melt compounding of poly (3-hydroxybutyrate-co-3-hydroxyvalerate)/ nanofibrillated cellulose nanocomposites, *Polymer Degradation and Stability*, 98 (2013), 1439–1449
- Srubar, W. V., Frank, C. W., & Billington, S. L.,** Modeling the kinetics of water transport and hydroexpansion in a lignocellulose-reinforced bacterial copolyester, *Polymer*, 53 (2012), 2152–2161
- Srubar, W. V., & Billington, S. L.,** A micromechanical model for moisture-induced deterioration in fully biorenewable wood–plastic composites. *Composites Part A: Applied Science and Manufacturing*, 50 (2013), 81–92
- Strawhecker, K. E., & Manias, E.,** Structure and Properties of Poly (vinyl alcohol)/ Na + Montmorillonite Nanocomposites. *Chemical Materials*, 12 (2000), 2943–2949
- Sun, L., Boo, W. J., Sue, H.-J., & Clearfield, A.,** Preparation of α -zirconium phosphate nanoplatelets with wide variations in aspect ratios. *New Journal of Chemistry*, 31 (2007), 39

- Sun, L., Boo, W.-J., Clearfield, A., Sue, H.-J., & Pham, H. Q.,** Barrier properties of model epoxy nanocomposites. *Journal of Membrane Science*, 318 (2008), 129–136
- Surdo, E. M., Khan, I. a, Choudhury, A. a, Saleh, N. B., & Arnold, W. A.,** Barrier properties of poly(vinyl alcohol) membranes containing carbon nanotubes or activated carbon, *Journal of hazardous materials*, 188 (2011), 334–40
- Suzuki, T., & Yamada, Y.,** Characterization of 6FDA-based hyperbranched and linear polyimide-silica hybrid membranes by gas permeation and ^{129}Xe NMR measurements, *Journal of Polymer Science Part B: Polymer Physics*, 44 (2006), 291–298
- Strutt, J.-W.,** On the influence of obstacles arranged in rectangular order upon the properties of a medium, *Phil. Mag.*, 34 (1892), 481–502
- Svagan, A. J., Hedenqvist, M. S., & Berglund, L.,** Reduced water vapour sorption in cellulose nanocomposites with starch matrix, *Composites Science and Technology*, 69 (2009), 500–506
- Swain, S. K., Dash, S., Behera, C., Kisku, S. K., & Behera, L.,** Cellulose nanobiocomposites with reinforcement of boron nitride: study of thermal, oxygen barrier and chemical resistant properties, *Carbohydrate polymers*, 95 (2013), 728–32
- Swannack, C., Cox, C., Liakos, A., & Hirt, D.,** A three-dimensional simulation of barrier properties of nanocomposite films, *Journal of Membrane Science*, 263 (2005), 47–56
- Takahashi, S., Goldberg, H. a., Feeney, C. a., Karim, D. P., Farrell, M., O'Leary, K., & Paul, D. R.,** Gas barrier properties of butyl rubber/vermiculite nanocomposite coatings, *Polymer*, 47 (2006), 3083–3093
- Takahashi, S., & Paul, D. R.,** Gas permeation in poly(ether imide) nanocomposite membranes based on surface-treated silica. Part 1: Without chemical coupling to matrix, *Polymer*, 47 (2006a), 7519–7534
- Takahashi, S., & Paul, D. R.,** Gas permeation in poly(ether imide) nanocomposite membranes based on surface-treated silica. Part 2: With chemical coupling to matrix, *Polymer*, 47 (2006b), 7535–7547
- Tang, X., Alavi, S., & Herald, T. J.,** Barrier and Mechanical Properties of Starch-Clay Nanocomposite Films, *Cereal Chemistry*, 85 (2008), 433–439
- Thellen, C., Orroth, C., Froio, D., Ziegler, D., Lucciarini, J., Farrell, R., ... Ratto, J. A.,** Influence of montmorillonite layered silicate on plasticized poly(L-lactide) blown films, *Polymer*, 46 (2005), 11716–11727
- Tunc, S., Angellier, H., Cahyana, Y., Chalier, P., Gontard, N., & Gastaldi, E.,** Functional properties of wheat gluten/montmorillonite nanocomposite films processed by casting, *Journal of Membrane Science*, 289 (2007), 159–168
- Ulutun, S., & Balkisse, D.,** Diffusivity, solubility and permeability of water vapor in flexible PVC / silica composite membranes, *Journal of Membrane Science*, 115 (1996), 217–224
- Vassiliou, A., Bikiaris, D., & Pavlidou, E.,** Optimizing Melt-Processing Conditions for the Preparation of iPP/Fumed Silica Nanocomposites: Morphology, Mechanical and Gas Permeability Properties, *Macromolecular Reaction Engineering*, 1 (2007), 488–501
- Vermogen, A., Masenelli-Varlot, K., Vigier, G., Slxou, B., Thollet, G., Duchet-Rumeau, J.,** Clay Dispersion and Aspect Ratios in Polymer-Clay Nanocomposites, *Journal of Nanoscience and Nanotechnology*, 7 (2007), 3160–3171
- Vinh-Thang, H. & Kaliaguine, S.,** Predictive Models for Mixed-Matrix Membrane Performance: A Review, *Chemical Reviews*, 113 (2013), 4980–5028

- Villaluenga, J. P. G., Khayet, M., López-Manchado, M. a., Valentin, J. L., Seoane, B., & Mengual, J. I.**, Gas transport properties of polypropylene/ clay composite membranes, *European Polymer Journal*, 43 (2007), 1132–1143
- Vladimirov, V., Betchev, C., Vassiliou, a., Papageorgiou, G., & Bikiaris, D.**, Dynamic mechanical and morphological studies of isotactic polypropylene/fumed silica nanocomposites with enhanced gas barrier properties, *Composites Science and Technology*, 66 (2006), 2935–2944
- Wang, Y., Zhang, H., Wu, Y., Yang, J., & Zhang, L.**, Preparation, structure, and properties of a novel rectorite/styrene-butadiene copolymer nanocomposite, *Journal of Applied Polymer Science*, 96 (2005), 324–328
- White, J. D., & Cussler, E. L.**, Anisotropic transport in water swollen flake-filled membranes, *Journal of Membrane Science*, 278 (2006), 225–231
- Xu, Z., Yu, L., & Han, L.**, Polymer-nanoinorganic particles composite membranes: a brief overview, *Frontiers of Chemical Engineering in China*, 3 (2009), 318–329
- Yang, C., Smyrl, W. H., & Cussler, E. L.**, Flake alignment in composite coatings, *Journal of Membrane Science*, 231 (2004), 1–12
- Yano, K., Usuki, A., & Okada, A.**, Synthesis and Properties of Polyimide-Clay Hybrid Films, *Journal of Polymer Science Part A: Polymer Chemistry*, 35 (2000), 2289–2294
- Yeh, J.-M., Huang, H.-Y., Chen, C.-L., Su, W.-F., & Yu, Y.-H.**, Siloxane-modified epoxy resin–clay nanocomposite coatings with advanced anticorrosive properties prepared by a solution dispersion approach, *Surface and Coatings Technology*, 200 (2006), 2753–2763
- Yu, H.-Y., Qin, Z.-Y., Sun, B., Yang, X.-G., & Yao, J.-M.**, Reinforcement of transparent poly(3-hydroxybutyrate-co-3-hydroxyvalerate) by incorporation of functionalized carbon nanotubes as a novel bionanocomposite for food packaging. *Composites Science and Technology*, 94 (2014), 96–104
- Yu, J., Yang, J., Liu, B., & Ma, X.**, Preparation and characterization of glycerol plasticized-pea starch/ZnO-carboxymethylcellulose sodium nano-composites, *Bioresource technology*, 100 (2009), 2832–41
- Zehetmeyer, Gislene, Soares, R. M. D., Brandelli, A., Mauler, R. S., & Oliveira, R. V. B.**, Evaluation of polypropylene/montmorillonite nanocomposites as food packaging material, *Polymer Bulletin*, 68 (2012), 2199–2217
- Zembouai, I., Kaci, M., Bruzaud, S., Benhamida, A., Corre, Y., & Grohens, Y.**, Material properties A study of morphological , thermal , rheological and barrier properties of Poly (3-hydroxybutyrate-Co-3-Hydroxyvalerate)/ polylactide blends prepared by melt mixing, *Polymer Testing*, 32 (2013), 842–851
- Zhang, B., & Wang, Q.**, Development of Highly Ordered Nanofillers in Zein Nanocomposites for Improved Tensile and Barrier Properties, *Journal of agricultural and food chemistry*, 60 (2012), 4162–4169
- Zheng, H., Ai, F., Chang, P. R., Huang, J., & Dufresne, A.**, Structure and Properties of Starch Nanocrystal-Reinforced Soy Protein Plastics, *Polymer Composites*, 30 (2009), 474–480
- Zhong, Y., Janes, D., Zheng, Y., Hetzer, M., & Kee, D. De.**, Mechanical and Oxygen Barrier Properties of Organoclay-Polyethylene Nanocomposite Films, *Polymer Engineering and Science*, 47 (2007), 1101–1107
- Zhou, J. J., Wang, S. Y., & Gunasekaran, S.**, Preparation and characterization of whey protein film incorporated with TiO₂ nanoparticles, *Journal of food science*, 74 (2009), 50–56

- Zhu, A., Cai, A., Zhang, J., Jia, H., & Wang, J.**, PMMA- grafted -Silica / PVC Nanocomposites : Mechanical Performance and Barrier Properties, *Journal of Applied Polymer Science*, 108 (2008), 2189–2196
- Zimm, B. H., & Lundberg, J. L.**, Sorption of vapors by high polymers, *Journal of Physical Chemistry*, 60 (1956), 425–428
- Zoppi, R. A., Neves, S., & Nunes, S. P.**, Hybrid films of poly (ethylene oxide-b-amide-6) containing sol-gel silicon or titanium oxide as inorganic fillers : effect of morphology and mechanical properties on gas permeability, *Polymer*, 41 (2000), 5461–5470
- Zou, H., Wu, S., & Shen, J.**, Polymer/silica nanocomposites: preparation, characterization, properties, and applications, *Chemical reviews*, 108 (2008), 3893–3957

PUBLICATIONS AND COMMUNICATIONS



Scientific papers

How various particle shapes affect structure & mass transfer relationships of nanocomposite materials?

C. Wolf, N. Gontard, H. Angellier-coussy, F. Doghieri, V. Guillard

In preparation for submission, (forthcoming (a))

State of the art and beyond, on multi-scale modelling of structure & mass transfer relationships in nanocomposite materials

C. Wolf, N. Gontard, F. Doghieri, V. Guillard

In preparation for submission, (forthcoming (b))

Water vapour sorption and diffusion in wheat straw fibres and impact on mass transfer in PHBV based bio-composites

C. Wolf, N. Gontard, G. Ghizzi Da Silva, V. Guillard

Composite Science and Technology, Submitted, (forthcoming (c))

Prediction of water vapour permeability in biocomposites using theoretical models

C. Wolf, N. Gontard, V. Guillard

In preparation for submission, (forthcoming (d))

A numerical model for predicting mass transfer in bio-composites: assessment of the permeable particles impact on the water vapour properties

C. Wolf, N. Gontard, V. Guillard

In preparation for submission, (forthcoming (e))

Oral communication

Multi-scale modelling of structure and mass transfer properties relationship

C. Wolf, V. Guillard, N. Gontard

Biopolymers 2013 - Nantes, France – 4-6th December 2013

Posters

Multi-scale modelling of structure and mass transfer properties relationship of composite materials

C. Wolf, V. Guillard, N. Gontard

Doctoral school day SP-SA – Montpellier, France – 21th June 2013

Multi-scale modelling of structure and mass transfer properties relationship - Application to biomaterials-based composites

C. Wolf, V. Guillard, N. Gontard

Recent advances in sustainable bio-based nano-composites for food packaging – Montpellier, France – 27th February 2014

ANNEXES

Contexte scientifique et technique dans le domaine de l'emballage alimentaire

Durant les dernières décennies, les recherches menées dans les centres de recherches et développement ont été majoritairement consacrées au design de matériaux barrières améliorés qui permettent d'augmenter la durée de vie tout en maintenant et en ayant un suivi en continu de la sécurité et de la qualité des aliments. Parallèlement, avec la prise de conscience internationale liée à l'usage intensif de plastiques dérivés de l'industrie pétrochimique dans les applications en emballage alimentaire, un intérêt considérable a été dédié à l'étude des biomatériaux [Petersen et al. (1999)]. Malgré le nombre croissant d'études associées au développement de nouveaux matériaux, la principale limitation est l'absence d'approches combinant à la fois les exigences des aliments et le développement de matériaux pour la mise en œuvre de « système aliment/emballage » intégrés aux filières alimentaires, du traitement à la consommation.

Un des rôles principal du matériau d'emballage en terme de qualité et de préservation des aliments est le contrôle des transferts de gaz et de vapeurs entre les aliments, le matériau d'emballage et l'environnement externe ; trois types de transferts peuvent avoir lieu (figure 1) :

- ➔ de l'environnement externe au travers de l'emballage, vers l'espace de tête et l'aliment, la perméation de gaz et de vapeurs doit être contrôlée pour la préservation de la qualité de l'aliment en évitant les réactions de dégradation de l'aliment ;

- ➔ de l'emballage vers l'aliment, la migration de molécules indésirables comme les additifs chimiques ne doivent pas excéder une limite maximum afin de ne pas être toxique pour les humains lors de l'exposition à long terme à ces éléments ;
- ➔ de l'aliment vers le matériau d'emballage, la sorption et la diffusion de composés de l'aliment comme les composés d'arôme qui doivent être contrôlés pour la conservation des propriétés organoleptiques des aliments.

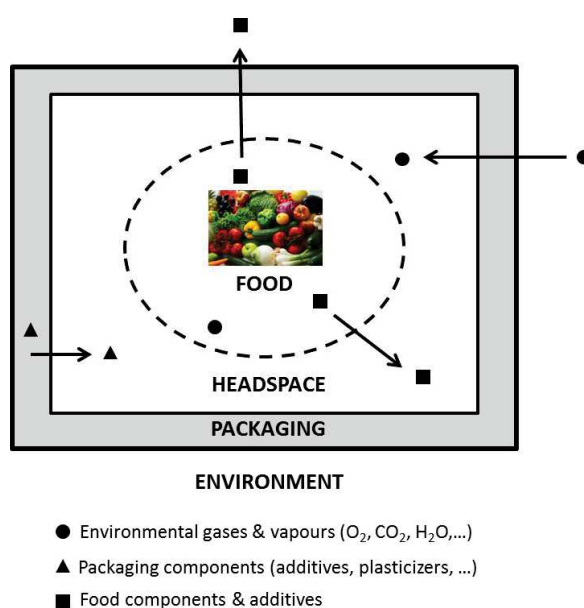


Figure 7: Représentation des transferts de matière au travers de l'emballage

Pour des applications en emballage alimentaire, une étape essentielle pour la proposition de nouveaux matériaux complexes, comme les composites par exemple, est le développement d'outils numériques d'aide à la décision basés sur la modélisation mathématique des transferts de matière afin de favoriser des structures composites adaptées aux besoins des aliments. Dans la perspective de modélisation multi-échelle, une compréhension plus en détail de la relation entre structure et transferts de matière, est nécessaire et établie à partir de la

caractérisation de la structure des composites (taille et forme de la particule in-situ la matrice polymérique, dispersion et orientation des particules), de l'impact des particules sur la structure et les propriétés de la matrice polymérique, de la modulation des transferts de masse dans le composites. Chaque particule est unique en terme de taille, de forme, de nature (imperméable ou perméable par exemple) et leurs effets sur les transferts de matière dans les composites ne sont pas les mêmes. Même si les effets des particules imperméables sur la modulation des transferts de matière a déjà été prouvés à de nombreuses reprises à l'aide d'approches expérimentales [Azeredo et al. (2009)], la formalisation (c.à.d. la modélisation) de la relation entre structure et transferts de matière demeure cependant limitée du fait de la difficulté d'atteindre une caractérisation optimale de la structure des propriétés de transfert à cause de deux verrous scientifiques majeurs :

- ➔ la difficulté d'atteindre une bonne caractérisation structurelle des matériaux composites, principalement une description précise de la taille, de la forme, de la dispersion et de l'orientation des particules à l'intérieur de la matrice polymérique ;
- ➔ le manque de méthodologies et d'outils expérimentaux pour la caractérisation des transferts de matières dans des particules perméables.

A l'état actuel, une richesse de données expérimentales sur les propriétés barrières des composites est disponible dans la littérature scientifique, et plus spécifiquement sur les nanocomposites renforcés avec des particules imperméables. En effet, les matériaux composites représentent une source de développement prometteuse pour les emballages actifs et intelligents mais aussi pour le développement

d'emballages respectueux de l'environnement avec l'utilisation de biopolymères. Alors que ces derniers présentent une grande sensibilité aux conditions extérieures, comme la température ou l'humidité qui peuvent limiter leur utilisation pour des applications en emballage alimentaire, la résistance à l'eau et mécanique peut être améliorés en ajoutant des fillers. [Rhim et al. (2013)] afin d'obtenir des matériaux avec des propriétés renforcées. De telles propriétés sont généralement atteintes à faible taux d'argiles, inférieur à 5% en comparaison aux fillers conventionnels qui présentent des taux entre 10 et 50%. Actuellement, les fibres végétales suscitent un grand intérêt pour des applications dans le domaine de l'emballage alimentaire du fait de leur large accessibilité ; en effet la cellulose nanocristalline est dix fois moins résistante mais des coûts de production qui sont 50 à 1000 fois plus faible [Faruk et al. (2012)]. L'incorporation de fibres végétales dans des matrices polymériques contribue à la diminution du coût du matériau, surtout avec de forts taux de renforts allant jusqu'à 40wt%, et permet de moduler les propriétés de transfert du composite comme par exemple la perméabilité à la vapeur d'eau.

Pour la prédiction des propriétés de transferts dans les composites, les approches de modélisation ont été basées sur soit l'application de modèles analytiques ou le développement de modèles numériques (modélisation de la dynamique des fluides computationnelle (CFD) comme par exemple la méthode des éléments finis). A présent, l'utilisation des modèles analytiques repose sur la prédiction de la perméabilité du composite à partir de la caractérisation de la structure composite avec pour entrées des modèles des paramètres géométriques (facteur de forme, fraction volumique, dispersion et orientation des particules), supposés être constant et homogène dans tout le matériau et à partir de la perméabilité de la matrice polymérique. Ces modèles ont été développées pour des distributions homogènes

de particules et exhibent des restrictions d'utilisation pour des composites présentant des structures hétérogènes. En ayant recours à des approches numériques, des structures plus complexes peuvent être abordées et étudiées en appliquant la méthode des éléments finis à des géométries 2D ou 3D représentant la structure du composites. Bhunia et al. (2012), entre autres, ont développés un modèle sur la base des éléments finis qui a permis de surmonter les limitations de la plupart des modèles analytiques en considérant des phénomènes structuraux complémentaires comme l'orientation et l'agglomération des particules.

Objectifs scientifiques du projet de thèse

Dans ce contexte, l'objectif de mon travail de thèse a été de contribuer à l'amélioration de la connaissance scientifique des transferts de matière dans des matériaux composites en atteignant une meilleure compréhension de la modulation des propriétés barrières avec l'incorporation de nano- et micro- perméables et imperméables particules dans des matrices polymériques.; et développer une approche multi-échelle innovante pour la prédiction des transferts de matière dans des composites biphasés, à partir de la méthode des éléments finis, en considérant à la fois les propriétés des particules et de la matrice polymérique dans des structures réalistes 2D du composites. Ce travail de thèse a été dans le cadre des activités de recherche de l'équipe de recherche Ingénierie des Agropolymères et des Techniques Emergentes et financée à l'aide d'une bourse ministérielle (bourse MENRT) délivrée par le gouvernement français. L'aspect innovant de ce projet a été de considérer des composites avec soit des particules perméables ou imperméables (comme des fibres végétales par exemple) qui contribuent de façon remarquable

au transfert global de vapeur d'eau. Un composite, créé à partir d'une matrice biopolyester et de fibre de paille de blé, a été employé comme matériau modèle pour le développement et la validation d'un modèle numérique. Ce composite é été développé au sein du projet européen EcoBioCap (<http://www.ecobiocap.eu/>); proposant des structures composites de pointes basées sur des constituants dérivés des sous-produits de l'industrie alimentaire.

Questions scientifiques du projet de thèse

Afin d'atteindre les objectifs de ma thèse, plusieurs réponses ont dû être trouvées aux questions suivantes :

- ➔ quel est l'impact de la nature, de la forme, de la taille des particules sur la perméabilité du composite ?
- ➔ quels sont les modèles communs les plus utilisés pour la prédiction des relations entre structure et transferts de matière ?
- ➔ quelle est la contribution des particules perméables, comme les fibres végétales par exemple, sur les transferts globaux de matière ?
- ➔ comment les caractéristiques structurales et les propriétés barrières, obtenues à partir de l'analyse de la structure et des transferts de matière, peuvent être réunis et liés aux transferts de matière dans un composite à l'aide d'une approche multi-échelle ?

Stratégies du projet de thèse

Afin de répondre aux questions relevées précédemment, la stratégie scientifique suivie, présentée dans la figure 2 a été adoptée : le plan de travail de ce projet de thèse est divisé en deux chapitres selon la nature de la particule soit imperméable, soit perméable.

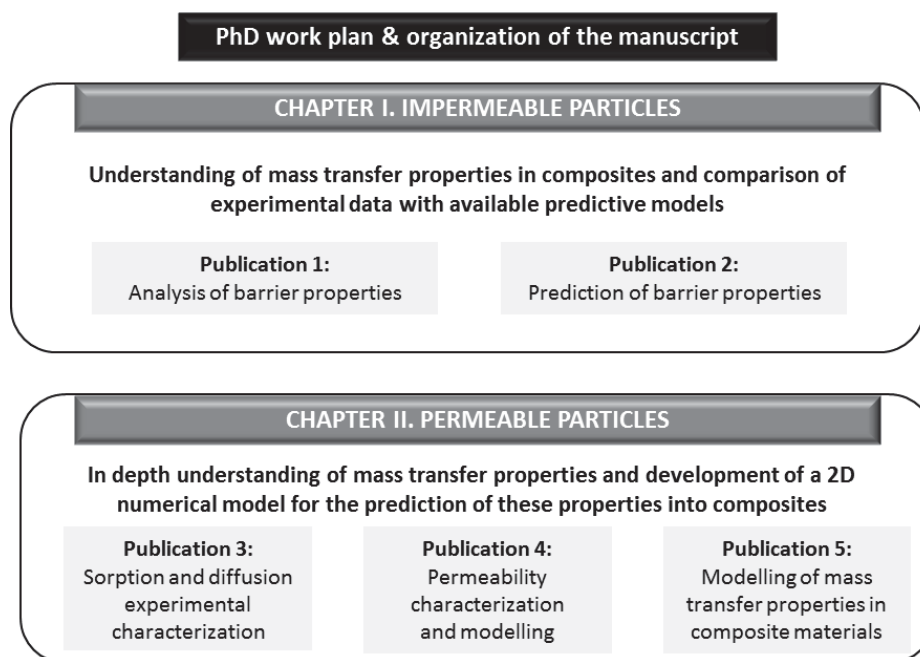


Figure 8: Organisation du travail de thèse

Le premier chapitre a été dédié à une analyse exhaustive des transferts de matière dans des composites et au listing de tous les modèles mathématiques proposés dans la littérature pour la prédiction des transferts de matière dans les composites. L'analyse des propriétés barrières a permis de déterminer les paramètres impactant les transferts de matière dans les composites et l'analyse des modèles a mis en évidence les verrous scientifiques rencontrés pour le développement de modèles permettant une bonne prédiction des propriétés barrières des composites.

Le second chapitre a été premièrement visant à fournir une meilleure compréhension de l'impact des particules perméable à la modulation des transferts de vapeur d'eau au travers d'un composite fibre de paille de blé/biopolyester à l'aide de supports expérimentaux et de modélisation. Il a été par la suite tenté de présenter d'une nouvelle approche multi-échelle, utilisant COMSOL Multiphysics Software, pour la prédiction des propriétés de transferts dans un composite biphasé ; en considérant à la fois les propriétés de transferts des particules perméables et de la matrice polymérique dans des structures réalistes 2D de composites.

Conclusion et discussion générale

Malgré l'intérêt croissant des structures composites pour le design de matériaux sur mesure répondant aux exigences des produits alimentaires en termes de propriétés barrières, la compréhension des transferts de matières au travers des matériaux composites reste un challenge pour le futur. D'une part, à cause de limitations expérimentales à la caractérisation tridimensionnelle de la structure des composites et la caractérisation des propriétés barrières des particules perméables reste difficile, d'autre part à cause du manque de méthode de modélisation efficace. Ce projet de thèse a été centré sur l'étude des transferts de gaz et de vapeurs dans les nano- et micro-composites contenant des particules imperméables et perméables (impact de la nature, taille, forme, etc.) et le développement d'un modèle numérique 2D pour la prédiction des relations structure/transferts de matière dans des matériaux composites.

La première partie de ce travail a été consacrée à l'étude de données disponible dans la littérature sur la perméabilité à l'oxygène, au dioxyde de carbone et à l'eau dans les nano- et micro-composites avec différents types de particules (inorganique et organique comme les nanowhiskers de cellulose), et différentes formes de particules (c.à.d sphérique, cylindrique et plaquettaire) et à l'examen des approches de modélisation prédictive de ces perméabilités. Les publications scientifiques ont été répertoriées et leurs résultats ont été comparés et discutés de façon à élucider le rôle de la forme et de la taille des particules sur la perméabilité du composite. Dans toutes les références collectées, les nanoparticules incluses dans les matrices polymériques ont été considérées imperméables et ont été ajoutées afin

de moduler et principalement de diminuer la perméabilité du composite en comparaison à celle de la matrice polymérique. Pour les particules sphériques ou cylindriques, la perméabilité a soit augmenté ou diminué avec l'ajout de particules imperméables. Cependant pour les particules plaquettaires, uniquement une diminution, parfois non-monotonique (c.à.d une diminution et ensuite une augmentation à taux de renfort plus élevé) de la perméabilité a été observée. Dans le cas des particules plaquettaire, la plus grande réduction de perméabilité pourrait être expliquée par la création d'un parcours plus tortueux pour les espèces diffusantes. Néanmoins, la modulation des propriétés barrières, notamment l'amélioration de ces propriétés, a été particulièrement reliée à la structure du composite. En effet, quand la structure du composite présente une bonne dispersion des particules, la diminution de la perméabilité est plus grande que dans le cas de mélange de particules bien dispersées et agglomérées. Lorsque les particules sont bien dispersées dans la matrice polymériques, la prédiction des modèles analytiques a été dans certain cas en bon accord avec les données expérimentales. Cependant en présence de particules agglomérées, les modèles ont été en limites de leurs conditions de validité et des écarts entre valeurs prédites et valeurs expérimentales ont été relevés. La dispersion des particules dépend fortement des modifications chimiques de la surface des particules et de l'optimisation des techniques de fabrication des composites qui sont de grandes importances pour accéder à des structures composites avec des particules bien dispersées dans une matrice polymérique. D'autres limitations d'utilisation des modèles analytiques comprennent la difficulté d'évaluer expérimentalement le facteur de forme des particules in-situ la matrice polymérique ; ainsi dans la plupart des cas, les modèles prédictifs ont été appliqués afin d'identifier ce paramètre géométrique. En général, les hypothèses reliées à la géométrie du composite dans ces modèles sont trop

simplifiées et ne représentent pas l'hétérogénéité des structures réelles des composites ; la polydispersité de la taille, de la forme, de la dispersion et de l'orientation des particules. De plus il est très compliqué de choisir un modèle analytique précis pour la prédiction des transferts de matière d'une série spécifique de données expérimentales ; l'utilisation de plusieurs théories est possible mais leurs prédictions ne convergent pas vers le même résultat, excepté pour les forts taux de renforts compte tenu des hypothèses de base trop simplistes. De plus peu de modèles sont disponibles pour la prédiction des transferts de matière dans des composites avec des particules sphériques et cylindriques et ces modèles ne permettent pas de prédire des augmentations de perméabilité dans les composites ; augmentations fréquemment observées dans les résultats expérimentaux.

Dans la littérature, un grand nombre d'études traite des particules imperméables et seulement peu d'études avec des particules perméables. Dans le cas des transferts de vapeur d'eau, les fibres végétales comme par exemple les fibres de paille de blé ne peuvent plus être considérées comme imperméables. Pour autant que nous sachions en ce qui concerne la modélisation prédictive de la perméabilité de ces composites renforcés avec des particules perméables qui contribuent énormément aux transferts globaux, aucune recherche scientifique n'a été menée à ce sujet dans le domaine de l'emballage alimentaire au début de ce travail. Par conséquent la deuxième partie de ce travail de thèse a été dédié à l'étude des transferts de matière dans un matériau composite contenant des particules perméables et au développement d'un modèle numérique pour prédire ces propriétés.

Du fait d'incapacité technique étant donné la taille et la forme des particules qui limitent leurs manipulations dans des cellules de perméabilité, la sorption, la diffusion et la perméabilité à la vapeur d'eau n'ont pas pu être analysées sur une particule élémentaire de paille de blé. Par conséquent, les tests de sorption à la vapeur d'eau ont été menés sur un morceau de paille de blé qui n'exhibe pas la même structure que celle des pailles de blé broyées. En comparaison avec la matrice polymérique poly(3-hydroxybutyrate-co-3-hydroxyvalérate) (PHBV), la sorption dans la paille de blé (PdB) est environ 40 fois plus grande et il a donc été démontré que les PdB améliorent la perméabilité dans les biocomposites PdB/PHBV du fait de leur caractère hydrophile. Bien que les transferts de vapeur d'eau dans le morceau de paille de blé n'est pas représentatif de ceux dans les PdB inclus dans la matrice polymérique, cela a permis de déterminer le coefficient de solubilité et de diffusivité et d'accéder au coefficient de perméabilité nécessaire pour l'application des modèles biphasés pour la prédiction de la perméabilité dans des composites perméables biphasés. A partir de la prédiction des modèles, il a été mis en évidence que plus de la moitié des modèles nécessitent l'ajustement d'au moins un paramètre aux données expérimentales (c.à.d l'évolution de P/P_0 en fonction de la fraction volumique de particules). Une fois ajusté aux données expérimentales, ces modèles ont bien évidemment convenablement représenté ces données avec une certaine incertitude mais n'ont pas pu être extrapolés. En réalité, ces modèles ont montrés des résultats peu concluants et des écarts avec les perméabilités expérimentales à de taux de renforts supérieurs à 10vol%. Similairement pour les modèles ne nécessitant aucun ajustement, des différences entre les valeurs prédites et les valeurs expérimentales sont apparus à plus forts taux de particules. Par conséquent l'utilisation de ces modèles analytiques biphasés n'est pas adaptée à nos structures composites hétérogènes. En ce sens, le développement d'une nouvelle approche

de modélisation 2D, reposant sur la méthode des éléments finis, a été proposé pour la prédiction des propriétés barrières des composites. Le modèle permet le calcul de la perméabilité à partir d'une valeur de flux dans un composite, en relation avec des paramètres structuraux des particules dispersées dans une matrice polymérique. Le modèle a été construit en prenant en compte les concentrations initiales et aux limites et les coefficients de diffusivité à la fois dans la matrice polymérique et dans les particules avec des représentations géométriques simplifiées (c.à.d. dispersion aléatoire d'ellipsoïdes) dans des structures composites. COMSOL Multiphysics a été utilisé comme logiciel pour le calcul approché du flux dans des structures composites établies. Le modèle a été mis en place avec pour entrées des données de transferts de vapeur d'eau dans les biocomposites PdB/PHBV. Les résultats de simulation ont montré que le flux dans les composites augmente avec une augmentation de la fraction volumique de particules ϕ et le facteur de forme α de ces particules. Cependant, à faible fraction volumique (c.à.d. environ inférieure à 2.5vol%) et à faible facteur de forme (c.à.d. environ 5) l'augmentation de la valeur du flux n'est pas significative en tenant en compte des incertitudes expérimentales obtenues lors de la mesure du flux de vapeur d'eau. Un essai de validation du modèle a été effectué sur une dispersion aléatoire d'ellipsoïdes avec différents gradient d'humidité relative au travers du composite avec des données expérimentales. La valeur prédite de perméabilité dans le composite est approximativement dix fois plus élevées que la valeur expérimentale. Selon la règle des mélanges, la prédiction de la sorption dans les composites est en bon accord avec la sorption expérimentale dans les biocomposites PdB/PHBV, les conditions initiales et aux limites ont donc été confirmées dans les PdB et le PHBV. Néanmoins comme énoncé précédemment, le coefficient de diffusivité dans les PdB a été identifié sur un morceau de paille de blé et non pas sur une fibre élémentaire. Une

fois incluse dans la matrice polymérique PHBV, la fibre broyée rencontre probablement des contraintes mécaniques qui l'empêchent de gonfler sous l'effet de la vapeur d'eau comme lors des tests de sorption sur des morceaux de paille. Cette caractéristique conduit à une modification du coefficient de diffusivité des PdB une fois incluses dans la structure composite. En confirmant ce fait, le coefficient de diffusivité identifié lors de simulations numériques a conduit à une valeur 12 fois plus faible que la valeur expérimentale, égale à $0.57 \times 10^{-12} \text{ m}^2 \cdot \text{s}^{-1}$ comparée à la valeur $6.91 \times 10^{-12} \text{ m}^2 \cdot \text{s}^{-1}$ calculée à partir du produit $D \times S$ mesuré sur un morceau de paille de blé. Ce résultat montre la difficulté rencontrée pour la caractérisation des transferts de matière dans une particule élémentaire broyée. En effet, de façon à améliorer la précision de la mesure, il pourrait être opportun de développer une technologie afin de suivre les transferts de matière dans une particule après son incorporation dans une matrice polymérique.

Tandis qu'il a été prouvé que les simulations numériques accordent une remarquable prédiction des propriétés barrières dans les composites composés de constituants présentant des comportements totalement opposés pour ce qui est des propriétés de transferts de vapeur d'eau, la convergence du modèle a pu être garantie en définissant une condition de continuité du flux à l'interface particule/matrice polymérique. Pour atteindre le niveau supérieur en développant un modèle numérique 3D pour la prédiction des transferts de matière dans des composites biphasés en simulant une structure 3D réelle, une caractérisation tridimensionnelle complète de la structure des composites avec la dispersion et l'orientation des particules sera primordiale.

MULTI-SCALE MODELLING OF STRUCTURE AND MASS TRANSFER PROPERTIES RELATIONSHIPS IN NANO- AND MICRO-COMPOSITES FOR FOOD PACKAGING

ABSTRACT: Despite the global growing interest in the food packaging field for the design of tailored composite structures with controlled mass transfer properties, the understanding of the modulation of the mass transfer properties with the incorporation of particles in polymer still remains very complex. In order to throw light on this scientific problem, the thesis work was focused on the following parts:

- providing a better understanding of mass transfer in composites. In this purpose an analysis of all experimental gas and vapour permeability data available in the literature has been carried out in nano- and micro- composites and a comparison of these data with predictions from tortuosity models based on few geometrical inputs has been achieved;

- performing a detailed study of water vapour mass transfer in composites (wheat straw fibres/bio-polyester). These data were compared with the prediction of bi-phasic analytical models coming from other disciplinary fields. This part of the work has highlighted the lack of comprehensive and complete models for the prediction of permeability in composite with permeable particles;

- developing of an innovative multi-scale approach for the prediction of mass transfer in bi-phasic composites considering both the particle and the polymer matrix properties with realistic 2D geometry of the composite structures has been proposed. For the sake of reaching a satisfactory validation level of the model, some experimental improvements are still needed to increase the accuracy of input parameters such as diffusivity of the particles.

This new modelling approach open the way for the creation of a reverse-engineering toolbox for the design of tailor made composites structures, tightly adjusted to barrier properties requirements of the packed food.

Keywords: Multi-scale modelling, Nano- and micro-composites, Mass transfers, Structure

MODELISATION MULTI-ECHELLE DES RELATIONS ENTRE STRUCTURE ET PROPRIETES DE TRANSFERT DE MATIERE DANS DES NANO- ET MICRO-COMPOSITES POUR L'EMBALLAGE

Abstract: Malgré l'intérêt croissant que représente dans le domaine de l'emballage alimentaire la conception raisonnée de structures composites aux propriétés de transfert contrôlées, la compréhension des transferts de gaz et de vapeurs avec l'ajout de particules dans des polymères reste complexe. En vue d'apporter un nouvel éclairage à ce verrou scientifique, les travaux de thèse se sont focalisés sur les trois parties suivantes :

- contribuer à une meilleure compréhension des transferts de matière dans les composites. Pour ce faire, une analyse exhaustive des données expérimentales de transfert de gaz et de vapeurs disponibles dans la littérature a été menée pour les nano- et micro-composites et une comparaison de ces données a été réalisée avec des modèles de tortuosité, basés sur des paramètres géométriques ;

- comprendre et modéliser la perméabilité dans des composites avec deux phases perméables. Pour cela, les transferts de vapeur d'eau dans un composite (fibre de paille/bio-polyester) chargé avec des particules perméables ont été mesurés et décrits en détail, et une comparaison de ces données avec des modèles analytiques issus d'autres champs disciplinaires, prenant en compte la perméabilité dans la particule et dans la matrice, a été menée. Cette étude a mis en avant le manque de modèles adaptés pour la prédiction de P dans les composites contenant des particules perméables ;

- développer une nouvelle approche multi-échelle pour la prédiction de la perméabilité dans des composites prenant en compte les propriétés de transfert dans les particules et dans la matrice polymérique avec une représentation 2D de la structure du composite. Afin d'atteindre un niveau satisfaisant de validation du modèle, la détermination des paramètres expérimentaux tels que la diffusion dans les particules doit être améliorée.

Cette nouvelle approche de modélisation ouvre la voie à la création d'outils d'ingénierie inverse pour le design de structures composites, ajustés aux besoins des aliments en termes de propriétés barrières.

Mots clés: Modélisation multi-échelle, Nano- et micro-composites, Transfer de gaz et de vapeur, Structure